

**PETROLOGICAL AND GEOCHRONOLOGICAL CONSTRAINTS ON THE
METAMORPHIC EVOLUTION OF HIGH-PRESSURE GRANULITES AND
ECLOGITES OF THE SNOWBIRD TECTONIC ZONE, CANADA**

by

Julia A. Baldwin

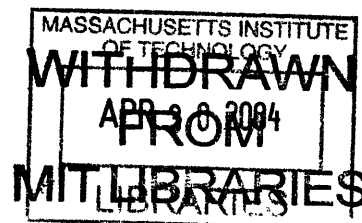
B.S. Geology
University of North Carolina at Chapel Hill, 1996

SUBMITTED TO THE DEPARTMENT OF EARTH, ATMOSPHERIC, AND PLANETARY SCIENCES
IN PARTIAL FULFILLMENT OF THE REQUIREMENTS FOR THE DEGREE OF

DOCTOR OF PHILOSOPHY
AT THE
MASSACHUSETTS INSTITUTE OF TECHNOLOGY

SEPTEMBER 2003

© 2003 Massachusetts Institute of Technology. All rights reserved.



Signature of Author: _____
Department of Earth, Atmospheric, and Planetary Sciences
July 18, 2003

Certified by: _____
Samuel A. Bowring
Professor of Geology
Thesis Supervisor

Accepted by: _____
Maria T. Zuber
E.A. Griswold Professor of Geophysics and Planetary Science
Department Head

LINDGREN

PETROLOGICAL AND GEOCHRONOLOGICAL CONSTRAINTS ON THE METAMORPHIC EVOLUTION OF HIGH-PRESSURE GRANULITES AND ECLOGITES OF THE SNOWBIRD TECTONIC ZONE, CANADA

by

Julia A. Baldwin

Submitted to the Department of Earth, Atmospheric, and Planetary Sciences at the Massachusetts Institute of Technology on July 18, 2003 in Partial Fulfillment of the Requirements for the Degree of Doctor of Philosophy in Geology

ABSTRACT

This thesis examines the petrology and geochronology of high-pressure granulites and eclogites within the Snowbird tectonic zone of the western Canadian Shield. The focus of this study is the East Athabasca mylonite triangle (EAmt), a well-exposed terrane of granulite facies mylonitic rocks along the trace of the Snowbird tectonic zone in northern Saskatchewan. This study focuses on the 400 km² Southern Domain of the EAmt, which contains a spectacular suite of high-pressure granulites and eclogites that have been metamorphosed at conditions exceeding 1.5 GPa and 1000°C.

Each chapter of this thesis focuses on a different lithology within the Southern Domain – mafic granulite, eclogite, sapphirine granulite, and felsic granulite. The approach that is taken in understanding each of these rock types is an integrated study of the petrological and geochronological constraints that yield important information about the metamorphic evolution of these unique rocks. The main discovery through these integrated studies is that the Snowbird tectonic zone records a significant Paleoproterozoic high-pressure metamorphism that was previously unrecognized.

Petrological and geochronological studies of each of these rock types constrains the pressure-temperature-time path of these rocks from their initial formation to their ultimate exhumation. The granulites and eclogites of the Southern Domain are derived from Archean igneous and sedimentary protoliths. The dominant rock type of the Southern Domain, the felsic gneiss, is interpreted to be derived from a pelitic protolith that underwent an early metamorphism at 2.62-2.60 Ga. Protoliths of the mafic lithologies intruded at mid-crustal levels by 2.55-2.52 Ga. The eclogite protolith was derived from a plagioclase-bearing cumulate source at pressures <1.0 GPa. The eclogite and mafic granulite, and, to a lesser extent, the felsic gneiss record high-pressure metamorphism at 1.9 Ga. Near-isothermal decompression P-T paths in the mafic granulite and eclogite record rapid exhumation to medium-pressure granulite facies conditions of ~1.0 GPa, 800°C. Sapphirine-bearing veins within the eclogite record further decompression, cooling, and re-equilibration in the middle crust at ~0.6 GPa, 600-700°C. Final exhumation of these rocks occurred by more protracted erosional processes from 1.9 to 1.8 Ga.

Thesis Supervisor: Samuel A. Bowring

Title: Professor of Geology

Acknowledgements

As I sit down to write these acknowledgements, it overwhelms to me to think about just how many people have contributed to my life over the past six years at MIT, in both scientific and personal ways. First and foremost is my advisor Sam Bowring. His daily enthusiasm in my work and suggestion of no less than ten Ph.D. theses during the course of my time here provided ample motivation, as well as some frustration, but his genuine interest in the science is always at the center of everything. I thank him for taking a chance on a metamorphic petrologist and for his push to always think about the larger tectonic context. I also owe many thanks to my second advisor and colleague on this project, Mike Williams. Mike always treated me like his own student and was a great source of advice on the petrological aspects of this thesis research. In addition, I would like to thank the other members of my thesis committee, Tim Grove, Kip Hodges, and Brian Evans for their helpful input and broader thinking. I also would like to thank my advisor on my second generals project, Kelin Whipple, for his endless supply of ideas and for encouraging me to take on a project in a completely unfamiliar field that broadened my skills and appreciation for geomorphology. Thanks also to Wiki Royden for her support of the women graduate students.

I never would have pursued a Ph.D. in geology had it not been for the faculty at UNC whose incredible teaching lured me in to the wonders of rocks and minerals. Thanks are due in particular to the spectacular teaching abilities of Kevin Stewart and Michael Follo during my freshman year, followed by my introduction to petrology from both Allen Glazner and Donna Whitney. Once my fascination was peaked with the wonders of petrology and the allure of spectacular metamorphic rocks, I never turned back, and I thank Donna for a productive undergraduate research experience and the guidance that helped lead me to where I am today.

The many and varied problems surrounding the Snowbird Zone would never have been unearthed without mapping by the Geological Survey of Canada led by Simon Hanmer. The early work by Mike and Simon laid much of the solid foundation on which this thesis was built. This project could never have been completed without three incredible women who assisted me in the field for many buggy weeks on end: Jessie Scott, Annie Crawford, and Julie Herrick. I owe a world of gratitude for their patience and good company during the long and sometimes stressful field seasons. In addition, I would like to thank the many folks in Stony Rapids who helped make the field logistics much easier: Ron and Al at the float plane base, the numerous bush pilots over the years that flew us safely from camp to camp, our expeditor Scott, and the folks at the Whitewater Inn.

I was grateful to interact with the department at UMass during the course of this research. Thanks to Mike Jercinovic for use of the electron microprobe lab. Field work and help with logistical support with Chris Kopf and Lori Krikorian is appreciated. I benefited from productive interactions in both the field and lab with Kevin Mahan and, more recently, the Perplex expertise of Philippe Goncalves.

The TIMS lab, known affectionately as “Sam’s Lab” is the center point of the 11th floor and there are many people that I have interacted with over the years that deserve much thanks. I learned the ropes of the lab from Kathy Keefe and Mark Martin. I am grateful to have shared time with

many people in the lab over the years: Kalsoum Abassi, Valerie Chavagnac, Greg Hoke, Aaron Reiter, Mark Schmitz, Michael Stewart, and Greg Weiss. The current group of staff, postdocs, and grad students has provided a supportive network, both scientifically and socially. Thanks go to Dan Condon, Jim Crowley, Frank Dudas, Becky Flowers, Jenny Matzel, Bill Olszweski, Jahan Ramezani, and Blair Schoene. Many thanks go to Pat Walsh who navigates the administrative hurdles with ease and provides a fresh perspective on things day to day. Neel Chatterjee's expertise and training on the microprobe is also greatly appreciated.

I am grateful for the supportive network of graduate students within EAPS and thankful for the many wonderful friendships I have formed during my time here. Firstly, life would not have been nearly so bearable during the pre-generals crunch and beyond had it not been for my fellow students who started in the G&G program in 1997: Sinan Akciz, Simon Brocklehurst, Marin Clark, Lindy Elkins Tanton, and Karen Viskupic. I truly feel honored to be associated with this group and am looking forward to where the future takes us all. I am particularly grateful to have shared an office with Anke Friedrich during my first year, and who helped show me the ropes of grad school. My long-time officemates in the "pink streamer" office on the 11th floor, Jenny Matzel and Karen Viskupic provided an incredibly supportive environment that I will certainly miss. The greatest strength of MIT is the cohesive graduate student population, and I am grateful to have overlapped with so many other wonderful individuals during my time here: Bridget Bergquist, Jeremy Boyce, Ben Crosby, Amy Draut, Shichuan Huang, Jose Hurtado, Joel Johnson, Eric Kirby, Greg Lawson, Danny MacPhee, Kirsten Nicolaysen, Steve Parman, Kate Ruhl, Lindsay Schoenbohm, Steven Singletary, Noah Snyder, Chris Studnicki-Gizbert, Jim Van Orman, Cam Wobus, and Arthur White, among many others.

Thanks to the Education Office personnel over the years that have made the administrative paperwork flow smoothly, most recently, Carol Sprague and Vicki McKenna. The staff of Lindgren Library has always been helpful to provide support, Kathy Keefe and Joe Hankins.

Last, but most importantly, I wish to thank my family. My parents, Phil and Norma Hyatt, for instilling in me a sense of curiosity, allowing me the freedom to choose my own path, and for always supporting me even if they didn't have a clue what I was doing or why I was doing it. My in-laws, Fred and Margie Baldwin, for always providing much needed rest and relaxation during the holidays. Hop and Georgie Powers for many wonderful Thanksgivings in Oswego. And finally, my husband Aaron, whose enduring love and support throughout this crazy roller-coaster ride, and reminder of the importance of "life outside of school" allowed me to keep a balance between work and home that is so important. I am grateful for his continued support and encouragement in future endeavors and I look forward to what the future holds for us. Thank you everyone!

Julie Baldwin
August 8, 2003

Table of Contents

Abstract	3
Acknowledgements	4
Table of Contents	6
Chapter 1. Introduction	11
Chapter 2. Petrological and geochronological constraints on high pressure, high temperature metamorphism in the Snowbird tectonic zone, Canada	19
Abstract	20
1. Introduction	20
2. Geological Background	21
3. The Upper Deck	22
4. Petrology and Phase Relationships	23
4.1 <i>Textural observations and reaction histories</i>	23
4.1.1 <i>Mafic granulite</i>	23
4.1.2 <i>Godfrey granite</i>	25
5. Mineral Compositions and Thermobarometry	26
5.1 <i>Mafic granulite</i>	26
5.1.1 <i>Mineral Compositions</i>	26
5.1.2 <i>Thermobarometry</i>	27
5.2 <i>Godfrey Granite</i>	28
5.2.1 <i>Mineral Compositions</i>	28
5.2.2 <i>Thermobarometry</i>	28
6. U-Pb Geochronology	29
6.1 <i>Mafic granulite</i>	29
6.1.1 <i>SZ00-118C, coronitic mafic granulite</i>	29
6.1.2 <i>SZ00-148A, mafic granulite with coronitic (decompression textures)</i>	29
6.1.3 <i>SZ00-141A, mafic granulite</i>	31
6.2 <i>Godfrey granite</i>	32
6.2.1 <i>SZ00-125A</i>	32
6.2.2 <i>SZ00-118E</i>	32
7. Discussion	33
7.1 <i>P-T history of the upper deck and Godfrey granite</i>	33
7.2 <i>Timing of high P-T metamorphism and juxtaposition of the upper and lower decks</i>	34
7.3 <i>Previous geochronological constraints and summary of preferred model</i>	34
8. Conclusions	35

Acknowledgements	36
References	36
Appendix 1	38
Appendix 2	42

Chapter 3. Eclogites of the Snowbird tectonic zone: evidence for Paleoproterozoic high-pressure metamorphism in the western Canadian Shield

pressure metamorphism in the western Canadian Shield	45
Abstract	46
1. Introduction	47
2. Geological Setting	49
3. Whole Rock Geochemistry	51
4. Petrography and Mineral Chemistry	51
4.1 Garnet	52
4.2 Clinopyroxene	53
4.3 Kyanite	53
4.4 Plagioclase	54
4.5 Pargasitic amphibole	54
4.6 Minor Phases	54
5. Geothermobarometry	54
5.1 Peak conditions	55
5.2 Decompression Path	56
6. U-Pb Geochronology	57
6.1 Dating eclogite facies metamorphism	57
6.2 Analytical techniques	60
6.3 U-Pb Results	61
7. Discussion	64
8. Conclusions	68
Acknowledgements	68
References	69
Figure Captions	75
Figures	78
Tables	88

Chapter 4. Decompressional reaction textures in sapphirine granulites from the Snowbird tectonic zone, Canada

tectonic zone, Canada	97
Abstract	98
1. Introduction	99
2. Geological Setting	100
3. Outcrop Description	103
4. Petrology and Mineral Chemistry	103

4.1 Quartz-bearing sapphirine granulites	104
4.2 Quartz-absent sapphirine-bearing vein granulites	105
4.3 Sapphirine Chemistry	106
5. Textures and Reaction History	107
5.1 Textures	107
5.2 Reactions in the garnet-sapphirine-quartz granulite	107
5.3 Symplectite-forming reactions in the veins	108
6. Thermobarometry	109
7. Petrologic Modeling	110
8. Discussion and Conclusions	112
References	114
Figure Captions	117
Figures	121
Tables	135

Chapter 5. High-pressure metamorphism of lower crustal felsic granulites, Snowbird tectonic zone, northern Saskatchewan, Canada: Implications for the U-Pb systematics of monazite

of monazite	139
Abstract	140
1. Introduction	141
2. Regional Geologic Setting	144
3. The Southern Domain	145
4. The Snowbird Felsic High-Pressure Granulites	146
4.1 Petrology of the “White” Gneiss	146
4.2 Petrographic description of 01SZ90	148
4.3 Evidence for Partial Melting of a Pelitic Protolith?	149
5. Geochemistry of the Felsic Gneiss	150
6. Electron Microprobe Characterization and Dating of Monazite	151
6.1 Mapping and Characterization of Monazite in Thin Section	151
6.2 Electron Microprobe Results	153
7. U-Pb IDTIMS Geochronology	155
7.1 ID-TIMS monazite data from thin sections	155
7.2 Summary of comparison between EPMA and ID-TIMS data	157
7.3 Imaged monazite grains in epoxy mounts	158
7.4 Zircon data from 01SZ90	159
8. Sm-Nd isotope systematics	160
9. Discussion	161
9.1 Nature of felsic gneiss protolith	161
9.2 Significance of U-Pb geochronological dates	162

9.3 Implications for behavior of monazite under high-grade metamorphic and anatectic conditions	165
9.4 Implications of geochemical data for melt sources and processes	167
10. Conclusions	168
Acknowledgements	169
Appendix A: Analytical Techniques	169
References	170
Figure Captions	175
Figures	179
Tables	194

Chapter 6. Synthesis of Thesis Findings and New Directions: Regional U-Pb

<i>geochronological constraints on the metamorphism and juxtaposition of crustal blocks across the East Athabasca mylonite triangle, northern Saskatchewan, Canada</i>	203
1. Introduction	204
2. The debate surrounding the STZ	204
3. Summary of Thesis Findings	206
2.1 Nature of the Southern Domain – Northwestern Domain Boundary	206
2.2 First record of eclogite facies metamorphism in the STZ	207
2.3 Decompression P-T path of the eclogite and sapphirine granulites	208
2.4 Metamorphic evolution of the high-pressure felsic granulite.....	208
4. Regional U-Pb geochronological constraints from the EAmT	209
3.1 Northwestern Domain (Bohica mafic complex).....	209
3.2 Southeastern Domain (Chipman dikes and tonalite)	209
3.3 Southern Domain (High-pressure granulites)	210
3.4 Summary of regional geochronological data	211
5. Tectonic model for the Snowbird tectonic zone	213
6. Future Work	214
7. Concluding Statement	215
References.....	216
Figure Captions	217
Figures	219
Tables	227

Chapter 1

Introduction

High-pressure (HP) granulites are exposed in both young and old metamorphic terranes (e.g., Namche Barwa, Eastern Himalaya, 45 Ma; European Variscides, 400-340 Ma; Hengshan, China, 1.8 Ga). Documented metamorphic pressures in these terranes typically exceed 1.4 GPa, at temperatures above 800°C (O'Brien & Rötzler, 2003), implying that the lower levels of thickened crust, or crust undergoing subduction, can be subjected to particularly high thermal regimes. Additionally, HP granulites are sometimes associated with eclogites (e.g., Indares, 1993; Indares & Dunning, 1997; Möller, 1998). Understanding the P - T evolution of HP granulites in these metamorphic terranes, and their relationship to eclogites, can provide important constraints on the thermal evolution of the lower crust involved in crustal thickening or continental subduction processes.

High-pressure granulites are characterized by the key mineral associations of garnet-clinopyroxene-plagioclase-quartz in mafic rocks, and kyanite-K-feldspar in metapelites and felsic rocks. HP granulites are a sub-facies of the granulite field that lies above the 'garnet-in' reaction in quartz tholeiite (for basic compositions) (Green & Ringwood, 1967). The upper pressure limit of the HP mafic granulite assemblage is marked by the disappearance of plagioclase that gives rise to garnet-omphacite assemblages, characteristic of eclogites (Carswell, 1990). The occurrence of HP granulites in association with eclogites can be controlled by a variety of factors, including equilibration at different P - T conditions along a P - T path, or distinct P - T evolution for the different rock types. However, this delineation between HP granulite and eclogite facies can also be controlled by bulk composition, rather than P - T conditions, in that the upper P - T limit of plagioclase stability field depends on the Al content of the original gabbro (Green & Ringwood, 1967; Green & Ringwood, 1972). This limit coincides with the granulite-eclogite transition only for quartz-tholeiite compositions, whereas

CHAPTER 1 - INTRODUCTION

plagioclase in high-Al bulk compositions persists at pressures well within the eclogite facies. Thus the spatial association of HP granulites and eclogites need not reflect variation in peak P - T conditions or the metamorphic evolution, and importantly, implies that many of these occurrences reflect regional high- T eclogite facies conditions.

Rocks of pelitic bulk compositions, although less common, are also found in many regional HP granulite terranes. At these P - T conditions, pelitic granulites should be kyanite- and K-feldspar-bearing, and at high temperatures, show evidence for dehydration melting of biotite (Vielzeuf & Montel, 1994). Ternary feldspar homogenization thermometry of HP hypersolvus ternary feldspars in felsic granulites is generally considered the most robust method of deducing temperature conditions for these granulites (Kröner et al., 2000; O'Brien & Rötzler, 2003; Rötzler & Romer, 2001; Snoeyenbos et al., 1995). Consistent ultrahigh temperatures of over 1000°C have been deduced by this method, which, in conjunction with the coexistence of kyanite, requires pressures of at least 1.5 GPa. This important observation shows that ultrahigh-temperature (UHT) granulites are not just restricted to rocks formed at normal crustal pressures, but can also occur in overthickened crust or subducted continental crust.

The Snowbird tectonic zone (STZ) is a ~2800-km-long linear feature in the horizontal gravity gradient map of the western Canadian Shield that separates the Archean Rae and Hearne Domains (Goodacre et al., 1987). Authors have long speculated on the tectonic significance of the STZ. Some have argued that the STZ represents a Paleoproterozoic suture (Hoffman, 1988), whereas others argue that the structure is fundamentally an Archean intracratonic shear zone with only local Paleoproterozoic reactivation (Hanmer et al., 1994; Hanmer et al., 1995a; Hanmer et al., 1995b). This thesis attempts to resolve some of these outstanding questions related to the tectonic significance of the STZ through a focused petrological, geochronological, and geochemical study of high-pressure granulites and eclogites that occur within a segment of the STZ.

The Striding-Athabasca (S-A) mylonite zone, northern Saskatchewan, Canada, is host to a spectacular suite of HP granulites and eclogites. The S-A mylonite zone is a ~400-km-long segment of the STZ. This well-exposed 125 x 80 x 75 km southwestern segment of the S-A mylonite zone has been described as the East Athabasca mylonite

CHAPTER 1 - INTRODUCTION

triangle (EAmt), and consists of anastomosing lower crustal granulite facies mylonites (Hanmer, 1994; Hanmer, 1997; Hanmer et al., 1994; Hanmer et al., 1995a; Hanmer et al., 1995b). The EAmt has been interpreted as an Archean intra-continental strike-slip shear zone (Hanmer, 1994; Hanmer, 1997; Hanmer et al., 1994; Hanmer et al., 1995a; Hanmer et al., 1995b). The work contained in this thesis has focused on the highest-pressure rocks exposed within the Southern Domain of the EAmt. Consisting of rocks that have been metamorphosed at pressures of >1.5 GPa and temperatures of 900-1000°C (Baldwin et al., 2003; Snoeyenbos et al., 1995), the Southern Domain provides a unique natural laboratory for understanding the thermal evolution of the lower crust during extreme metamorphic conditions.

The primary motivation behind this thesis research was to obtain a more complete understanding of these unusual rocks, within both a metamorphic and a temporal framework. This research aims at obtaining a better understanding of the evolution of the high-pressure granulites of the EAmt from their formation to their ultimate exhumation through an integrated petrological and geochronological study. Previous studies of these types of rocks tended to focus primarily on the petrology and P - T paths, and largely neglected the timescales of metamorphism, residence in the lower crust, and exhumation. This study attempts to quantify these processes and obtain a better understanding of the behavior and growth of accessory phases under extreme metamorphic conditions.

This dissertation consists of four chapters that have been written for publication in international geologic journals. Chapter 2, published in the *Journal of Metamorphic Geology*, describes the nature of the boundary between the structurally lowest levels of the Southern Domain and the charnockitic granulites to the north. Well-preserved corona textures in the mafic granulite of the Southern Domain record a near-isothermal decompression path from maximum pressures of 1.9 GPa to 1.0 GPa. Zircon in the mafic granulites records two metamorphic events, at 2.55-2.52 Ga and 1.9 Ga. This study provides the first evidence for Paleoproterozoic high-pressure metamorphism within the EAmt.

Chapter 3, submitted to *Contributions to Mineralogy and Petrology*, describes the petrology of the eclogites of the EAmt. This eclogite unit is remarkable in its structural preservation as a thin, 15-m-thick layer contained within a host felsic gneiss that occurs

CHAPTER 1 - INTRODUCTION

along strike for over 10 km. This study documents the occurrence of the eclogite through a detailed study of its geochemistry and mineral chemistry. The eclogite was derived from a plagioclase-bearing gabbroic protolith, and experienced peak metamorphic conditions of 1.8-2.0 GPa at 920-1000°C. Reaction textures in the eclogite record near-isothermal decompression to similar conditions recorded in the mafic granulite of ~1.0 GPa, 800°C. U-Pb geochronology of zircon from the eclogite records high-pressure metamorphism at 1.9 Ga. Thus this study provides the best evidence so far for an important Paleoproterozoic high-P event in the STZ.

Chapter 4, prepared for submission to the *Journal of Petrology*, is a focused study of the reaction textures preserved in sapphirine granulites associated with the decompressed kyanite eclogites. The results of this petrological study suggest that these rocks re-equilibrated at mid-crustal depths following the high-*PT* metamorphism. Spectacular reaction textures are preserved in these rocks that allow for detailed petrological modeling and construction of petrogenetic grids that are applicable to a variety of sapphirine assemblages in decompressed kyanite eclogites in the literature.

Chapter 5, prepared for submission to *Contributions to Mineralogy and Petrology*, is a petrological, geochronological, and geochemical study of the most abundant lithology in the Southern Domain, the felsic HP granulites. This chapter presents important evidence for an Archean (2.6 Ga) metamorphic history. This study presents detailed investigations of monazite from the felsic gneiss using combined electron microprobe and ID-TIMS methods, and reveals that monazite records a complex growth history from 2.6 to 1.9 Ga. This study shows how the petrographic setting of monazite affects its ability to participate in later metamorphic reactions and also shows how the geochemistry of the individual grains vary depending on the petrographic setting as inclusions in garnet or as matrix grains. Additionally, this chapter presents important Sm-Nd geochemical data that bears on the isotopic source region during the formation of monazite at different times. Petrological observations imply that the felsic gneiss is interpreted to largely be a product of dehydration melting in the lower crust, but the precise timing and nature of the 2.6 versus 1.9 Ga history of this rock remains somewhat elusive. Nevertheless, an important conclusion of this study is the empirical verification of the high closure temperature for Pb diffusion in monazite. This study provides

CHAPTER 1 - INTRODUCTION

evidence that despite temperatures as great as 1000°C, monazite that is well-armored in garnet does not show any evidence for diffusional Pb loss.

The final chapter of this dissertation, Chapter 6, summarizes the main conclusions drawn from this research, and also presents additional regional geochronological data that bears on the regional implications of this study. U-Pb geochronological data from each of the three distinct lithotectonic domains of the EAmt are presented. These data highlight the differences in metamorphic histories from each domain. The Northwestern Domain, consisting largely of 2.6 Ga meta-igneous rocks, shows little evidence for any Paleoproterozoic metamorphism recorded in accessory phase growth. In contrast, the Southeastern Domain, experienced an important magmatic and metamorphic event at 1890-1895 Ma as manifested by the Chipman mafic dike swarm. This mafic dike swarm was previously thought to be Archean in age (Williams et al., 1995), and the presence of voluminous mafic magmatism in close temporal association with the HP metamorphism in the Southern Domain raises intriguing questions. Finally, this chapter presents additional data from three lithologies of the Southern Domain: the felsic gneiss, mafic granulite, and sapphirine granulite. These data are meant to complement the detailed data set for one sample presented in Chapter 5. These samples record similar metamorphic histories from 2.6 to 1.9 Ga. In addition, rutile data from the felsic gneiss bear evidence for protracted exhumation from ~1.9-1.8 Ga.

The Snowbird tectonic zone provides a unique area in which to understand the metamorphic evolution of high-pressure granulites from both a petrological and temporal perspective. This study offers a view of the structural and tectonic context that is generally not possible in xenolith studies. This field-based study provides an important and necessary structural context, without which would make the interpretation of the complex thermochronologic data impossible. Thus, the work contained in this study highlights the complexities of the lower crust from both a metamorphic and geochronological perspective.

References

- Baldwin, J. A., Bowring, S. A. & Williams, M. L., 2003. Petrological and geochronological constraints on high pressure, high temperature metamorphism in the Snowbird tectonic zone, Canada. *Journal of Metamorphic Geology*, **21**, 81-98.
- Carswell, D. A., 1990. Eclogites and the eclogite facies: definitions and classification. In: *Eclogite Facies Rocks* (ed Carswell, D. A.), pp. 1-13, Chapman and Hall, New York.
- Goodacre, A. K., Grieve, R. A. F., Halpenny, J. F. & Sharpton, V. L., 1987. Horizontal gradient of the Bouguer gravity anomaly map of Canada, Canadian Geophysical Atlas, Map 5, Geological Survey of Canada, Ottawa.
- Green, D. H. & Ringwood, A. E., 1967. An experimental investigation of the gabbro to eclogite transformation and its petrological applications. *Geochimica et Cosmochimica Acta*, **31**, 767-833.
- Green, D. H. & Ringwood, A. E., 1972. A comparison of recent experimental data on the gabbro-garnet granulite-eclogite transition. *Journal of Geology*, **80**, 277-288.
- Hanmer, S., 1994. Geology, East Athabasca mylonite triangle, Saskatchewan. In: *Geological Survey of Canada Map 1859A*.
- Hanmer, S., 1997. Geology of the Striding-Athabasca mylonite zone, northern Saskatchewan and southeastern District of Mackenzie, Northwest Territories. *Geological Survey of Canada Bulletin*, **501**, 1-92.
- Hanmer, S., Parrish, R., Williams, M. & Kopf, C., 1994. Striding-Athabasca mylonite zone: Complex Archean deep-crustal deformation in the East Athabasca mylonite triangle, northern Saskatchewan. *Canadian Journal of Earth Sciences*, **31**, 1287-1300.
- Hanmer, S., Williams, M. & Kopf, C., 1995a. Modest movements, spectacular fabrics in an intracontinental deep-crustal strike-slip fault: Striding-Athabasca mylonite zone, NW Canadian Shield. *Journal of Structural Geology*, **17**(4), 493-507.
- Hanmer, S., Williams, M. & Kopf, C., 1995b. Striding-Athabasca mylonite zone: implications for the Archean and Early Proterozoic tectonics of the western Canadian Shield. *Canadian Journal of Earth Sciences*, **32**, 178-196.
- Hoffman, P. F., 1988. United Plates of America, the birth of a craton: Early Proterozoic assembly and the growth of Laurentia. *Annual Reviews of Earth and Planetary Science Letters*, **16**, 543-603.
- Indares, A., 1993. Eclogitized gabbros from the eastern Grenville Province; textures, metamorphic context, and implications. *Canadian Journal of Earth Sciences*, **30**(1), 159-173.
- Indares, A. & Dunning, G. R., 1997. Coronitic metagabbro and eclogite from the Grenville Province of western Quebec; interpretation of U-Pb geochronology and metamorphism. *Canadian Journal of Earth Sciences*, **34**(7), 891-901.
- Kröner, A., O'Brien, P. J., Nemchin, A. A. & Pidgeon, R. T., 2000. Zircon ages for high pressure granulites from South Bohemia, Czech Republic, and their connection to Carboniferous high temperature processes. *Contributions to Mineralogy and Petrology*, **138**(2), 127-142.
- Möller, C., 1998. Decompressed eclogites in the Sveconorwegian (-Grenvillian) orogen of SW Sweden: petrology and tectonic implications. *Journal of Metamorphic Geology*, **16**, 641-656.

CHAPTER 1 - INTRODUCTION

- O'Brien, P. J. & Rötzler, J., 2003. High-pressure granulites: formation, recovery of peak conditions and implications for tectonics. *Journal of Metamorphic Geology*, **21**, 3-20.
- Rötzler, J. & Romer, R. L., 2001. P-T-t evolution of ultrahigh-temperature granulites from the Saxon Granulite Massif, Germany. Part I: Petrology. *Journal of Petrology*, **42**, 1995-2013.
- Snoeyenbos, D. R., Williams, M. L. & Hanmer, S., 1995. Archean high-pressure metamorphism in the western Canadian Shield. *European Journal of Mineralogy*, **7**, 1251-1272.
- Vielzeuf, D. & Montel, J. M., 1994. Partial melting of metagreywackes. Part I. Fluid-absent experiments and phase relationships. *Contributions to Mineralogy and Petrology*, **117**, 375-393.
- Williams, M. L., Hanmer, S., Kopf, C. & Darrach, M., 1995. Syntectonic generation and segregation of tonalitic melts from amphibolite dikes in the lower crust, Striding-Athabasca mylonite zone, northern Saskatchewan. *Journal of Geophysical Research*, **100**(B8), 15717-15734.

Chapter 2

Petrological and geochronological constraints on high pressure, high temperature metamorphism in the Snowbird tectonic zone, Canada

Published in the Journal of Metamorphic Geology, January 2003

Baldwin, J.A., Bowring, S.A., and Williams, M.L., 2003, Journal of Metamorphic Geology, v. 21, n. 1, 81-98.

Reprinted with permission from Blackwell Science, Inc.

Petrological and geochronological constraints on high pressure, high temperature metamorphism in the Snowbird tectonic zone, Canada

J. A. BALDWIN,¹ S. A. BOWRING¹ AND M. L. WILLIAMS²

¹*Department of Earth, Atmospheric and Planetary Sciences, Massachusetts Institute of Technology, Cambridge, MA 02139, USA (jbaldwin@mit.edu)*

²*Department of Geosciences, University of Massachusetts, Amherst, MA 01003, USA*

ABSTRACT The upper deck of the East Athabasca mylonite triangle (EAMt), northern Saskatchewan, Canada, contains mafic granulites that have undergone high P – T metamorphism at conditions ranging from 1.3 to 1.9 GPa, 890–960 °C. Coronitic textures in these mafic granulites indicate a near-isothermal decompression path to 0.9 GPa, 800 °C. The Godfrey granite occurs to the north adjacent to the upper deck high P – T domain. Well-preserved corona textures in the Godfrey granite constrain igneous crystallization and early metamorphism in the intermediate-pressure granulite field (Opx + Pl) at 1.0 GPa, 775 °C followed by metamorphism in the high pressure granulite field (Grt + Cpx + Pl) at 1.2 GPa, 860 °C. U–Pb geochronology of zircon in upper deck mafic granulite yields evidence for events at both *c.* 2.5 Ga and *c.* 1.9 Ga. The oldest zircon dates are interpreted to constrain a minimum age for crystallization or early metamorphism of the protolith. A population of 1.9 Ga zircon in one mafic granulite is interpreted to constrain the timing of high P – T metamorphism. Titanite from the mafic granulites yields dates ranging from 1900 to 1894 Ma, and is interpreted to have grown along the decompression path, but still above its closure temperature, indicating cooling following the high P – T metamorphism from *c.* 960–650 °C in 4–10 Myr. Zircon dates from the Godfrey granite indicate a minimum crystallization age of 2.61 Ga, without any evidence for 1.9 Ga overgrowths. The data indicate that an early granulite facies event occurred at *c.* 2.55–2.52 Ga in the lower crust (*c.* 1.0 GPa), but at 1.9 Ga the upper deck underwent high P – T metamorphism, then decompressed to 0.9–1.0 GPa. Juxtaposition of the upper deck and Godfrey granite would have occurred after or been related to this decompression. In this model, the high P – T rocks are exhumed quickly following the high pressure metamorphism. This type of metamorphism is typically associated with collisional orogenesis, which has important implications for the Snowbird tectonic zone as a fundamental boundary in the Canadian Shield.

Key words: geochronology; granulites; high pressure metamorphism; petrology; Saskatchewan.

INTRODUCTION

The discovery of granulites in metamorphic terranes that have experienced very high pressures (> 1.5 GPa), and in some cases also very high temperatures (> 900–1000 °C), has led to a significant expansion in the P – T limits of crustal petrology. High pressure granulites have been recognized in at least two distinct tectonic settings: those that formed in overthickened crust in collisional orogens and those that evolved near the base of a normal thickness continental crust and were exhumed by a mechanism unrelated to their formation. High pressure granulites in collisional orogens include the Variscides (e.g. Vielzeuf & Pin, 1989; Carswell & O'Brien, 1993; O'Brien & Carswell, 1993), the Grenville Province (e.g. Indares, 1995; Indares *et al.*, 1998; Indares & Dunning, 2001), the eastern Himalayas (e.g. Liu & Zhong, 1997), and the Hengshan Complex of the North China Craton (e.g. Zhao *et al.*, 2001). In each

case, these rocks were metamorphosed at high pressures and exhumed relatively quickly (on the order of tens of millions of years) following the peak metamorphic event (Indares & Dunning, 1997; Kröner *et al.*, 2000). In contrast, high pressure granulites that formed near the base of a 'normal' thickness (*c.* 30–35 km) continental crust generally record a thermal perturbation at the base of the crust followed by isobaric cooling towards a cratonic geotherm. These rocks are thought to record the long-term evolution of the lower crust. Examples of such rocks may include the Ivrea Zone (Zingg, 1990; Handy & Zingg, 1991), the Kapuskasing uplift (Percival & Card, 1983; Percival & McGrath, 1986; Percival & West, 1994).

The Snowbird tectonic zone in northern Saskatchewan is exposed in the East Athabasca mylonite triangle (EAMt) (Fig. 1). The EAMt is a *c.* 3000 km² terrane of Archean rocks that have undergone metamorphism at minimum P – T conditions of 1.0 GPa, 800 °C

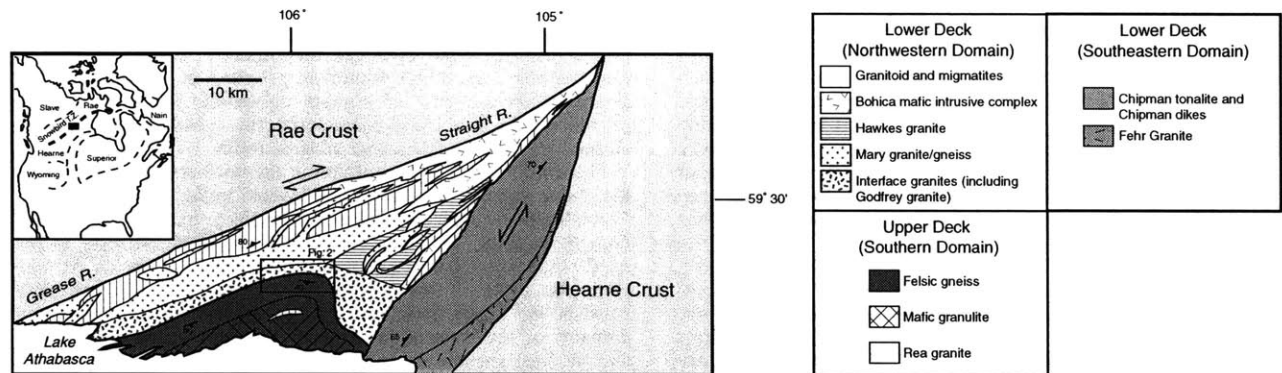


Fig. 1. Geological and structural elements of the East Athabasca mylonite triangle (EAMt), northern Saskatchewan (modified after Hanmer, 1994). Explanations for the three main structural subdomains are shown separately. Inset shows location of EAMt along the Snowbird tectonic zone (Hoffman, 1988).

(Williams *et al.*, 1995; Williams *et al.*, 2000). Embedded within this terrane is a *c.* 400 km² litho-tectonic domain termed the 'upper deck' (Hanmer, 1994). This high grade terrane consists of granulite facies mylonites, which have been metamorphosed at conditions exceeding 1.5 GPa and 900–1000 °C (Snoeyenbos *et al.*, 1995). The upper deck was noted as being unusual compared to other high pressure terranes in both its setting within a much larger granulite terrane as well as by its apparent intracratonic tectonic setting (Snoeyenbos *et al.*, 1995). In addition, the high temperature metamorphism (900–1000 °C) is relatively unusual in association with such high pressure rocks. In order to understand the setting and history of these granulites within the Snowbird tectonic zone, it is critical to constrain the timing of high pressure metamorphism and the specific relationship between these high pressure granulites and other gneisses of the EAMt.

Although the occurrence of high *P–T* metamorphism in the upper deck of the EAMt is well-established (Snoeyenbos *et al.*, 1995), the timing of this metamorphism has been uncertain. It was proposed that the high *P–T* metamorphism occurred at >2.6 Ga (Snoeyenbos *et al.*, 1995), and that these rocks resided in the lower crust for *c.* 700 Myr prior to exhumation. However, evidence is mounting for an important 1.9 Ga metamorphic event in this segment of the Snowbird tectonic zone, and identification of the *P–T* conditions and nature of this event have important implications for the tectonic evolution of the Canadian Shield. Accordingly, the specific goals of this study are: (1) to describe the distribution and extent of high *P–T* metamorphism in the upper deck; (2) to place *P–T* constraints on metamorphism across the boundary between these high pressure rocks and the granulites to the north; and (3) to place constraints on the timing of high *P–T* metamorphism and juxtaposition of the upper deck with the other domains of the EAMt (Fig. 1). Our broader goal is to use the nature of the contact

between the upper deck and granulites to the north, as well as the differences in crustal level exposed across this tectonic boundary to gain insight into the larger scale behaviour and evolution of the lower crust in this region.

GEOLOGICAL BACKGROUND

The western Canadian Shield is a collage of Archean crustal provinces bounded by anastomosing Palaeoproterozoic orogenic belts (Hoffman, 1988). The boundary between the Rae and Hearne domains of the western Churchill Province, the Snowbird tectonic zone, coincides with a 3000 km-long gravity anomaly, which extends from the Canadian Cordillera northeast to Hudson Bay (Fig. 1) (Goodacre *et al.*, 1987; Hoffman, 1988). In northern Saskatchewan, a well-exposed 125 × 80 × 75 km segment of the Snowbird tectonic zone has been described as the East Athabasca mylonite triangle (EAMt), and consists of anastomosing lower crustal granulite facies mylonites (Hanmer, 1994, 1997; Hanmer *et al.*, 1994, 1995a,b). The EAMt is the south-western segment of the Striding-Athabasca mylonite zone that has been interpreted as an Archean intracontinental strike-slip shear zone (Hanmer, 1994; Hanmer *et al.*, 1994, 1995a,b).

The EAMt is bounded to the northwest and southeast by wallrocks of the Rae and Hearne provinces, respectively, and is overlain to the south by the *c.* 1.7 Ga Athabasca sandstone. Although both the Rae and Hearne wallrocks adjacent to the EAMt are lithologically similar, consisting dominantly of pelitic schist, paragneiss, amphibolite and granitoid rocks, their overall metamorphic grade is different. Recent work in the Neil Bay area about 40 km west of the EAMt (Kopf, 1999) suggests that much of the Rae Province in this area experienced intermediate-*P* granulite facies conditions (*c.* 0.8 GPa, 900 °C) at *c.* 1.9 Ga. In contrast, the Hearne Province wallrocks are separated from the EAMt by a major amphibolite facies shear zone and record lower pressure amphibolite facies metamorphic conditions (0.5 GPa, 600–700 °C) (Mahan *et al.*, 2001). Recent work in the northern Hearne Province by Stern & Berman (2001) has identified a Palaeoproterozoic high pressure (> 1.0 GPa) corridor in the northern segment of the Snowbird tectonic zone, which includes the Kramanitar Complex (1.5–1.2 GPa, 850–900 °C) (Sanborn-Barrie *et al.*, 2001) as well as the Uvauk Complex (1.3–1.1 GPa, 800–875 °C). Stern & Berman (2001) interpreted this high *P* metamorphism to overprint an earlier *c.* 2.5 Ga metamorphism at 0.4–0.6 GPa and *c.* 625–700 °C.

The EAMt is divided into three structural domains (Fig. 1). The southern domain of the EAMt, termed the upper deck, consists of garnet-kyanite quartzofeldspathic gneiss, mafic two-pyroxene garnet granulite, and a semicontinuous 10–15 m-thick layer of eclogitic

garnet clinopyroxenite with associated sapphirine granulites. The northwestern domain is dominated by felsic to mafic plutonic rocks, the largest of which is the 2.6 Ga Mary granite (Fig. 1). Williams *et al.* (2000) proposed that the Mary granite was emplaced and then metamorphosed at 1.0 GPa during dextral shearing. The southeastern domain is dominated by the *c.* 3.2 Ga Chipman tonalite batholith which is intruded by the 1.9 Ga Chipman mafic dyke swarm (Williams *et al.*, 1995; Baldwin *et al.*, 2000). The Chipman dyke swarm consists of 1–100 m thick mafic dykes that were metamorphosed and partially melted at granulite facies conditions (Williams *et al.*, 1995).

The northwestern and southeastern domains are collectively referred to as the 'lower deck', in recognition of their relationship to the structurally overlying mylonites of the upper deck (Hanmer, 1994; Hanmer *et al.*, 1995; Hanmer *et al.*, 1994). Calculated pressures for both the NW and SE domains of the lower deck are approximately 1.0 GPa (Williams *et al.*, 1995, 2000). In contrast, the northern part of the upper deck records minimum pressures of 1.5 GPa, translating into a 10–15 km difference in crustal level across this boundary. The differences in peak metamorphic conditions between the upper and lower decks are interpreted to indicate that these two terranes had different metamorphic histories prior to their juxtaposition (Snoeyenbos *et al.*, 1995).

As described by Hanmer (1994), the boundary between the upper deck and lower deck is a several-km-wide zone. It consists of a suite of granitic gneisses that vary in metamorphic grade from amphibolite to granulite facies. These rocks have been termed the 'interface granites' and are generally characterized by a relatively low strain state compared to the associated mylonites (Hanmer, 1994, 1997; Hanmer *et al.*, 1995a,b). The focus of this report is on the region between the base of the upper deck domain and one of these 'interface' granitic gneisses, the Godfrey granite (Fig. 2).

THE UPPER DECK

Within the upper deck there are three dominant lithological units: felsic gneiss, eclogitic garnet clinopyroxenite and mafic granulite (Fig. 1). The structurally higher levels in the southern upper deck are dominated by mafic granulite, whereas the lower structural levels to the north are dominated by felsic gneiss. The most abundant lithology in the northern upper deck is a massive garnet-kyanite quartzofeldspathic gneiss. This felsic gneiss is an anhydrous mylonitic rock (Grt + Pl + Qtz ± Ky + Rt) with a shallow SW-plunging lineation. Garnet is ubiquitous throughout the felsic gneiss, and typically comprises 5–40% of the rock. Kyanite-bearing assemblages are locally preserved; kyanite occurs as inclusions in garnet and as a matrix phase wrapping around garnet. Kyanite-bearing assemblages are particularly well-preserved in the *c.* 5 km thick zone between Axis Lake and Currie Lake (Fig. 2). Peak metamorphic conditions for the felsic gneiss have been calculated at 900–1000 °C and > 1.5 GPa (Snoeyenbos *et al.*, 1995).

A distinctive and important lithological unit for constraining the *P-T* history of the northern upper deck, is a thin 10–15 m-thick band

of eclogitic garnet clinopyroxenite and associated sapphirine granulites which have been mapped along strike for *c.* 15 km (Fig. 2). Garnet-clinopyroxene exchange thermometry yields 950–1000 °C (Snoeyenbos *et al.*, 1995). Minimum pressures of 1.5 GPa are suggested by the presence of primary corundum. Research is being carried out to more fully characterize the petrology and thermochronology of these distinctive eclogitic rocks.

The third major lithological unit in the northern upper deck, and the major focus of this study, is a layered mafic granulite (Fig. 2). These layers are typically several metres thick, but are locally more than 10 m thick. They contain a foliation, dipping steeply to the south, that is parallel to foliation in the host felsic gneiss. At map scale, the strike of this foliation is sub-parallel to the boundary between the upper deck and the northwestern and southeastern domains of the lower deck (Fig. 1). Most mafic granulite layers, and the host gneisses, have a strong mineral lineation that plunges shallowly to the southwest. Previous workers have interpreted the mafic granulite layers as a series of intrusive sills with northeast-striking intrusive contacts (Baer, 1969; Slimmon, 1989). However, given the highly deformed nature of these rocks, the original contacts have likely been completely transposed into their present orientation.

In the southern upper deck (Fig. 1), a *c.* 5 km thick exposure of layered mafic granulite is interlayered with very thin cm-scale layers of felsic gneiss. Gabbroic textures are locally preserved in low strain zones but in general the rocks display spectacular coronitic textures. Peak metamorphism and deformation occurred in the high pressure granulite field (garnet + clinopyroxene + quartz; 1.4–1.2 GPa at 750–800 °C) (Kopf, 1999). A transition to intermediate-pressure granulite conditions (orthopyroxene + plagioclase; 0.9 GPa at 700–750 °C) involved a period of near-isothermal decompression, possibly related to the thrust emplacement of the upper deck onto the lower deck (Kopf, 1999). This decompression is inferred to have been followed by isobaric cooling that involved development of garnet-plagioclase-magnetite symplectite textures.

Previous geochronological constraints on the timing of granulite facies metamorphism in the upper deck include zircon dates from mafic granulite of *c.* 2600 Ma. This age is interpreted to constrain the granulite facies metamorphism (Hanmer, 1997). In addition, monazite from a sample of felsic gneiss at the western end of Axis Lake yielded a date of 2629 ± 2 Ma, which has been interpreted to be the minimum age for the high pressure metamorphism and associated granulite facies mylonitization in the upper deck (Hanmer, 1997). The clinopyroxene-bearing leucocratic Rea granite outcrops along the south shore of Axis Lake. Hanmer (1997) observed that although the contact relationships of the Rea granite with the mafic granulite are not exposed, the granite is penetratively mylonitized with a well-developed ribbon fabric. A U-Pb zircon date of $2584 \pm 40/-15$ Ma was interpreted as a crystallization age and therefore a maximum age for the mylonitization of the Rea granite (Hanmer, 1997). These geochronological data led Snoeyenbos *et al.* (1995) to conclude that the minimum age

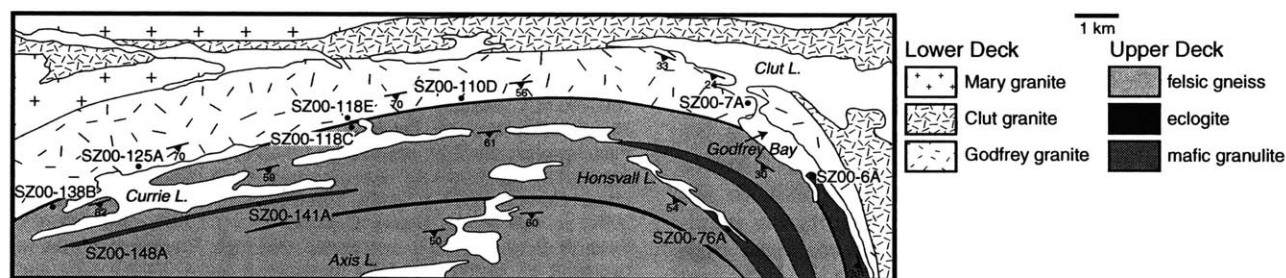


Fig. 2. Detailed geological map of the northern upper deck and Godfrey granite contact region showing lithologies and sample locations used for thermobarometry and U-Pb geochronology. Mappable mafic granulite layers are shown. Other mafic granulite sample localities (SZ00-118C and SZ00-138B) are only a few-m-thick and are shown only as points and not as mappable layers on the map. A thin eclogitic garnet clinopyroxenite layer is shown in black.

for the high P - T metamorphism and juxtaposition of the upper and lower deck was 2.62–2.59 Ga. However, this study presents new petrological and U–Pb geochronological evidence and a model which favours high P - T metamorphism in the upper deck and final juxtaposition of the upper and lower deck domains at c. 1.9 Ga.

PETROLOGY AND PHASE RELATIONSHIPS

Lithologies, textures and mineral compositions are described for both mafic granulite from the northern upper deck and the Godfrey granite (Fig. 2), with an emphasis on assemblages and textures relevant to thermobarometry. In order to evaluate compositional zonation, high resolution compositional maps of these assemblages were collected on the Cameca SX-50 microprobe at the University of Massachusetts.

Textural observations and reaction histories

Mafic granulite

The main assemblage in the mafic granulites of the northern upper deck is $\text{Grt} + \text{Cpx} + \text{Pl} \pm \text{Opx} \pm \text{Qtz}$. Accessory phases include zircon, titanite, rutile and apatite. Ilmenite, magnetite and pyrite are present in some samples. Hornblende occurs as a secondary phase. These rocks are typically fine-grained with a broad range of textures (Fig. 3a–d). Garnet is usually < 1 mm in size but a few layers contain coarser grained (up to 4 mm) garnet. Clinopyroxene occurs both as fine-grained aggregates and as larger porphyroblasts. Larger grains of clinopyroxene (>1 mm) locally exhibit a spongy appearance with exsolution lamellae of Na-rich plagioclase (Fig. 3c). Orthopyroxene is

commonly present, but typically occurs as rims on clinopyroxene grains or as an orthopyroxene-plagioclase symplectite around garnet (Fig. 3d). Pargasitic to ferro-pargasitic hornblende is locally present as rims on clinopyroxene, and likely formed from the breakdown of clinopyroxene.

A several metre thick band of mafic granulite occurs at the base of the northern upper deck and is in contact with the Godfrey granite to the north. Corona textures are particularly well-preserved in this layer (Figs 3a & 4a–c). Relatively large 1–2 mm clinopyroxene and plagioclase grains are dominant. Clinopyroxene shows weak zoning with slightly Mg-richer rims but relatively unzoned cores. Large matrix plagioclase crystals typically preserve small, relict calcic cores but grade outward into more sodic compositions. A second generation of more calcic plagioclase occurs between garnet and clinopyroxene (Fig. 4a,c). Clinopyroxene is rimmed by fine-grained tips of orthopyroxene, which is in turn rimmed by plagioclase (Fig. 4a,b). Garnet is typically < 500 μm , unzoned, and occurs as trains of euhedral grains around the clinopyroxene. Some slight Fe-enrichment at the rims is present in some of the larger garnet crystals. Abundant ilmenite and magnetite typically occur as interstitial phases, and commonly occur at the rims of the clinopyroxene grains.

Reaction textures in these granulites indicate a two-stage metamorphic history. The corona textures in the mafic granulites suggest that these rocks likely crystallized as clinopyroxene-plagioclase rocks and then were subsequently metamorphosed in the high pressure ($\text{Grt} + \text{Cpx} + \text{Pl}$) granulite facies. This metamor-

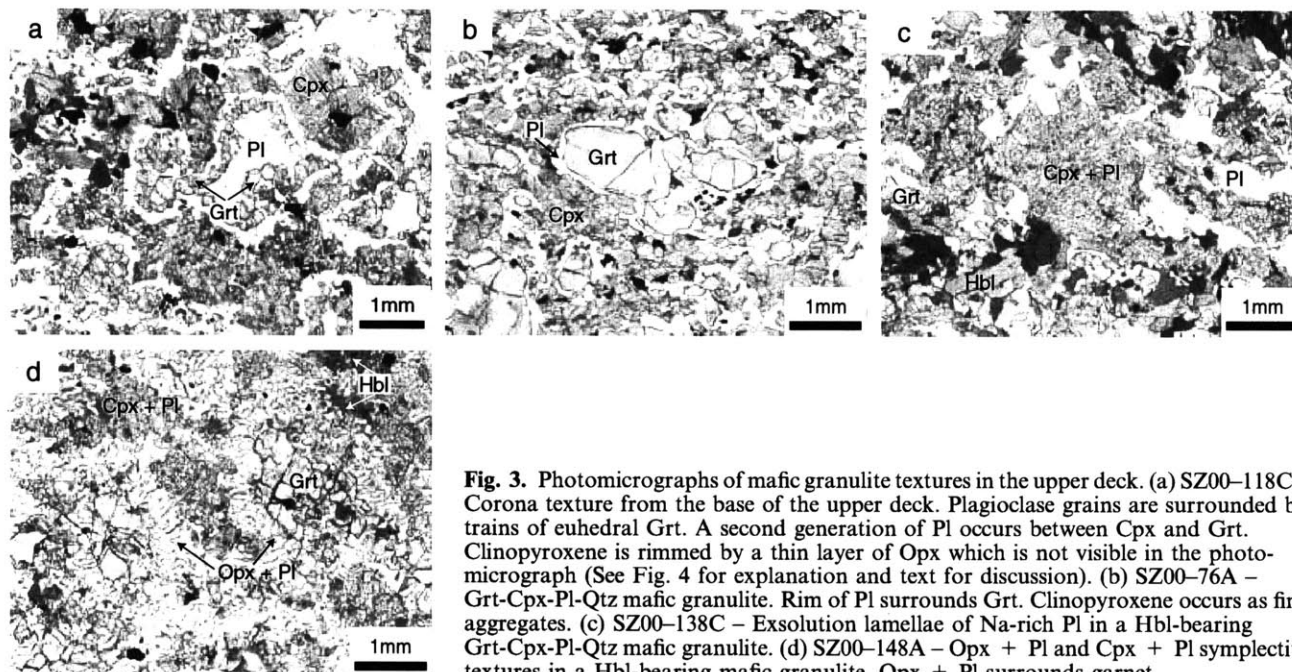


Fig. 3. Photomicrographs of mafic granulite textures in the upper deck. (a) SZ00-118C – Corona texture from the base of the upper deck. Plagioclase grains are surrounded by trains of euhedral Grt. A second generation of Pl occurs between Cpx and Grt. Clinopyroxene is rimmed by a thin layer of Opx which is not visible in the photomicrograph (See Fig. 4 for explanation and text for discussion). (b) SZ00-76A – Grt-Cpx-Pl-Qtz mafic granulite. Rim of Pl surrounds Grt. Clinopyroxene occurs as fine aggregates. (c) SZ00-138C – Exsolution lamellae of Na-rich Pl in a Hbl-bearing Grt-Cpx-Pl-Qtz mafic granulite. (d) SZ00-148A – Opx + Pl and Cpx + Pl symplectite textures in a Hbl-bearing mafic granulite. Opx + Pl surrounds garnet.

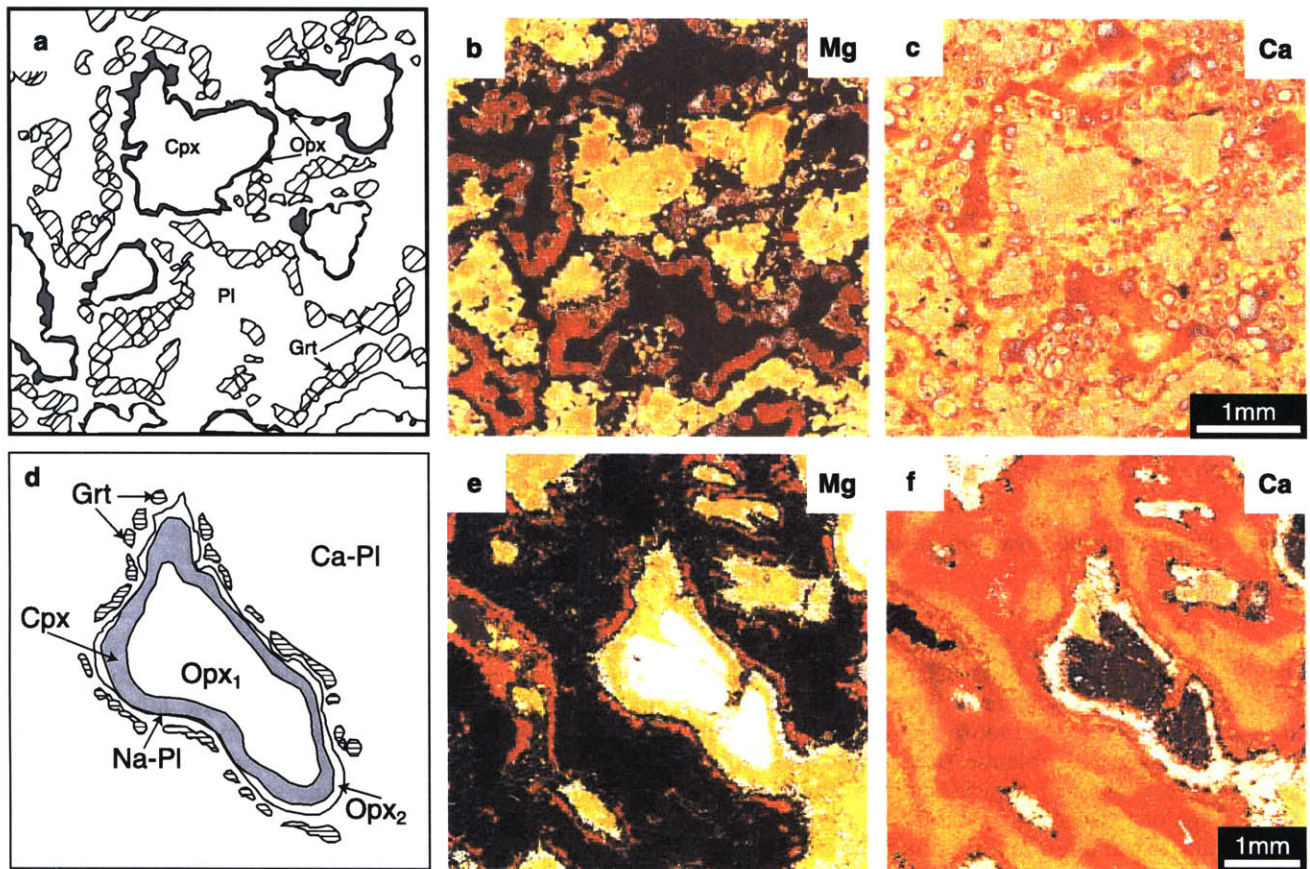


Fig. 4. Sketches and X-ray compositional maps of an upper deck mafic granulite (SZ00-118C) (a-c) and low-strain Godfrey granite (SZ00-7A) (d-f). (a) Sketch of phase relationships. Clinopyroxene is rimmed by a thin layer of Opx (black) which is in turn surrounded by Pl (white). Necklace of small Grt (ruled pattern) occurs between Pl surrounding Cpx and matrix Pl (b) Mg X-ray compositional map. The bright yellow rim around Cpx is Opx (c) Ca X-ray compositional map. Plagioclase has relict Ca-rich cores grading into more Na-rich Pl with a slight increase in Ca adjacent to Grt (d) Sketch showing phase relationships in SZ00-7A. Large, relict Opx grains (Opx_1) are surrounded by rim of fine-grained Cpx which is surrounded by a second generation of Opx (Opx_2). A thin rim of Na-rich Pl surrounds Opx_2 which is in turn rimmed by small Grt. Matrix Pl is more calcic. See text for interpretation of reaction relationships. (e) Mg X-ray compositional map. Brighter yellow is Opx. Note second generation of Opx surrounding Cpx. (f) Ca X-ray compositional map. Note zonation in matrix Pl from calcic cores to more sodic and then back to slightly more calcic adjacent to garnet.

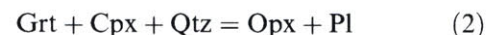
phism resulted in the breakdown of clinopyroxene and Ca-plagioclase (Pl_1) to form garnet and a more sodic plagioclase (Pl_2) (Fig. 4) by a reaction such as:



Zonation in the plagioclase is consistent with this interpretation (Fig. 4a). Garnet and clinopyroxene core compositions combined with the most sodic plagioclase composition are thus considered to be representative of peak pressure conditions, although this may not also be representative of peak temperature conditions since $Opx + Pl$ (reaction 2) can be produced by an increase in temperature during decompression. We therefore interpret this as a minimum estimate of the temperature corresponding to the high *P* event.

A second generation of plagioclase and orthopyroxene occurs between trains of garnet and the large clinopyroxene grains. The orthopyroxene-plagioclase

assemblage is interpreted to be the breakdown product of garnet and clinopyroxene by a reaction such as:



This reaction represents the transition from the high pressure ($Grt + Cpx + Qtz$) to the intermediate-pressure ($Opx + Pl + Grt + Cpx + Qtz$) granulite field (Green & Ringwood, 1967). Thus the postpeak metamorphic conditions are given by the equilibria defined by the garnet, orthopyroxene, and the late Ca-rich plagioclase.

A notable mafic granulite in this study, SZ00-141A, occurs south of Currie Lake (Fig. 2), and consists of the assemblage $Grt + Cpx + Pl + Qtz + Ttn + Hbl$. The rock has 1–5 mm porphyroblasts of garnet and clinopyroxene. Garnet typically displays a resorbed texture, surrounded by a corona of plagioclase. Most clinopyroxene contains inclusions of sodic feldspar.

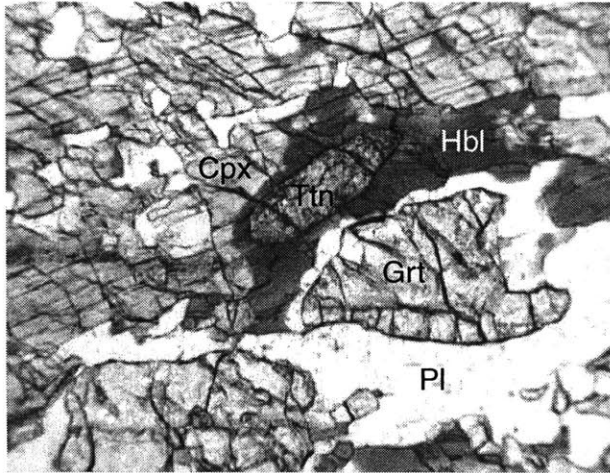
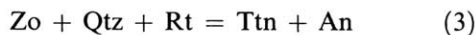
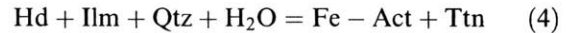


Fig. 5. Photomicrograph of the petrographic setting of titanite in upper deck mafic granulite (SZ00-141A). Field of view is 1.5 mm. Ttn is surrounded by Hbl and occurs at the tip of Cpx grains. Note resorbed texture of Grt and corona of Pl surrounding Grt. See text for full discussion.

The matrix consists of fine-grained quartz and feldspar. Amphibole forms rims on clinopyroxene and commonly nucleates around titanite crystals (Fig. 5); ilmenite is locally present in the Ttn + Hbl domains. Titanite also occurs (without amphibole), in the plagioclase coronas surrounding garnet. A reasonable interpretation is that the Ttn + Hbl formed as the breakdown product of Cpx + Grt in the presence of water. Another possibility is that this rock crystallized in the high pressure granulite field with the assemblage Grt + Cpx + Qtz. Plagioclase coronas formed from the breakdown of the Grt + Cpx + Qtz assemblage. There is a systematic association of titanite within feldspar, either with or without the rim of amphibole, indicating that it grew at the time of plagioclase and amphibole formation along the retrograde path. One reaction that may have produced the titanite is:



There is no rutile or zoisite present in SZ00-141A, indicating that it may have been entirely consumed. The association of titanite with hornblende and ilmenite also indicates that a reaction such as



may have contributed some titanite as well.

Another reaction texture, which is preserved in some of the mafic granulites is a symplectite of Opx + Pl surrounding garnet (Fig. 3d). This is a second example of reaction (2), where Opx + Pl is interpreted to have formed from the breakdown of the high pressure Grt + Cpx + Qtz assemblage. These mafic granulites also display clinopyroxene with exsolved Na-rich plagioclase (Fig. 3c), further indicating the transition from the high pressure back to the intermediate-pressure granulite field.

Godfrey granite

The Godfrey granite is an orthopyroxene-bearing granulite that is part of the lower deck domain and occurs along much of the northern margin of the upper deck (Figs 1 & 2). It typically has a penetrative and locally mylonitized fabric, although areas of coarse igneous (protolith) textures are locally preserved. Typical exposures exhibit ribbons of polycrystalline feldspar interlayered with garnet + orthopyroxene + hornblende layers and a finer matrix of plagioclase and quartz. Biotite is locally present but very scarce.

Low-strain varieties of the Godfrey granite, such as SZ00-7A (Fig. 6a), occur at the entrance to Godfrey Bay on Clut Lake (Fig. 2). In this sample, large 1–4 mm orthopyroxene crystals, interpreted to be relict igneous grains (Opx₁), are set in a fine-grained matrix of Ca-plagioclase (Pl₁) and quartz (Figs 6a & 4d–f). The Opx₁ grains are rimmed by a thick corona of fine-grained clinopyroxene which is in turn rimmed by a second thin corona of fine-grained orthopyroxene (Opx₂) (Fig. 4d). Around these fine orthopyroxene grains is a rim of more Na-rich plagioclase (Pl₂). A train of small garnet crystals typically surrounds the Na-plagioclase. The reaction suggested by these textures is



The left side of reaction (5) is interpreted to represent the relict igneous assemblage consisting of Opx₁ + Pl₁ + Qtz. Peak pressure conditions were achieved as the reaction proceeded into the high pressure granulite field represented by the assemblage of Grt + Cpx + Pl₂ + Qtz. The second generation

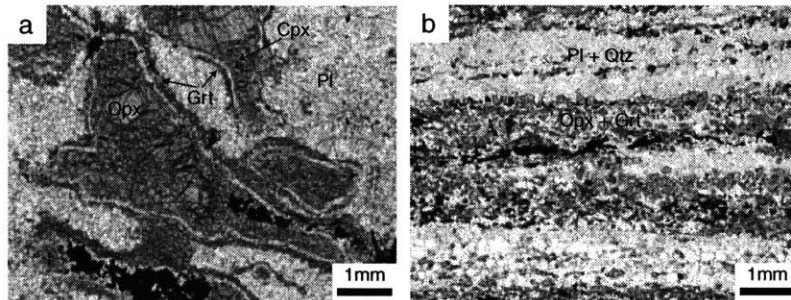


Fig. 6. Photomicrographs of the Godfrey granite. (a) Low strain variety (SZ00-7A) showing large, relict Opx grains surrounded by fine-grained Cpx. Na-rich Pl occurs between Cpx and Grt. Necklace of small Grt surrounds Opx-Cpx-Pl corona. Matrix Pl is more calcic. (b) Mylonitized Godfrey granite. Grt + Opx occurs in layers with thin rims of Pl surrounding the small Grt. Ribbons of Pl and Qtz separate the Grt-Opx layers.

of orthopyroxene, Opx_2 , is interpreted to have formed by reaction (5) proceeding back to the left into the intermediate-pressure granulite field.

In highly strained samples (SZ00-110D and SZ00-118E) of Godfrey granite (Fig. 6b), clinopyroxene is extremely rare, and the main assemblage is garnet + orthopyroxene + plagioclase + quartz + ilmenite. Where present, clinopyroxene typically occurs as minor, extremely small (tens of μm) inclusions in orthopyroxene. Garnet and orthopyroxene are concentrated in layers along with the ilmenite. Plagioclase typically forms thin rims around garnet and is antiperthitic. Quartz occurs as thin ribbons and matrix feldspar is fine grained. Ribbons of matrix feldspar tend to be more homogeneous with less extensive exsolution of feldspar compared to the low-strain varieties.

MINERAL COMPOSITIONS AND THERMOBAROMETRY

Mineral compositions in key assemblages were measured on the JEOL Superprobe 733 at MIT using an accelerating voltage of 15 kV and a beam current of 10 nA. Locations of spot analyses and quantitative traverses were selected based on the zonation and variation evident in high resolution compositional maps. Pressure-temperature conditions for a variety of mafic layers near the base of the upper deck as well as for the structurally underlying Godfrey granite of the lower deck were determined with the TWQ software (Berman, 1991) using the internally consistent thermodynamic database of Berman & Aranovich (1996). Representative mineral

compositions from mafic granulite and Godfrey granite samples are summarized in Tables 1 and 2. Calculated pressures and temperatures are reported in Table 3.

Mafic granulite

Mineral compositions

Garnet ranges from $\text{Alm}_{50}\text{Grs}_{30}\text{Prp}_{20}$ to $\text{Alm}_{60}\text{Grs}_{20}\text{Prp}_{20}$. In general, X_{Alm} is negatively correlated with X_{Grs} , while X_{Prp} remains nearly constant. Garnet cores are unzoned, and are interpreted to represent the peak pressure conditions. Garnet rims show increasing X_{Alm} and decreasing X_{Prp} , which are interpreted to represent diffusional re-equilibration with clinopyroxene during cooling. X_{Alm} is nearly constant from core to rim.

Plagioclase feldspar spans a wide range of compositions from An_{27} to An_{85} , depending on its petrographic setting. Typical core feldspar is An_{45-50} , however, some samples have cores as sodic as An_{20-30} . Some grains show slight zonation from An_{20} cores to An_{40} rims or An_{30} cores to An_{45} rims. Coronitic mafic granulites have some relict high Ca cores of An_{76} but most matrix plagioclase is approximately An_{45-50} . Plagioclase that occurs between clinopyroxene and garnet is slightly more calcic (An_{50-55}). Plagioclase that occurs in samples with orthopyroxene-plagioclase symplectite around garnet (e.g. SZ00-148A) is generally calcic (An_{85}), likely forming from the breakdown of garnet at significantly lower pressures. Plagioclase that occurs as exsolved lamellae in clinopyroxene is An_{35-40} . Matrix feldspar in this same sample is also sodic with cores of An_{30} zoning to rims of An_{45} . The composition of plagioclase surrounding garnet is similar to the matrix feldspar composition (An_{35-45}).

Clinopyroxene (augite) is variable in composition between samples. Clinopyroxene ranges in $\text{Mg}\#$ [$100 \text{ Mg}/(\text{Mg} + \text{Fe})$] from 57 to 75, but most mafic granulites have $\text{Mg}\# = 60-65$. Individual crystals have unzoned interiors but locally show an increase in $\text{Mg}\#$ near

Table 1. Representative mineral compositions of selected upper deck mafic granulite samples.

Sample	SZ00-118C					SZ00-148A					SZ00-141A		
	Grt (core)	Pl (matrix)	Pl (adj grt)	Cpx	Opx	Grt (core)	Pl (matrix)	Pl (adj grt)	Cpx	Opx	Grt (core)	Pl (rim)	Cpx
SiO_2	38.41	56.70	55.37	51.45	51.01	39.30	56.71	46.74	53.09	52.34	38.73	58.35	49.93
TiO_2	<dl	na	na	0.06	0.31	<dl	na	na	0.35	0.30	<dl	na	0.60
Al_2O_3	22.06	27.66	29.04	2.93	1.29	22.55	28.34	34.44	1.43	0.93	22.01	26.72	5.59
Cr_2O_3	<dl	na	na	<dl	0.05	<dl	na	na	0.07	0.08	<dl	na	0.03
FeO	22.40	0.06	0.17	11.13	28.76	23.96	0.16	0.48	7.77	25.58	19.46	0.34	10.14
MnO	0.58	na	na	0.10	0.31	0.31	na	na	0.03	0.25	1.28	na	0.13
MgO	4.22	<dl	<dl	12.22	18.08	8.54	<dl	<dl	14.48	20.53	4.36	<dl	11.33
CaO	12.15	9.59	11.25	22.28	<dl	6.13	9.82	17.38	22.84	<dl	14.20	8.36	21.63
Na_2O	0.02	6.26	5.73	0.46	0.06	<dl	6.12	1.79	0.28	0.08	<dl	6.97	0.64
K_2O	na	0.09	0.05	na	na	na	0.14	0.02	na	na	na	0.22	na
Σ	99.84	100.36	101.61	99.43	99.87	100.78	101.29	100.86	100.32	100.09	100.05	100.96	100.02
Cations													
Si	2.99	2.54	2.46	1.95	1.96	2.98	2.52	2.13	1.96	1.97	2.99	2.59	1.87
Ti	—	—	—	0.00	0.01	—	—	—	0.01	0.01	—	—	0.02
Al	2.02	1.46	1.52	0.13	0.06	2.02	1.48	1.85	0.06	0.04	2.00	1.40	0.25
Cr	—	—	—	0.00	0.00	—	—	0.00	0.00	0.00	—	0.00	—
Fe	1.45	0.00	0.01	0.35	0.92	1.52	0.01	0.02	0.24	0.81	1.26	0.01	0.32
Mn	0.04	—	—	0.00	0.01	0.02	—	—	0.00	0.01	0.08	—	0.00
Mg	0.49	—	—	0.66	1.04	0.97	—	—	0.80	1.15	0.50	0.00	0.63
Ca	1.01	0.46	0.54	0.87	—	0.50	0.47	0.85	0.91	0.00	1.17	0.40	0.87
Na	0.00	0.54	0.49	0.04	0.00	—	0.53	0.16	0.02	0.01	—	0.60	0.05
K	—	—	0.00	—	—	—	0.01	0.00	—	—	—	0.01	—
X_{Mg}	—	—	—	0.65	0.53	—	—	—	0.77	0.59	—	—	0.66
An	—	0.46	0.54	—	—	—	0.46	0.85	—	—	—	0.39	—
Ab	—	0.54	0.49	—	—	—	0.53	0.15	—	—	—	0.59	—
Kfs	—	0.00	0.00	—	—	—	0.01	0.00	—	—	—	0.00	—
Alm	0.49	—	—	—	—	0.51	—	—	—	—	0.42	—	—
Sps	0.01	—	—	—	—	0.01	—	—	—	—	0.03	—	—
Pyr	0.16	—	—	—	—	0.32	—	—	—	—	0.17	—	—
Grs	0.34	—	—	—	—	0.17	—	—	—	—	0.39	—	—

na, not analyzed; dl, detection limit.

Table 2. Representative mineral compositions of selected Godfrey granite samples.

Sample	SZ00-7A					SZ00-118E		
	Grt (core)	Pl (matrix)	Pl (adj cpx)	Cpx (core)	Opx	Grt	Pl	Opx
SiO ₂	39.27	51.06	57.08	52.28	52.78	37.75	59.28	50.13
TiO ₂	0.01	na	na	0.26	0.05	0.09	na	0.03
Al ₂ O ₃	22.66	31.75	27.77	3.20	2.56	21.33	26.25	1.05
Cr ₂ O ₃	<dl	na	na	0.02	0.38	0.02	na	0.04
FeO	22.28	0.09	0.37	7.59	19.48	23.82	0.15	32.88
MnO	1.00	na	na	0.12	0.22	0.63	na	0.48
MgO	9.36	0.01	<dl	13.99	24.17	3.14	0.02	14.90
CaO	9.36	13.95	9.45	22.03	0.80	12.34	7.90	0.50
Na ₂ O	0.01	3.42	6.32	0.77	0.03	0.03	7.08	<dl
K ₂ O	na	0.28	0.04	na	na	na	0.29	na
Σ	100.49	100.55	101.04	100.26	100.47	99.14	100.96	100.00
Cations								
Si	2.98	2.31	2.54	1.93	1.93	2.99	2.63	1.97
Ti	0.00	—	—	0.01	0.00	0.01	—	0.00
Al	2.02	1.69	1.46	0.14	0.11	1.99	1.37	0.05
Cr	—	—	—	0.00	0.01	0.00	—	0.00
Fe	1.41	0.00	0.01	0.23	0.60	1.58	0.01	1.08
Mn	0.06	—	—	0.00	0.01	0.04	0.02	—
Mg	1.06	0.00	—	0.77	1.32	0.37	0.00	0.87
Ca	0.48	0.68	0.45	0.87	0.03	1.05	0.37	0.02
Na	0.00	0.30	0.55	0.06	0.00	0.00	0.61	—
K	—	0.02	0.00	—	—	—	0.02	—
X _{Mg}				0.77	0.69			0.45
An		0.68	0.45				0.38	
Ab		0.30	0.55				0.61	
Kfs		0.02	0.00				0.02	
Alm	0.47					0.52		
Sps	0.02					0.01		
Pyr	0.35					0.12		
Grs	0.16					0.34		

na, not analyzed; dl, detection limit.

Table 3. Thermobarometric results.

Sample	Lithology	Temperature (°C)		Pressure (GPa)	
		Grt-Cpx	Grt-Opx	Grt-Cpx Pl-Qtz	Grt-Opx Pl-Qtz
SZ00-6A	mafic granulite	890		1.5	
SZ00-76A	mafic granulite	940		1.3	
SZ00-118C	mafic granulite	910	800	1.6	0.9
SZ00-138B	mafic granulite	940		1.6	
SZ00-148A	mafic granulite	800		1.0	
SZ00-141A	mafic granulite	960		1.9	
SZ00-110D	Godfrey granite		880		1.1
SZ00-118E	Godfrey granite		980		1.2
SZ00-7A	Godfrey granite	860	775	1.2	1.0

Clinopyroxene mixing properties are given by Berman *et al.* (1995). Nonideal interactions for Mg-Al-Fe in pyroxenes are given by Berman & Aranovich (1996). Garnet solution model of Berman (1990). Feldspar solution model of Fuhrman & Lindsley (1988).

the rims which likely reflects diffusional exchange with garnet during cooling. Where present, orthopyroxene generally only occurs as rims on clinopyroxene or as an orthopyroxene-plagioclase symplectite surrounding garnet. Orthopyroxene Mg#s range from 50 to 60. Rims on clinopyroxene have Mg# = 50–55, while orthopyroxene in the symplectites has Mg# ≈ 60. Amphibole, where present, ranges from pargasite to hornblende in composition.

Thermobarometry

Pressures and temperatures were calculated for six samples of mafic granulite layers in the upper deck

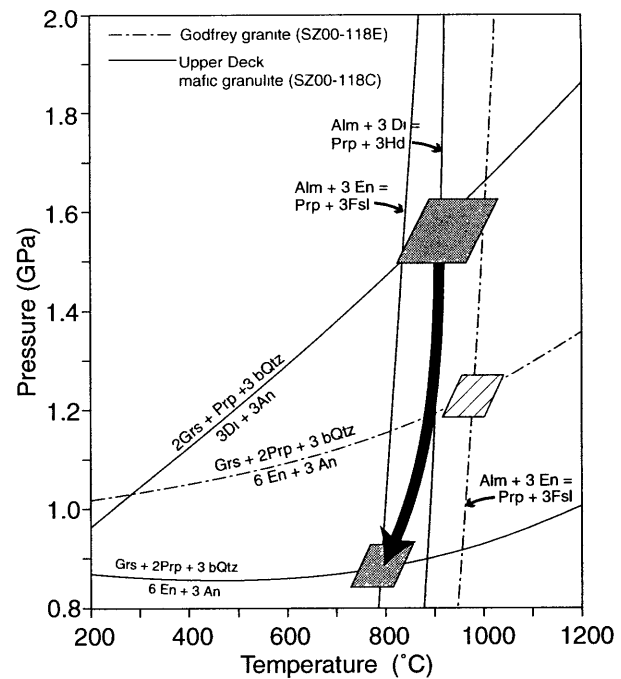


Fig. 7. Pressure–temperature diagram for upper deck mafic granulite and adjacent Godfrey granite. Coronitic mafic granulite (SZ00-118C) yields peak conditions of 1.6 GPa, 910 °C. Grt-Opx-Pl-Qtz equilibria show decompression to 0.9 GPa, 800 °C. Mylonitic sample of the Godfrey granite (SZ00-118E) adjacent to this mafic granulite layer constrains peak conditions at 1.2 GPa, 980 °C.

(Table 3). *P–T* conditions for the early high pressure metamorphism are constrained by Grt–Cpx–Pl–Qtz equilibria. Late stage metamorphic conditions were calculated in relevant samples using the Grt–Opx–Pl–Qtz equilibria. Garnet core compositions were used in both sets of calculations since zoning profiles are generally flat and only the outermost rim of garnet has been modified by late stage net transfer reactions. The best constraints on the *P–T* path of the mafic granulites come from the coronitic samples, such as SZ00-118C (Fig. 7). Peak *P–T* conditions are approximately 1.6 GPa and 910 °C (Fig. 7). A transition to intermediate-pressure granulite facies via reaction (2) is evidenced by orthopyroxene rimming clinopyroxene and more calcic plagioclase forming from the breakdown of garnet and clinopyroxene. Late stage metamorphic conditions are 0.9 GPa and 800 °C.

Sample SZ00-141A also yields firm constraints on the high *P–T* metamorphic conditions. Garnet core, average clinopyroxene, and plagioclase rim compositions yield 1.9 GPa, 960 °C (Fig. 8). We consider this to represent a point closely following peak metamorphism, but along the retrograde path because the plagioclase appears to have formed from the breakdown of Grt + Cpx. We infer that at these high temperatures, diffusion would have taken place rapidly enough to equilibrate the Grt + Cpx + new-Pl assemblage. In addition, for the composition of

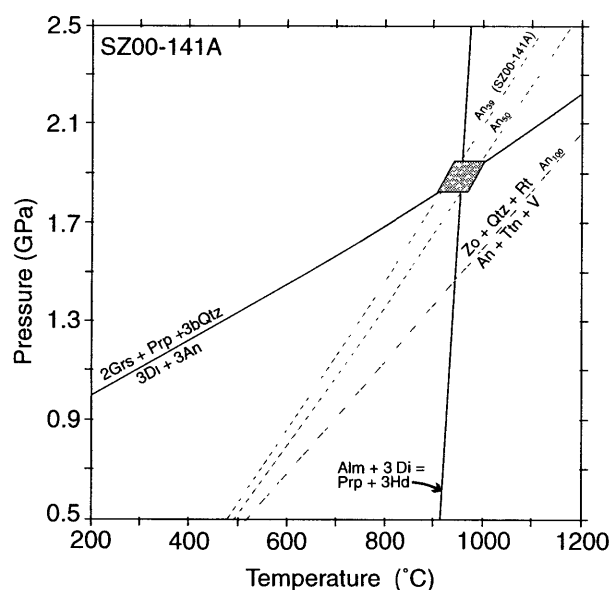


Fig. 8. Pressure-temperature diagram for upper deck mafic granulite (SZ00-141A). Solid lines are the Grt-Cpx-Pl-Qtz equilibria and shaded box shows the *P*-*T* conditions calculated for this sample of 1.9 GPa, 960 °C. Dashed lines are drawn for the reaction $Zo + Qtz + Rt = An + Ttn + Vapour$ for different An contents (An_{39} , An_{50} , & An_{100}). An_{39} is the composition for sample SZ00-141A used in the thermobarometric calculations. Note increasing stability of the An + Ttn assemblage with increasing Na content in plagioclase.

plagioclase in SZ00-141A, the stability of Ttn + An nearly coincides with the calculated *P*-*T* conditions (Fig. 9), which is consistent with titanite forming along the retrograde path. The *P*-*T* limits of titanite stability increase with increasing Na in plagioclase. Given that titanite is not stable above *c.* 1.9 GPa at the temperature calculated (960 °C), we infer that it was probably not present at the time of peak metamorphism, but instead formed along the retrograde path above its closure temperature (*c.* 650 °C).

The mafic granulites examined in this study yield a range of calculated peak pressures (Table 3). The range is likely due to varying amounts of re-equilibration during decompression. Samples that yield higher pressures generally show very little evidence for decompression. In contrast, samples with abundant decompression textures (Opx-Pl symplectite surrounding garnet; exsolution lamellae of Na-rich Pl in Cpx), such as SZ00-148A (Fig. 3d), yield lower pressures (*c.* 1.0 GPa).

The thermobarometric data from these rocks suggest that the mafic granulites have a simple two stage metamorphic history. First, these rocks were metamorphosed in the high pressure granulite field at minimum pressures of 1.6 GPa, 910-960 °C, followed by decompression to lower crustal conditions of 0.9 GPa and 800 °C. The delicate reaction textures preserved in the coronitic mafic granulites are interpreted to have formed during this decompression.

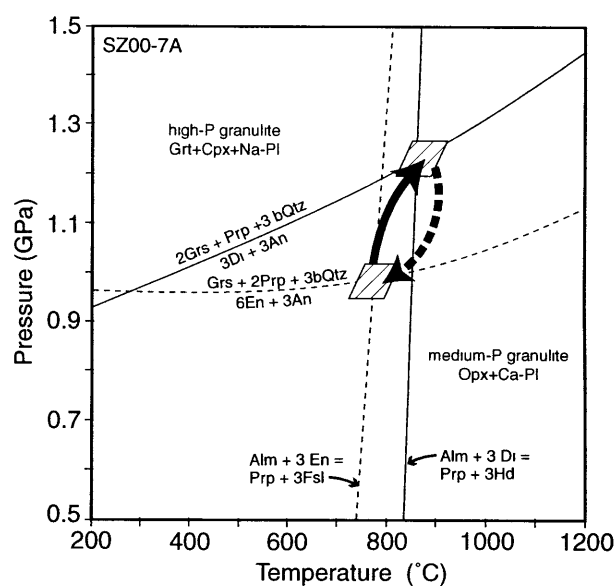


Fig. 9. Pressure-temperature diagram for low strain Godfrey granite (SZ00-7A). Igneous crystallization or early metamorphism in the intermediate-pressure granulite field at 1.0 GPa, 775 °C was followed by higher-pressure metamorphism at 1.2 GPa, 860 °C. Prograde path shown by solid arrow. Second generation of Opx surrounding Cpx indicates there may have been decompression following peak metamorphism. Possible path shown by dashed arrow.

Godfrey granite

Mineral compositions

Garnet in the highly strained samples (SZ00-110D and SZ00-118E) of Godfrey granite is $Alm_{60}Grs_{20-25}Prp_{15-20}$. In the low-strain variety (SZ00-7A) garnet has a significantly higher X_{Prp} with an average composition of $Alm_{47}Grs_{16}Prp_{35}$. Garnet cores are unzoned, and are interpreted to represent peak metamorphic conditions. Garnet rims have slightly higher X_{Alm} and lower X_{Prp} , consistent with diffusional exchange of Fe-Mg between garnet and pyroxene on cooling.

Plagioclase in the highly strained samples is homogeneous with compositions of An_{35-40} . In the low strain sample, there are two plagioclase compositions (Fig. 4d). Plagioclase cores are calcic with more sodic domains closer to the rims. Our interpretation is that the first plagioclase to form was calcic (*c.* An_{68}) (left side of reaction 5), so this composition was used to calculate the early metamorphic conditions. The second generation of plagioclase, which occurs between clinopyroxene and garnet, was used to calculate the later metamorphic conditions.

Clinopyroxene (augite) is only present in the low strain sample and has $Mg\# = 77$. Orthopyroxene (ferrosilite) occurs in the highly strained Godfrey granite with $Mg\# = 44$ for SZ00-118E to 50 for SZ00-110D. Large relict orthopyroxene (enstatite) grains in the low strain sample SZ00-7A (Fig. 6a) are unzoned with an average $Mg\# = 68$.

Thermobarometry

Pressures and temperatures were calculated for three samples of Godfrey granite (Table 3). Two samples, SZ00-110D and SZ00-118E, are highly strained mylonitic gneisses, and record comparable pressures

and temperatures (880–980 °C and 1.1–1.2 GPa) based on garnet–orthopyroxene–plagioclase–quartz equilibria. Textural criteria for equilibrium in these rocks is difficult to evaluate however, because of the fine-grained nature of these mylonites and the concentration of garnet + orthopyroxene in separate domains from the plagioclase + quartz. Therefore more robust *P–T* constraints on metamorphism of the Godfrey granite are interpreted to come from the least deformed sample, SZ00–7A, in which interpretations of mineral textures can be made with greater confidence.

Calculated *P–T* conditions for the early stage metamorphism based on the Opx + Grt + Ca-rich Pl + Qtz assemblage yields 775 °C and 1.0 GPa (Fig. 9). Peak *P–T* conditions of 1.2 GPa and 860 °C for SZ00–7A are recorded by Grt + Cpx + Na-Pl assemblages. In addition, a second generation of orthopyroxene forms a thin rim around the clinopyroxene (Fig. 4d–f), indicating that the reaction (5) was again crossed from the high pressure back into the intermediate-pressure granulite field following the peak metamorphic conditions. This is further supported by the zonation of the plagioclase (Fig. 4d–f) from highly calcic relict cores in the interior of the matrix to more sodic rims, and then becoming slightly more calcic adjacent to garnet. Thus the coronitic textures preserved in the Godfrey granite indicate a three-stage history from (1) igneous crystallization and early metamorphism in the intermediate pressure granulite field at 775 °C, 1.0 GPa; (2) high pressure granulite facies metamorphism at 860 °C, 1.2 GPa; and (3) decompression into the intermediate-pressure granulite facies (Fig. 9, dashed arrow).

U-PB GEOCHRONOLOGY

The main goals of our ongoing U–Pb geochronological investigations are to constrain the timing of high pressure metamorphism in the upper deck, to determine the crystallization age of the Godfrey granite, and to constrain the timing of juxtaposition of the upper deck with the Godfrey granite. High precision isotope dilution thermal ionization mass spectrometry (IDTIMS) was used in concert with cathodoluminescence (CL) and backscattered electron (BSE) imaging. CL reveals information about the growth history of zircon by providing a map of chemical variation in chemical composition related to the REE content (Mariano, 1989; Hanchar & Rudnick, 1995).

Accessory minerals were isolated from the samples by standard crushing, heavy liquid and magnetic separation techniques. Fractions of accessory minerals consisting of both single grains and multigrain fractions were carefully picked to yield consistent grain sizes, which were measured and recorded by digital photography. Zircon crystals were air-abraded with pyrite after the method of Krogh (1982), and acid rinsed in 3M HNO₃ for 5–6 h, followed by ultrasonication. Accessory mineral fractions were loaded into Teflon FEP microcapsules and washed again in 3M HNO₃ (zircon) or high purity water (titanite and apatite) at *c.* 50 °C for 3–4 h, followed by rinsing with several capsule volumes of 3 M HNO₃ (zircon) or water (titanite). Samples were spiked with a mixed ²⁰⁵Pb, ²³³U, ²³⁵U tracer and dissolved in 29 M HF at 220 °C for 48–96 h, followed by conversion to 6 M HCl at 180 °C for 24 h. Pb and U were separated from all mineral solutions using anion

exchange chromatography procedures modified after Krogh (1973). U–Pb analyses were done at the Massachusetts Institute of Technology on the VG Sector 54 thermal ionization multicollector mass spectrometer. Pb and U were loaded on single Re filaments with a dilute silica gel-0.1 H₃PO₄ emitter solution with U run as an oxide. U–Pb data as well as the details of fractionation and blank corrections are given in Table 4.

Mafic granulite

SZ00–118C, coronitic mafic granulite

Zircon and titanite were analyzed from this coronitic mafic granulite to temporally calibrate the inferred isothermal decompression path (Fig. 7) for this sample. Zircon in this rock is pink, typically < 80 μm in diameter, irregularly shaped with jagged edges, and contains inclusions of plagioclase feldspar. In this section, zircon is associated with abundant Fe-oxides, and in particular, zircon forms irregular tips on ilmenite. CL images of zircon show evidence for thin (< 10 μm) rim overgrowths on weakly oscillatory-zoned cores (Fig. 10a). Six abraded single grains of zircon were analyzed which have ²⁰⁷Pb/²⁰⁶Pb dates ranging from 2531 to 2339 Ma (Fig. 11). This spread in age is interpreted to reflect protracted crystallization of zircon along a retrograde *P–T* path, with a minimum igneous protolith or earliest metamorphism at 2.53 Ga. Given the extremely thin rims on these grains and treatment with aggressive air abrasion, it is not likely that this spread in dates is the result of the mixing between two or more components.

In addition, two titanite fractions were analyzed. The first (s1) was a large (*c.* 150 μm) single grain. The second fraction (s3) consisted of six small (*c.* 60 μm) grains. These analyses yield a weighted mean ²⁰⁷Pb/²⁰⁶Pb date of 1898 ± 1.3 Ma, which is interpreted as a cooling age following decompression of this sample from 1.6 GPa, 910 °C to 0.9 GPa, 800 °C because the closure temperature of titanite is *c.* 650 °C (Cherniak, 1993). This date is interpreted to place a minimum constraint on the growth of the coronas around garnet and clinopyroxene. However, since the petrographic setting of titanite does not conclusively link its growth to the high pressure metamorphism, precise geochronological constraints cannot yet be placed on the timing of the peak *P–T* conditions in this sample.

SZ00–148A, mafic granulite with coronitic (decompression) textures

This mafic granulite (SZ00–148A) has abundant decompression textures, which are described above. Zircon in this sample occurs as large (150–200 μm), anhedral to rounded, pink grains which are generally inclusion-free. CL images show rim overgrowths on oscillatory zoned cores, and evidence for resorption around the cores with embayments filled by younger overgrowths (Fig. 10b). Six abraded single grains of

Table 4. U-Pb isotopic data for mafic granulites and Godfrey granite.

Fractions ^a	Weight (μg) ^b	Compositions				Isotopic ratios						Dates (Ma)			Discordance (%)		
		U (p.p.m.)	Pb (p.p.m.)	Th/U	Pb ζ (pg)	²⁰⁶ Pb*/ ²⁰⁴ Pb	²⁰⁸ Pb/ ²⁰⁶ Pb	²⁰⁶ Pb ϵ / ²³⁸ U	% err	²⁰⁷ Pb ϵ / ²³⁵ U	% err	²⁰⁷ Pb ϵ / ²⁰⁶ Pb	% err	²⁰⁶ Pb/ ²³⁸ U		²⁰⁷ Pb/ ²³⁵ U	²⁰⁷ Pb/ ²⁰⁶ Pb
<i>SZ00-118C, mafic granulite</i>																	
z1	2.6	92	45	0.14	4.8	1446	0.0404	0.46790	(0.38)	10.46413	(0.40)	0.16220	(0.12)	2474.4	2476.7	2478.7 \pm 2.0	0.2
z2	2.0	35	17	0.26	1.9	1095	0.0740	0.45654	(0.23)	9.95751	(0.26)	0.15819	(0.13)	2424.3	2430.9	2436.4 \pm 2.1	0.6
z3	7.5	9	5	0.34	3.3	660	0.0968	0.46888	(0.45)	10.81461	(0.47)	0.16728	(0.13)	2478.6	2507.3	2530.6 \pm 2.2	2.5
z4	2.6	14	8	0.42	8.4	125	0.1243	0.42247	(1.77)	8.70151	(1.79)	0.14938	(0.22)	2271.7	2307.2	2338.9 \pm 3.7	3.4
z5	5.8	14	7	0.36	4.8	484	0.1021	0.46148	(0.76)	10.27865	(0.76)	0.16154	(0.11)	2446.1	2460.2	2471.8 \pm 1.9	1.3
z11	2.2	29	15	0.34	1.5	1398	0.0952	0.48139	(0.16)	11.04227	(0.19)	0.16636	(0.09)	2533.3	2526.7	2521.4 \pm 1.4	-0.6
s1	18	5	2	1.05	6.5	334	0.2989	0.34766	(1.15)	5.57093	(1.17)	0.11622	(0.15)	1923.4	1911.6	1898.8 \pm 2.5	-1.5
s3 (6)	39	8	3	1.24	7.6	857	0.3606	0.34241	(0.40)	5.48578	(0.41)	0.11620	(0.09)	1898.2	1898.4	1898.5 \pm 1.5	0.0
<i>SZ00-148 A, mafic granulite</i>																	
z1	14.9	60	34	0.75	1.9	14156	0.2132	0.47397	(0.07)	10.87473	(0.09)	0.16640	(0.05)	2501.0	2512.5	2521.8 \pm 0.8	1.0
z2	7.1	37	19	0.60	3.7	2076	0.1722	0.45827	(0.24)	10.14505	(0.25)	0.16056	(0.06)	2431.9	2448.1	2461.6 \pm 1.0	1.4
z3	5.0	44	17	0.57	4.5	1102	0.1666	0.35155	(0.35)	5.83520	(0.37)	0.12039	(0.10)	1942.0	1951.7	1961.9 \pm 1.8	1.2
z4	9.9	62	34	0.67	23.8	665	0.1946	0.44317	(0.21)	9.67628	(0.26)	0.15836	(0.15)	2364.8	2404.5	2438.2 \pm 2.6	3.6
z5	6.5	42	21	0.74	7.7	891	0.2179	0.41289	(0.27)	8.31602	(0.30)	0.14608	(0.12)	2228.1	2266.1	2300.5 \pm 2.0	3.7
z6	10.4	28	15	0.66	12.6	593	0.1917	0.43166	(0.28)	9.06125	(0.47)	0.15225	(0.33)	2313.2	2344.2	2371.3 \pm 5.7	2.9
<i>SZ00-141 A, mafic granulite</i>																	
z1	16.2	54	19	0.15	3.5	5548	0.0430	0.34342	(0.14)	5.51883	(0.15)	0.11655	(0.05)	1903.1	1903.5	1904.0 \pm 0.9	0.1
z2	11.5	50	17	0.10	2.0	6373	0.0287	0.34439	(0.07)	5.53063	(0.10)	0.11647	(0.06)	1907.7	1905.4	1902.8 \pm 1.1	-0.3
z3	3.8	53	18	0.09	3.3	1353	0.0266	0.34439	(0.26)	5.54000	(0.31)	0.11667	(0.15)	1907.8	1906.8	1905.8 \pm 2.7	-0.1
z4	14.3	26	9	0.07	6.6	1182	0.0203	0.34289	(0.28)	5.53089	(0.37)	0.11699	(0.23)	1900.6	1905.4	1910.7 \pm 4.1	0.6
z5	5.9	472	184	0.09	5.0	13323	0.0281	0.38610	(0.06)	7.57126	(0.07)	0.14222	(0.04)	2104.7	2181.5	2254.5 \pm 0.7	7.8
z6	3.7	207	84	0.11	1.9	10560	0.0327	0.40175	(0.09)	7.96786	(0.10)	0.14384	(0.04)	2177.1	2227.4	2274.0 \pm 0.8	5.0
z8	1.9	511	246	0.27	4.3	6443	0.0770	0.45315	(0.11)	9.89287	(0.12)	0.15833	(0.05)	2409.3	2424.8	2437.9 \pm 0.8	1.4
z9	3.3	400	176	0.19	0.7	49780	0.0547	0.42612	(0.15)	8.72995	(0.16)	0.14859	(0.05)	2288.2	2310.2	2329.7 \pm 0.8	2.1
s2	11.6	20	10	1.52	11.9	407	0.4550	0.33099	(0.49)	5.28867	(0.51)	0.11588	(0.10)	1843.2	1867.0	1893.7 \pm 1.7	3.1
s4	88.4	16	9	2.45	102.2	280	0.7183	0.33745	(0.11)	5.39286	(0.16)	0.11591	(0.11)	1874.4	1883.7	1894.0 \pm 2.1	1.2
s5	96.4	19	10	1.87	44.5	825	0.5414	0.34347	(0.09)	5.50619	(0.12)	0.11627	(0.07)	1903.3	1901.6	1899.6 \pm 1.2	-0.2
<i>SZ00-125 A, Godfrey granite</i>																	
z1	7.5	94	60	0.99	23.0	858	0.2785	0.49215	(0.17)	11.79127	(0.21)	0.17376	(0.11)	2580.0	2588.0	2594.2 \pm 1.9	0.7
z2	1.7	87	51	0.72	8.1	519	0.2011	0.47763	(0.43)	10.86000	(0.44)	0.16491	(0.09)	2516.9	2511.2	2506.6 \pm 1.6	-0.5
z3	1.9	149	98	0.68	23.1	350	0.1877	0.50295	(0.22)	12.16311	(0.29)	0.17540	(0.16)	2626.4	2617.1	2609.8 \pm 2.7	-0.8
z4	2.2	186	113	0.50	40.5	266	0.1505	0.45285	(0.18)	10.70267	(0.19)	0.17141	(0.07)	2407.9	2497.7	2571.5 \pm 1.2	7.6
z5	2.0	172	89	0.42	1.0	10561	0.1264	0.46127	(0.09)	10.96374	(0.11)	0.17239	(0.06)	2445.2	2520.1	2581.0 \pm 1.0	6.3
z6	0.9	269	135	0.29	1.6	4463	0.0844	0.46572	(0.11)	10.72808	(0.13)	0.16707	(0.07)	2464.7	2499.9	2528.5 \pm 1.1	3.0
<i>SZ00-118E, Godfrey granite</i>																	
z1	2.5	75	44	0.70	1.5	4101	0.1974	0.49248	(0.12)	11.91935	(0.13)	0.17554	(0.05)	2581.4	2598.1	2611.1 \pm 0.8	1.4
z2	2.5	121	73	0.67	11.8	743	0.1890	0.49236	(0.24)	11.85864	(0.25)	0.17468	(0.07)	2580.9	2593.3	2603.0 \pm 1.1	1.0
z3	2.2	121	73	0.87	1.7	4898	0.2438	0.49309	(0.14)	11.87335	(0.15)	0.17464	(0.06)	2584.0	2594.5	2602.6 \pm 1.0	0.9
z4	3.9	116	70	0.85	5.5	2458	0.2400	0.49099	(0.14)	11.77094	(0.15)	0.17387	(0.06)	2575.0	2586.4	2595.3 \pm 0.9	0.9
z8*	5.0	84	48	0.60	1.4	9504	0.1695	0.49552	(0.09)	11.98624	(0.10)	0.17544	(0.05)	2594.5	2603.3	2610.2 \pm 0.9	0.7
z10b*	4.5	104	55	0.49	4.2	3270	0.1403	0.46648	(0.23)	10.77981	(0.24)	0.16760	(0.05)	2468.1	2504.3	2533.8 \pm 0.9	3.1
z10t*	5.4	105	63	0.59	19.5	824	0.1672	0.49242	(0.14)	11.87579	(0.15)	0.17491	(0.05)	2581.1	2594.7	2605.2 \pm 1.0	1.1
z19*	3.4	40	22	0.62	1.4	3144	0.1751	0.48719	(0.22)	11.54229	(0.23)	0.17183	(0.06)	2558.5	2568.0	2575.5 \pm 0.8	0.8

^a All grains analyzed were single grains with the exception of SZ00-118C, s3 (6 grains) (z = zircon, s = titanite). * Indicates broken tip that was analyzed after imaging.

^b Sample weights were estimated to within 40% using measured grains dimensions, and nominal density 4.5 g cm⁻³ for zircon or 3.5 g cm⁻³ for titanite.

^c Common Pb.

^d Measured ratio corrected for fractionation and spike contribution; Pb fractionation correction is 0.12 \pm 0.04% per a.m.u. (2 σ) for multicollector analyses and 0.15 + 0.04% per a.m.u. (2 σ) for single collector analyses based on repeated daily analysis of NBS 981.

^e Pb/U isotopic ratios corrected for fractionation, spike, blank, and initial common Pb; U blank 0.1 pg \pm 50%; data was reduced using a Pb blank of 3.5 \pm 50%; initial common Pb composition was estimated using the model for terrestrial Pb evolution of Stacey & Kramers (1975); numbers in parentheses are the percentage error reported at the 2-sigma confidence interval.

^f Uncertainty in the Pb-Pb date in My at the 2-sigma confidence interval.

zircon were analyzed. Three large, relatively round grains (z1, z2, z4) are slightly different morphologically from the other three grains (z3, z5, z6) that are flatter and more irregularly shaped. After abrasion both z5 and z6 still showed optical evidence for rim overgrowths whereas z3 is a small relatively homogenous fragment of a grain. The first population (z1, z2, z4) yielded older $^{207}\text{Pb}/^{206}\text{Pb}$ dates ranging from 2522 to 2438 Ma (Fig. 12). Both z6 and z5 are discordant with younger $^{207}\text{Pb}/^{206}\text{Pb}$ dates of 2371.3 ± 5.7 and 2300.5 ± 2.0 Ma, respectively. One zircon grain (z3) yields a $^{207}\text{Pb}/^{206}\text{Pb}$ date of 1961.9 ± 1.8 Ma. The simplest interpretation is that these analyses represent mixtures of *c.* 2.5 Ga protolith igneous or metamorphic zircon and *c.* 1.9 Ga overgrowths. A statistically insignificant (MSWD = 29) linear array can be drawn with an upper intercept of 2.55 Ga and a lower intercept of 1.92 Ga, consistent with either Pb-loss or mixing, indicating a minimum protolith/early metamorphic age of *c.* 2.55–2.52 Ga followed by metamorphism *c.* 1.9 Ga.

SZ00-141A, mafic granulite

In this sample, two morphological populations of zircon are present. The first displays a rounded morphology, ranges in size from *c.* 100 to $> 200 \mu\text{m}$, and is pink and inclusion-free. This population of zircon makes up *c.* 90% of the total zircon population. The second zircon population is rounded as well, but is smaller (90–120 μm), metamict, extremely cloudy, and brown in colour. In thin section, zircon occurs as inclusions within garnet, clinopyroxene, and plagioclase

feldspar. CL imaging of the first population shows that the interiors of the crystals display sector zoning, which is typical of high pressure metamorphic zircon (Fig. 10c) (Vavra *et al.*, 1996). Four single abraded zircon crystals (z1, z2, z3, z4) from the pink, inclusion-free population yield a range in $^{207}\text{Pb}/^{206}\text{Pb}$ dates from 1911 to 1903 Ma (Fig. 13, Table 4). The oldest, most discordant (0.6%) analysis in this population, z4, yields a $^{207}\text{Pb}/^{206}\text{Pb}$ date of 1910.7 ± 4.1 Ma, which may represent slight inheritance. We consider z1, which is nearly concordant, with a $^{207}\text{Pb}/^{206}\text{Pb}$ date of 1904.0 ± 0.9 Ma to be the best estimate of the age of metamorphic zircon growth. Low Th/U ratios for all four analyses, ranging from 0.07 to 0.15 (Table 4), are consistent with a metamorphic origin for the zircon. The range in $^{207}\text{Pb}/^{206}\text{Pb}$ dates reflects either a protracted period of growth and/or slight inheritance.

The second metamict zircon population (z5, z6, z8, z9) yields variably discordant analyses (1.41–7.78%) with a range in $^{207}\text{Pb}/^{206}\text{Pb}$ dates of 2438–2255 Ma. This population has a significantly higher U content than the younger population (200–500 p.p.m. in the metamict population compared to 25–50 p.p.m. in the pink, inclusion-free population). We interpret the two populations as follows: the metamict population likely formed during crystallization of the original protolith and is similar in its discordance pattern to *c.* 2.5 Ga zircon from other lithologies examined in this study. We thus interpret the oldest $^{207}\text{Pb}/^{206}\text{Pb}$ date of 2437.9 ± 0.8 Ma as a minimum protolith age for this sample. The younger, low-U population likely formed during *c.* 1.9 Ga metamorphism. Petrographic

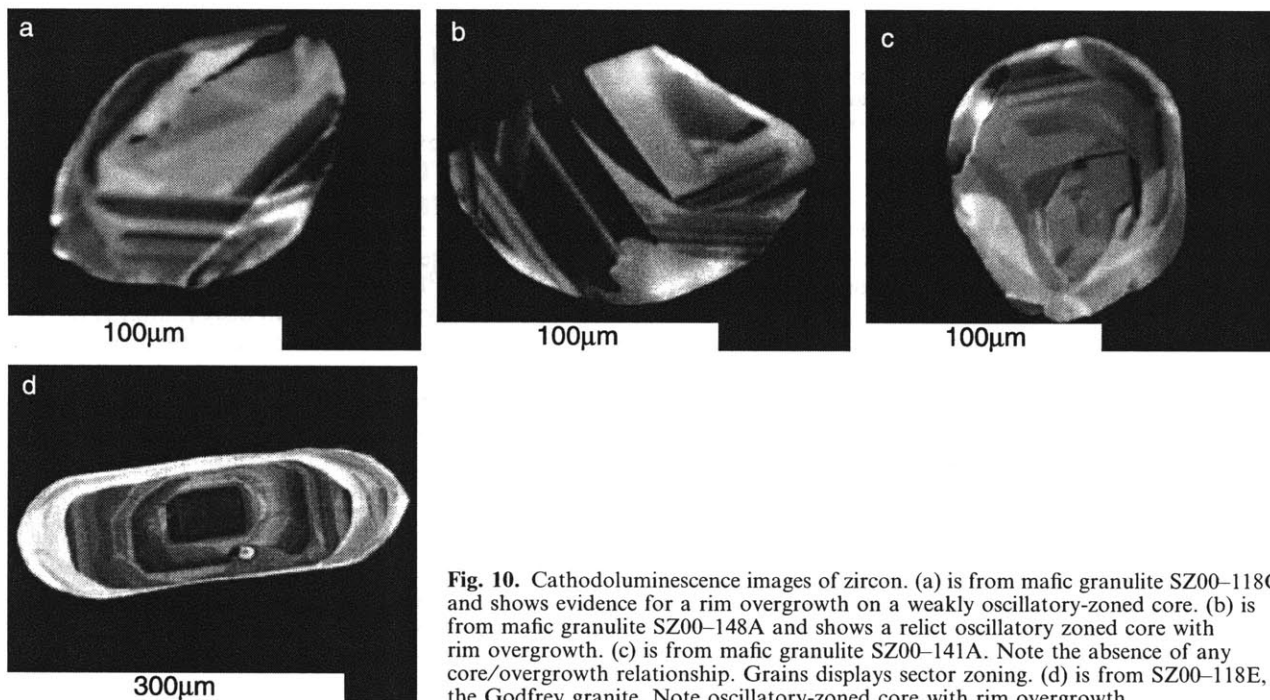


Fig. 10. Cathodoluminescence images of zircon. (a) is from mafic granulite SZ00-118C and shows evidence for a rim overgrowth on a weakly oscillatory-zoned core. (b) is from mafic granulite SZ00-148A and shows a relict oscillatory zoned core with rim overgrowth. (c) is from mafic granulite SZ00-141A. Note the absence of any core/overgrowth relationship. Grains displays sector zoning. (d) is from SZ00-118E, the Godfrey granite. Note oscillatory-zoned core with rim overgrowth.

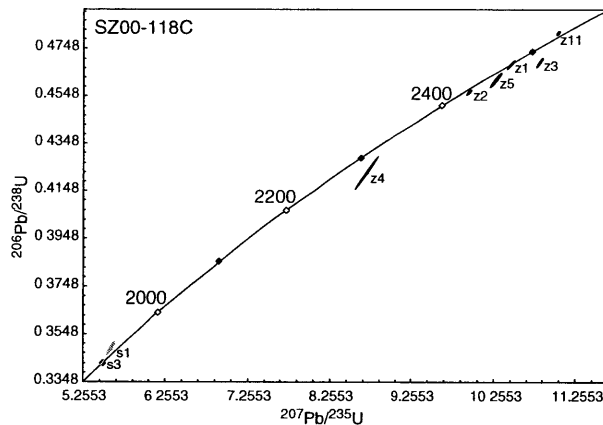


Fig. 11. U-Pb concordia diagram for upper deck coronitic mafic granulite, SZ00-118C. z indicates the zircon analyses and s indicates titanite analyses. Error ellipses are 2σ .

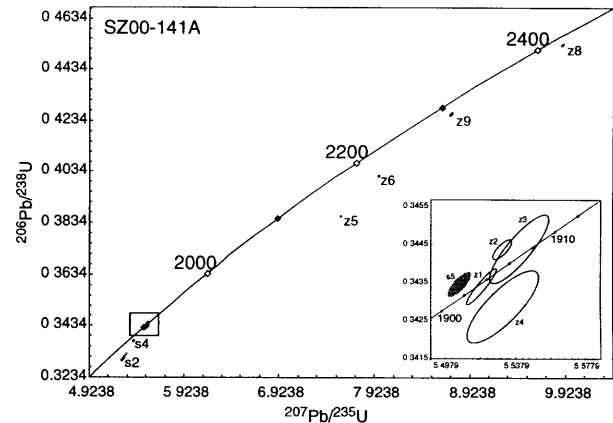


Fig. 13. U-Pb concordia diagram for upper deck mafic granulite, SZ00-141A. Inset shows area outlined in box around 1900 Ma. Zircon analyses (z) are in black. Titanite analyses (s) are shaded in grey. Note two distinct age populations of zircon. See text for discussion. Error ellipses are 2σ .

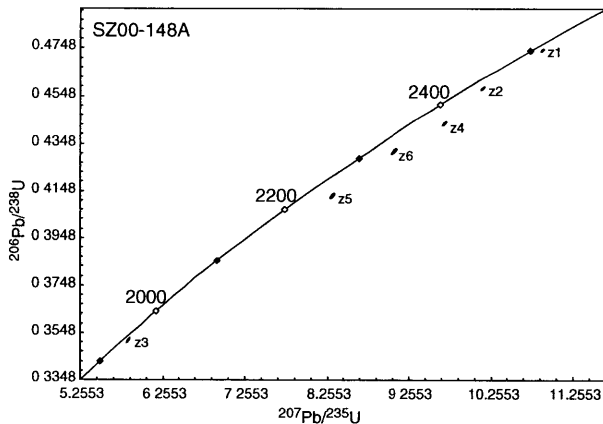


Fig. 12. U-Pb concordia diagram for zircon from upper deck mafic granulite, SZ00-148A. Crude linear array indicates mixture between igneous zircon and metamorphic overgrowths. Error ellipses are 2σ .

examination has not permitted us to distinguish between these two zircon populations, so there is some ambiguity in interpreting the metamorphic conditions associated with each population. However, given the petrographic setting of zircon within high pressure garnet and clinopyroxene, and the abundance of this younger population, we believe that it is most likely that this population of 1.9 Ga zircon is linked to the 1.9 GPa, 960 °C metamorphic conditions.

In addition to zircon, three single grains of titanite were analyzed from this sample, which ranged from 150 to 430 μm in diameter. These analyses have a range in $^{207}\text{Pb}/^{206}\text{Pb}$ dates from 1900 to 1895 Ma (Fig. 13). We argue above that the petrographic setting of the titanite indicates that it likely formed after peak metamorphic conditions. Also, given that the stability of the Ttn + An assemblage in the coronas surrounding

garnet is limited to *c.* 1.9 GPa at the temperature of the metamorphism (960 °C), we infer that the titanite formed above its closure temperature (near 1.9 GPa, 960 °C) and cooled to *c.* 650 °C by *c.* 1.9 Ga.

Godfrey granite

SZ00-125A

Sample SZ00-125A is a mylonitic sample of Godfrey granite. Petrographic examination and CL imaging of zircon reveal two morphologic populations of zircon: one of colourless, cloudy euhedral grains with some inclusions, and a second of clear, anhedral rounded grains that are generally inclusion-free. One grain (z1) from this second population was analyzed. The other grains are all from the first population. CL images reveal relatively simple oscillatory-zoned cores with local rim overgrowths on some of the more irregularly shaped grains. There was no apparent correlation between the morphological populations and the dates obtained. The round, anhedral grain yielded a $^{207}\text{Pb}/^{206}\text{Pb}$ date of 2594.2 ± 1.9 Ma. The other grains yielded $^{207}\text{Pb}/^{206}\text{Pb}$ dates ranging from 2610 to 2529 Ma with varying degrees of discordancy (Fig. 14). Our interpretation of these data is that there were likely two episodes of zircon growth at *c.* 2.61 and *c.* 2.51 Ga with zircon representing physical mixtures of the two ages. The systematics of these data cannot be accounted for by 1.9 Ga disturbance or zircon growth.

SZ00-118E

This sample is similar petrologically to the previous sample. Zircon occurs as euhedral grains that are needle to ovoid in shape. However, CL images reveal a very complex internal structure (Fig. 10d). Most

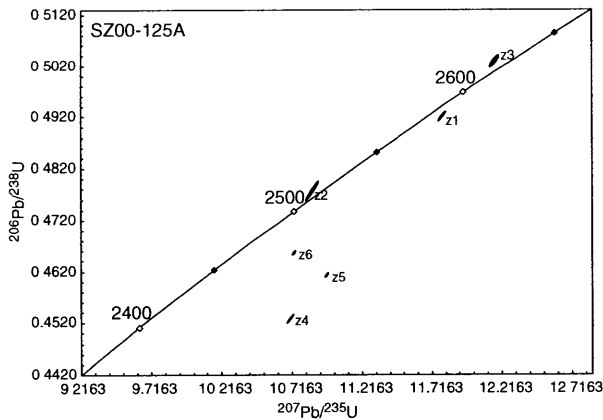


Fig. 14. U-Pb concordia diagram for Godfrey granite, SZ00-125 A. Error ellipses are 2σ .

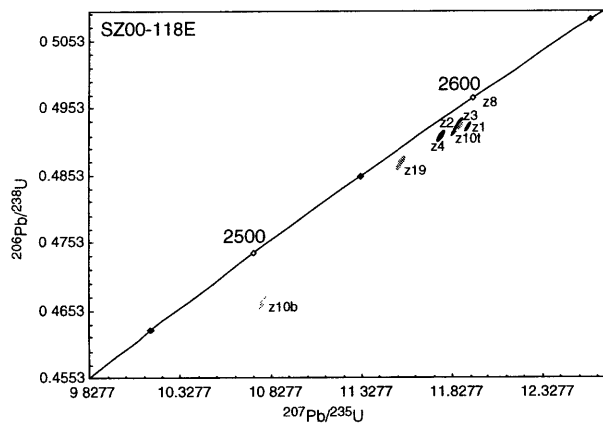


Fig. 15. U-Pb concordia diagram for Godfrey granite, SZ00-118E. Gray ellipses are from broken tip fragments. A representative CL image is shown in Fig. 10(d). Black ellipses are from whole, abraded grains. Note the overlap in $^{207}\text{Pb}/^{206}\text{Pb}$ dates. z10t and z10b are the top and bottom fragments from the same grain and define a discordia between *c.* 2637 and 1876 Ma, indicating episodic Pb loss at *c.* 1.9 Ga. Error ellipses are 2σ .

images show cores with substantial rim overgrowths. The core is generally oscillatory-zoned, whereas the rim lacks any zonation. Four abraded single zircon grains were analyzed from this sample. The first two grains (z1 & z2) are ovoid in shape and the other two grains (z3 & z4) are long (200–250 μm) needles. $^{207}\text{Pb}/^{206}\text{Pb}$ zircon dates form a cluster, ranging from 2611 to 2595 Ma and are moderately discordant (0.9–1.4%) (Fig. 15). In addition, the tips of four zircon grains that display substantial overgrowths in the CL images were plucked directly from the grain mounts and analyzed. These tips yield similar $^{207}\text{Pb}/^{206}\text{Pb}$ dates of 2610–2533 Ma, indicating that the rims are not dramatically younger metamorphic overgrowths but instead probably grew during igneous crystallization. Two fragments of tips (z10b & z10t) from the same zircon define a discordia between

c. 2.64 Ga and *c.* 1.88 Ga suggestive of episodic Pb-loss at *c.* 1.9 Ga, but not metamorphic growth. Taken at face value, the data from these two samples of Godfrey granite suggest relatively simple systematics and a minimum crystallization age of *c.* 2.61 Ga, with a possible metamorphic event at 2.53–2.51 Ga, and no evidence for new zircon growth at *c.* 1.9 Ga.

DISCUSSION

P-T history of the upper deck and Godfrey granite

One goal of this investigation was to establish and compare *P-T* paths for the upper deck mafic granulite and adjacent structurally underlying Godfrey granite. Thermobarometric constraints on both the felsic gneiss and the gneiss-hosted eclogitic garnet clinopyroxenite in the northern upper deck indicate minimum *P-T* conditions of 1.5 GPa and 1000 °C (Snoeyenbos *et al.*, 1995). The thermobarometric data presented here confirm that all lithological units in the northern upper deck, including the felsic gneiss, mafic granulite, and eclogitic clinopyroxenite, experienced this phase of high *P-T* metamorphism (>1.5 GPa, 900–1000 °C). New thermobarometric data from this study also show that this high *P-T* metamorphism was followed by near-isothermal decompression from >1.5 GPa to lower crustal conditions of approximately 0.9–1.0 GPa. This *P-T* path is similar to that reported by Kopf (1999) in a study of mafic granulite from the southern upper deck (1.2–1.4 GPa, 750–800 °C decompressing to 0.9 GPa, 700–750 °C); however, maximum pressures and temperatures recorded by mafic granulite in the northern upper deck are slightly higher.

Thermobarometric data from the Godfrey granite to the north (1.2 GPa, 860 °C) indicate that there is at least a 0.3 GPa discontinuity in peak metamorphic pressures across the upper deck-Godfrey granite contact, and a minimum difference in pressure of 0.5 GPa between the upper deck domain and other lithological units of the lower deck (1.0 GPa; Williams *et al.* 1995, 2000). Our interpretation for the history of this region is that the upper deck domain experienced a period of high *P-T* metamorphism (>1.5 GPa, 900–1000 °C) prior to its juxtaposition with the Godfrey granite and other domains of the lower deck.

The presence of relict orthopyroxene in the Godfrey granite is interpreted to indicate that it either crystallized or underwent an early metamorphism in the intermediate-pressure granulite field (1.0 GPa, 775 °C) prior to being metamorphosed in the high pressure granulite field (1.2 GPa, 860 °C). The igneous crystallization conditions in the Godfrey granite are comparable to those recorded in the Mary granite (1.0 GPa, 900 °C), which occurs along the northern margin of the Godfrey granite (Fig. 2) (Williams *et al.*, 2000). The Mary granite is interpreted to have been emplaced

at 900 °C and 1.0 GPa and records *P-T* conditions achieved during cooling of 750 °C and 1.0 GPa (Williams *et al.*, 2000). U–Pb dates of zircon from the Mary granite by Hanmer *et al.* (1994) of 2618 ± 4 and $2606 + 13/-11$ Ma indicate that the Mary granite is similar in age to the Godfrey granite. Compositionally and texturally, these two granites are very similar. These similarities in crystallization conditions, U–Pb zircon ages, and textures in the Godfrey and Mary granites suggests that they both may be part of the same suite of igneous intrusion and probably both crystallized at *c.* 1.0 GPa at *c.* 2.6 Ga. Unlike the Godfrey granite, however, the Mary granite does not record an increase in pressure following crystallization (see fig. 10 in Williams *et al.*, 2000 compared to Fig. 9 this study).

In terms of the relationship of *P-T* paths recorded in each of these lithologies, our interpretation is that the 1.2 GPa pressure recorded in the Godfrey granite is a consequence of loading the upper deck onto the Godfrey granite during the juxtaposition and thrusting of the upper deck rocks onto the Godfrey granite. The interpretation that the Godfrey granite initially crystallized and resided at 1.0 GPa prior to its juxtaposition with the upper deck is consistent with *P-T* data from the rest of the lower deck, which indicate pressures and temperatures in the 0.9–1.0 GPa, 750–850 °C range (Williams *et al.*, 1995, 2000). The second generation of orthopyroxene is interpreted to have formed via decompression due to subsequent isostatic adjustments.

Timing of high *P-T* metamorphism and juxtaposition of the upper and lower decks

The outstanding questions regarding the timing of events in the upper deck–Godfrey granite contact region include: (1) what is the timing of the high *P-T* metamorphism in the upper deck? (2) what is the crystallization age and timing of metamorphic events in the Godfrey granite? (3) what is the timing of the juxtaposition of the upper deck and Godfrey granite? We present two possible scenarios for the metamorphic evolution of this part of the Snowbird tectonic zone.

U–Pb data presented in this study show that there is evidence for accessory phase growth at *c.* 2.5 and 1.9 Ga in the upper deck mafic granulite. Zircon in the mafic granulites investigated in this study yields a wide range of $^{207}\text{Pb}/^{206}\text{Pb}$ dates, from 2531 to 1903 Ma. Two mafic granulites (SZ00–148A & SZ00–141A) show evidence for zircon growth at 1.9 Ga. The geochronological data for zircon from the mafic granulite sample SZ00–148A implies a mixing between a *c.* 2.5 Ga protolith and 1.9 Ga metamorphic growth that is supported by CL imaging of core/overgrowth relationships. In contrast, sample SZ00–141A has a population of 1.9 Ga zircon which is interpreted to have formed during peak high *P-T* conditions given

the inclusion of zircon within garnet and clinopyroxene and *P-T* conditions calculated for this sample (1.9 GPa, 960 °C). Taken at face value, these data suggest either (1) *c.* 2.55–2.52 Archean protolith ages overprinted by a high *P-T* Palaeoproterozoic metamorphism, or (2) high *P-T* metamorphism at *c.* 2.55–2.52 Ga and a second metamorphic event at 1.9 Ga.

Lower temperature chronometers provide constraints on the thermal magnitude and duration of the 1.9 Ga metamorphic event in the upper deck. Titanite from mafic granulite layers (SZ00–118C & SZ00–141A) in the upper deck is 1900–1894 Ma, and given the stability of titanite + plagioclase in SZ00–141A (Fig. 9), we believe that titanite formed during or shortly following the high *P-T* metamorphism. The titanite likely formed above its closure temperature but cooled from *c.* 960–650 °C in 4–10 Myr. Additional thermochronological constraints are given by rutile ages from the felsic gneiss, which indicate that the upper deck terrane cooled below *c.* 400 °C between 1890 and 1850 Ga (Baldwin *et al.*, 2000).

The U–Pb data presented here for the Godfrey granite indicate a crystallization age of *c.* 2.61 Ga. The range in dates and the moderate amount of discordance in zircon from samples SZ00–118E and SZ00–125A of Godfrey granite is most likely due to Pb loss associated with metamorphism soon after emplacement (*c.* 2.5 Ga). The Godfrey granite does not show any evidence for 1.9 Ga zircon growth nor has it undergone the high *P-T* metamorphism that the upper deck experienced. Petrological data suggest that the Godfrey granite records a loading effect from the juxtaposition with the upper deck. Because the Godfrey granite shows no evidence for the 1.9 Ga event, then it is likely that this juxtaposition did not occur until after 1.9 Ga. However, if the metamorphism of the Godfrey granite resulted from the juxtaposition of the upper deck, then the Godfrey granite might be expected to show some evidence of mineral growth or episodic Pb loss at *c.* 1.9 Ga or slightly later. This may be represented by the rim fragment U–Pb data from SZ00–118E in which two tip fragments from the same zircon grain suggest a lower intercept age of *c.* 1.9 Ga.

Previous geochronological constraints and summary of preferred model

Previous geochronological investigations in the EAmt yielded little evidence for Proterozoic metamorphism or deformation (Hanmer *et al.*, 1994, 1995a,b; Hanmer, 1997) and must be reconciled with the new data and interpretations arising from this study. First, the relatively high precision of the ages obtained from mafic granulite in this study (2.55–2.52 Ga) compared to the *c.* 2.6 Ga date reported by Hanmer (1997) indicate that this lithological unit is distinguishably younger than its host felsic gneiss and therefore could

not have experienced the 2.6 Ga granulite facies metamorphism and deformation that Hanmer (1997) reports. Second, the felsic gneiss into which the mafic granulite is intruded experienced an older metamorphic event at *c.* 2.62 Ga which is constrained by a monazite date from the felsic gneiss (Hanmer, 1997). However, the suggestion that this age reflects cooling through the closure temperature of monazite (Hanmer, 1997) should be reconsidered in light of new estimates for the closure temperature of Pb diffusion in monazite of ≥ 900 °C (Cherniak & Watson, 2001). Instead we interpret the 2.62 Ga monazite in the felsic gneiss to have formed along the prograde path during a Late Archean metamorphic event of unconstrained *P–T* conditions which did not exceed the closure temperature of monazite. In addition, the maximum age for the high *P–T* metamorphism and juxtaposition of the upper and lower decks was interpreted to be 2.55–2.52 Ga, contemporaneous with the age of the protolith or earliest metamorphism of the mafic granulite. However, our preferred interpretation based on the U–Pb data from mafic granulite SZ00–141A is that the highest *P–T* event occurred at *c.* 1904 Ma.

With the new geochronological data presented in this study, our preferred model for the evolution of this segment of the Snowbird tectonic zone is as follows. The felsic gneiss of the EAmt underwent an early metamorphic and deformational event at *c.* 2.62 Ga in the lower crust, and was later intruded by the protolith to the mafic granulite by 2.55–2.52 Ga. Then at 1.9 Ga the upper deck underwent high *P–T* metamorphism (>1.5 GPa), followed by decompression to 0.9–1.0 GPa. The pressure discontinuity recorded across the upper deck–Godfrey granite contact indicates that the lower deck did not undergo the same high *P–T* metamorphism. Juxtaposition of the upper deck and Godfrey granite would have occurred after or been related to this decompression. In this scenario, the high *P–T* rocks were exhumed relatively quickly following the high pressure metamorphism, given the 4–10 Myr difference between zircon and titanite dates in the mafic granulite. In contrast to other domains in the EAmt (Williams *et al.*, 1995), the upper deck shows little evidence for isobaric cooling paths (Kopf, 1999).

CONCLUSIONS

The main conclusions of this study are first that all three lithological units in the upper deck, including felsic gneiss, gneiss-hosted eclogitic clinopyroxenite and mafic granulite, experienced a high *P–T* event not seen in the adjacent Godfrey granite. Second, minimum conditions for this high *P–T* event are constrained at >1.5 GPa and 900–1000 °C, which was followed by near-isothermal decompression of the upper deck to *c.* 0.9–1.0 GPa. Juxtaposition of the upper deck and Godfrey granite likely

occurred at pressures of *c.* 0.9–1.0 GPa during decompression. Inferred igneous crystallization and possibly early metamorphic conditions in the Godfrey granite *c.* 2.5 Ga record intermediate-pressure granulite conditions (1.0 GPa, 775 °C), followed by *c.* 1.9 Ga metamorphism in the high pressure granulite field related to thrusting of upper deck rocks and resulting in transient pressures of 1.2 GPa followed by a return to intermediate-pressure granulite conditions.

Previous studies in the EAmt have concluded that granulite facies mylonitization occurred in the lower crust at *c.* 2.6 Ga in a transpressional shear zone setting (Hanmer *et al.*, 1994, 1995a,b), followed by long-term storage of these high *P–T* rocks in the lower crust for *c.* 700 My prior to their exhumation between *c.* 1.9–1.8 Ga. This study shows that, although these rocks may have resided in the lower crust at depths of *c.* 30 km for several hundred million years, they did not reside at depths corresponding to the high *P–T* conditions documented in this study for a protracted period of time. We conclude that there is an important 1.9 Ga high *P–T* metamorphic event in this segment of the Snowbird tectonic zone that overprints an earlier Archean metamorphism (*c.* 2.52–2.55 Ga), in which rocks that were metamorphosed at depths of *c.* 30 km *c.* 2.5 Ga were taken to depths of 50–60 km, followed by rapid exhumation. The precise timing and nature of the juxtaposition of the various domains of the EAmt is not yet certain, but we interpret it to have occurred following the high *P–T* metamorphism since the Godfrey granite does not show the high *P–T* overprint.

The implications for 1.9 Ga high *P–T* metamorphism in this part of the Canadian Shield are important for at least two major reasons. First, although this part of the Snowbird tectonic zone is contained within dominantly Archean rocks, it has experienced a major high *P–T* event in the Palaeoproterozoic, a type of metamorphism normally found exclusively in collisional settings. Second, remarkably, the age of this high *P–T* metamorphism falls between the ages of the bounding orogens on either side of the Rae (Taltson–Thelon, 2.02–1.91 Ga) and Hearne (Trans-Hudson, 1.91–1.81 Ga) cratons. An important question that this study raises is what the history of the rocks in the Snowbird Tectonic zone is between 2.5 and 1.9 Ga. Since the thermobarometric and thermochronological data is dominated by the 1.9 Ga event, there are as yet no firm constraints on the *P–T–t* path of these rocks during this time period. This is a crucial question to answer before developing a comprehensive model for the Snowbird tectonic zone. The data presented in this study suggests that aspects of both models for high pressure granulite formation, including collisional orogenesis and exhumation of lower crustal rocks by younger structures unrelated to their formation may be correct. The data presented in this study does not

directly answer the question as to whether the Snowbird tectonic zone represents an important collisional suture, but the style and timing of metamorphism and exhumation are most consistent with this tectonic setting.

ACKNOWLEDGEMENTS

We acknowledge support from NSF grant EAR-0001131 to S.A.B. and M.L.W. as well as a research grant from the Mineralogical Society of America to J.A.B. Thorough and constructive reviews by R. Berman, J. Martignole, and N. Wodicka greatly improved the manuscript. Special thanks go to A. Indares and J. Martignole for organizing this special volume on high pressure granulites.

REFERENCES

- Baer, A. J., 1969. The Precambrian geology of Fond-du-Lac map-area (74-0), Saskatchewan. *Geological Survey of Canada Paper*, **68-61**, 17p.
- Baldwin, J. A., Bowring, S. A. & Williams, M. L., 2000. A unique view of Archean lower crust. *EOS Transactions, American Geophysical Union*, **81**, 1250.
- Berman, R. G., 1990. Mixing properties of Ca-Mg-Fe-Mn garnets. *American Mineralogist*, **75**, 328-344.
- Berman, R. G., 1991. Thermobarometry using multi-equilibrium calculations: a new technique, with petrological applications. *Canadian Mineralogist*, **29**, 833-855.
- Berman, R. G. & Aranovich, L. Y., 1996. Optimized standard state and solution properties of minerals. I. Model calibration for olivine, orthopyroxene, cordierite, garnet, and ilmenite in the system FeO-MgO-CaO-Al₂O₃-TiO₂-SiO₂. *Contributions to Mineralogy and Petrology*, **126**, 1-24.
- Berman, R. G., Aranovich, L. Y. & Pattison, D. R. M., 1995. Reassessment of the garnet-clinopyroxene Fe-Mg exchange thermometer: II. Thermodynamic analysis. *Contributions to Mineralogy and Petrology*, **119**, 30-42.
- Carswell, D. A. & O'Brien, P. J., 1993. Thermobarometry and geotectonic significance of high-pressure granulites: Examples from the Moldanubian zone of the Bohemian Massif in lower Austria. *Journal of Petrology*, **34**, 427-459.
- Cherniak, D. J., 1993. Lead diffusion in titanite and preliminary results on the effects of radiation damage on Pb transport. *Chemical Geology*, **110**, 177-194.
- Cherniak, D. J. & Watson, E. B., 2001. The influence of diffusion on U-Pb systematics. *11th Annual V.M. Goldschmidt Conference*, Abstract 3260.
- Fuhrman, M. L. & Lindsley, D. H., 1988. Ternary-feldspar modeling and thermometry. *American Mineralogist*, **73**, 201-215.
- Goodacre, A. K., Grieve, R. A. F., Halpenny, J. F. & Sharpton, V. L., 1987. Horizontal gradient of the Bouguer gravity anomaly map of Canada, Canadian Geophysical Atlas, Map 5, Geological Survey of Canada, Ottawa.
- Green, D. H. & Ringwood, A. E., 1967. An experimental investigation of the gabbro to eclogite transformation and its petrological applications. *Geochimica Cosmochimica Acta*, **48**, 767-833.
- Hanchar, J. M. & Rudnick, R. L., 1995. Revealing hidden structures; the application of cathodoluminescence and back-scattered electron imaging to dating zircons from lower crustal xenoliths. *Lithos*, **36**, 289-303.
- Handy, M. R. & Zingg, A., 1991. The tectonic and rheological evolution of an attenuated cross section of the continental crust; Ivrea crustal section, southern Alps, northwestern Italy and southern Switzerland. *Geological Society of America Bulletin*, **103**, 236-253.
- Hanmer, S., 1994. Geology, East Athabasca mylonite triangle, Saskatchewan. In: *Geological Survey of Canada Map 1859A*.
- Hanmer, S., 1997. Geology of the Striding-Athabasca mylonite zone, northern Saskatchewan and southeastern District of Mackenzie, Northwest Territories. *Geological Survey of Canada Bulletin*, **501**, 1-92.
- Hanmer, S., Parrish, R., Williams, M. & Kopf, C., 1994. Striding-Athabasca mylonite zone: Complex Archean deep-crustal deformation in the East Athabasca mylonite triangle, northern Saskatchewan. *Canadian Journal of Earth Sciences*, **31**, 1287-1300.
- Hanmer, S., Williams, M. & Kopf, C., 1995a. Modest movements, spectacular fabrics in an intracontinental deep-crustal strike-slip fault: Striding-Athabasca mylonite zone, NW Canadian Shield. *Journal of Structural Geology*, **17**, 493-507.
- Hanmer, S., Williams, M. & Kopf, C., 1995b. Striding-Athabasca mylonite zone: implications for the Archean and Early Proterozoic tectonics of the western Canadian Shield. *Canadian Journal of Earth Sciences*, **32**, 178-196.
- Hoffman, P. F., 1988. United Plates of America, the birth of a craton: Early Proterozoic assembly and the growth of Laurentia. *Annual Reviews of Earth and Planetary Science Letters*, **16**, 543-603.
- Indares, A., 1995. Metamorphic interpretation of high-pressure-temperature metapelites with preserved growth zoning in garnet, eastern Grenville Province, Canadian Shield. *Journal of Metamorphic Geology*, **13**, 475-486.
- Indares, A. & Dunning, G. R., 1997. Coronitic metagabbro and eclogite from the Grenville Province of western Quebec; interpretation of U-Pb geochronology and metamorphism. *Canadian Journal of Earth Sciences*, **34**, 891-901.
- Indares, A. & Dunning, G., 2001. Partial melting of high-P-T metapelites from the Tshenukutish terrane (Grenville Province): Petrography and U-Pb geochronology. *Journal of Petrology*, **42**, 1547-1565.
- Indares, A., Dunning, G., Cox, R., Gale, D. & Connelly, J., 1998. High-pressure, high-temperature rocks from the base of thick continental crust: Geology and age constraints from the Manicouagan Imbricate Zone, eastern Grenville Province. *Tectonics*, **17**, 426-440.
- Kopf, C. F., 1999. Deformation, metamorphism, and magmatism in the East Athabasca mylonite triangle, northern Saskatchewan: implications for the Archean and Early Proterozoic crustal structure of the Canadian Shield, *University of Massachusetts*, Unpublished PhD Thesis.
- Krogh, T. E., 1973. A low contamination method for hydrothermal decomposition of zircon and extraction of U and Pb for isotopic age determinations. *Geochimica et Cosmochimica Acta*, **37**, 485-494.
- Krogh, T. E., 1982. Improved accuracy of U-Pb zircon ages by the creation of more concordant systems using an abrasion technique. *Geochimica et Cosmochimica Acta*, **46**, 637-649.
- Kröner, A., O'Brien, P. J., Nemchin, A. A. & Pidgeon, R. T., 2000. Zircon ages for high pressure granulites from South Bohemia, Czech Republic, and their connection to Carboniferous high temperature processes. *Contributions to Mineralogy and Petrology*, **138**, 127-142.
- Liu, Y. & Zhong, D., 1997. Petrology of high-pressure granulites from the eastern Himalayan syntaxis. *Journal of Metamorphic Geology*, **15**, 451-466.
- Mahan, K. H., Williams, M. L., Baldwin, J. A. & Bowring, S. A., 2001. Juxtaposition of deep crustal and middle crustal rocks across the Legs Lake shear zone in northern Saskatchewan. Summary of Investigations 2001. *Saskatchewan Geological Survey, Sask. Energy Mines Miscellaneous Report 2001-4.*, **2** (2), 76-86.
- Mariano, A. N., 1989. Cathodoluminescence emission spectra of rare earth element activators in minerals. In: *Geochemistry and Mineralogy of Rare Earth Elements, Reviews in Mineralogy 21*

- (eds Lipin, B. R. & McKay, G. A.), pp. 339–348. Mineralogical Society of America.
- O'Brien, P. J. & Carswell, D. A., 1993. Tectonometamorphic evolution of the Bohemian Massif: evidence from high pressure metamorphic rocks. *Geologische Rundschau*, **82**, 531–555.
- Percival, J. A. & Card, K. D., 1983. Archean crust as revealed in the Kapuskasing Uplift, Superior Province, Canada. *Geology*, **11**, 323–326.
- Percival, J. A. & McGrath, P. H., 1986. Deep crustal structure and tectonic history of the northern Kapuskasing Uplift of Ontario; an integrated petrological-geophysical study. *Tectonics*, **5**, 553–572.
- Percival, J. A. & West, G. F., 1994. The Kapuskasing Uplift; a geological and geophysical synthesis. *Canadian Journal of Earth Sciences*, **31**, 1256–1286.
- Sanborn-Barrie, M., Carr, S. D. & Theriault, R., 2001. Geochronological constraints on metamorphism, magmatism, and exhumation of deep-crustal rocks of the Kramanitar Complex, with implications for the Paleoproterozoic evolution of the Archean western Churchill Province, Canada. *Contributions to Mineralogy and Petrology*, **141**, 592–612.
- Slimmon, W. L., 1989. Compilation bedrock geology Fond-du-Lac. *NTS Area 74-0, Saskatchewan Geological Survey, Map247A*, **1**, 250000.
- Snoeyenbos, D. R., Williams, M. L. & Hanmer, S., 1995. Archean high-pressure metamorphism in the western Canadian Shield. *European Journal of Mineralogy*, **7**, 1251–1272.
- Stacey, J. S. & Kramers, J. D., 1975. Approximation of terrestrial lead isotope evolution by a two-stage model. *Earth and Planetary Science Letters*, **26**, 207–221.
- Stern, R. A. & Berman, R. G., 2001. Monazite U-Pb and Th-Pb geochronology by ion microprobe, with an application to in situ dating of an Archean metasedimentary rock. *Chemical Geology*, **172**, 113–130.
- Vavra, G., Gebauer, D., Schmid, R. & Compston, W., 1996. Multiple zircon growth and recrystallization during polyphase Late Carboniferous to Triassic metamorphism in granulites of the Ivrea Zone (Southern Alps); an ion microprobe (SHRIMP) study. *Contributions to Mineralogy and Petrology*, **122**, 337–358.
- Vielzeuf, D. & Pin, C., 1989. Geodynamic implications of granulitic rocks in the Hercynian Belt. *Geological Society Special Publications*, **43**, 343–348.
- Williams, M. L., Hanmer, S., Kopf, C. & Darrach, M., 1995. Syntectonic generation and segregation of tonalitic melts from amphibolite dykes in the lower crust, Striding-Athabasca mylonite zone, northern Saskatchewan. *Journal of Geophysical Research*, **100**, 15717–15734.
- Williams, M. L., Melis, E. A., Kopf, C. & Hanmer, S., 2000. Microstructural tectonometamorphic processes and the development of gneissic layering: a mechanism for metamorphic segregation. *Journal of Metamorphic Geology*, **18**, 41–57.
- Zhao, G. C., Cawood, P. A., Wilde, S. A. & Lu, L. Z., 2001. High-pressure granulites (retrograded eclogites) from the Hengshan Complex, North China craton: Petrology and tectonic implications. *Journal of Petrology*, **42**, 1141–1170.
- Zingg, A., 1990. The Ivrea crustal cross-section (northern Italy and southern Switzerland). Exposed cross-sections of the continental crust; proceedings. *NATO Advanced Study Institute on Exposed Cross-Sections of the Continental Crust*, 317, 1–19.

Received 28 December 2001; revision accepted 13 August 2002.

Appendix 1: Uncertainties in Thermobarometry and Choice of Solution Models

The development of geothermobarometry over the past few decades has allowed petrologists to quantify the conditions of metamorphism, leading to a better understanding of tectonic processes. But the question still remains as to how accurate the data are, since the uncertainties in pressure and temperature estimation are rarely reported, largely because it can be difficult to identify the sources of errors. Such sources for uncertainties may include: the accuracy of the experimentally determined end-member reaction, volume measurement errors (for net transfer barometers), analytical imprecision of mineral analyses using an electron microprobe, thermometer calibration errors, variation in activity models for minerals such as garnet and plagioclase, and compositional heterogeneity of natural minerals. Two of the most significant sources of error are the analytical imprecision of the analysis and the systematic errors associated with experimental calibrations (Hodges & McKenna, 1987). Below, I explore the former in an estimation of the uncertainty in pressure and temperature on the P-T calculations for the mafic granulites. It is important to note that by using comparative thermobarometry, some of these systematic errors can be avoided, and result in precise calculations of the relative difference in P-T conditions recorded by different samples.

The analytical uncertainties associated with an electron microprobe analysis are of two types. The first is the standardization, X-ray counting, and correction uncertainties. The second are variations in chemical composition that are associated with varying scales of domainal equilibrium. The latter involves careful compositional mapping prior to analysis in order to choose areas that are in compositional equilibrium. Careful characterization like this can avoid many of the pitfalls that plagued early thermobarometric studies. The analysis below propagates the analytical uncertainties associated with the analysis thus providing a minimum estimate of the precision of a P-T calculation for three mafic granulite samples presented in Baldwin et al. (2003).

The method used in the error analysis follows the method outlined by Hodges & McKenna (1987). First, I assumed a conservative uniform 2% analytical uncertainty on the oxide measurements from the electron microprobe data. Errors were propagated to calculate the uncertainty in the mole fractions that were input into the solution models. A

Monte Carlo approach to the calculation of the compositional uncertainties was followed by the method of Hodges & McKenna (1987). The results of this analysis are shown in Table 1 and Figure 2.

Table 1. P-T results

Sample	Pressure (kbar)	$\pm 1\sigma$	Temperature ($^{\circ}\text{C}$)	$\pm 1\sigma$
SZ00-141A	17.6	1.7	950	55
SZ00-118C	14.0	1.4	874	42
SZ00-148A	9.6	1.1	785	48

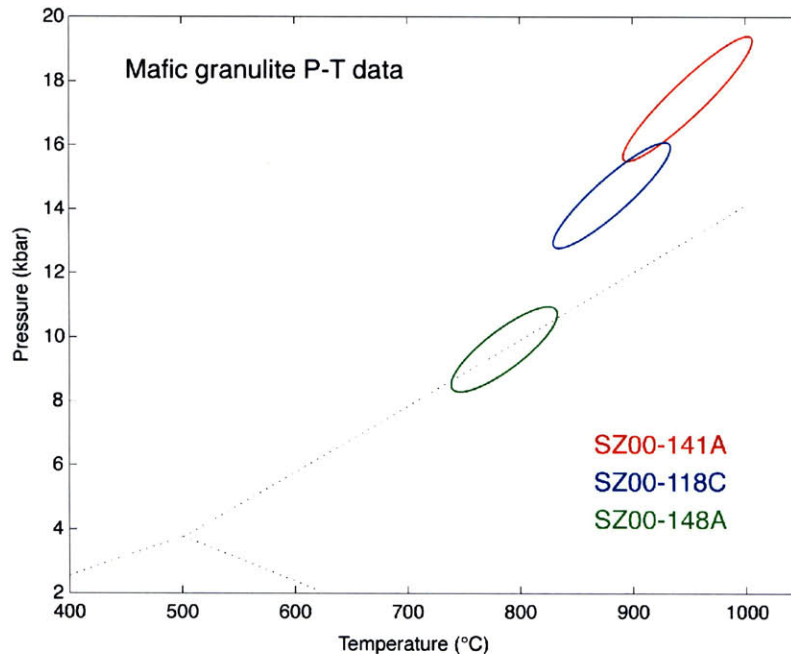


Figure 1. P-T diagram for mafic granulites. Error ellipse reflects precision on the electron microprobe analysis calculated following the method of Hodges and McKenna (1987).

For these calculations, I used the garnet-clinopyroxene exchange thermometer of Berman et al. (1995) using the Berman (1990) solution model for garnet, and non-ideal Mg-Fe-Al interactions for clinopyroxene given by Berman & Aranovich (1996). The garnet-clinopyroxene-plagioclase-quartz barometer of Pattison & Newton was used with the feldspar solution model of Elkins & Grove (1990).

This can be compared to the output from the TWQ computer program given in Table 1 of Baldwin et al. (2003). The temperatures and pressures calculated using the above calibrations and solution models differ slightly, which highlights the importance of being consistent in one's choice of geothermobarometers and solution models. The relative difference using each of these techniques is similar, however there are systematic differences of ~10-35°C and 0.4-2 kbar. However, within the analytical uncertainty on the microprobe analysis these two methods agree.

The choice of solution models and particular calibrations in geothermobarometry is important, as there are many to choose from, and understanding the similarities, and magnitude of the differences is important. In choosing solution models and calibrations, I routinely used a variety of thermometers and barometers, focusing on those that are currently in use in the literature. There have been numerous reevaluations of thermobarometers in recent years, due to more sophisticated experiments and better thermodynamic data (e.g., Pattison et al., 2003). There are certain standards in the literature that have prevailed through time, particularly with regard to eclogite facies rocks. The calibration of Holland (1980) for the Jd + Qtz = Ab barometer is most frequently used for pressure estimation in eclogites, and can be useful to apply when comparing one's data to other eclogites from the literature. The choice of calibrations and solution models is very particular to the problem being addressed, and it is most important to maintain consistency within a single study so that relative differences among related samples can be addressed.

References

- Baldwin, J. A., Bowring, S. A. & Williams, M. L., 2003. Petrological and geochronological constraints on high pressure, high temperature metamorphism in the Snowbird tectonic zone, Canada. *Journal of Metamorphic Geology*, **21**, 81-98.
- Berman, R. G., 1990. Mixing properties of Ca-Mg-Fe-Mn garnets. *American Mineralogist*, **75**(3-4), 328-344.
- Berman, R. G. & Aranovich, L. Y., 1996. Optimized standard state and solution properties of minerals: I. Model calibration for olivine, orthopyroxene, cordierite, garnet, and ilmenite in the system FeO-MgO-CaO-Al₂O₂-TiO₂-SiO₂. *Contributions to Mineralogy and Petrology*, **126**, 1-24.
- Berman, R. G., Aranovich, L. Y. & Pattison, D. R. M., 1995. Reassessment of the Garnet-Clinopyroxene Fe-Mg Exchange Thermometer; 2. Thermodynamic Analysis. *Contributions to Mineralogy and Petrology*, **119**(1), 30-42.

- Elkins, L. T. & Grove, T. L., 1990. Ternary feldspar experiments and thermodynamic models. *American Mineralogist*, **75**, 544-559.
- Hodges, K. V. & McKenna, L. W., 1987. Realistic propagation of uncertainties in geologic thermobarometry. *American Mineralogist*, **72**, 671-680.
- Holland, T. J. B., 1980. The reaction albite = jadeite + quartz determined experimentally in the range 600-1200°C. *American Mineralogist*, **65**, 129-134.
- Pattison, D.R.M., Chacko, T., Farquhar, J., & McFarlane, C.R.M. 2003. Temperatures of granulite-facies metamorphism: constraints from experimental phase equilibria and thermobarometry corrected for retrograde exchange. *Journal of Petrology*, **44**, 867-900.

Appendix 2: Diffusion during cooling in granulites

Chemical diffusivities are sufficiently rapid at high temperatures of metamorphism for most minerals to homogenize. It is therefore appropriate to assume as a starting point homogeneous minerals during peak metamorphism. Whether minerals continue to re-equilibrate during cooling and decompression is a function of both the cooling rate and grain size. For example, a 5-mm-diameter garnet in a rock that is exhumed 10 km without significant cooling will equilibrate more slowly than a 1-mm-diameter garnet in the same rock. How much more slowly is an important question since diffusion rates are dependent on grain size. In thermobarometry, garnet of differing grain sizes is typically used, and depending on the choice of compositions, one could be looking at garnet that equilibrated at significantly different times in the history of the rock. In order to examine this problem, I used the FeMg⁻¹ diffusion data of Freer & Edwards (1999) with a $D = 1.22 \times 10^{-6} \exp(-270.4 \text{ kJ/RT}) \text{ m}^2 \text{ s}^{-1}$. The characteristic length scale for diffusion is given by the equation $x = (Dt)^{1/2}$. Figure 1 shows a plot of temperature versus time for grain sizes ranging from 1-5 mm, grain sizes that are typical of the mafic granulites examined in this study. This diagram shows that at the temperatures calculated by the Grt-Cpx exchange thermometer (900-1000°C), diffusion occurs very rapidly such that garnet in the 1-5 mm range will re-equilibrate in < 1 Ma. As the rock cools, however, diffusion rates decrease significantly such that at ~800°C, the garnet will re-equilibrate over progressively longer timescales of a few Ma to ~10 Ma.

This simple calculation shows that for the rate of decompression calculated for the Snowbird mafic granulites of ~1 km/Ma, that garnet would equilibrate over the entire decompression path. Thus the composition of garnet preserved is likely related to equilibration at some point along the retrograde path, not the composition during the peak of metamorphism. Once the rock cooled below ~800°C, diffusion rates decrease and the composition of the garnet would equilibrate on timescales that are much longer than the timescale for the decompression of these rocks. The implications for this are that the “peak” pressures and temperatures calculated are likely minimums and evidence for the maximum P-T conditions in these rocks is likely lost because of the fast diffusion and re-equilibration of garnet along the entire retrograde path.

References

Freer, R., & A. Edwards, 1999, An experimental study of Ca-(Fe,Mg) interdiffusion in silicate garnets. *Contributions to Mineralogy and Petrology*, **134**, 370-379.

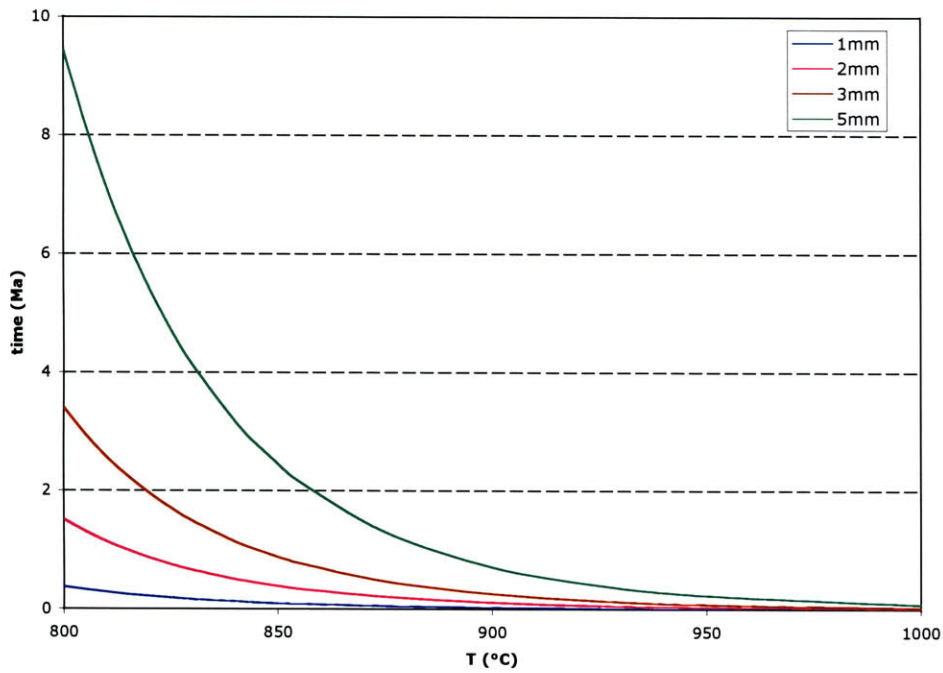


Figure 1. Plot of time versus temperature showing the characteristic lengthscale of diffusion for garnet of varying radii. Calculated using the FeMg^{-1} diffusion coefficient of Freer & Edwards (1999).

Chapter 3

Eclogites of the Snowbird tectonic zone: evidence for Paleoproterozoic high-pressure metamorphism in the western Canadian Shield

Submitted to Contributions to Mineralogy and Petrology, May 2003

*Julia A. Baldwin and Samuel A. Bowring
Department of Earth, Atmospheric and Planetary Sciences,
Massachusetts Institute of Technology, Cambridge, MA 02139*

*Michael L. Williams
University of Massachusetts, Department of Geosciences, Amherst, MA 01003*

*Ian S. Williams
Research School of Earth Sciences, The Australian National University
Canberra, ACT 0200, Australia*

Abstract

The past decade has seen considerable controversy surrounding the relative importance of Archean and Paleoproterozoic deformation and metamorphism of the Snowbird tectonic zone, Canada. Two end-member models have emerged: one suggests a *ca.* 1.9 Ga reactivation of what has been inferred to be an Archean boundary, and the other that the Snowbird tectonic zone records a Paleoproterozoic collision. This contribution addresses this controversy in a petrological and geochronological study of eclogites that occur in the East Athabasca mylonite triangle, northern Saskatchewan. In addition to eclogite, this area contains a variety of lower crustal high-pressure rocks that record a complex metamorphic history from 2.6 to 1.9 Ga. The eclogites occur at the boundary between the Archean Rae and Hearne Provinces of the western Canadian Shield. Temperatures are constrained by garnet-clinopyroxene exchange thermometry at 920-1000°C. At these temperatures, minimum pressure conditions in the eclogite are recorded by the $Jd + Qtz = Ab$ geobarometer at 1.8-2.0 GPa. A near-isothermal decompression path to granulite facies conditions is inferred from retrograde reaction textures. U-Pb IDTIMS zircon geochronology of the eclogite yields a weighted mean $^{207}\text{Pb}/^{206}\text{Pb}$ date of 1904.2 ± 0.2 Ma, which we interpret as the time of eclogite facies metamorphism. SHRIMP analyses of zircons included within omphacitic clinopyroxene support this interpretation with a weighted mean $^{207}\text{Pb}/^{206}\text{Pb}$ date of 1903.3 ± 9.6 Ma ($1-\sigma$). Inclusion suites of high-pressure phases, sector-zoning patterns, and the petrographic setting of zircon are a direct link between zircon growth and eclogite facies metamorphism. Zircon from one eclogite sample has older cores that are 2.54 Ga, which is a minimum age for the emplacement or earliest metamorphism of the gabbroic protolith. U-Pb rutile data indicate slow cooling at $\sim 1^\circ\text{C}/\text{Ma}$ below $\sim 500^\circ\text{C}$ from 1.88 to 1.85 Ga. The formation and exhumation of the eclogites *ca.* 1.9 Ga has important implications for the tectonic significance of the Snowbird tectonic zone during the Paleoproterozoic. The eclogites described here are consistent with a model of transport of continental crust to mantle depths during the Paleoproterozoic, followed by rapid buoyancy-driven exhumation to normal lower crustal depths.

Key words: eclogite, geochronology, geothermobarometry, reaction texture, Snowbird tectonic zone, zircon

1. Introduction

Eclogites form under a wide range of P - T conditions in deeply subducted oceanic and continental crustal rocks, as well as under ambient lower crustal and upper mantle conditions. During the past decade there has been an emphasis on the classification of eclogites based on a temperature subdivision of high ($>900^{\circ}\text{C}$), medium (550 - 900°C), and low ($<550^{\circ}\text{C}$) (Carswell, 1990). These temperature subdivisions broadly correlate with geological settings of the upper mantle/lower crust, tectonically thickened continental crust, and subducted oceanic crust, respectively. Experimental studies of phase equilibria indicate that eclogite mineral assemblages should be stable in the lower crust and upper mantle of cratonic areas (Ellis & Maboko, 1992; Green & Ringwood, 1967; Green & Ringwood, 1972). The extrapolation of the experimental data of Green & Ringwood (1967) to the range of probable geothermal gradients in cratonic regions predicts that the lower crust should consist of a mixture of eclogites and granulites. However, this prediction is difficult to verify through direct observation. Many uplifted deep crustal sections (e.g. the Ivrea Zone and Kapuskasing Uplift) contain mafic granulites but not eclogites (Fountain, 1976; Percival & Card, 1983). However, these sections typically do not extend to the base of the crust, and maximum pressures calculated are typically ≤ 1.0 GPa corresponding to ~ 30 km depth. In contrast, xenoliths of eclogite of lower crustal and upper mantle origin are common in kimberlites, are typically associated with granulite xenoliths, and can record temperatures $\geq 800^{\circ}\text{C}$, implying depths of 100 km or more, assuming a conductive cratonic geotherm (Griffin et al., 1990). Reaction textures in these eclogites are often indicative of isobaric cooling paths that are consistent with the evolution from gabbro to granulite to eclogite with declining temperature (Griffin et al., 1990).

In contrast, orogenic eclogites that form in tectonically thickened crust typically fall into the medium temperature classification and commonly preserve isothermal decompression P - T paths that are apparent through reaction textures and mineral zoning. These eclogites that form through the processes of plate collision and subduction are often cited as evidence for modern-style plate tectonic processes. The temporal

CHAPTER 3 – ECLOGITES OF THE SNOWBIRD TECTONIC ZONE

distribution of eclogite facies metamorphism in the geologic record has thus been proposed as a proxy for the onset of "modern" plate tectonics (Ernst, 1972; Maruyama & Liou, 1998; Maruyama et al., 1996). The paucity of eclogites older than *ca.* 550 Ma has been inferred by some to be indicative of higher heat production/steeper geotherms in the Precambrian and thus the lack of high-P, low-T environments required for the formation of eclogite. Documented examples of such "old" collisional eclogites include the 620 Ma Mali ultrahigh-pressure (UHP) eclogites in West Africa (700-750°C, >2.7 GPa) (Caby, 1994; Caby et al., 1981; Jahn et al., 2001), *ca.* 1.1 Ga eclogites from the eastern Grenville Province in Canada (700-750°C, 1.2-1.4 GPa) (Indares, 1993; Indares & Dunning, 1997), and *ca.* 2 Ga eclogites in the Usagaran belt of Tanzania (750°C, 1.8 GPa), which are the oldest documented occurrence of subduction-related eclogites (Möller et al., 1995).

The occurrence of Precambrian eclogites provides important constraints on possible secular changes in the thermal structure of collisional zones. First, it has been argued by some that the rarity of HP and UHP rocks in the Precambrian may be ascribed to higher heat production and heat flow, which prevented the formation and survival of deeply subducted cold plates (Jahn et al., 2001; Maruyama & Liou, 1998). This is at odds with xenolith data that have been interpreted as evidence for Archean subduction and formation of eclogite ~3.4 Ga in the Man Shield, West Africa (Barth et al., 2002). The lack of blueschists and eclogites in the Precambrian has encouraged caution in a simple application of Phanerozoic-style plate tectonic models (Maruyama et al., 1996), although their paucity may instead reflect the low preservation potential of these rocks (Möller et al., 1995).

In this paper, we document the *P-T* evolution, geochemistry, and geochronology of an occurrence of eclogite in the Snowbird tectonic zone (STZ), northern Saskatchewan, Canada. The STZ is a dramatic, regional northeast-trending positive linear anomaly in the horizontal gravity gradient map of the Canadian Shield, which extends from the Canadian Rocky Mountains to the coast of Hudson Bay (Fig. 1) (Goodacre et al., 1987; Hanmer et al., 1995b). Since its original definition and interpretation as a Proterozoic suture (Hoffman, 1988), this enigmatic structure has been

CHAPTER 3 – ECLOGITES OF THE SNOWBIRD TECTONIC ZONE

alternatively interpreted as a Proterozoic escape structure (Hoffman, 1989), an Archean suture with Proterozoic reactivation (Hanmer et al., 1994), and an Archean suture with Archean reactivation (Hanmer et al., 1994; Hanmer et al., 1995a; Hoffman, 1989). The STZ is clearly a fundamental lithospheric-scale structure in the western Canadian Shield, but its significance for the architecture and history of Laurentia has remained elusive.

The eclogite occurs near the boundary between the Rae and Hearne Archean crustal provinces within the Striding-Athabasca segment of the STZ (Hanmer et al., 1994), and within a 400 km² terrane of high-pressure granulite facies rocks that has experienced minimum metamorphic conditions of 900-1000°C, >1.5 GPa (Baldwin et al., 2003; Snoeyenbos et al., 1995). The discovery of this eclogite was first reported by Snoeyenbos et al. (1995), who inferred that the eclogite facies metamorphism formed in an intraplate setting during the Archean (*ca.* 2.6 Ga). However, this was based on geochronological data from the host felsic gneiss to the eclogite that record a complex and uncertain metamorphic history from 2.6 to 1.9 Ga. This contribution reports precise U-Pb zircon geochronological data that constrain the timing of eclogite facies metamorphism to 1904 Ma and discusses the implications of this date both for the geological setting for the formation of this eclogite as well as the tectonic evolution of the western Canadian Shield.

2. Geological Setting

In northern Saskatchewan, a well-exposed 125 x 80 x 75 km segment of the STZ has been described as the East Athabasca mylonite triangle (EAmt) (Tantato Domain of Gilboy, 1978), and consists of anastomosing lower crustal granulite facies mylonites (Hanmer, 1994; Hanmer, 1997; Hanmer et al., 1994; Hanmer et al., 1995a; Hanmer et al., 1995b). The EAmt is the southwestern segment of the Striding-Athabasca mylonite zone that has been interpreted as an Archean intra-continental strike-slip shear zone (Hanmer, 1994; Hanmer, 1997; Hanmer et al., 1994; Hanmer et al., 1995a; Hanmer et al., 1995b). Based on field and structural studies, the EAmt has been divided into three tectonic domains, each with distinct rock types, structures, and *P-T* histories (Fig. 2a). The southern domain (or “upper deck”) of the EAmt is a 400 km² terrane of high-pressure

CHAPTER 3 – ECLOGITES OF THE SNOWBIRD TECTONIC ZONE

granulite and eclogite facies rocks (Fig. 2b) that consists of garnet-kyanite quartzofeldspathic gneiss, mafic two-pyroxene garnet granulite, and eclogite with associated sapphirine granulites. Minimum P - T conditions of 1.5-1.9 GPa and 900-1000°C have been documented in the felsic gneiss and mafic granulites (Baldwin et al., 2003; Snoeyenbos et al., 1995), although the timing has been difficult to constrain. The northwestern domain is dominated by felsic to mafic plutonic rocks, the largest of which is the *ca.* 2.6 Ga Mary granite. Williams et al. (2000) concluded that the Mary granite was synchronously emplaced, metamorphosed and deformed at 1.0 GPa. The southeastern domain of the EAmt is dominated by the *ca.* 3.0-3.2 Ga Chipman tonalite batholith and the 1.9 Ga Chipman mafic dike swarm (Flowers et al., 2002). The Chipman dike swarm consists of 1 to 100 m thick amphibolite dikes that were metamorphosed and partially melted at granulite facies conditions (Williams et al., 1995). Thermobarometry from the Chipman dikes have yielded metamorphic pressures and temperatures of 1.0 GPa and 750-850 C (Williams et al., 1995).

The southern domain eclogite is preserved as a single concordant ~10-15 m-thick sheet that is semi-continuous and traceable for a minimum of 10 km (Fig. 2b). The eclogite is coarse-grained, consisting of garnet-omphacite, with minor kyanite, pargasite, orthopyroxene, and spinel. It is typically slightly discordant to the foliation in the host gneiss. Within the eclogite are veins of interlayered sillimanite and orthopyroxene that display reaction textures involving peraluminous sapphirine, spinel, corundum, and anorthite. At the margin of the eclogite, where it is in contact with felsic gneiss, there is a 1-2 m-wide zone of garnet-kyanite-quartz granulites with well-preserved decompressional reaction textures involving the breakdown of kyanite to form peraluminous sapphirine, spinel, and anorthite symplectites and the breakdown of garnet to orthopyroxene + plagioclase.

The felsic granulites that host the eclogite have had a complex metamorphic history from 2.6 to 1.9 Ga. U-Pb geochronological data from monazite in the felsic gneiss indicate that the felsic gneiss experienced an early protracted granulite facies event starting at 2.62 Ga with metamorphic zircon growth at ~2.58-2.53 Ga (Baldwin, unpublished data). Garnet zoning profiles in the felsic gneiss indicate a substantial

CHAPTER 3 – ECLOGITES OF THE SNOWBIRD TECTONIC ZONE

increase in pressure during growth of garnet rims, which we interpret to reflect an increase in pressure conditions following the early granulite metamorphism. This likely coincides with the high-pressure metamorphic event that produced the eclogite.

3. Whole Rock Geochemistry

Four samples of eclogite were analyzed for major and trace elements (Table 1). Sample locations are shown in Figure 2. The analyses were obtained by XRF analysis for major elements and ICPMS for trace elements. The four samples have a limited range of major element concentrations, and are basaltic in composition with SiO₂ ranging from 42.8% to 45.1%. All four samples are high in Al (18.3-20.4 wt.%) with Mg/Mg+Fe²⁺ ranging from 0.71-0.76. Total REE abundances are relatively low and show an enrichment in LREE ((La/Yb)_N=3.44-8.79) (Fig. 3). Pronounced positive Eu anomalies in three of the samples suggest that plagioclase fractionation was involved in their origin, and that the protolith of the eclogites did not crystallize from a primary mantle melt. The high Al content, positive Eu anomaly, and LREE fractionation are consistent with a low-P (<1.0 GPa) plagioclase cumulate source for the eclogite protolith. This interpretation is consistent with normative calculations, which indicate 46-52% anorthite. Based on the projection into the Cpx-Ol-Pl ternary system, the protolith may be classified as a troctolite or troctolitic gabbro, with minor clinopyroxene. Numerous examples of eclogites with similar geochemistry and REE patterns showing LREE enrichment and positive Eu anomalies have been described in the literature (Brastad, 1985; Gebauer et al., 1985; Kornprobst et al., 1990; O'Brien & Vrána, 1995; Paquette et al., 1989) and have also been interpreted as being derived from a plagioclase cumulate source.

4. Petrography and Mineral Chemistry

The high-P mineral assemblage in the eclogite includes garnet, omphacite, kyanite, rutile, zoisite, and quartz. The eclogites have a granoblastic texture and relative grain size and mineral proportions vary significantly on the outcrop scale. The degree of overprinting by hydrous phases or breakdown reactions also varies considerably, but within a single outcrop the degree of preservation is relatively constant. Retrograde

CHAPTER 3 – ECLOGITES OF THE SNOWBIRD TECTONIC ZONE

mineral reactions have produced plagioclase, orthopyroxene, secondary clinopyroxene, phlogopite, pargasite, spinel, and sapphirine.

4.1 Garnet

Garnet is anhedral and ranges in size from <0.5 mm to several mm in diameter (Fig. 4a-c). Most eclogites contain a high ratio of garnet to clinopyroxene (>50%). Inclusions are common in garnet. Garnet in the kyanite-bearing eclogites invariably have cores rich in inclusions of kyanite ± zoisite and locally contain thin, 1-3 µm-wide needles of rutile (Fig. 5a,b). The inclusions are typically confined to the cores of the garnet and do not extend to the outer few hundred micron rim areas. Kyanite inclusions are oval to elongate in shape and usually show preferred alignment within single crystals. Zoisite inclusions are typically larger than coexisting kyanite inclusions. This inclusion pattern of kyanite + zoisite is similar to that seen in garnet growing in domains of plagioclase breakdown in metagabbros (O'Brien, 1993; O'Brien et al., 1992; O'Brien & Vrána, 1995). Kyanite-absent eclogites usually have rounded inclusions of quartz and rutile, and invariably contain abundant needles of rutile. Less common inclusions are omphacitic clinopyroxene and phlogopite.

Representative garnet analyses are given in Table 2. There is a compositional range in garnet with cores of $\text{Alm}_{33-23}\text{Prp}_{43-55}\text{Grs}_{17-29}$ and rims of $\text{Alm}_{41-23}\text{Prp}_{38-52}\text{Grs}_{21-25}$. Garnet is typically unzoned with X_{Mg} decreasing at the rim. An exception to this involves garnet cores that are rich in kyanite inclusions. The area around the inclusions shows an increase in X_{Ca} and decrease in X_{Mg} near the inclusions, with garnet rims that have higher X_{Mg} and lower X_{Ca} . Within a single thin section, X_{Ca} decreases slightly from cores of garnet containing inclusions to inclusion-free rims. The most pyrope-rich garnet typically occurs in samples with the least Jd-rich omphacite. Kyanite-bearing eclogites tend to preserve the least Mg-rich, most Ca-rich garnet and most Jd-rich omphacite.

Garnet rims have reacted to form either a pargasite + plagioclase symplectite or complex symplectite of orthopyroxene + plagioclase and clinopyroxene + spinel + orthopyroxene symplectite, depending on the availability of water to form amphibole (Fig. 4c,d and 5c,d). These textures are described below.

4.2 Clinopyroxene

CHAPTER 3 – ECLOGITES OF THE SNOWBIRD TECTONIC ZONE

Sodic clinopyroxene is present in all eclogite samples, but there is a large variation in degree of preservation, grain size, and modal abundance. The most sodic clinopyroxene preserved in unzoned cores is omphacite with a composition of Jd_{23} (~4 wt% Na_2O) (Table 3). A decrease in X_{Jd} occurs in the outer region of the grain where the Cpx contains inclusions of Na-rich plagioclase (An_{29-44}) (Fig. 5d). This suggests a reaction such as:



The outer 100-200 μm rims of clinopyroxene grains typically do not contain plagioclase inclusions, presumably because the Na component has been lost to the matrix. Partially to completely amphibolitized samples contain the least sodic pyroxene ($X_{Jd} \leq 0.10$). Clinopyroxene rims with the lower Jd-component have higher Ca-Tschermaks contents ($X_{CaTs} = 0.14-0.17$) than in omphacite cores ($X_{CaTs} = 0.10-0.11$).

4.3 *Kyanite*

Primary kyanite occurs as inclusions in garnet cores (Fig. 5a). Kyanite is typical in eclogites derived from Mg-Al rich gabbro, and is usually interpreted to form from the breakdown of paragonite (Mottana et al., 1990) (Table 1). Kyanite inclusions are locally associated with inclusions of zoisite (Fig. 5a). The zoisite inclusions probably represent sites of former plagioclase, since zoisite forms from the breakdown of anorthite with increasing pressure. Fine-grained symplectites of corundum, spinel, sapphirine, and anorthite commonly occur in the eclogite matrix. The typical structure of these symplectites is a Crn + An core, rimmed by a secondary symplectite of Spl + Spr + An. These symplectites typically occur in a “moat” of plagioclase and are interpreted to be pseudomorphs after kyanite, where first the Crn + An symplectite replaced kyanite by reaction with garnet, followed by the formation of the Spl + Spr + An symplectite around the Crn + An. Kyanite and/or sillimanite also occurs as veins within the eclogite, with reaction textures involving Crn, Spl, and Spr. These sapphirine-bearing assemblages and their significance will be discussed in detail in a separate contribution.

CHAPTER 3 – ECLOGITES OF THE SNOWBIRD TECTONIC ZONE

4.4 Plagioclase

Garnet and omphacite rims are surrounded by kelyphitic rims and symplectites with secondary plagioclase. Garnet rims commonly break down to pargasite + plagioclase with a Ca-rich plagioclase (An_{84-91}) (Fig. 4c,d, Fig. 5c) (Table 4). Plagioclase in these symplectites shows dramatic zoning over small distances (100-200 μm) away from the garnet rim (An_{91} adjacent to garnet to An_{44} outside of kelyphitic rim). Omphacite grains have rims of orthopyroxene + plagioclase \pm spinel (Fig. 4c,d and 5c). Plagioclase in this symplectite is An_{47} . Plagioclase also occurs as discrete rims on omphacite, where it is not intergrown with orthopyroxene and this plagioclase has the most Na-rich composition of all plagioclase in the eclogites (An_{27-30}) (Fig. 5c). This plagioclase is interpreted to have formed by the breakdown of the primary omphacite during decompression.

4.5 Pargasitic Amphibole

Pargasite occurs in kelyphitic rims around garnet and typically forms a symplectite with Ca-plagioclase (Table 5). Pargasite also occurs as large secondary matrix grains with a similar composition to that in the symplectites surrounding garnet. Both kelyphitic and matrix amphibole are calcic and pargasite by the classification of Leake (1978).

4.6 Minor Phases

Common inclusions are zoisite, rutile, and quartz. Quartz occurs only as inclusions in garnet, but does not occur in the same garnet as the $Ky \pm Zo$ inclusions. Corundum occurs rarely as inclusions in garnet and in symplectites with anorthite, interpreted to be after kyanite. Orthopyroxene occurs as rims on Cpx and is enstatite with X_{Mg} of 0.74. Ti-rich phlogopite occurs throughout the matrix (Table 5). Other minor phases include spinel and sapphirine replacing kyanite, and more rarely ilmenite, apatite, and zircon. Spinel is more Fe-rich than coexisting Fe-Mg phases with X_{Mg} of 0.61 to 0.67. Representative compositions of spinel and zoisite are given in Table 6.

5. Geothermobarometry

Mineral compositions were measured on the JEOL JXA-733 Superprobe at MIT using an accelerating voltage of 15 kV and a beam current of 10 nA. Locations of spot

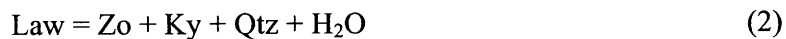
CHAPTER 3 – ECLOGITES OF THE SNOWBIRD TECTONIC ZONE

analyses and quantitative traverses were selected based on the zonation and variation evident in high-resolution compositional maps and backscattered electron (BSE) images. Representative mineral compositions from the eclogite are summarized in Tables 2-6. Various geothermobarometers can be applied to the assemblages in the eclogite. For the decompression conditions, disequilibrium reaction textures require that we define small domains where equilibrium assumptions may be tested.

5.1 Peak Conditions

Temperatures for the eclogite facies event have been derived from the garnet-clinopyroxene Fe-Mg exchange thermometer using the calibration of Powell (1985). Using the most Mg-rich garnet compositions and most Jd-rich clinopyroxene yields a range in temperatures of 920-1000°C at pressures of 1.8 GPa (Table 7). Using the experimental calibration of Holland (1980) for the reaction $Ab = Jd + Qtz$, minimum pressures may be calculated from the Jd content of the core omphacite and the most sodic feldspar formed from the breakdown of omphacite. Measured X_{Jd} values of 0.18-0.23 indicate pressures of 1.8-2.0 GPa at 920-1000°C (Fig. 6) (Table 7).

The presence of zoisite and kyanite inclusions in garnet also has important implications for the P - T path of the eclogite during prograde metamorphism. The equilibria shown in Figure 6 were derived using THERMOCALC, based on the ideal activity for zoisite (see O'Brien 1993) and Grs component in garnet according to the activity model of Berman (1990) (Fig. 6). The absence of lawsonite or margarite in these samples places minimum conditions based on the following reactions (Fig. 6) (Chatterjee et al., 1984):

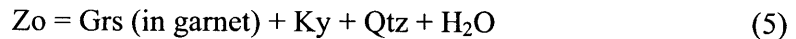


Inclusion textures in garnet indicate that the initial formation of zoisite probably occurred by the breakdown of plagioclase at relatively low pressures by the reaction:



CHAPTER 3 – ECLOGITES OF THE SNOWBIRD TECTONIC ZONE

Reaction 4 occurs at 0.9-1.4 GPa at 700-900°C (Fig. 6). The breakdown reaction of zoisite gives an indication of the peak pressures the studied samples may have experienced:



Reaction 5 yields pressures of 1.9-2.0 GPa for temperatures of 920-1000°C. The relatively scarcity of zoisite and abundance of kyanite inclusions in garnet, as well as the lack of zoisite in the matrix are good evidence that this reaction was crossed during prograde metamorphism. In addition, the following equilibrium has been suggested as a useful geobarometer in eclogites (Poli & Schmidt, 1998):



Using the ideal activity model for zoisite, garnet model of Berman (1990), and Wood & Banno (1973) model for diopside we calculate this equilibrium at 1.9-2.2 GPa at 920-1000°C.

5.2 Decompression Path

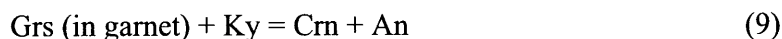
The decompression reactions recorded in the eclogite include (i) breakdown of primary omphacitic clinopyroxene to form a symplectite of less sodic clinopyroxene and albite-rich feldspar (by reaction 1); (ii) breakdown of garnet to form a kelyphitic rims of either pargasite and calcic plagioclase or orthopyroxene + spinel + clinopyroxene + plagioclase by reactions such as:



(iii) breakdown of clinopyroxene to form orthopyroxene and plagioclase by a reaction such as:



(iv) breakdown of kyanite to form a symplectite of corundum and anorthite, followed by development of symplectites of spinel, sapphirine, and anorthite. The formation of corundum + anorthite symplectites after kyanite is probably due to the reaction:



Using the activities for the phases present, and THERMOCALC (Powell & Holland 1988), the equilibrium represented by reaction 9 was calculated. This reaction lies between 1.1-1.3 GPa at 700-900°C (Fig. 6).

All of these reactions imply a P-T path from eclogite to granulite facies conditions. The small area of domainal equilibrium preserved in these samples makes calculations of these equilibria difficult. However, we attempted to estimate the breakdown conditions of reactions 7 and 8 for sample 01SZ40B (Figure 5c) using the TWQ software (Berman, 1991) and internally consistent thermodynamic database of Berman & Aranovich (1996) using rim garnet compositions in equilibrium with the symplectite phases. Garnet-orthopyroxene-plagioclase-quartz equilibrium yields P-T conditions of 1.2 GPa, 810°C and garnet-hornblende-plagioclase-quartz equilibrium yields conditions of 1.1 GPa, 790°C (Table 7). This is consistent with the conditions calculated for the breakdown of kyanite by reaction 9.

6. U-Pb Geochronology

6.1 Dating eclogite facies metamorphism

The successful unambiguous dating of eclogite facies metamorphism using U-Pb zircon geochronology is relatively rare, in part because geochronological data from eclogitic zircon can be complex and difficult to interpret. It is therefore useful to review other examples of U-Pb dating of eclogitic zircon by a variety of techniques (IDTIMS, SHRIMP, and LA-ICPMS) in order to illustrate the complexities of relating zircon

CHAPTER 3 – ECLOGITES OF THE SNOWBIRD TECTONIC ZONE

growth to eclogite facies metamorphism and the subsequent interpretation of the geochronology. Zircon in eclogite has been variably interpreted as dating the peak eclogite facies metamorphic event, growth along the cooling path, inherited components in the protolith, growth during post-peak metasomatism, or the age of protolith emplacement (Bröcker & Enders, 1999; Gebauer et al., 1985; Rubatto et al., 1999; Schmitz & Bowring, 2001). The first report of eclogite zircons dated by U-Pb geochronology were from the Western Gneiss Region of Norway (Krogh et al., 1974). The morphology of these small rounded grains, along with the presence of inclusions of omphacite, rutile, and quartz, led to the interpretation that the Caledonian ages obtained on this zircon dated the formation of the eclogite body. In a further study on the age and origin of Norwegian eclogites, Gebauer et al. (1985) reported both U-Pb zircon and geochemical data to distinguish between basaltic and gabbroic protoliths based on morphology and size of zircons. A Caledonian age of eclogite formation was reported for all of these samples, in agreement with the data of Krogh et al. (1974).

Since these early studies, *in situ* studies using the ion microprobe have made it possible to obtain geochronological information on domains within individual crystals and to distinguish multiple growth zones within zircon. The first published example of *in situ* dating was on retrograded eclogites from the Central Alps (Gebauer, 1990; Gebauer et al., 1988). This study found composite grains with Archean inherited magmatic cores and Caledonian overgrowths that defined the age of HP metamorphism (Gebauer, 1990).

More recent studies have utilized both the spatial resolution provided by *in situ* SHRIMP and LA-ICPMS methods, as well as the high-precision afforded by IDTIMS analysis (Bingen et al., 2001a; Bingen et al., 2001b; Creaser et al., 1997; Johansson et al., 2001; Root et al., *in review*; Rubatto et al., 1999; Rubatto et al., 2001; Schmitz & Bowring, 2001; Sun et al., 2002). An essential component of successfully interpreting geochronological data is the characterization of the grains using cathodoluminescence (CL) imaging. CL reveals information about the growth history of zircon by providing a map of variation in REE content (Hanchar & Rudnick, 1995; Mariano, 1989). A common characteristic of eclogitic zircon is the presence of inherited, oscillatory zoned cores with thin, bright CL overgrowths that formed during the eclogite facies event (Liat

CHAPTER 3 – ECLOGITES OF THE SNOWBIRD TECTONIC ZONE

et al., 2001; Rubatto et al., 1999; Rubatto et al., 2001; Sun et al., 2002). These metamorphic rims typically have distinctly lower U concentrations and low Th/U ratios (<0.3) (Creaser et al., 1997). Low Th/U ratios in eclogitic zircon are generally attributed to co-precipitation of metamorphic zircon with epidote group minerals (Bingen et al., 2001a). In some eclogites, there is a single population of metamorphic zircon interpreted to have formed during the eclogite facies event (Creaser et al., 1997; Gebauer et al., 1985; Johansson et al., 2001). These are typically identified by morphology (round and multi-faceted) and are usually unzoned to sector zoned with distinctly low Th/U ratios.

In addition, trace element concentrations of zircon, and especially the REE patterns may be used to infer co-precipitating phases (Rubatto, 2002). Zircon grown under eclogite facies conditions commonly have depleted heavy REE indicating that garnet was present during growth, and commonly have little or no negative Eu anomaly (plagioclase absent) (Rubatto, 2002). Combining trace element data with inclusion suites within zircon is compelling evidence for growth of metamorphic rims during eclogite facies metamorphism. Sun et al. (2002) show that inclusions of high-pressure phases are restricted to overgrowths, indicative of late zircon growth under eclogite facies conditions, and is consistent with REE patterns in the zircon.

There are a few studies that convincingly link zircon growth to eclogite facies metamorphic conditions and reactions (Bingen et al., 2001a; Johansson et al., 2001; Root et al., in review). Understanding the solid state reactions involving the breakdown of magmatic or metamorphic Zr-bearing phases is important for determining which domains of zircon formed during different parts of the P-T-t path (Bingen et al., 2001a). Zircon often occurs in association with Ti-bearing phases such as rutile and ilmenite in granulite and eclogite facies rocks. Ilmenite typically contains 125-1920 ppm Zr and is the largest potential reservoir of Zr in eclogite protoliths (Bingen et al., 2001a; Stimac & Hickmott, 1994). Spectacular textures involving coronas of small zircon around rutile have been described in the Western Gneiss region of Norway (Bingen et al., 2001a; Root et al., in review). The interpretation of these textures is that rutile forms from the breakdown of ilmenite in the presence of a silica-bearing fluid to form the zircon corona (Bingen et al., 2001a). Another study has suggested that zircon forms from the

CHAPTER 3 – ECLOGITES OF THE SNOWBIRD TECTONIC ZONE

breakdown of clinopyroxene along the cooling path (e.g., Schmitz & Bowring, 2001). The relative scarcity of zircon in eclogites makes it difficult to document the petrographic setting of zircon at the scale of a thin section, yet the context of zircon remains one of the most powerful tools when combined with trace element analysis and dating by linking zircon growth to specific *P-T* conditions. Below we present U-Pb geochronological data, both by IDTIMS and SHRIMP, from zircon contained within the Snowbird eclogite layer and discuss the petrographic setting of the zircon and the implications for interpreting the significance of the U-Pb data. This combined approach allows us the high spatial resolution of in situ analyses of zircon in thin section as well as the high precision afforded by IDTIMS to allow us to accurately determine the timing of high-*P* metamorphism and link the growth of zircon to the eclogite facies metamorphism.

6.2 Analytical Techniques

Zircon and rutile were isolated from the eclogite samples by standard crushing, heavy liquid, and magnetic separation techniques. Fractions of accessory minerals consisting of both single grains and multi-grain fractions (rutile) were picked and measured and recorded by digital photography. Zircon crystals were air-abraded with pyrite after the method of Krogh (1982), and acid rinsed in 3M HNO₃ for 5-6 hours, followed by ultrasonication. Accessory mineral fractions were loaded into Teflon FEP microcapsules and washed again in 3M HNO₃ (zircon) or high-purity water (rutile) at *c.* 50°C for 3-4 hours, followed by rinsing with several capsule volumes of 3M HNO₃ (zircon) or water (rutile). Samples were spiked with a mixed ²⁰⁵Pb-²³³U-²³⁵U tracer and dissolved in 29M HF at 220°C for 48-96 hours, followed by conversion to 6M HCl at 180°C for 24 hours. Pb and U were separated from all mineral solutions using anion exchange chromatography procedures modified after Krogh (1973). U-Pb IDTIMS analyses were done at the Massachusetts Institute of Technology on the VG Sector 54 thermal ionization multicollector mass spectrometer. Pb and U were loaded on single Re filaments with a dilute silica gel-0.1 H₃PO₄ emitter solution with U run as an oxide. U-Pb data as well as the details of fractionation and blank corrections are given in Table 3.

Sample 01SZ40B was prepared for SHRIMP U-Pb dating as a 25 mm diameter, Au-coated, polished thin section. Spots within the composite zircon cluster and isolated

CHAPTER 3 – ECLOGITES OF THE SNOWBIRD TECTONIC ZONE

grains, selected using optical and CL imaging, were analysed using a 10 μm diameter, 1 nA, 10kV, negative O_2 primary ion beam. Positive secondary ions were extracted at 10 kV and mass analysed at mass resolution 5000 using a single ETP electron multiplier and magnetic field switching. The Pb isotopic composition was measured directly. Pb/U and Pb/Th were determined relative to chips of zircon standard QGNG (1842 Ma) mounted in an adjacent sample holder. The standard also provided an estimate of Pb isotopic fractionation (~ 0.4).

6.3 U-Pb Results

High-precision isotope dilution thermal ionization mass spectrometry (IDTIMS) was used in concert with in situ SHRIMP analysis and cathodoluminescence (CL) imaging to constrain the timing of high-pressure metamorphism in the STZ. Sample 01SZ41A is from the interior of a ~ 15 m-wide outcrop of eclogite and represents one of the least retrograded eclogite samples. Zircon from this sample is scarce, and occurs as spherical grains, ranging in diameter from 80-250 μm . They generally display sector-zoning when viewed in CL (Fig. 7a,b), and contain inclusions of the high-pressure mineral paragenesis including garnet, kyanite, corundum, and quartz (Fig. 7c,d). The largest zircon grains have highly irregular, pocked surfaces, and BSE images reveal what appears to be an agglomeration of several zircon nuclei that have coalesced (Fig. 7d). The two largest grains with this morphology (z1,z2) analyzed from this sample have high calculated Th/U ratios of 1.0-2.0. The range in Th/U ratios for the remaining grains is 0.04-0.46. The $^{207}\text{Pb}/^{206}\text{Pb}$ dates for 9 abraded single zircons range from 1903.7 to 1906.2 Ma (Table 8). One analysis, z12, yields a distinguishably older $^{207}\text{Pb}/^{206}\text{Pb}$ date (1906.2 ± 0.9 Ma) than the rest of the grains. This may represent a small amount of inheritance or indicate protracted zircon growth over a few million years. Excluding the youngest discordant (z5) and oldest (z12) grains, the data form a tight cluster with weighted mean $^{207}\text{Pb}/^{206}\text{Pb}$, $^{206}\text{Pb}/^{238}\text{U}$, and $^{207}\text{Pb}/^{235}\text{U}$ dates of 1904.2 ± 0.2 Ma (MSWD = 0.13), 1903.8 ± 0.6 Ma (MSWD = 0.43), and $1903.9 \text{ Ma} \pm 0.3 \text{ Ma}$ (MSWD = 0.09) respectively (Fig. 8a).

Sample 01SZ40B is from the edge of the outcrop, near a ~ 1 -2 m-wide reaction zone of sapphirine granulites, and has undergone much more extensive retrograde

CHAPTER 3 – ECLOGITES OF THE SNOWBIRD TECTONIC ZONE

overprinting and development of reaction textures (Fig. 4c,d). Nine abraded single zircon grains define a mixing line between two components, 2.54 and 1.91 Ga (anchored by concordant analyses at 1904.0 Ma and 2542.9 Ma) (Table 8, Fig. 8b). The $^{207}\text{Pb}/^{206}\text{Pb}$ date for the youngest grain is 1904.0 ± 1.4 Ma and has a distinctly lower Th/U ratio (0.14) than the remaining grains (0.63-1.13). The oldest concordant zircon analyzed has a $^{207}\text{Pb}/^{206}\text{Pb}$ date of 2542.9 ± 0.9 Ma. The largest zircon grains in this sample are anhedral and have irregular rims nucleated on rounded cores that are evident from optical inspection (Fig. 7f-h). A second population of spherical grains is present, which range in diameter from 100-250 μm . CL images reveal that many grains display sector-zoning (Fig. 7e), but in contrast to sample 01SZ41A, also contain relict dark cores, which may correspond to either an early 2.54 Ga metamorphism, or possibly reflect inheritance caused by interaction of eclogite protolith with host gneisses (Fig. 7f-h). In addition, the outer sector-zoned portions of the zircon grains from this sample contain inclusions of corundum and rutile, indicating that this part likely grew during or after the eclogite facies event at 1.9 Ga.

In order to link the growth of zircon to the high-pressure metamorphism it is necessary to understand the petrographic setting of zircon, and specifically its relationship to the high-P mineral paragenesis. We examined a large cluster of zircon grains in 01SZ40B (Fig. 9). The cluster occurs within omphacitic ($\sim\text{Jd}_{20}$) clinopyroxene, and is in contact with garnet and plagioclase. The morphology and large number of free surfaces in this cluster imply that the zircon grew first and was included by the large clinopyroxene grain as it grew during the eclogite facies metamorphism. CL imaging of this cluster of grains reveals that each individual grain consists of a dark core and thin, bright, low U rim (Fig. 9b). Two relatively small ($\sim 20 \mu\text{m}$) zircon grains occur as inclusions well-armed in clinopyroxene (Fig. 10). These grains also display dark cores with bright overgrowths in CL (Fig. 10a,b). Zircons from this cluster were dated in situ using the SHRIMP and analyses are reported in Table 9. All of the analyses indicate *ca.* 1.9 Ga dates within the cluster of zircon. Though CL imaging reveals two distinct chemical domains, there does not appear to be a difference in calculated dates between cores and overgrowths (Table 9). However, the low U, bright CL rims are low in

CHAPTER 3 – ECLOGITES OF THE SNOWBIRD TECTONIC ZONE

radiogenic Pb, with concentrations of only 6-7 ppm, resulting in large 1- σ errors in the SHRIMP analyses of 100-200 Ma, precluding any means of detecting small differences in age. Th/U ratios of these in situ analyses are varied, and are slightly lower in the overgrowths (0.17-0.26) compared to the cores (0.41-0.77). Six analyses of the dark core zones within the cluster (analyses 2.1, 2.2, 2.4, 2.7, 2.9, and 2.10 in Table 9) define a weighted mean $^{207}\text{Pb}/^{206}\text{Pb}$ date of 1903.3 ± 9.6 Ma (1- σ), which is similar to the IDTIMS date for the Proterozoic zircon growth (1904.2 ± 0.2 Ma). The isotopic compositions of the six higher-U cores are concordant and indistinguishable within the analytical uncertainties. There is no evidence in the U/Pb or Pb isotopic composition, even on the micro-scale, for any pre-1.9 Ga component. Further, despite the much larger uncertainties on the overgrowth analyses, there is also no evidence for zircon growth substantially later than 1.9 Ga. One analysis was obtained for the grain shown in Figure 10, which is well-armored in omphacitic clinopyroxene and displays a dark core with bright overgrowth. This yielded an imprecise $^{207}\text{Pb}/^{206}\text{Pb}$ date of 1856 ± 40 Ma. This texture implies that the high-P omphacitic clinopyroxene grew during or following the growth of zircon *ca.* 1.9 Ga.

Distinguishing magmatic from metamorphic zircon is a difficult task. Many studies of metamorphic zircon have cited low Th/U (<0.1) as a means of distinguishing metamorphic from magmatic zircon (Creaser et al., 1997; Rubatto, 2002; Rubatto et al., 1999; Rubatto et al., 2001; Williams et al., 1996). However, the relatively high and varied Th/U ratios measured in zircons in this study indicate that metamorphic zircons formed under eclogite facies conditions do not always exhibit low Th/U, or alternatively, that the magmatic and metamorphic ages are similar. Thus, the growth environment of the zircon cannot necessarily be distinguished by solely relying upon Th/U and probably merely reflects the Th budget in the protolith of the metamorphic rock. In many eclogites, low Th/U is attributed to co-precipitation of metamorphic zircon with epidote group minerals (Bingen et al., 2001a). Because the Snowbird eclogite has experienced sufficiently high temperatures during metamorphism above the stability field of epidote, it is possible that more Th was available during the crystallization of zircon, resulting in higher calculated Th/U.

CHAPTER 3 – ECLOGITES OF THE SNOWBIRD TECTONIC ZONE

Five fractions of rutile from 01SZ40B were analyzed. Four fractions consisted of single grains ranging from 300-700 μm in diameter, whereas one fraction (r3) consisted of five grains, each ~ 250 μm in diameter. Invariably rutile occurs as inclusions in garnet, so the rutile dates obtained are interpreted to reflect the time at which the rutile grain cooled below its closure temperature ($\sim 500^\circ\text{C}$ for grain sizes in the range analyzed) (Mezger et al., 1989). The $^{207}\text{Pb}/^{206}\text{Pb}$ dates range from 1882 to 1851 Ma and the four single grain analyses show a grain size dependence reflected in the cooling ages, with the largest grain yielding the oldest $^{207}\text{Pb}/^{206}\text{Pb}$ age (Fig. 8c). Calculated cooling rates using the empirical data of Mezger et al. (1989) are $\sim 1^\circ\text{C}/\text{Ma}$, consistent with conductive cooling in the lower crust.

7. Discussion

The occurrence of eclogite in the Snowbird tectonic zone has important implications for the history and significance of the zone itself. The physical conditions necessary to produce this eclogite require either substantial crustal thickening and heating or transport of these rocks to mantle (~ 2 GPa, 1000°C). Inclusion patterns in garnet and geochemical data suggest that the eclogites were derived from protoliths of troctolitic gabbros that crystallized at moderate (~ 1.0 GPa) crustal pressures. The presence of zoisite + kyanite inclusions in garnet supports an evolution from a plagioclase-bearing cumulate protolith (without garnet) to a rock with Ca-bearing garnet \pm zoisite \pm kyanite \pm quartz (O'Brien, 1993; O'Brien & Vrána, 1995). The presence of high-Ca cores in garnet with increasing Mg at the inclusion-free rim, suggests that the growth of garnet occurred during prograde metamorphism. The minimum pressures recorded in the eclogites are 1.8-2.0 GPa. These petrological data imply that the eclogites formed from a protolith of troctolitic gabbro that crystallized at a maximum depths of *ca.* 1.0 GPa and were then transported to mantle depths where the eclogite facies assemblages developed. The high-pressure metamorphism was followed by near-isothermal decompression to granulite facies conditions, based on the presence of reaction rims of secondary phases around the high-pressure minerals garnet, omphacite, and kyanite. The breakdown reactions record decompression back to normal lower crustal pressures of *ca.* 1.0 GPa. This was probably

CHAPTER 3 – ECLOGITES OF THE SNOWBIRD TECTONIC ZONE

achieved during rapid, buoyancy-driven exhumation following the high-pressure metamorphism, and as indicated by the rutile data, was followed by more protracted exhumation consistent with a conductive geotherm.

The timing of the high-pressure metamorphism is constrained by high-precision U-Pb geochronology of metamorphic zircons from two eclogite samples. Zircon in the most pristine eclogite contains a single population of multi-faceted, sector-zoned, zircon that yield crystallization ages of 1904 Ma. A second sample from the margin of the eclogite outcrop records a mixture of two components, 1904 and 2544 Ga. The older age may reflect magmatic interaction of the eclogitic protolith with the host felsic gneiss and thus may indicate the timing of emplacement of the eclogite protolith. The in situ SHRIMP data supports the interpretation that the high-P metamorphism occurred at 1.9 Ga. Zircon included within omphacitic clinopyroxene records exclusively 1.9 Ga dates, indicating that growth of the high-P omphacite was either contemporaneous with or followed the zircon growth.

The Snowbird eclogites occur within a much more extensive 400 km² package of high-pressure granulites. Peak P-T conditions recorded in the host rock to the eclogite, a garnet-kyanite quartzofeldspathic gneiss, are >1.5 GPa and 1000°C (Snoeyenbos et al., 1995). Mafic granulite layers interlayered with the felsic gneiss in the vicinity of the eclogite record variable *P-T* conditions of 1.3-1.9 GPa, 890-960°C; the variation in pressures is interpreted to represent varying degrees of re-equilibration during decompression (Baldwin et al., 2003). Near-isothermal decompression paths to medium pressure granulite facies conditions are recorded in all the lithological units in the southern domain of the EAmt (Baldwin et al., 2003). Mafic granulites in the structurally higher levels of the southern domain record slightly lower pressures of 1.2-1.4 GPa (Kopf, 1999). Uniform P-T conditions of 1.0 GPa, 800°C are observed in the northwestern and southeastern domains (Williams et al., 1995; Williams et al., 2000).

The high temperatures recorded in all of the lithologies in the southern domain as well as the high pressures that lie outside the normal, stable Archean continental crustal thickness of 35-40 km, implies that there was a burial event along a relatively high dP/dT gradient. Similar models have been proposed for high-pressure granulites in the Variscan

CHAPTER 3 – ECLOGITES OF THE SNOWBIRD TECTONIC ZONE

Bohemian Massif (O'Brien & Rötzler, 2003). The temperatures preserved in the Snowbird eclogite are somewhat unusual with respect to other examples of eclogites associated with high-pressure granulites. These occurrences are summarized in O'Brien & Rötzler (2003), and typically preserve maximum temperatures of $\sim 800^{\circ}\text{C}$. There is at least one example of eclogite associated with high-pressure granulites in the Gföhl terrane of the Variscan Bohemian Massif that does record higher temperatures of $>1000^{\circ}\text{C}$ and maximum pressures of 2.0 GPa (Medaris et al., 1995). Documented examples of Precambrian eclogites including the Mali, Grenville, and Tanzanian eclogites all record maximum temperatures of $\sim 750^{\circ}\text{C}$ (Caby, 1994; Indares, 1993; Möller et al., 1995). These high temperatures recorded in the Snowbird eclogite require an additional heat source are consistent with burial to mantle depths, delamination of continental lithospheric mantle and heating from asthenospheric upwelling, consistent with a scenario that involves transport of these rocks to mantle depths. Perhaps high-T eclogites such as these record a signature of lithospheric delamination during continental collision rather than secular change.

Constraining the timing and P-T evolution of high-pressure metamorphism in the STZ has important implications. The timing constraints from this study show that the high-pressure metamorphism is much younger than previously thought, and the 1.9 Ga age corresponds to a major period of assembly of the various micro-continents forming Laurentia. The age of high-pressure metamorphism falls in between the ages of the bounding orogens on either side, the Taltson-Thelon (1.9-2.0 Ga) and the Trans-Hudson (1.8-1.9 Ga). The STZ may either be a Paleoproterozoic suture, or represent an Archean structure that experienced a component of convergence that resulted in collisional type metamorphism and decompression to normal lower crustal depths.

The evidence for 1.9 Ga timing of high-pressure metamorphism in the eclogite unit is consistent with geochronological data from one mafic granulite sample described in Baldwin et al. (2003). This sample contains metamorphic zircon that is 1904.0 ± 0.9 Ma, which occurs as inclusions in the high-P mineral phases such as garnet, clinopyroxene, and plagioclase. Other mafic granulites record metamorphic zircon growth from ca. 2.55-2.52 Ga, indicating that some mafic granulite samples record an

CHAPTER 3 – ECLOGITES OF THE SNOWBIRD TECTONIC ZONE

earlier granulite facies metamorphism. Additionally, felsic gneiss samples with protomylonitic fabrics and largely anhydrous assemblages that are the host rock to the eclogite record an extremely complex history from >2.6 to 1.9 Ga. Both the mafic granulite and eclogite layers are typically slightly discordant to the strong fabric developed in the felsic gneiss, indicating that their emplacement postdates this fabric development. This implies that the fabric in the felsic gneiss developed sometime prior to 1.9 Ga, either during the early granulite facies metamorphism at 2.60-2.62 Ga or related to the metamorphic event at ~2.55 Ga. These rocks show abundant evidence for dehydration melting reactions that result in a predominantly anhydrous garnet-kyanite-feldspar-quartz assemblage. Following the emplacement of the protolith to the eclogite, the maximum age of which is 2.54 Ga but is not well-constrained, the entire package of rocks underwent a high-P metamorphism during which the protomylonitic fabric in the felsic gneiss remained undisturbed. This is largely due to the anhydrous nature of the assemblage as well as the short-lived duration of the high-P metamorphic event.

It should also be noted that there is significant mafic magmatism that post-dates the high-pressure metamorphism by ~10 Ma. The 1895 Ma Chipman dike swarm occurs in the southeastern domain to the east of the high-pressure rocks (Flowers et al., 2002) (Fig. 2). This dike swarm is inferred to have been emplaced at pressures of 1.0 GPa (Williams et al., 1995). A model for the exhumation of the eclogites to normal deep crustal conditions involving delamination of the continental lithosphere, which may have triggered asthenospheric upwelling and mafic magmatism could be applicable (Kay & Kay, 1993). This asthenospheric upwelling may be an explanation for the very high-temperatures (900-1000°C) associated with the eclogite facies metamorphism. However the lag of about 10 Ma between eclogite facies metamorphism and mafic magmatism is problematic.

Exhumation to mid-crustal depths is recorded in rutile data from the eclogite. These data indicate that decompression of the eclogites occurred between ~1.88 and 1.85 Ga. Rutile data indicate a cooling rate of ~1°C/Ma, which is consistent with slow cooling following the rapid exhumation and implies that this stage of exhumation of the eclogite

CHAPTER 3 – ECLOGITES OF THE SNOWBIRD TECTONIC ZONE

brought the rocks to mid-crustal levels, followed by more protracted exhumation (a few tens of millions of years) prior to their exposure at the surface.

8. Conclusions

- (1) Eclogite containing the diagnostic assemblage of omphacite + Mg-rich garnet is present in the Snowbird tectonic zone.
- (2) Inclusion suites in garnet and bulk geochemical data (LREE enrichment and positive Eu anomalies) indicates a plagioclase cumulate source for the Snowbird eclogites. Bulk geochemical data indicate that they were probably derived from Mg-Al gabbro. These data indicate a lower pressure crustal history prior to the high-P metamorphism.
- (3) Pressures and temperatures derived from empirical and experimentally calibrated equilibria indicate minimum pressures of 1.8-2.0 GPa at 900-1000°C. Prograde inclusion textures in garnet suggest that pressure could have been as high as 2.0 GPa.
- (4) Partial re-equilibration during uplift led to the development of multiple reaction textures which indicate overprinting by granulite facies assemblages at ≥ 1.0 GPa.
- (5) U-Pb IDTIMS geochronology of sector-zoned zircon with inclusions of the high-P mineral paragenesis and SHRIMP analyses of zircons included within clinopyroxene indicates an age of 1904 Ma for the high-P metamorphism. This is in contrast of previous estimates of 2.6 Ga high-P metamorphism and this new interpretation has important tectonic implications for the nature of this boundary.
- (6) A range in U-Pb rutile data indicate that from 1.88-1.85 Ga the eclogite cooled below *ca.* 500°C at a rate of $\sim 1^\circ\text{C}/\text{Ma}$. This is consistent with rapid uplift of the rocks to moderate pressures (~ 1.0 GPa) followed by more protracted cooling and subsequent exhumation from normal lower crustal depths.

Acknowledgements

This research was supported by National Science Foundation grant EAR-0001131 to SAB and MLW and a research grant from the Mineralogical Society of America to JAB. We thank John Hanchar for providing the CL image shown in Figure 9c as well as trace element analyses of zircon.

References

- Baldwin, J. A., Bowring, S. A. & Williams, M. L., 2003. Petrological and geochronological constraints on high pressure, high temperature metamorphism in the Snowbird tectonic zone, Canada. *Journal of Metamorphic Geology*, **21**, 81-98.
- Barth, M. G., Rudnick, R. L., Carlson, R. W., Horn, I. & McDonough, W. F., 2002. Re-Os and U-Pb geochronological constraints on the eclogite-tonalite connection in the Archean Man Shield, West Africa. *Precambrian Research*, **118**, 267-283.
- Berman, R. G., 1990. Mixing properties of Ca-Mg-Fe-Mn garnets. *American Mineralogist*, **75**(3-4), 328-344.
- Berman, R. G., 1991. Thermobarometry using multi-equilibrium calculations: a new technique, with petrological applications. *Canadian Mineralogist*, **29**, 833-855.
- Berman, R. G. & Aranovich, L. Y., 1996. Optimized standard state and solution properties of minerals: I. Model calibration for olivine, orthopyroxene, cordierite, garnet, and ilmenite in the system FeO-MgO-CaO-Al₂O₃-TiO₂-SiO₂. *Contributions to Mineralogy and Petrology*, **126**, 1-24.
- Bingen, B., Austrheim, H. & Whitehouse, M., 2001a. Ilmenite as a source for zirconium during high-grade metamorphism? Textural evidence from the Caledonides of Western Norway and implications for zircon geochronology. *Journal of Petrology*, **42**, 355-375.
- Bingen, B., Davis, W. J. & Austrheim, H., 2001b. Zircon U-Pb geochronology in the Bergen arc eclogites and their Proterozoic protoliths, and implications for the pre-Scandian evolution of the Caledonides in western Norway. *Geological Society of America Bulletin*, **113**, 640-649.
- Brastad, K., 1985. Relationships between peridotites, anorthosites, and eclogites in Bjorkedalen, western Norway. In: *The Caledonide Orogen - Scandinavia and Related Areas* (eds Gee, D. G. & Sturt, B. A.), pp. 859-872, John Wiley & Sons, Chichester.
- Bröcker, M. & Enders, M., 1999. U-Pb zircon geochronology of unusual eclogite-facies rocks from Syros and Tinos (Cyclades, Greece). *Geological Magazine*, **136**, 111-118.
- Caby, R., 1994. Precambrian coesite from northern Mali; first record and implications for plate tectonics in the trans-Saharan segment of the Pan-African belt. *European Journal of Mineralogy*, **6**(2), 235-244.
- Caby, R., Bertrand, J. M. & Black, R., 1981. Oceanic closure and continental collision in the Hogger-Iforas Pan-African segment. In: *Precambrian Plate Tectonics* (ed Kröner, A.), pp. 407-434, Elsevier, Amsterdam.
- Carswell, D. A., 1990. Eclogites and the eclogite facies: definitions and classification. In: *Eclogite Facies Rocks* (ed Carswell, D. A.), pp. 1-13, Chapman and Hall, New York.
- Chatterjee, N. D., Johannes, W. & Leistner, H., 1984. The system CaO-Al₂O₃-SiO₂-H₂O: new phase equilibria data, some calculated phases relations, and their petrological applications. *Contributions to Mineralogy and Petrology*, **88**, 1-13.

CHAPTER 3 – ECLOGITES OF THE SNOWBIRD TECTONIC ZONE

- Creaser, R. A., Heaman, L. M. & Erdmer, P., 1997. Timing of high-pressure metamorphism in the Yukon-Tanana terrane, Canadian Cordillera: constraints from U-Pb zircon dating of eclogite from the Teslin tectonic zone. *Canadian Journal of Earth Sciences*, **34**, 709-715.
- Ellis, D. J. & Maboko, M. A. H., 1992. Precambrian tectonics and the physiochemical evolution of the continental crust. I. The gabbro-eclogite transition revisited. *Precambrian Research*, **55**, 491-506.
- Ernst, W. G., 1972. Occurrence and mineralogic evolution of blueschist belts with time. *American Journal of Science*, **272**, 657-668.
- Flowers, R. M., Baldwin, J. A., Bowring, S. A. & Williams, M. L., 2002. Age and significance of the Proterozoic Chipman dike swarm, Snowbird Tectonic Zone, northern Saskatchewan. *Geological Association of Canada - Mineralogical Association of Canada Annual Meeting Abstracts*.
- Fountain, D. M., 1976. The Ivrea-Verbano zone and Strona-Ceneri zones, northern Italy: a cross section of the continental crust - new evidence from seismic velocities. *Tectonophysics*, **33**, 145-166.
- Gebauer, D., 1990. Isotopic systems - geochronology of eclogites. In: *Eclogite Facies Rocks* (ed Carswell, D. A.), pp. 141-159, Chapman and Hall, New York.
- Gebauer, D., Lappin, M. A., Grünenfelder, M. & Wytttenbach, A., 1985. The age and origin of some Norwegian eclogites: a U-Pb zircon and REE study. *Chemical Geology*, **52**, 227-247.
- Gebauer, D., Quadt, A., Williams, I. S., Compston, W. & Grünenfelder, M., 1988. Archean zircons in a retrograded Caledonian eclogite of the Gotthard Massif (Central Alps, Switzerland). *Schweiz. Mineral. Petrogr. Mitt.*, **68**, 485-490.
- Gilboy, C. F., 1978. Reconnaissance geology, Stony Rapids area (part of NTS area 74P). In: *Summary of Investigations, Saskatchewan Geological Survey* (eds Christopher, J. E. & Macdonald, R.), pp. 35-42.
- Goodacre, A. K., Grieve, R. A. F., Halpenny, J. F. & Sharpton, V. L., 1987. Horizontal gradient of the Bouguer gravity anomaly map of Canada, Canadian Geophysical Atlas, Map 5, Geological Survey of Canada, Ottawa.
- Green, D. H. & Ringwood, A. E., 1967. An experimental investigation of the gabbro to eclogite transformation and its petrological applications. *Geochimica Cosmochimica Acta*, **48**, 767-833.
- Green, D. H. & Ringwood, A. E., 1972. A comparison of recent experimental data on the gabbro-garnet granulite-eclogite transition. *Journal of Geology*, **80**, 277-288.
- Griffin, W. L., O'Reilly, S. Y. & Pearson, N. J., 1990. Eclogite stability near the crust-mantle boundary. In: *Eclogite Facies Rocks* (ed Carswell, D. A.), pp. 291-314, Chapman and Hall, New York.
- Grove, T. L., Kinzler, R. J. & Bryan, W. B., 1992. Fractionation of Mid-Ocean Ridge Basalt (MORB). In: *Mantle Flow and Melt Generation at Mid-Ocean Ridges, Geophysical Monograph 71*, pp. 281-310, American Geophysical Union.
- Hanchar, J. M. & Rudnick, R. L., 1995. Revealing hidden structures; the application of cathodoluminescence and back-scattered electron imaging to dating zircons from lower crustal xenoliths. *Lithos*, **36**(3-4), 289-303.

CHAPTER 3 – ECLOGITES OF THE SNOWBIRD TECTONIC ZONE

- Hanmer, S., 1994. Geology, East Athabasca mylonite triangle, Saskatchewan. In: *Geological Survey of Canada Map 1859A*.
- Hanmer, S., 1997. Geology of the Striding-Athabasca mylonite zone, northern Saskatchewan and southeastern District of Mackenzie, Northwest Territories. *Geological Survey of Canada Bulletin*, **501**, 1-92.
- Hanmer, S., Parrish, R., Williams, M. & Kopf, C., 1994. Striding-Athabasca mylonite zone: Complex Archean deep-crustal deformation in the East Athabasca mylonite triangle, northern Saskatchewan. *Canadian Journal of Earth Sciences*, **31**, 1287-1300.
- Hanmer, S., Williams, M. & Kopf, C., 1995a. Modest movements, spectacular fabrics in an intracontinental deep-crustal strike-slip fault: Striding-Athabasca mylonite zone, NW Canadian Shield. *Journal of Structural Geology*, **17**(4), 493-507.
- Hanmer, S., Williams, M. & Kopf, C., 1995b. Striding-Athabasca mylonite zone: implications for the Archean and Early Proterozoic tectonics of the western Canadian Shield. *Canadian Journal of Earth Sciences*, **32**, 178-196.
- Hoffman, P. F., 1988. United Plates of America, the birth of a craton: Early Proterozoic assembly and the growth of Laurentia. *Annual Reviews of Earth and Planetary Science Letters*, **16**, 543-603.
- Hoffman, P. F., 1989. Precambrian geology and tectonic history of North America. In: *The Geology of North America - An overview* (eds Bally, A. W. & Palmer, A. R.), pp. 447-512, Geological Society of America, Boulder, Colorado.
- Holland, T. J. B., 1980. The reaction albite = jadeite + quartz determined experimentally in the range 600-1200°C. *American Mineralogist*, **65**, 129-134.
- Indares, A., 1993. Eclogitized gabbros from the eastern Grenville Province; textures, metamorphic context, and implications. *Canadian Journal of Earth Sciences*, **30**(1), 159-173.
- Indares, A. & Dunning, G. R., 1997. Coronitic metagabbro and eclogite from the Grenville Province of western Quebec; interpretation of U-Pb geochronology and metamorphism. *Canadian Journal of Earth Sciences*, **34**(7), 891-901.
- Jahn, B., Caby, R. & Monie, P., 2001. The oldest UHP eclogites of the World: age of UHP metamorphism, nature of protoliths and tectonic implications. *Chemical Geology*, **178**, 143-158.
- Johansson, L., Möller, C. & Söderlund, U., 2001. Geochronology of eclogite facies metamorphism in the Sveconorwegian Province of SW Sweden. *Precambrian Research*, **106**, 261-275.
- Kay, R. W. & Kay, S., 1993. Delamination and delamination magmatism. *Tectonophysics*, **219**, 177-189.
- Kopf, C. F., 1999. Deformation, metamorphism, and magmatism in the East Athabasca mylonite triangle, northern Saskatchewan: implications for the Archean and Early Proterozoic crustal structure of the Canadian Shield, *University of Massachusetts, Unpublished Ph.D. thesis*.
- Kornprobst, J., Piboule, M., Roden, M. & Tabit, A., 1990. Corundum-bearing garnet clinopyroxenites at Beni Bousera (Morocco): Original plagioclase-rich gabbros recrystallized at depth within the mantle? *Journal of Petrology*, **31**, 717-745.

CHAPTER 3 – ECLOGITES OF THE SNOWBIRD TECTONIC ZONE

- Krogh, T. E., 1973. A low-contamination method for hydrothermal decomposition of zircon and extraction of U and Pb for isotopic age determination. *Geochimica Cosmochimica Acta*, **46**, 485-494.
- Krogh, T. E., 1982. Improved accuracy of U-Pb zircon ages by the creation of more concordant systems using an abrasion technique. *Geochimica et Cosmochimica Acta*, **46**, 637-649.
- Krogh, T. E., Mysen, B. O. & Davis, G. L., 1974. A Paleozoic age for the primary minerals of a Norwegian eclogite. *Yearb. Carnegie Inst. Washington*, **73**, 575-576.
- Leake, B. E., 1978. Nomenclature of amphiboles. *American Mineralogist*, **63**, 1023-1052.
- Liati, A., Gebauer, D., Froitzheim, N. & Fanning, C. M., 2001. U-Pb SHRIMP geochronology of an amphibolitized eclogite and an orthogneiss from the Furgg zone (Western Alps) and implications for its geodynamic evolution. *Schweiz. Mineral. Petrogr. Mitt.*, **81**, 379-393.
- Mariano, A. N., 1989. Cathodoluminescence emission spectra of rare earth element activators in minerals. In: *Geochemistry and Mineralogy of Rare Earth Elements, Reviews in Mineralogy 21* (eds Lipin, B. R. & McKay, G. A.), pp. 339-348, Mineralogical Society of America.
- Maruyama, S. & Liou, J. G., 1998. Initiation of ultrahigh-pressure metamorphism and its significance on the Proterozoic-Phanerozoic boundary. *The Island Arc*, **7**, 6-35.
- Maruyama, S., Liou, J. G. & Terabayashi, M., 1996. Blueschists and eclogites of the world and their exhumation. *International Geology Review*, **38**, 485-594.
- Medaris, G., Jelínek, E. & Mísar, Z., 1995. Czech eclogites: Terrane settings and implications for Variscan tectonic evolution of the Bohemian Massif. *European Journal of Mineralogy*, **7**, 7-28.
- Mezger, K., Hanson, G. N. & Bohlen, S. R., 1989. High-precision U-Pb ages of metamorphic rutile: application to the cooling history of high-grade terranes. *Earth and Planetary Science Letters*, **96**, 106-118.
- Möller, A., Appel, P., Mezger, K. & Schenk, V., 1995. Evidence for a 2 Ga subduction zone: Eclogites in the Usagaran belt of Tanzania. *Geology*, **23**(12), 1067-1070.
- Mottana, A., Carswell, D. A., Chopin, C. & Oberhänsli, R., 1990. Eclogite facies mineral parageneses. In: *Eclogite Facies Rocks* (ed Carswell, D. A.), pp. 14-52, Chapman and Hall, New York.
- O'Brien, P. J., 1993. Partially retrograded eclogites of the Münchberg Massif, Germany: records of a multi-stage Variscan uplift history in the Bohemian Massif. *Journal of Metamorphic Geology*, **11**, 241-260.
- O'Brien, P. J., Röhr, C., Okrusch, M. & Patzak, M., 1992. Eclogite facies relics and multistage breakdown in metabasites of the KTB pilot hole, NE Bavaria: implications for the Variscan tectonometamorphic evolution of the NW Bohemian Massif. *Contributions to Mineralogy and Petrology*, **112**, 261-278.
- O'Brien, P. J. & Rötzler, J., 2003. High-pressure granulites: formation, recovery of peak conditions and implications for tectonics. *Journal of Metamorphic Geology*, **21**, 3-20.

CHAPTER 3 – ECLOGITES OF THE SNOWBIRD TECTONIC ZONE

- O'Brien, P. J. & Vrána, S., 1995. Eclogites with a short-lived granulite facies overprint in the Moldanubian Zone, Czech Republic: petrology, geochemistry, and diffusion modeling of garnet zoning. *Geol Rundsch*, **84**, 473-488.
- Paquette, J.-L., Menot, R.-P. & Peucat, J.-J., 1989. REE, Sm-Nd, and U-Pb zircon study of eclogites from the Alpine External Massifs (Western Alps): evidence for crustal contamination. *Earth and Planetary Science Letters*, **96**, 181-198.
- Percival, J. A. & Card, K. D., 1983. Archean crust as revealed in the Kapuskasing Uplift, Superior Province, Canada. *Geology*, **11**(6), 323-326.
- Poli, S. & Schmidt, M. W., 1998. The high-pressure stability of zoisite and phase relationships of zoisite-bearing assemblages. *Contributions to Mineralogy and Petrology*, **130**, 162-175.
- Powell, R., 1985. Regression diagnostics and robust regression in geothermometer/geobarometer calibration: the garnet-clinopyroxene geothermometer revisited. *Journal of Metamorphic Geology*, **3**, 231-243.
- Root, D. B., Hacker, B. R., Mattinson, J. M. & Wooden, J. L., in review. Young age and rapid exhumation of Norwegian ultrahigh-pressure rocks: an ion microprobe and chemical abrasion study. *Chemical Geology*.
- Rubatto, D., 2002. Zircon trace element geochemistry: partitioning with garnet and the link between U-Pb ages and metamorphism. *Chemical Geology*, **184**, 123-138.
- Rubatto, D., Gebauer, D. & Compagnoni, R., 1999. Dating of eclogite-facies zircons: the age of Alpine metamorphism in the Sesia-Lanzo Zone (Western Alps). *Earth and Planetary Science Letters*, **167**, 141-158.
- Rubatto, D., Schaltegger, U., Lombardo, B., Colombo, F. & Compagnoni, R., 2001. Complex Paleozoic magmatic and metamorphic evolution in the Argentera Massif (Western Alps) resolved with U-Pb dating. *Schweiz. Mineral. Petrogr. Mitt.*, **81**, 213-228.
- Schmitz, M. D. & Bowring, S. A., 2001. The significance of U-Pb zircon dates in lower crustal xenoliths from the southwestern margin of the Kaapvaal craton, southern Africa. *Chemical Geology*, **172**, 59-76.
- Snoeyenbos, D. R., Williams, M. L. & Hanmer, S., 1995. Archean high-pressure metamorphism in the western Canadian Shield. *European Journal of Mineralogy*, **7**, 1251-1272.
- Stimac, J. & Hickmott, D., 1994. Trace-element partition coefficients for ilmenite, orthopyroxene and pyrrhotite in rhyolite determined by micro-PIXE analysis. *Chemical Geology*, **117**, 313-330.
- Sun, W., Williams, I. S. & Shuguang, L., 2002. Carboniferous and Triassic eclogite in the western Dabie Mountains, east-central China: evidence for protracted convergence of the North and South China Blocks. *Journal of Metamorphic Geology*, **20**, 873-886.
- Williams, I. S., Buick, I. S. & Cartwright, I., 1996. An extended episode of early Mesoproterozoic metamorphic fluid flow in the Reynolds Range, Central Australia. *Journal of Metamorphic Geology*, **14**, 29-47.
- Williams, M. L., Hanmer, S., Kopf, C. & Darrach, M., 1995. Syntectonic generation and segregation of tonalitic melts from amphibolite dikes in the lower crust, Striding-

CHAPTER 3 – ECLOGITES OF THE SNOWBIRD TECTONIC ZONE

- Athabasca mylonite zone, northern Saskatchewan. *Journal of Geophysical Research*, **100**(B8), 15717-15734.
- Williams, M. L., Melis, E. A., Kopf, C. & Hanmer, S., 2000. Microstructural tectonometamorphic processes and the development of gneissic layering: a mechanism for metamorphic segregation. *Journal of Metamorphic Geology*, **18**, 41-57.
- Wood, B. J. & Banno, S., 1973. Garnet-orthopyroxene and orthopyroxene-clinopyroxene relationships in simple and complex systems. *Contributions to Mineralogy and Petrology*(42), 109-124.

Figure Captions

Figure 1. Geologic map of the western Canadian Shield showing major tectonic elements (inset shows location of map). Abbreviations are as follows: AB – Athabasca basin, BL – Baker Lake basin, KX – Kramanitaur Complex, STZ – Snowbird tectonic zone, THO – Trans-Hudson Orogen, TO – Talston Orogen, TMZ – Thelon Magmatic Zone, UX – Uvauk Complex, VR – Virgin River Shear Zone. The Striding-Athabasca mylonite zone occurs within the East Athabasca mylonite triangle, the northern tip of the Athabasca lozenge, as well along the eastern margin of the Selwyn lozenge to the northeast (shown in black). Other examples of high-pressure granulites in the STZ include the Kramanitaur Complex and Uvauk Complex. Outline shown for East Athabasca mylonite triangle shown in Figure 2.

Figure 2. (a) Lithotectonic domains of the East Athabasca mylonite triangle, northern Saskatchewan. Outline of study area shown in b, (b) Geologic map of the northern extent of the southern domain showing the location of the eclogite. Locations of samples described in this study are marked with stars.

Figure 3. REE diagram for eclogite samples. Chondrite values from Sun and McDonough (1989).

Figure 4. Photomicrographs of the eclogite. (a) Primary mineralogy is garnet + omphacitic clinopyroxene with secondary development of symplectite textures, (b) Photomicrograph showing reaction rims of Opx + Pl around Cpx and Prg + Pl around Grt, (c) Photomicrograph showing delicate symplectite textures. More extensive reaction results in development of discrete plagioclase domains, (d) Reaction rims are typically ~50-150µm in width. Note plagioclase exsolution from Cpx in bottom right. This is the reaction of Omp + Qtz breaking down to Cpx + Pl.

CHAPTER 3 – ECLOGITES OF THE SNOWBIRD TECTONIC ZONE

Figure 5. BSE images from the eclogite. (a) Garnet with abundant inclusions of kyanite and zoisite, (b) Image shows reaction rim around garnet (bottom of field of view). In anhydrous assemblages, Grt breaks down to form a composite Opx + Pl and Spl + Cpx + Opx symplectite, (c) BSE image showing the various reaction textures in the eclogite. Omp breaks down to Cpx + Na-Pl, which breaks down to Opx + Pl. Garnet breaks down to form pargasite + Ca-Pl. Difference in contrast in image reflects different plagioclase compositions in the symplectites. Plagioclase also occurs in direct contact with Omp (top left field of view). This is the most sodic plagioclase present, with the exception of exsolved plagioclase in Cpx, (d) Omphacite porphyroblast. Difference in contrast in image reflects the variation in Na content in Cpx. Dark region is highest in Na (~Jd₂₃). Outer region of grain is breaking down to a less sodic Cpx + Na-Pl. Panel below is a traverse along A-A'. Maximum Na contents in the omphacite are Jd₂₅.

Figure 6. *P-T* diagram for eclogite. Abbreviations are as follows: an = anorthite, coe = coesite, crn = corundum, di = diopside, gr = grossular, ky = kyanite, law = lawsonite, ma = margarite, py = pyrope, q = quartz, zo = zoisite. Pressures were calculated with the Ab = Jd + Qtz equilibria and are shaded in dark grey for the range in X_{Jd} contents observed in the samples (Holland, 1980). Temperatures were calculated using the Grt-Cpx Fe-Mg exchange reaction using the calibration of Powell (1985) and are shaded in light grey showing the range in calculated temperatures for the samples investigated. Equilibria involving zoisite were calculated using THERMOCALC and activities corresponding to the actual compositions observed in the eclogites, which are indicated by the subscripts. The reaction gr + ky + q = an corresponds to the breakdown reaction of kyanite. Gray arrow shows possible *P-T* path based on the inclusion and reaction textures. Box outlines *P-T* conditions for adjacent mafic granulites from Baldwin et al. (2003). See text for discussion.

CHAPTER 3 – ECLOGITES OF THE SNOWBIRD TECTONIC ZONE

Figure 7. (a) and (b) CL images of zircons from eclogite sample 01SZ41A. Sector and fir-tree zoning are typical in CL. (c) and (d) BSE images showing inclusion suites of high-P phases in relatively large zircon grains from 01SZ41A. (E-H) CL images for 01SZ40B (e) Sector-zoned grain without core (f-h) Other images reveal two distinct CL domains, with variably-sized dark cores surrounded by brighter rims.

Figure 8. (a) Concordia diagram for 01SZ41A zircon, (b) Concordia diagram for 01SZ41B zircon showing mixture between two age components. Mixture is pinned by concordant analyses at 2543 Ma and 1904 Ma, (c) Concordia diagram for rutile from 01SZ40B. All analyses are single grains with the exception of r3 which consisted of 5 grains. Single grain analyses show a correlation with grain size reflecting variations in closure temperature.

Figure 9. (a) BSE image of 01SZ40B showing petrographic setting of zircon. Zircon is mostly contained within Cpx. For the analyses shown in Table 9, grain 1 is shown at left, grain 2 is the cluster, and grain 3 is in the lower right corner and is also shown in Figure 9, (b) Sketch of zircon cluster in thin section showing location of SHRIMP analysis pits, (c) CL image showing bright rims on most of the individual zircon grains.

Figure 10. (a) BSE image of well-armored zircon inclusions within Cpx. SHRIMP data indicate a Proterozoic age for the zircon shown in b and c, (b) CL image of grain outlined in (a), (c) BSE image of grain shown in b showing location of SHRIMP analysis pit.

CHAPTER 3 - ECLOGITES OF THE SNOWBIRD TECTONIC ZONE

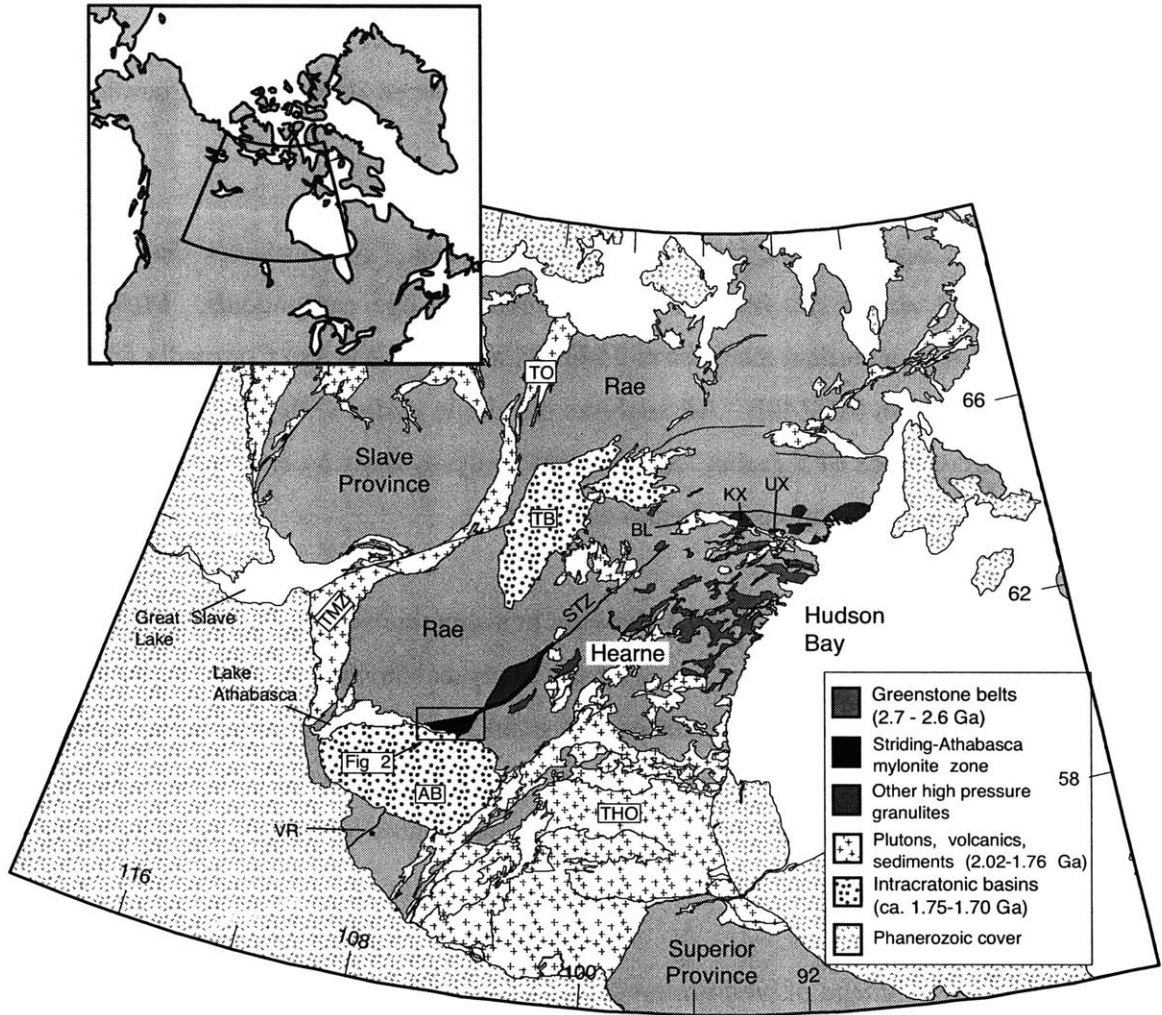


Figure 1

CHAPTER 3 - ECLOGITES OF THE SNOWBIRD TECTONIC ZONE

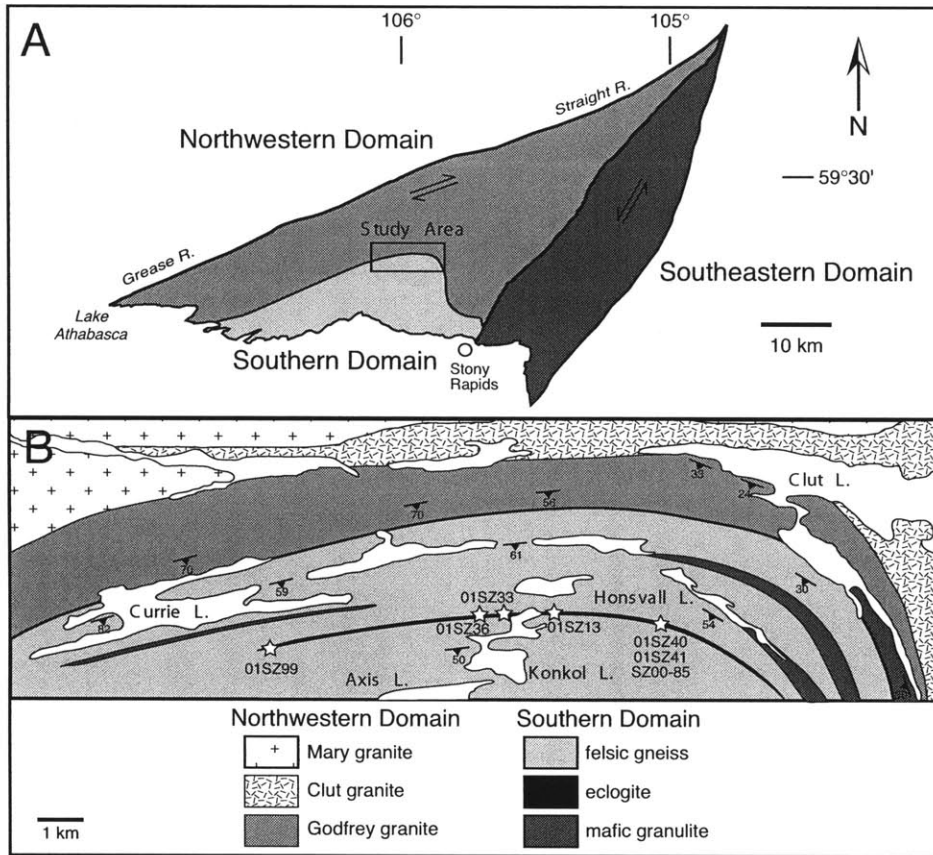


Figure 2

CHAPTER 3 - ECLOGITES OF THE SNOWBIRD TECTONIC ZONE

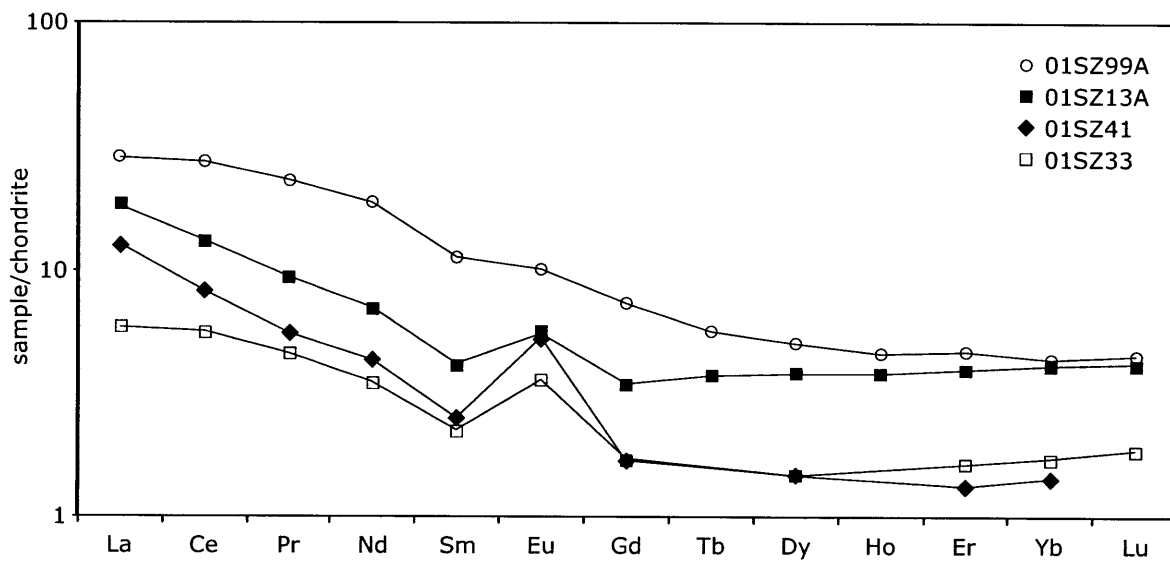


Figure 3

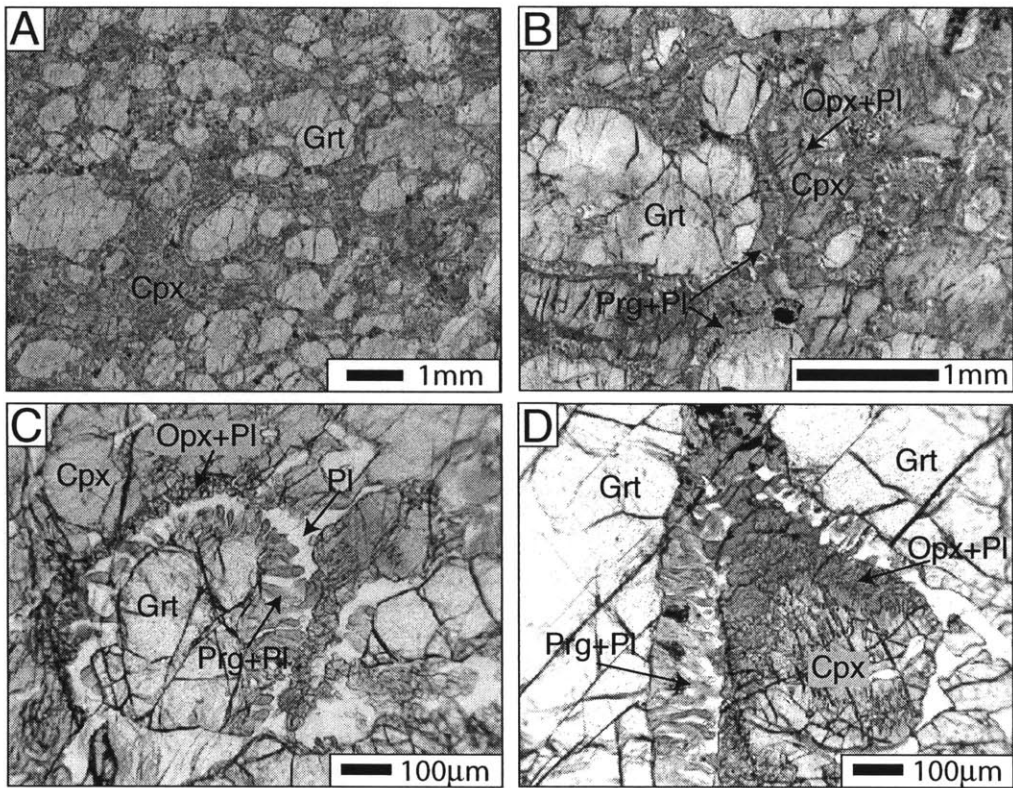


Figure 4

CHAPTER 3 - ECLOGITES OF THE SNOWBIRD TECTONIC ZONE

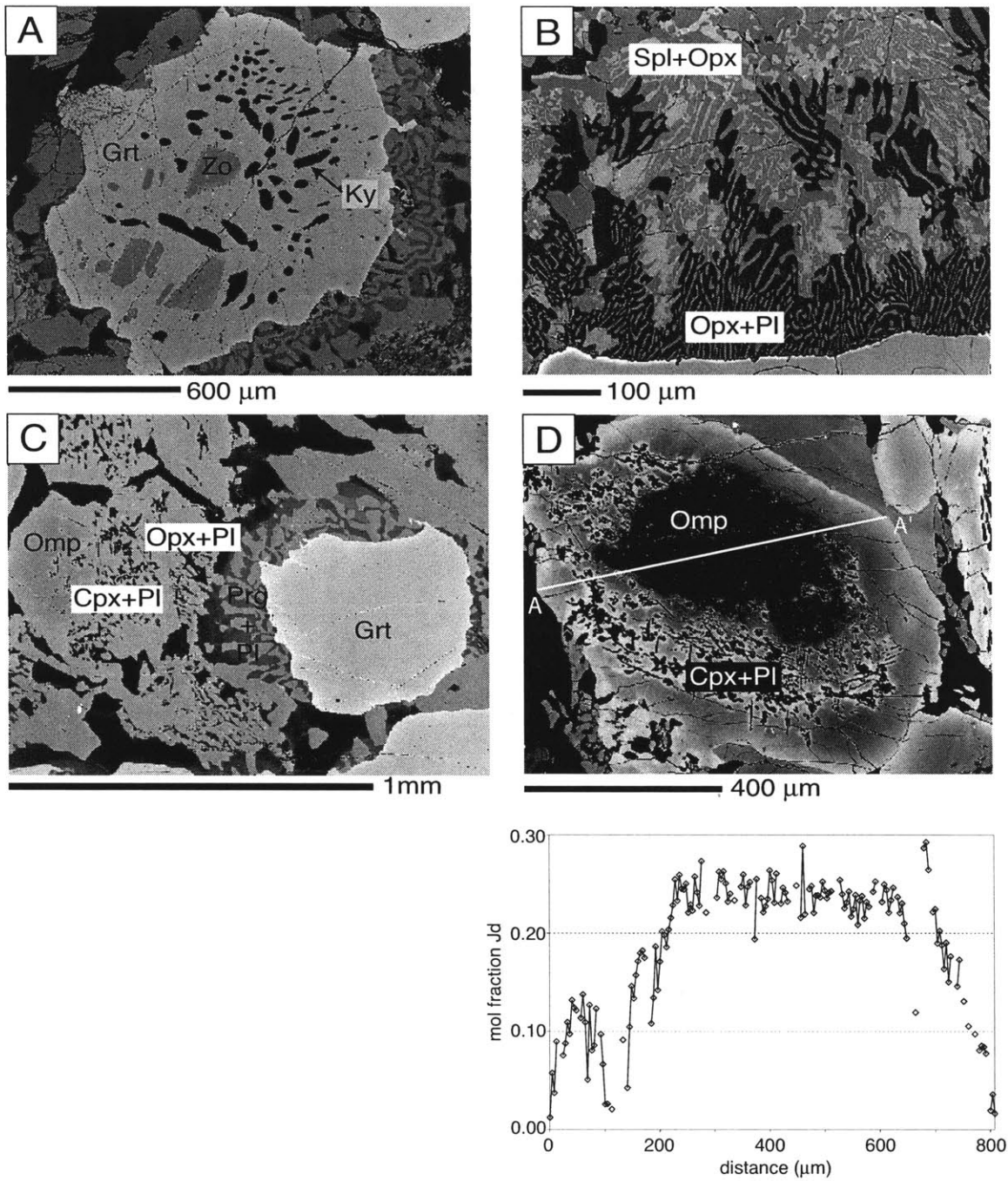


Figure 5

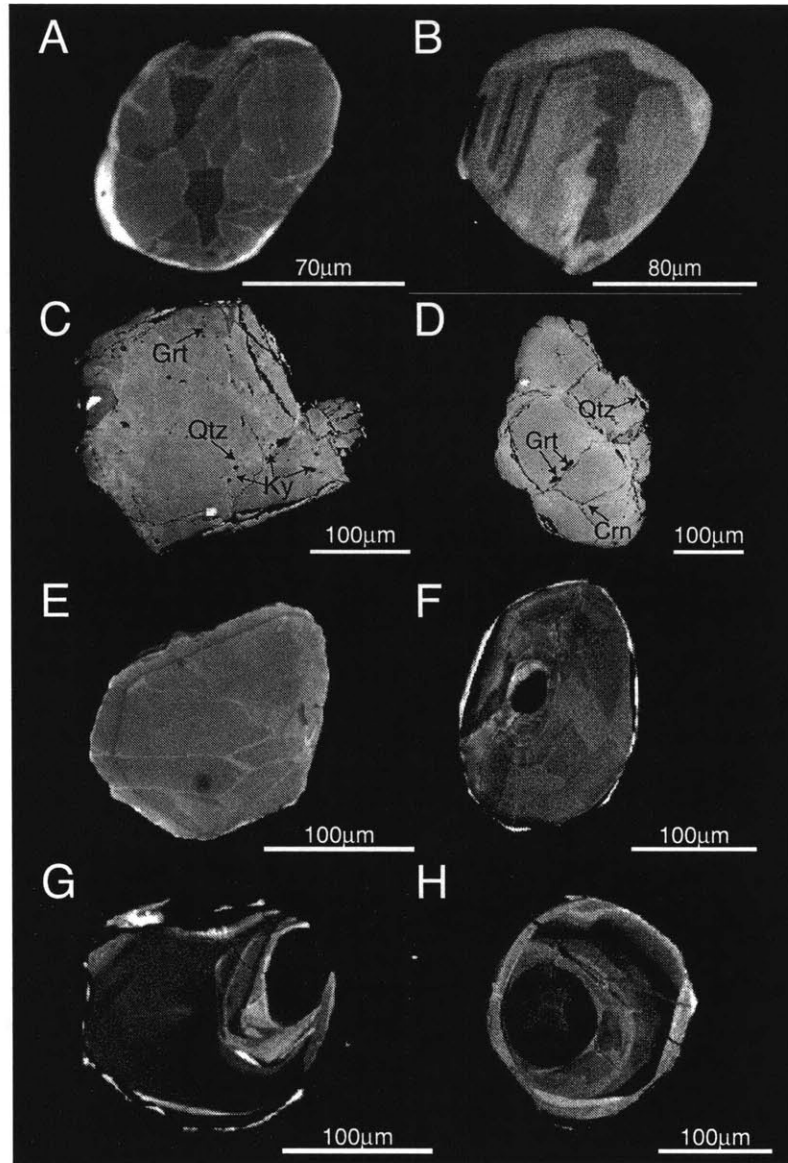


Figure 7

CHAPTER 3 - ECLOGITES OF THE SNOWBIRD TECTONIC ZONE

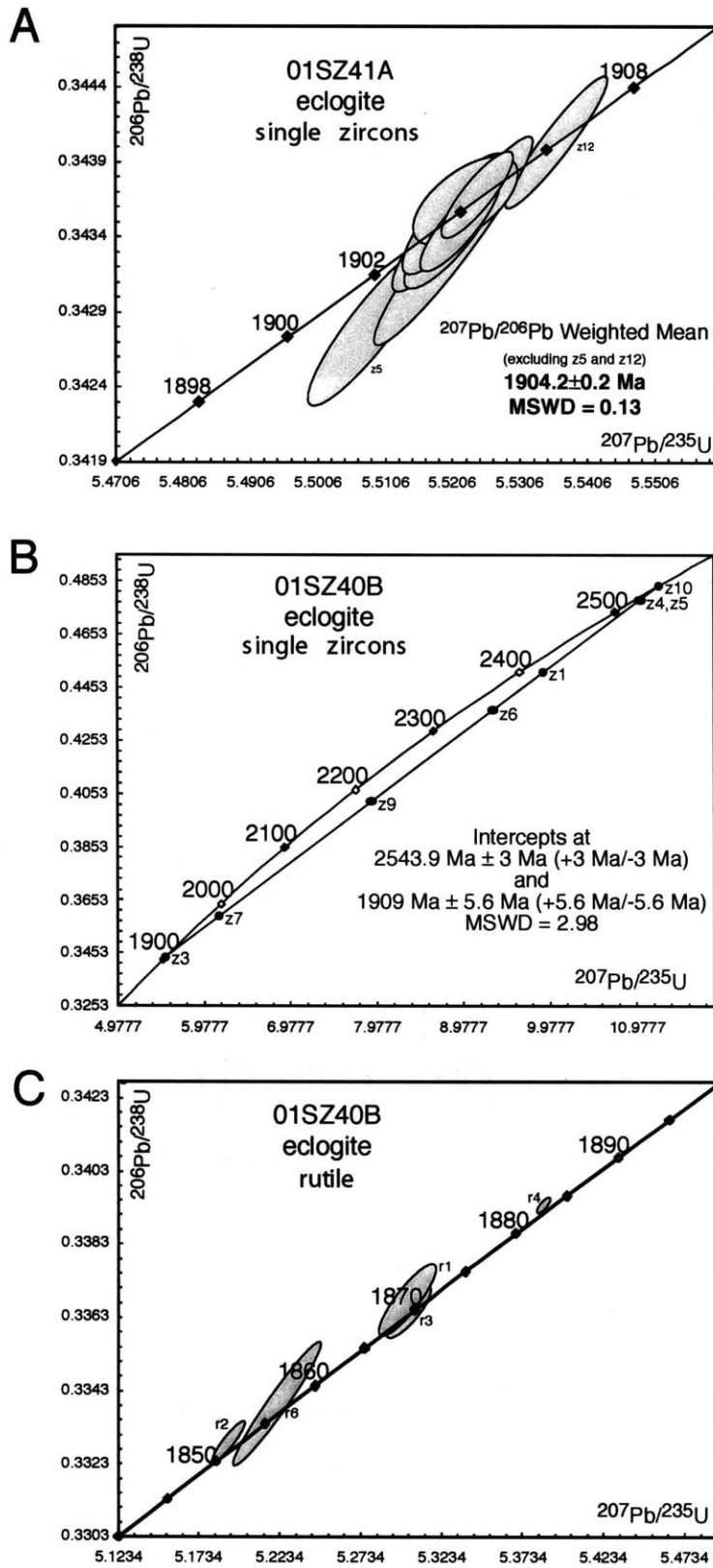


Figure 8

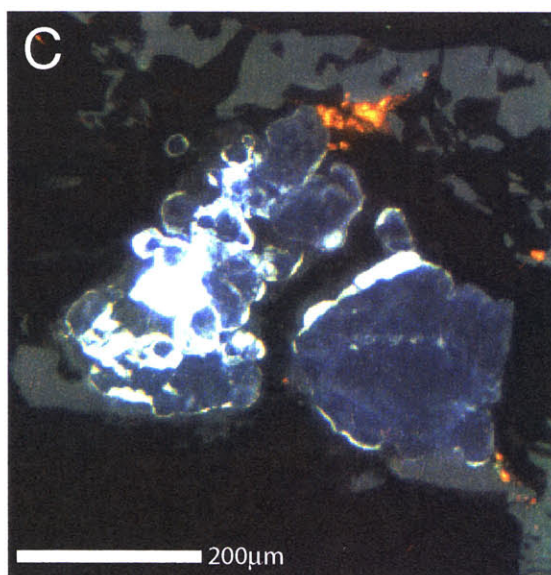
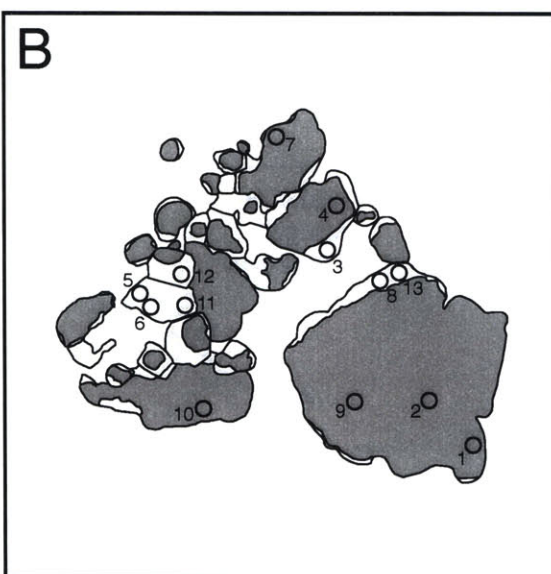
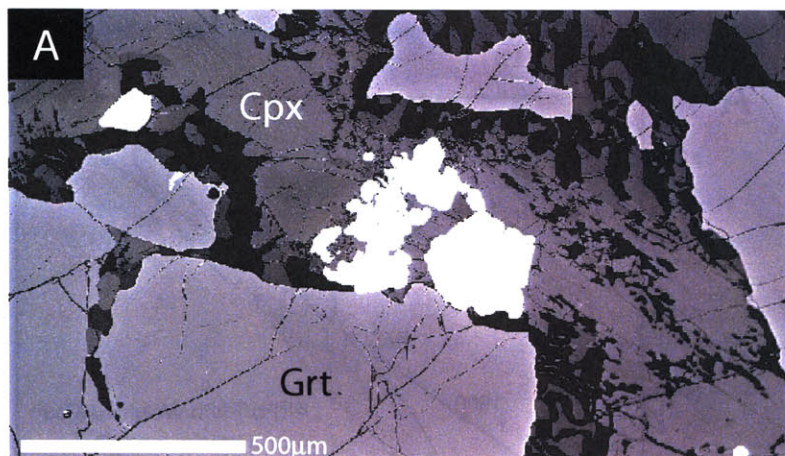


Figure 9

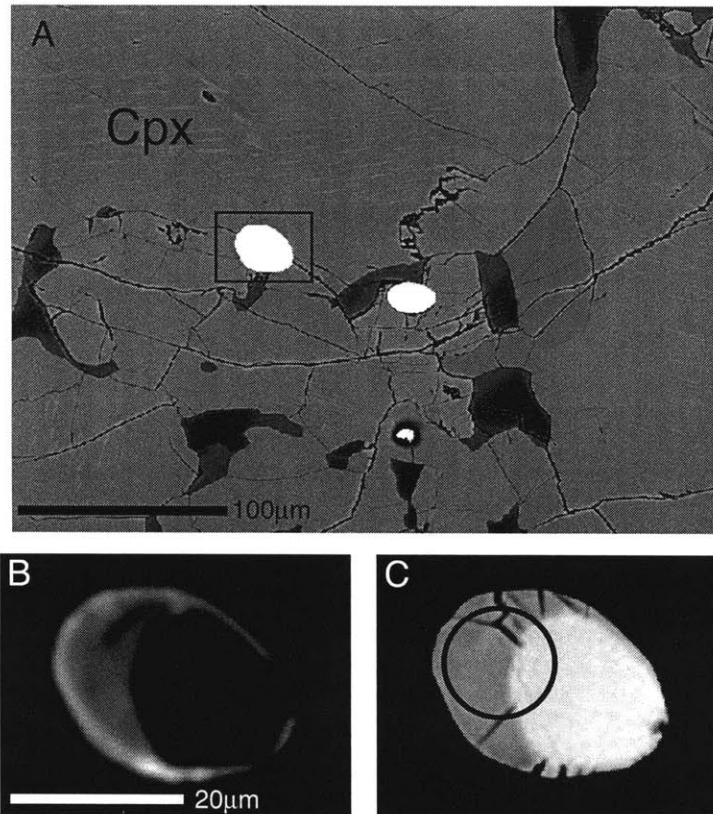


Figure 10

CHAPTER 3 - ECLOGITES OF THE SNOWBIRD TECTONIC ZONE

Table 1. Major and trace element data for eclogite

Sample:	01SZ41	01SZ13A	01SZ33	01SZ99A
SiO ₂	42.75	45.09	43.67	44.76
Al ₂ O ₃	20.37	19.90	18.25	18.73
Fe ₂ O ₃	9.58	8.75	9.69	9.91
MnO	0.13	0.13	0.14	0.14
MgO	14.86	13.10	15.66	12.29
CaO	10.29	11.52	10.33	12.32
Na ₂ O	1.05	1.26	1.28	1.41
K ₂ O	0.45	0.19	0.35	0.29
TiO ₂	0.16	0.14	0.06	0.21
P ₂ O ₅	0.03	0.02	0.01	0.01
L.O.I.	0.37	-0.04	0.67	0.19
Total	100.03	100.06	100.12	100.27
Sc	11.00	19.00	12.00	28.00
V	59.33	84.68	42.55	120.43
Cr	104.55	183.27	128.47	267.39
Co	85.27	76.45	89.50	73.50
Ni	245.58	229.75	255.24	184.62
Ga	14.85	13.12	11.51	14.99
Ge	1.14	1.01	1.36	1.70
Rb	6.52	2.25	5.06	3.44
Sr	84.03	66.71	96.65	77.56
Y	2.14	5.89	2.34	7.01
Zr	19.39	18.07	6.54	27.12
Nb	0.00	1.31	0.00	0.00
Ba	27.97	26.38	21.79	40.40
La	2.97	4.31	1.39	6.77
Ce	5.00	8.02	3.42	16.73
Pr	0.53	0.89	0.44	2.18
Nd	2.02	3.27	1.64	8.78
Sm	0.39	0.63	0.34	1.71
Eu	0.31	0.32	0.21	0.58
Gd	0.35	0.71	0.36	1.51
Tb	0.00	0.14	0.00	0.21
Dy	0.37	0.96	0.38	1.29
Ho	0.00	0.22	0.00	0.26
Er	0.22	0.65	0.27	0.76
Tm	0.00	0.11	0.00	0.12
Yb	0.24	0.70	0.29	0.73
Lu	0.00	0.10	0.05	0.11
Hf	0.48	0.52	0.00	0.70
Th	0.43	0.49	0.00	0.43
Eu/Eu*	12.8	16.4	14.6	5.3
Mg #	75	75	76	71

Recalculation of composition of protolith (Grove et al., 1992)

An	0.524	0.502	0.456	0.464
Ol	0.352	0.290	0.353	0.266
Ab	0.100	0.118	0.122	0.134
Or	0.028	0.012	0.022	0.018
Cpx	0.012	0.071	0.065	0.136
Sp	0.003	0.003	0.001	0.004
Qtz	-0.019	0.005	-0.020	-0.022
Ternary normalization				
Cpx	0.011	0.071	0.065	0.136
Pl	0.631	0.632	0.580	0.597
Ol	0.359	0.297	0.355	0.268

Table 2. Representative garnet microprobe analyses from eclogite

Sample	01SZ40b	01SZ40b	SZ00-85A	SZ00-85A	SZ00-85A	SZ00-85A	01SZ99A	01SZ99A	01SZ99A	01SZ99B	01SZ99B	01SZ36A	01SZ36A
Type	core	rim	core (ky)	rim	core	rim	core (ky+zo)	rim	core (ky)	core	core	core	rim
SiO ₂	40.38	39.43	40.41	40.73	41.04	41.14	40.38	39.42	40.25	40.92	40.56	40.49	40.14
TiO ₂	0.02	0.08	0.06	0.00	0.04	0.06	0.13	0.05	0.06	0.04	0.07	0.04	0.02
Al ₂ O ₃	23.25	22.85	23.21	23.28	23.80	23.46	23.25	23.07	23.20	23.58	23.42	23.39	23.20
Cr ₂ O ₃	0.089	0.068	0.00	0.00	0.03	0.02	0.02	0.06	0.07	0.02	0.00	0.012	0.083
FeO	15.97	19.45	12.98	11.53	11.49	12.86	14.20	17.20	13.30	13.58	12.28	14.72	16.46
MnO	0.24	0.54	0.34	0.15	0.25	0.24	0.28	0.47	0.28	0.21	0.17	0.26	0.33
MgO	12.39	10.08	13.24	14.33	14.77	13.65	12.21	10.55	11.85	15.14	13.81	13.17	11.29
CaO	7.84	7.72	9.89	9.30	8.60	9.76	9.69	8.98	10.81	6.73	9.54	8.02	8.75
Na ₂ O	0.05	bd	bd	bd	bd	bd	bd	0.02	bd	0.02	0.05	bd	0.02
Total	100.23	100.23	100.11	99.32	100.01	101.20	100.17	99.82	99.83	100.24	99.89	100.10	100.29
Si	2.982	2.967	2.968	2.986	2.979	2.981	2.977	2.958	2.976	2.977	2.970	2.978	2.979
Ti	0.001	0.005	0.003	0.000	0.002	0.003	0.007	0.003	0.003	0.002	0.004	0.002	0.001
Al	2.024	2.026	2.009	2.011	2.036	2.003	2.020	2.041	2.022	2.022	2.021	2.028	2.030
Cr	0.005	0.004	0.000	0.000	0.002	0.001	0.001	0.004	0.004	0.001	0.000	0.001	0.005
Fe ²⁺	0.986	1.224	0.797	0.707	0.697	0.779	0.876	1.079	0.823	0.827	0.752	0.905	1.022
Mn	0.015	0.034	0.021	0.010	0.015	0.015	0.017	0.030	0.018	0.013	0.010	0.016	0.021
Mg	1.364	1.130	1.449	1.565	1.599	1.474	1.342	1.180	1.306	1.642	1.507	1.443	1.249
Ca	0.620	0.623	0.778	0.731	0.669	0.758	0.765	0.722	0.857	0.525	0.748	0.632	0.696
Na	0.008	0.000	0.000	0.000	0.000	0.000	0.000	0.003	0.001	0.003	0.007	0.000	0.003
X _{Grs}	0.21	0.21	0.26	0.24	0.22	0.25	0.26	0.24	0.29	0.17	0.25	0.21	0.23
X _{Sps}	0.01	0.01	0.01	0.00	0.01	0.00	0.01	0.01	0.01	0.00	0.00	0.01	0.01
X _{Alm}	0.33	0.41	0.26	0.23	0.23	0.26	0.29	0.36	0.27	0.27	0.25	0.30	0.34
X _{Prp}	0.46	0.38	0.48	0.52	0.54	0.49	0.45	0.39	0.43	0.55	0.50	0.48	0.42

Normalized to 12 oxygens. bd, below detection limit. Core (ky), core (ky+zo), garnet core contains kyanite or kyanite and zoisite inclusions.

Table 3. Representative pyroxene microprobe analyses from eclogite

Sample	01SZ40b	01SZ40b	01SZ40b	SZ00-85A	SZ00-85A	SZ00-85A	01SZ99A	01SZ99A	01SZ99B	01SZ36A	01SZ36A	01SZ36A
Type	cpx core	cpx rim	opx sym	cpx core	cpx rim	opx sym	cpx core	cpx rim	cpx core	cpx core	opx sym grt	opx adj cpx
SiO ₂	52.54	50.76	53.80	52.53	50.86	54.38	53.10	50.36	52.75	52.48	53.24	53.19
TiO ₂	0.29	0.36	0.04	0.06	0.07	bd	0.20	0.21	0.12	0.27	0.01	bd
Al ₂ O ₃	10.57	6.74	2.62	9.57	9.07	3.82	10.56	9.35	9.69	9.76	3.98	3.30
Cr ₂ O ₃	0.04	0.06	0.05	bd	bd	bd	bd	0.06	0.03	0.06	0.04	0.00
FeO	5.38	5.61	16.90	3.04	6.10	13.72	3.22	4.45	3.62	3.43	15.54	16.39
MnO	0.04	0.01	0.20	0.01	0.06	0.26	0.03	0.06	0.01	bd	0.16	0.20
MgO	10.52	13.03	26.37	12.42	15.60	28.36	11.41	13.10	11.95	11.77	26.99	26.58
CaO	17.17	22.04	0.31	19.81	17.09	0.26	18.93	21.89	18.55	19.34	0.34	0.30
Na ₂ O	4.02	1.40	bd	2.65	1.12	bd	3.38	1.18	3.15	3.16	0.03	bd
Total	100.58	100.00	100.30	100.10	99.98	100.80	100.83	100.67	99.86	100.28	100.32	99.98
Si	1.882	1.855	1.924	1.888	1.838	1.922	1.892	1.821	1.899	1.883	1.906	1.918
Al ^{IV}	0.118	0.145	0.076	0.112	0.162	0.078	0.108	0.179	0.101	0.117	0.094	0.082
Ti	0.008	0.010	0.001	0.002	0.001	0.000	0.005	0.006	0.003	0.007	0.000	0.000
Al ^{VI}	0.328	0.145	0.047	0.293	0.235	0.081	0.336	0.219	0.310	0.295	0.073	0.059
Cr	0.001	0.002	0.001	0.000	0.000	0.000	0.000	0.002	0.001	0.002	0.001	0.000
Fe ²⁺	0.110	0.093	0.488	0.091	0.083	0.405	0.101	0.105	0.105	0.078	0.444	0.471
Fe ³⁺	0.051	0.078	0.027	0.000	0.039	0.000	0.000	0.029	0.004	0.025	0.021	0.023
Mn	0.001	0.000	0.007	0.000	0.001	0.008	0.001	0.002	0.000	0.000	0.005	0.006
Mg	0.562	0.710	1.417	0.665	0.697	1.494	0.606	0.706	0.641	0.630	1.440	1.429
Ca	0.659	0.863	0.012	0.763	0.829	0.010	0.723	0.848	0.715	0.743	0.013	0.012
Na	0.279	0.099	0.000	0.185	0.114	0.000	0.233	0.083	0.220	0.220	0.002	0.000
Ac	0.05	0.08		0.00	0.04		0.00	0.03	0.00	0.03		
Jd	0.23	0.02		0.18	0.08		0.23	0.05	0.22	0.20		
CaTs	0.11	0.14		0.11	0.15		0.10	0.17	0.09	0.11		
Aug	0.72	0.90		0.82	0.88		0.77	0.92	0.78	0.78		
X _{Mg}	0.84	0.88	0.74	0.88	0.89	0.79	0.86	0.87	0.86	0.89	0.76	0.75
En			0.66			0.70					0.66	0.66
Fs			0.36			0.32					0.34	0.35

Normalized to 6 oxygens. Ferric iron calculated by charge balance. bd, below detection limit. $X_{Mg} = Mg/(Mg+Fe^{2+})$

Table 4. Representative plagioclase microprobe analyses from eclogite.

Sample	01SZ40b		01SZ40b		01SZ40b		01SZ99A		01SZ99B		01SZ36A		01SZ36A		SZ00-85A	
Type	opx	sym adj cpx	amph	sym adj grt	adj cpx	incl in cpx	inner adj grt	outer rim grt	incl in cpx	adj cpx	amph	sym adj grt	adj cpx	opx	sym adj grt	
SiO ₂		55.99		46.77	60.40	61.40	47.62	57.34	61.55	57.13		45.75		58.35		44.66
Al ₂ O ₃		28.26		34.41	24.93	25.19	34.72	27.96	24.50	27.12		35.69		27.27		36.22
FeO		0.30		0.26	0.12	bd	0.25	0.09	0.09	0.16		0.36		0.07		0.26
MgO		0.01		0.01	bd	bd	0.03	bd	0.01	0.01		0.01		bd		0.01
CaO		9.89		17.17	6.24	6.30	17.06	9.30	5.70	8.89		18.55		8.90		18.90
Na ₂ O		6.03		1.76	7.90	8.20	1.82	6.47	8.30	6.46		1.04		7.00		0.72
K ₂ O		0.15		0.02	0.21	0.21	0.05	0.08	0.22	0.21		bd		0.03		bd
Total		100.62		100.40	99.80	101.30	101.54	101.25	100.36	99.99		101.40		101.61		100.77
Si		2.506		2.141	2.693	2.696	2.153	2.542	2.724	2.5637		2.082		2.575		2.047
Al		1.491		1.857	1.310	1.304	1.850	1.461	1.278	1.434		1.914		1.418		1.957
Fe ²⁺		0.011		0.010	0.005	0.000	0.009	0.004	0.003	0.006		0.014		0.003		0.010
Mg		0.001		0.001	0.000	0.000	0.002	0.000	0.001	0.001		0.001		0.000		0.001
Ca		0.475		0.842	0.298	0.296	0.827	0.442	0.270	0.428		0.904		0.421		0.928
Na		0.523		0.156	0.683	0.699	0.159	0.556	0.712	0.562		0.092		0.599		0.064
K		0.008		0.001	0.012	0.012	0.003	0.005	0.012	0.012		0.000		0.002		0.000
X _{An}		0.47		0.84	0.30	0.29	0.84	0.44	0.27	0.43		0.91		0.41		0.94

Normalized to 8 oxygens. bd, below detection limit.

CHAPTER 3 - ECLOGITES OF THE SNOWBIRD TECTONIC ZONE

Table 5. Representative amphibole and biotite microprobe analyses from eclogite

Sample	01SZ40b	SZ00-85A	01SZ99A	01SZ99A	01SZ99A	01SZ99B	01SZ99B
Type	sym around grt	matrix	matrix	sym around grt	incl in grt	phlogopite	phlogopite
SiO ₂	41.36	42.81	43.04	42.16	43.29	38.36	38.47
TiO ₂	0.22	0.28	0.57	0.21	0.65	5.16	5.42
Al ₂ O ₃	16.47	16.26	15.55	16.86	16.40	16.36	16.02
Cr ₂ O ₃	0.09	0.10	0.10	0.08	0.06	0.03	0.06
FeO	9.25	6.82	7.59	8.73	5.84	5.66	5.50
MnO	0.01	0.06	0.06	0.07	0.07	0.01	bd
MgO	14.38	16.33	15.69	14.33	16.04	20.55	20.32
CaO	11.97	11.97	11.87	11.99	11.76	bd	0.02
Na ₂ O	2.45	2.60	2.61	2.76	2.43	0.19	0.14
K ₂ O	1.32	1.31	0.92	0.65	1.65	10.00	9.96
Total	97.51	98.54	97.99	97.84	98.18	96.33	95.91
Si	5.962	6.026	6.105	6.025	6.117	5.432	5.466
Ti	0.024	0.030	0.061	0.022	0.069	0.550	0.579
Al	2.798	2.697	2.599	2.839	2.731	2.730	2.682
Cr	0.010	0.011	0.011	0.009	0.006	0.001	0.002
Fe ²⁺	0.519	0.176	0.334	0.540	0.322	0.670	0.653
Fe ³⁺	0.596	0.627	0.565	0.504	0.368		
Mn	0.001	0.007	0.007	0.009	0.008	0.002	0.000
Mg	3.090	3.427	3.317	3.052	3.379	4.338	4.304
Ca	1.848	1.805	1.803	1.836	1.780	0.000	0.003
Na	0.685	0.709	0.719	0.763	0.666	0.052	0.040
K	0.243	0.235	0.167	0.118	0.297	1.806	1.805
X _{Mg}	0.86	0.95	0.91	0.85	0.91	0.87	0.87
Classification:	pargasite	pargasite	pargasite	pargasite	pargasite		

Normalized to 23 oxygens. Ferric iron calculated by charge balance. bd, below detection. $X_{Mg} = Mg/(Mg+Fe^{2+})$

Amphibole classification according to Leake (1978).

CHAPTER 3 - ECLOGITES OF THE SNOWBIRD TECTONIC ZONE

Table 6. Representative zoisite and spinel microprobe analyses from eclogite.

Sample	01SZ99A	01SZ99A	01SZ40b	SZ00-85A	SZ00-85A	01SZ99A
Mineral	Zo	Zo	Spl	Spl	Spl	Spl
Type	incl in grt	incl in grt	matrix	sym grt	sym grt	sym grt
SiO ₂	39.84	40.10	0.03	0.03	0.00	0.04
TiO ₂	0.10	0.05	0.02	0.00	0.00	0.00
Al ₂ O ₃	32.78	32.61	65.54	64.74	63.70	64.58
Cr ₂ O ₃	na	na	0.09	0.08	0.06	0.07
FeO	1.37	1.16	16.36	18.53	20.24	17.91
MnO	0.05	0.02	0.11	0.09	0.14	0.05
MgO	0.04	0.07	17.30	15.83	15.64	15.93
CaO	24.69	24.69	0.11	0.11	0.00	0.10
NiO	na	na	0.27	0.24	0.00	0.23
Total	98.88	98.70	99.83	99.65	99.77	98.92
Si	3.000	3.023	0.000	0.001	0.000	0.001
Ti	0.006	0.003	0.000	0.000	0.000	0.000
Al	2.908	2.897	1.976	1.975	1.950	1.981
Cr	na	na	0.002	0.002	0.001	0.001
Fe ³⁺	0.080	0.050	0.020	0.021	0.048	0.016
Fe ²⁺	0.006	0.023	0.330	0.380	0.391	0.374
Mn	0.003	0.001	0.002	0.002	0.003	0.001
Mg	0.005	0.008	0.660	0.611	0.606	0.618
Ca	1.992	1.994	0.003	0.003	0.000	0.003
Ni	na	na	0.005	0.005	0.000	0.005
X_{Mg}			0.67	0.62	0.61	0.62

Zoisite normalized to 12.5 and spinel to 4 oxygens. Ferric iron calculated by charge balance.

Abbreviations: na, not analyzed; bd, below detection; $X_{Mg} = Mg/(Mg+Fe^{2+})$

CHAPTER 3 - ECLOGITES OF THE SNOWBIRD TECTONIC ZONE

Table 7. Thermobarometric Results.

Sample	UTM North	UTM East	T (P85) ¹ °C	a _{jd} ²	a _{Ab}	P (H80) ³ GPa	GOPQ ⁴ P,T	GHPQ ⁴ P,T
01SZ36A	6582803	0444022	970	0.18	0.60	1.9		
01SZ40B	6582213	0448256	920	0.22	0.70	1.8	1.2, 810	1.1, 790
SZ00-85A	6582304	0448095	1000	0.15	0.56	1.8		
01SZ99A	6582389	0440226	990	0.21	0.57	2.0		
01SZ99B	6582389	0440226	960	0.20	0.72	1.8		

¹ Temperatures calculated using Grt-Cpx calibration of Powell (1985), ² Activity of jadeite calculated from Holland (1980), ³ Ab-Jd-Qtz barometer of Holland (1980). Pressures calculated at intersection of Grt-Cpx and Ab-Jd-Qtz curves, ⁴ Garnet-orthopyroxene-plagioclase-quartz and garnet-hornblende-plagioclase-quartz equilibria calculated for reaction rims around Garnet and Cpx (Fig. 5c) using TWQ software (Berman 1991).

Table 8. U-Pb IDTIMS isotopic data for eclogite zircon and rutile

Fractions ^a	Weight (mg) ^b	Compositions				Isotopic Ratios						Dates (Ma)			Dis- cordance (%)		
		U	Pb	Th	Pb ^c	206 Pb* ^d	208 Pb	206 Pb ^e	207 Pb ^e	207 Pb ^e	206 Pb	207 Pb	207 Pb ^f				
		(ppm)	(ppm)	U	(pg)	204 Pb	206 Pb	238 U	% err	235 U	% err	206 Pb	% err	238 U		235 U	206 Pb
<i>01SZ41A eclogite</i>																	
z1	41.5	33.4	14.0	1.04	2.6	11776	0.301	0.34360	(0.12)	5.52082	(0.14)	0.11653	(0.07)	1903.9	1903.8	1903.7 ± 1.3	0.0
z2	39.8	277.2	142.2	2.03	90.7	2423	0.588	0.34341	(0.10)	5.51785	(0.11)	0.11653	(0.06)	1903.1	1903.4	1903.7 ± 1.1	0.0
z3	21.8	43.9	16.2	0.46	0.7	30249	0.133	0.34345	(0.10)	5.52025	(0.12)	0.11657	(0.07)	1903.2	1903.8	1904.3 ± 1.2	0.1
z4	15.4	41.4	14.7	0.29	3.0	4658	0.083	0.34352	(0.09)	5.52174	(0.11)	0.11658	(0.06)	1903.6	1904.0	1904.4 ± 1.0	0.0
z5	3.2	59	19.7	0.06	2.0	2085	0.016	0.34285	(0.15)	5.50858	(0.17)	0.11653	(0.07)	1900.3	1901.9	1903.7 ± 1.3	0.2
z8	11.6	24.5	8.5	0.19	2.2	2855	0.054	0.34342	(0.20)	5.52078	(0.21)	0.11659	(0.07)	1903.1	1903.8	1904.6 ± 1.2	0.1
z9	10.8	15.3	5.3	0.20	0.8	4568	0.057	0.34368	(0.09)	5.52270	(0.14)	0.11654	(0.11)	1904.4	1904.1	1903.9 ± 1.4	0.0
z10	12.4	30	10.8	0.33	1.2	6743	0.097	0.34372	(0.08)	5.52434	(0.10)	0.11657	(0.05)	1904.6	1904.4	1904.2 ± 0.9	0.0
z12	9.7	75.7	25.9	0.07	7.9	1960	0.020	0.34408	(0.13)	5.53611	(0.14)	0.11669	(0.05)	1906.2	1906.2	1906.2 ± 0.9	0.0
<i>01SZ40B eclogite</i>																	
z1	18.5	90.2	47.0	0.63	3.6	13393	0.1824	0.45114	(0.07)	9.90090	(0.08)	0.15917	(0.04)	2400.3	2425.6	2446.9 ± 0.7	2.3
z3	5.5	46.9	16.4	0.14	5.1	1091	0.0413	0.34373	(0.32)	5.52380	(0.33)	0.11655	(0.08)	1904.6	1904.3	1904.0 ± 1.4	0.0
z4	40.1	68.4	38.0	0.65	3.7	22568	0.1824	0.47822	(0.05)	11.02176	(0.07)	0.16715	(0.04)	2519.5	2525.0	2529.4 ± 0.7	0.5
z5	16.2	101.6	56.8	0.67	5.8	8274	0.1867	0.47840	(0.07)	11.02989	(0.08)	0.16722	(0.04)	2520.3	2525.7	2530.0 ± 0.7	0.5
z6	50.0	57.8	28.7	0.58	2.3	35165	0.1685	0.43663	(0.07)	9.32434	(0.08)	0.15488	(0.04)	2335.5	2370.4	2400.6 ± 0.7	3.2
z7	19.8	59.7	26.9	1.13	2.0	13594	0.3321	0.35908	(0.05)	6.14527	(0.07)	0.12412	(0.04)	1977.8	1996.7	2016.3 ± 0.7	2.2
z8	3.6	67.5	29.8	0.78	1.8	3246	0.2293	0.37691	(0.10)	6.83983	(0.13)	0.13162	(0.08)	2061.8	2090.9	2119.6 ± 1.4	3.2
z9	5.9	30.8	14.7	0.80	2.4	2009	0.2365	0.40266	(0.14)	7.91586	(0.15)	0.14258	(0.06)	2181.3	2221.5	2258.8 ± 1.0	4.0
z10	6.0	47.3	26.5	0.63	2.2	4092	0.1751	0.48367	(0.08)	11.23781	(0.10)	0.16851	(0.06)	2543.2	2543.1	2542.9 ± 0.9	0.0
r1	274.4	3.0	1.0	0.00	12.2	1381	0.0012	0.33699	(0.29)	5.30857	(0.33)	0.11425	(0.16)	1872.2	1870.2	1868.1 ± 2.9	-0.3
r2	117.0	1.8	0.6	0.02	3.0	1489	0.0068	0.33311	(0.17)	5.19734	(0.19)	0.11316	(0.08)	1853.5	1852.2	1850.8 ± 1.4	-0.2
r3	225.0	1.9	0.6	0.00	4.2	2184	0.0014	0.33647	(0.21)	5.30321	(0.25)	0.11431	(0.14)	1869.7	1869.4	1869.0 ± 2.6	0.0
r4	447.9	8.8	2.9	0.03	18.9	4194	0.0076	0.33939	(0.06)	5.38663	(0.07)	0.11511	(0.04)	1883.7	1882.7	1881.6 ± 0.8	-0.1
r6	56.0	4.0	1.5	0.02	15.9	295	0.0059	0.33397	(0.50)	5.22162	(0.52)	0.11340	(0.13)	1857.6	1856.2	1854.5 ± 2.4	-0.2

^a Abbreviation z for zircon and r for rutile. All fractions are single grains with the exception of r3, which consisted of 5 grains

^b Sample weights were estimated to within 40% using measured grains dimensions, and nominal density 4.5g/cm³ for zircon and 4.2g/cm³ for rutile

^c common Pb

^d Measured ratio corrected for fractionation and spike contribution; Pb fractionation correction is 0.12 ± 0.04% per a m u (2s) for multicollector analyses and 0.15 ± 0.04% per a m u (2s) for single collector analyses based on repeated daily analysis of NBS 981

^e Pb/U isotopic ratios corrected for fractionation, spike, blank, and initial common Pb; U blank = 0.1 pg ± 50%, data was reduced using a Pb blank of 3.5 ± 50%, initial common Pb composition was estimated using the model for terrestrial Pb evolution of Stacey & Kramers (1975); numbers in parentheses are the % error reported at the 2-sigma confidence interval

^f Uncertainty in the Pb-Pb date in My at the 2-sigma confidence interval

Table 9. SHRIMP U-Th-Pb analyses of zircon from the eclogite. Errors are given at 1 sigma level.

Label ^a	U (ppm)	Th (ppm)	Th/U	Pb* (ppm) ^b	²⁰⁶ Pb/ ²³⁸ U	± 1σ	²⁰⁷ Pb/ ²³⁵ U	± 1σ	²⁰⁷ Pb/ ²⁰⁶ Pb	± 1σ	²⁰⁷ Pb/ ²⁰⁶ Pb Date (Ma)	± 1σ
1.1C	92	55	0.60	36	0.352	0.010	5.87	0.22	0.1208	0.0025	1968	37
1.2C	85	54	0.63	33	0.349	0.009	5.68	0.23	0.1181	0.0032	1928	49
2.1C	199	78	0.39	74	0.355	0.006	5.68	0.14	0.1159	0.0018	1894	29
2.2C	141	108	0.76	56	0.347	0.008	5.60	0.17	0.1172	0.0021	1913	33
2.3O	27	15	0.56	10	0.328	0.019	5.04	0.46	0.1115	0.0070	1823	118
2.4C	284	118	0.41	107	0.356	0.007	5.74	0.12	0.1170	0.0010	1911	15
2.5O	20	5	0.26	7	0.346	0.018	5.77	0.56	0.1211	0.0093	1972	143
2.6O	22	5	0.23	8	0.341	0.017	5.80	0.74	0.1233	0.0136	2004	211
2.7C	204	131	0.64	80	0.355	0.007	5.70	0.14	0.1163	0.0016	1901	24
2.8O	20	7	0.33	7	0.339	0.019	5.46	0.46	0.1169	0.0065	1909	104
2.9C	108	83	0.77	43	0.351	0.009	5.60	0.17	0.1156	0.0015	1890	23
2.10C	111	83	0.74	44	0.347	0.010	5.58	0.21	0.1167	0.0027	1906	41
2.11O	21	4	0.17	6	0.318	0.015	4.42	0.48	0.1007	0.0092	1636	181
2.12O	30	10	0.32	11	0.362	0.013	5.25	0.47	0.1052	0.0081	1718	149
2.13O	22	5	0.22	7	0.330	0.025	5.67	0.53	0.1246	0.0059	2024	86
3.1O	119	28	0.24	44	0.369	0.010	5.78	0.22	0.1135	0.0025	1856	40

^a 1,2, and 3 refer to individual grains shown on Figure 9A, followed by the analysis number; C refers to core analysis, O refers to overgrowth; ^b Pb* = radiogenic lead

Chapter 4

Decompressional reaction textures in sapphirine granulites from the Snowbird tectonic zone, Canada

To be submitted to the *Journal of Petrology*

Baldwin, J.A., Williams, M.L., Goncalves, P., and Bowring, S.A.

Abstract

The East Athabasca mylonite triangle, northern Saskatchewan, Canada, contains high-pressure granulites and eclogites that were metamorphosed at P - T conditions of 1.5-2.0 GPa, 900-1000°C. Associated with these high-pressure rocks is a suite of sapphirine-bearing granulites that preserve a rich variety of reaction textures. Two varieties of sapphirine-bearing rocks are described in this contribution, both of which are associated with eclogites. The first occurs as a 1-2 m reaction zone structurally above the eclogite unit. The peak assemblage of garnet-kyanite-quartz occurred at near 2.0 GPa, 900°C and developed during the eclogite facies metamorphism. A near-isothermal decompression path is inferred from reaction textures that developed around the primary porphyroblasts. Rims of orthopyroxene and plagioclase developed around garnet and sapphirine-spinel-anorthite reaction rims developed around kyanite. The second variety of sapphirine-bearing assemblages occurs in kyanite veins within the eclogite. The peak assemblage preserved in the veins contains garnet, orthopyroxene, kyanite, and plagioclase, and these veins are interpreted to have formed following the eclogite facies metamorphism. Evidence for a decompression path includes the replacement of kyanite by sillimanite and the development of reaction rims involving sapphirine, spinel, corundum, and anorthite around the aluminum silicate. Based on petrological modeling in the CFMAS system, the sapphirine + spinel + corundum assemblage in the veins is interpreted to have formed at ~0.6 GPa and 600-700°C. The P - T path for this suite of rocks is one of an initial near-isothermal decompression P - T path from ~2.0 GPa to ~1.0 GPa followed by cooling from ~900 to ~600°C during decompression to ~0.6 GPa. These results indicate that the final equilibration of these rocks occurred at mid-crustal levels. This study implies that the reaction textures developed in these rocks may not be isochronous and that each sub-domain may record different stages of the decompression P - T path.

Key words: decompression, kyanite eclogite, reaction textures, sapphirine, Saskatchewan

1. Introduction

Sapphirine is a relatively common mineral in Mg and Al-rich granulite-facies rocks. In silica-undersaturated rocks, sapphirine commonly forms as a symplectite product with anorthite at the expense of earlier aluminous phases, such as kyanite. Because this assemblage is very sensitive to changes in pressure and temperature, they commonly preserve ‘frozen’ reaction textures that provide valuable information to decipher the P - T evolution and tectonic history of the host terranes (e.g., Droop, 1989; Kriegsman & Schumacher, 1999; Windley et al., 1984). Sapphirine is most often interpreted to form during isothermal decompression in a clockwise P - T path (Baba, 1999; Brown & Raith, 1996; Möller, 1999; Windley et al., 1984); however, other workers have found sapphirine forming coronas or porphyroblasts in isobarically cooled terranes (Coscombe, 1992; Harley, 1998; Sandiford et al., 1987). Since sapphirine can form on both types of P - T paths and is stable over a wide range of P - T conditions, then it is important to constrain the metamorphic evolution of the associated lithologies. In the case of this study, the well-constrained P - T history of the associated eclogites is of crucial importance to interpreting the petrologic context of the sapphirine-bearing textures.

Numerous petrological studies over the past 25 years have resulted in petrogenetic grids for ultrahigh-temperature (UHT) sapphirine granulites that contain the stable assemblage sapphirine + quartz (Harley, 1989; Harley et al., 1990; Hensen & Green, 1973; Hensen & Harley, 1990; McDade & Harley, 2001). These grids have been constructed for granulite-facies assemblages derived from metapelitic compositions in the model systems FMAS and KFMASH. However, less work has been done to constrain similar grids for sapphirine-bearing silica-undersaturated assemblages involving plagioclase that form within or related to decompressed kyanite eclogites, despite the fact that reaction textures and mineral compositions in such rocks are remarkably similar from a variety of localities worldwide (Austria: Carswell et al., 1989; Norway: Johansson & Möller, 1986; Greece: Liati & Seidel, 1994; SW Sweden: Möller, 1999; O'Brien, 1992).

CHAPTER 4 – REACTION TEXTURES IN SAPPHIRINE GRANULITES

The common reaction histories from a broad variety of localities and ages creates the need to place more quantitative constraints on their P - T evolution.

This paper is the first to document the occurrence of sapphirine granulites associated with eclogites from the Snowbird tectonic zone, northern Saskatchewan, Canada. These eclogites have been metamorphosed at minimum P - T conditions of 1.8-2.0 GPa, 920-1000°C (Chapter 3). There are two varieties of sapphirine granulites preserved, both quartz-bearing and quartz-absent, neither of which has the stable assemblage of sapphirine+quartz. Reaction textures in the eclogite unit with which these rocks are associated record an isothermal decompression path from eclogite facies conditions of ~2.0 GPa, 920-1000°C to granulite facies conditions at ~1.0 GPa. In contrast, the sapphirine-bearing kyanite veins in the eclogite record re-equilibration at lower pressures and temperatures and indicate that these rocks equilibrated at mid-crustal levels at ~0.6 GPa, 600-700°C. This contribution describes the reaction textures preserved in the sapphirine granulites and gives evidence for the crossing of several univariant reactions in a model CFMAS system. Peak pressures and temperatures from the various lithologies preserved in the Snowbird zone provide independent constraints on the P - T evolution of this region and provide a means of calibrating such grids with the observed reaction sequences.

2. Geological Setting

The Snowbird tectonic zone is a 3000-km-long linear element in the horizontal gravity gradient map of the Canadian Shield that extends from the Canadian Cordillera northeast to Hudson Bay (Fig. 1) (Goodacre et al., 1987). It occurs at the boundary between the Rae and Hearne Archean domains of the western Churchill Province (Hoffman, 1988). In northern Saskatchewan, a well-exposed 125 x 80 x 75 km wedge-shaped segment of the Snowbird tectonic zone has been described as the East Athabasca mylonite triangle (EAmt), and consists of anastomosing lower crustal high-grade granulite facies mylonites (Hanmer, 1994; Hanmer, 1997; Hanmer et al., 1994; Hanmer et al., 1995a; Hanmer et al., 1995b). The EAmt is the southwestern segment of the Striding-Athabasca mylonite zone that has been interpreted as an Archean intra-

CHAPTER 4 – REACTION TEXTURES IN SAPPHIRINE GRANULITES

continental strike-slip shear zone (Hanmer, 1994; Hanmer et al., 1994; Hanmer et al., 1995a; Hanmer et al., 1995b).

The EAmt is bounded to the northwest and southeast by rocks of the Rae and Hearne provinces, respectively, and is overlain to the south by the *ca.* 1.77 Ga Athabasca sandstone (Cumming et al., 1987; Kopf, 1999). The wallrocks of the Rae and Hearne domains adjacent to the EAmt are lithologically similar, consisting dominantly of pelitic schist, paragneiss, amphibolite, and largely undated granitoid rocks. However their metamorphic grade is different. Recent work in the Rae Province adjacent to the EAmt suggests that much of the Rae Province in this area experienced intermediate-P granulite facies conditions (~ 0.8 GPa, 900°C) at *ca.* 1.9 Ga (Williams & Hanmer, in press). In contrast, the Hearne Province wallrocks are separated from the EAmt by a major amphibolite-facies shear zone and record lower pressure amphibolite facies metamorphic conditions (0.5 GPa, $600\text{-}700^{\circ}\text{C}$) (Mahan et al., in press).

The EAmt is divided into three structural domains (Fig. 1). The northwestern and southeastern domains are dominated by felsic to mafic plutonic rocks that have been metamorphosed at uniform pressures and temperatures of 1.0 GPa, 800°C (Williams et al., 1995; Williams et al., 2000). The southeastern domain of the EAmt is dominated by the *ca.* 3.2 Ga Chipman tonalite batholith which is intruded by the 1.9 Ga Chipman mafic dike swarm (Baldwin et al., 2000; Flowers et al., 2002; Williams et al., 1995).

Within the southern domain there are two apparent domains, each composed of three dominant lithological units in varying proportions: felsic gneiss, eclogite, and mafic granulite (Fig. 1). The structurally higher levels in the southern extent are dominated by mafic granulite, whereas the lower structural levels to the north are dominated by felsic gneiss. The most abundant lithology in the northern part of the southern domain is a massive felsic garnet-kyanite quartzofeldspathic gneiss. This felsic gneiss is an anhydrous mylonitic rock (garnet+feldspar+quartz+kyanite/sillimanite+rutile) with a shallow SW-plunging lineation. Garnet is ubiquitous throughout the felsic gneiss, and typically comprises 5-40% of the rock. Kyanite-bearing assemblages are locally preserved; kyanite occurs both as inclusions in garnet and as a matrix phase wrapping around garnet. Kyanite-bearing assemblages are particularly well-preserved in the ~ 5 km

CHAPTER 4 – REACTION TEXTURES IN SAPPHIRINE GRANULITES

thick zone between Axis Lake and Currie Lake (Fig. 2). Peak metamorphic conditions for the felsic gneiss, eclogites, and mafic granulites have been calculated at 900-1000°C and 1.5-2.0 GPa (Baldwin et al., 2003; Snoeyenbos et al., 1995).

Mafic granulite occurs as layers that are typically several-m-thick, but are locally more than 10 m thick. They contain a foliation that dips steeply to the south and is parallel to foliation in the host felsic gneiss. At map scale, the strike of this foliation is sub-parallel to the boundary between the southern domain and the northwestern and southeastern domains of the lower deck (Fig. 1). Most mafic granulite layers and the host gneisses have a strong mineral lineation that plunges shallowly to the southwest. These mafic granulite layers have been interpreted as a series of intrusive sills with northeast-striking intrusive contacts (Baer, 1969; Slimmon, 1989). Pressures and temperatures have been calculated for mafic granulite layers within the felsic gneiss at 890-960°C, 1.3-1.9 GPa (Baldwin et al., 2003). Zircon in mafic granulite records 1.9 Ga dates, that are interpreted to date the timing of high-pressure metamorphism. Titanite yields cooling dates ranging from 1900-1894 Ma and is interpreted to have grown along the decompression path, indicating rapid decompression following the high-pressure metamorphism (Baldwin et al., 2003).

A distinctive and important lithological unit for constraining the pressure-temperature history of the southern domain, is a thin 10-15 m-thick band of eclogite that has been mapped along strike for ~15 km (Fig. 2) (Chapter 3). It consists of garnet + omphacite, with kelyphitic reaction rims of pargasite + plagioclase around garnet and orthopyroxene + plagioclase symplectite rims around clinopyroxene. The garnet contains abundant inclusions of kyanite ± zoisite. Pressures and temperatures are constrained at 920-1000°C, 1.8–2.0 GPa (Chapter 3). A near-isothermal decompression path to granulite facies conditions is inferred from the retrograde reaction textures. U-Pb zircon geochronology of the eclogite yields a weighted mean $^{207}\text{Pb}/^{206}\text{Pb}$ date of 1904.2 ± 0.2 Ma, which is interpreted as the time of eclogite facies metamorphism (Chapter 3). The sapphirine-bearing granulites are present adjacent to and within this eclogite layer and are described below.

3. Outcrop Description of Sapphirine Granulites

The sapphirine granulites occur in two distinct field settings, always in association with the eclogite layer shown in Figure 2. The overall structure of this part of the southern domain is characterized by steeply dipping foliations that wrap around from NE to SW with shallow SW-plunging lineations. The assemblage Grt-Qtz-Opx-Spr-Sp occurs as a narrow zone within the quartzofeldspathic gneiss ~1-2 m above the eclogite. Sapphirine and spinel disappear within 1-2 m of the eclogite contact (Fig. 3a). This field relationship implies that this rock with its anhydrous, restitic composition may represent the melt residue from melting of the host gneiss during emplacement of the gabbroic protolith to the eclogite. There is no evidence for the preservation of the melt indicating that it was likely extracted during a subsequent deformational event.

Silica-undersaturated granulites also occur as cm-scale veins within the eclogite. These are original kyanite or sillimanite after kyanite veins that have reacted to form sapphirine-spinel-corundum-bearing assemblages. The degree of breakdown of the kyanite and/or sillimanite is variable. In some instances, the aluminum silicate polymorph has been completely replaced by late aluminous phases such as sapphirine and spinel; in others, the kyanite is still well-preserved. These veins are typically a few cm wide and generally are concordant with the main foliation. In some locations, the veins form a more extensive network that crosscuts the foliation at large angles (Fig. 3b). In these outcrops, the veins form zones several-cm-wide of alternating bands of 1-3-mm garnet and orthopyroxene porphyroblasts (Fig. 3c).

4. Petrology and Mineral Chemistry

Lithologies, textures, and mineral compositions are described below for the sapphirine-bearing lithologies in the southern domain of the EAmt, with an emphasis on assemblages and textures relevant to petrologic modeling and thermobarometry. In order to evaluate compositional zonation, high-resolution compositional maps of these assemblages were collected on the Cameca SX-50 microprobe at the University of Massachusetts. Mineral compositions were measured on the JEOL Superprobe 733 at MIT using an accelerating voltage of 15 kV and a beam current of 10 nA. Locations of

CHAPTER 4 – REACTION TEXTURES IN SAPPHIRINE GRANULITES

spot analyses and quantitative traverses were selected based on the zonation and variation evident in high-resolution compositional maps. Representative analyses are given in Tables 1-4.

4.1 Quartz-Bearing Sapphirine Granulites

The quartz-bearing granulites that occur near the margin of the eclogite unit contain the primary high-pressure assemblage of Grt + Ky + Qtz. Garnet shows strong Ca-zoning at the rim with a decrease in Ca adjacent to surrounding plagioclase. There is a narrow zone of Fe-Mg exchange at the garnet rim. The Ca content of garnet cores is variable. Garnet core compositions range from Prp₄₀₋₃₀Alm₄₂₋₃₆Grs₁₇₋₃₃ (Table 1). There are two microstructures that surround garnet; it is either surrounded by a composite corona of plagioclase and orthopyroxene in the vicinity of quartz, or, when garnet is adjacent to kyanite, it is rimmed by a Spr-Spl-An symplectite. In the first setting, garnet is typically rimmed by a corona of plagioclase, which is, in turn, rimmed by orthopyroxene (Fig. 4a-c, Fig. 5a-c). Garnet typically contains abundant inclusions of kyanite, quartz, and plagioclase (Fig. 4c). Plagioclase between garnet and orthopyroxene is relatively sodic with a composition of An₄₃₋₄₈ (Table 2). Orthopyroxene has X_{Mg} of 0.66-0.67 (Table 3). Orthopyroxene, plagioclase, and quartz are typically separated by orthopyroxene grains even in the absence of garnet. Figure 6 shows an X-ray compositional map of this corona structure, where the depletion of Ca near garnet rim adjacent to plagioclase is apparent.

Kyanite occurs as either discrete or clustered 200-400 μm porphyroblasts (Fig. 4e,f, Fig. 5d). They are surrounded by reaction rims with Spr + Pl and Spl + Pl symplectites. These form two discrete symplectite microstructures around kyanite, with extremely fine-grained symplectites directly adjacent to the kyanite, surrounded by larger, discrete spinel grains (Fig. 5d). The composition of the plagioclase in these symplectites is typically An₇₇₋₇₉ (Fig. 5d) (Table 2). Sapphirine in these symplectites is more magnesian than coexisting spinel with X_{Mg} of 0.79-0.80 and 0.44-0.47, respectively (Table 4). Kyanite can be found in direct contact with garnet, but more commonly symplectites of Spr + Pl and Spl + Pl occur directly adjacent to garnet and are inferred to

CHAPTER 4 – REACTION TEXTURES IN SAPPHIRINE GRANULITES

be former kyanite domains that have been completely pseudomorphed by these symplectites (Fig. 4d).

Quartz is never observed to be in contact with the sapphirine-bearing microstructures. Throughout the matrix, there is typically a thin selvage of orthopyroxene between quartz and plagioclase, separating subdomains of these symplectite microstructures (Fig. 5e,f). These commonly surround Spl + Pl symplectites in the matrix (Fig. 5f). The composition of plagioclase in these symplectites is more sodic than the kyanite-bearing subdomains (An_{57}) (Fig. 5f) (Table 2).

Accessory minerals include rutile, ilmenite, zircon, and apatite. Rutile is very abundant and occurs both in association with the sapphirine symplectites and as inclusions in garnet. Apatite in one sample contains abundant needle-shaped inclusions and lamellae of monazite. Monazite has not been observed as a discrete phase in these rocks.

4.2 *Quartz-Absent Sapphirine-Bearing Vein Granulites*

Quartz-undersaturated sapphirine granulites occur as veins within the eclogite unit. These veins are typically a few-centimeter-wide and occur both as discrete aluminum silicate veins or in a network of connected veins. In some outcrops these veins are closely spaced, and form a “zone”, no more than 10-centimeter-wide, that consists of interlayered aluminum silicate veins and garnet and orthopyroxene porphyroblasts (Fig. 7). In these zones, garnet is slightly more Fe-rich and less Mg-rich in the vein compared to garnet in the eclogite ($Alm_{36}Prp_{36}Grs_{28}$ in vein compared to $Alm_{33-23}Prp_{43-55}Grs_{17-29}$ in the eclogite) (Table 1).

The aluminum silicate veins are bounded by a fine-grained symplectite of Spl+Pl (Fig. 8a). This symplectite is overgrown by symplectites of Spr+Pl and Crn+Pl (Fig. 8b). Plagioclase in these symplectites is near end-member anorthite with a composition of 0.87-0.93. The most calcic compositions occur adjacent to corundum. Sapphirine is more magnesian-rich than spinel with X_{Mg} of 0.79 and 0.46 respectively. Discrete crystals of sapphirine are generally aligned along the margin of the vein (Fig. 8c, Fig. 9a). Small inclusions (<10 μm) of monazite and allanite are common as inclusions in kyanite or sillimanite (Fig. 9b). Elongate and disrupted garnet porphyroblasts occur along the

CHAPTER 4 – REACTION TEXTURES IN SAPPHIRINE GRANULITES

perimeter of the veins and are separated from the symplectite microstructures by near end-member anorthite (Fig. 8d). The garnet is highly resorbed, due to its participation in the symplectite-forming reactions and replacement by plagioclase (Fig. 10). These elongate garnets are typically found in interlayered zones with plagioclase on the side with the symplectites and aluminum silicate vein and orthopyroxene on the opposite side (Fig. 10a,b). Figure 10c and d show this relationship with Opx+Pl symplectites along the bottom margin of the garnet. These garnets typically show highly asymmetric zoning profiles, with a strong depletion in Ca from Grs₂₈ adjacent to the Opx to Grs₁₂ adjacent to the vein. A less dramatic increase in Fe and Mg is observed from Alm₃₈Prp₃₄ adjacent to orthopyroxene to Alm₄₉Prp₃₉ adjacent to the vein (Fig. 11).

The large orthopyroxene porphyroblasts are surrounded by symplectites of Opx-Pl (Fig. 8e). These porphyroblasts have an X_{Mg} of 0.74 and are not very aluminous (1.5% Al₂O₃). Large 1-5 mm garnet porphyroblasts in the matrix not associated with the veins typically are surrounded by Opx+Pl symplectites and show a substantial drop in Grs near the rim (Fig. 8f, Fig. 10e,f). The interior of garnet is replaced by a more sodic plagioclase than the matrix. Adjacent to these garnet crystals are symplectite structures of discrete Spl+Pl symplectites that are rimmed by Spr+Pl symplectites. These probably represent sites of former kyanite porphyroblasts. These microstructures are rimmed by a moat of near-end-member anorthite. Accessory phases in the vein zones include monazite, allanite, rutile, ilmenite, and zircon.

4.3 Sapphirine Chemistry

Sapphirine compositions follow the general chemical formula $(Mg,Fe^{2+})_{16-n}(Al,Fe^{3+},Cr)_{32+2n}Si_{8-n}O_{80}$ (Vogt, 1947). Variations are linked to Mg₋₁Fe and Tschermak's substitutions. The end-member compositions for this formula (Mg,Fe²⁺: Al,Fe³⁺,Cr:SiO₂) are 2:2:1 (n = 0) and 7:9:3 (n = 2) (Higgins et al., 1979). The sapphirine in this study is more aluminous than the 7:9:3 endmember (n = 2.17-3.18) indicating substantial Tschermak's substitution (Fig. 12). The most aluminous sapphirine in the literature is from an American Massif eclogite (n = 3.46) (Godard & Mabit, 1998); similar compositions are reported for a eclogite from the Czech Republic by O'Brien (1992) (n = 3.42). These examples are also from kyanite eclogites in which the sapphirine formed

CHAPTER 4 – REACTION TEXTURES IN SAPPHIRINE GRANULITES

from the breakdown of kyanite in association with spinel, corundum, and plagioclase. Such sapphirine compositions were first described by Schreyer and Abraham (1975); they are classified as peraluminous and interpreted to be metastable. Both petrographic occurrences of sapphirine reported here have similar compositions and are magnesian, with $X_{Mg} = 0.79-0.80$.

5. Textures and Reaction History

5.1 Textures

The textures described above are interpreted to be the result of a complex reaction history following high-pressure metamorphism. These are predominantly disequilibrium textures that are ‘frozen in’, indicating that the reactions terminated before they ran to completion. Reaction rims and delicate symplectites around early-formed porphyroblasts are related to the exhumation of the rocks following the peak eclogite-facies metamorphism. Some of these reaction products probably developed isochronously, but others can be placed in a sequence that can then be compared to petrogenetic grids to elucidate the P - T conditions of these sequential reactions. The reaction textures and various subdomains indicate that despite the high temperatures of metamorphism, diffusion was restricted and equilibrium was obtained within these small subdomains.

5.2 Reactions in the garnet-sapphirine-quartz granulite

This rock is interpreted to have consisted of Grt + Ky + Qtz at peak eclogite facies conditions. Most of the plagioclase in this rock is texturally late, forming from the breakdown of the peak assemblage. Near garnet, plagioclase was produced by the GASP back reaction:

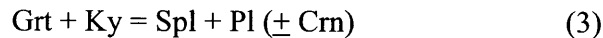


Then a reaction between Grt + Qtz produced a rim of orthopyroxene around garnet. This would indicate the classic high-pressure to medium-pressure granulite reaction of Green and Ringwood (1967):

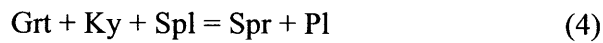
CHAPTER 4 – REACTION TEXTURES IN SAPPHIRINE GRANULITES



The origin of sapphirine-anorthite symplectites in similar rocks has been discussed by a number of authors (Carswell et al., 1989; Johansson & Möller, 1986; Liati & Seidel, 1994; Möller, 1999). In most eclogites, clinopyroxene is typically involved in such reactions. In this instance, there is no clinopyroxene in the marginal rocks, and garnet and kyanite are the main reactants. The nucleation and growth of the sapphirine and spinel symplectites took place around former kyanite grains. The Spl + Pl symplectites formed around kyanite first by a reaction such as:



This was followed by a reaction with garnet to produce Spr + Pl, such as:

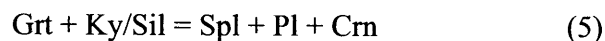


Contacts occur between garnet and kyanite, but kyanite is more commonly replaced by the symplectites. Where the garnet-orthopyroxene associations occur, kyanite is not present, although kyanite is observed as an inclusion phase in garnet.

5.3 Symplectite-forming reactions in the veins

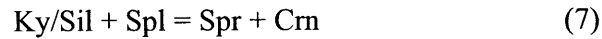
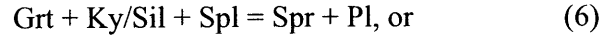
A similar set of reactions can be described for the sapphirine-bearing veins. The main differences between the two types of sapphirine-bearing granulites is the absence of quartz in the veins. However, even in the quartz-saturated granulites, quartz is not a reactant in the development of the sapphirine-bearing subdomains and is only involved in breakdown reactions involving garnet. The primary assemblage in the veins is interpreted to have been Grt+Opx+Ky. As is the case for the margin rocks, most of the plagioclase is secondary.

The Spl-Pl symplectite developed by a reaction such as:

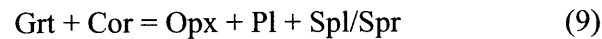
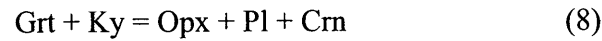


CHAPTER 4 – REACTION TEXTURES IN SAPPHIRINE GRANULITES

Then the formation of the Spr-Pl symplectites occurred with Spl as reactant:



In the absence of quartz, the development of Opx+Pl symplectites around garnet and around large Opx porphyroblasts involved a reaction with kyanite or corundum such as:



The important observation from the sapphirine-bearing vein rocks is that all of these reactions involve the introduction of plagioclase to the system. In the case of reactions involving kyanite, the plagioclase is generally close to pure anorthite, but in it is mmore sodic in reactions involving the breakdown of garnet plagioclase.

6. Thermobarometry

Peak pressures and temperatures were estimated using the TWQ software (Berman, 1991) and database of Berman & Aranovich (1996). In the sapphirine-bearing rocks adjacent to the eclogite, the peak assemblage is interpreted to have included garnet-kyanite-quartz. Evidence for GASP back reaction is given by the "moat" of plagioclase around garnet (reaction (1)). Using core garnet compositions, combined with the adjacent plagioclase yields minimum pressures of 2.1 GPa at 900°C for this breakdown reaction. The further breakdown of garnet to produce the orthopyroxene rims is given by reaction (2). Garnet-orthopyroxene-plagioclase-quartz equilibria yield *P-T* conditions of 1.1 GPa, 790°C. These reaction textures indicate an isothermal decompression *P-T* path from high-pressure granulite to medium-pressure granulites facies conditions.

The vast range of compositions in garnet, depending on its petrographic setting and adjacent phases in the sapphirine-bearing veins precludes the ability to quantitatively

CHAPTER 4 – REACTION TEXTURES IN SAPPHIRINE GRANULITES

determine peak P-T conditions for this rock. In addition, the plagioclase composition varies tremendously on a micron scale whether as a symplectite or matrix phase.

The lack of good thermodynamic data for sapphirine hinders the quantitative calculation of the P-T conditions recorded by the reaction textures involving this phase. One important question to answer is whether or not the reaction textures preserved in these rocks developed isochronously, at similar pressure-temperature conditions, or whether, for example, the reaction textures around kyanite porphyroblasts formed at different P-T conditions than the reaction textures around garnet. If the sapphirine-spinel-plagioclase reaction textures around kyanite formed at substantially lower P-T conditions than the reactions around garnet calculated quantitatively, then this would give some indication as to the final equilibration conditions of this assemblage in the middle to lower crust. In order to examine the stability of the textures involving sapphirine and spinel, it is necessary to study these assemblages in reaction space in order to determine the appropriate equilibration conditions for these assemblages.

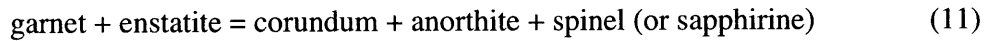
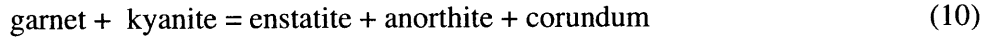
7. Petrologic Modeling

The *P-T* evolution of sapphirine + quartz-bearing UHT granulites is typically examined using petrogenetic grids for the model systems FMAS and KFMASH (Harley, 1998). These grids allow constraints to be placed on the evolution of the *P-T* conditions recorded by the reaction textures and mineral assemblages. Similar grids for quartz-undersaturated sapphirine granulites are lacking, although reaction textures, bulk compositions, and mineral assemblages in such rocks are remarkably similar from a variety of localities worldwide. In order to examine the stability of the assemblages observed in the silica-undersaturated granulites, we used the CFMAS model system and constructed petrogenetic grids using the Perplex phase equilibria program (Connolly & Pettrini, 2002) and the thermodynamic dataset of Holland & Powell (1998). We focus on the quartz-absent assemblage present in the kyanite veins and develop a model petrogenetic grid for this assemblage.

The first step towards constructing the grid was to start with the model CMAS system for the pure Mg-endmembers, and a pyrope-grossular garnet solution model. This

CHAPTER 4 – REACTION TEXTURES IN SAPPHIRINE GRANULITES

system consists of the phases garnet, kyanite, corundum, spinel, sapphirine, anorthite, and enstatite. Two invariant points are stable in this system: kyanite- and spinel-absent points (Fig. 13). This grid shows several univariant reactions for Mg-endmember compositions delimiting main CMAS divariant assemblages:



These two reactions constrain the formation of anorthite in the model system. Above pressures of ~1.1 GPa in this grid, assemblages are anorthite-free, and the formation of anorthite occurs by the breakdown of garnet, the only other Ca-bearing phase in the system. Singularities along these univariant reactions involve variation in the Mg-phases on either side of the reaction, however, garnet is always on the high-P side of the reaction because it is required for anorthite production.

In order to more realistically model the assemblages observed in the veins, iron must be added to the system. In addition, Al in Opx must also be incorporated. Figure 13 shows a CFMAS grid that incorporates solution models for the Fe-Mg phases including orthopyroxene, spinel, sapphirine, and garnet. The grid also takes into account Al in Opx, adding ~1.9 wt % Al₂O₃ to the Opx composition. The brown lines indicate the most Mg-rich compositions that are stable in this grid, indicating the maximum P-T conditions. As in the CMAS system, the two stable invariant points involve kyanite-absent [ky] and spinel-absent [spl] assemblages. In addition, the pseudoinvariant point, labeled [x] in Figure 13, is the point on the P-T diagram where all phases coexist stably. Adding iron to the system results in a shift of the [ky] and [spl] invariant points along the univariant reactions in the direction indicated by the arrows in Figure 14. An important observation is that the [ky] and [spl] invariant points are stable only above higher X_{Mg} than the pseudoinvariant point [x]. At a bulk X_{Mg} lower than that of [x], the [ky] and [spl] invariant points are metastable. The compositions of the phases stable at [x] are Spr₈₉, Alm₂₅Prp₇₀, Spl₇₁, and En₈₁. These are considerably more Mg-rich compositions than observed in the sapphirine-bearing veins. For lower bulk X_{Mg}, the reactions around

CHAPTER 4 – REACTION TEXTURES IN SAPPHIRINE GRANULITES

the pseudo-invariant point [spr] were constructed for compositions ranging from En_{81} to En_{77} , with 1.9 wt% Al_2O_3 . This represents a more accurate estimation of the composition of the sapphirine-bearing veins. The main univariant reactions in this grid occur at substantially lower P-T conditions than for the pure Mg endmember case. Reactions (10) and (11) in this grid occur at ~6 kbar, 600-700°C. It is important to note that these reactions do not involve sapphirine as a stable phase, but are consistent with the mineral compositions in the other phases in the sapphirine-bearing vein rocks. In this CFMAS grid all of the univariant reactions involving sapphirine are at high T. An explanation for this could be that the thermodynamic data for sapphirine is not well-constrained. In addition, an ideal solution model is used that may not be accurate. Other workers have attempted to modify the Holland & Powell (1998) thermodynamic data for sapphirine to be more consistent with experimental results (Ouzegane et al., 2003). This modification appears to produce grids that are more consistent with the observed assemblages.

8. Discussion and Conclusions

The high-pressure granulites and eclogites of the Snowbird tectonic zone underwent a high-PT metamorphism at 1904 Ma (Baldwin et al., 2003, Chapter 3). The development of the reaction textures in these rocks occurred following high-PT metamorphism and are interpreted to have formed along the decompression path. Peak pressures in the eclogite, constrained by the $Jd + Qtz = Ab$ geobarometer, were 1.8-2.0 GPa at 920-1000°C (Chapter 3). In the eclogite unit, a near-isothermal decompression path to granulite facies conditions is inferred from retrograde reaction textures that indicate a transition from high-pressure to medium-pressure granulite facies (Green & Ringwood, 1967). Development of the peak assemblages in the sapphirine-bearing rocks of Grt-Ky-Qtz in the marginal rocks. Grt-Ky-Opx in the veins within the eclogite likely formed at these eclogite facies conditions. The rocks marginal to the eclogite contain restitic assemblages, but no evidence of leucosome is present. Two possibilities are that the bulk rock composition was inappropriate to produce melt, or if melt was generated, then it was extracted completely during a later deformational event. Evidence for biotite dehydration melting of the host felsic gneiss during high-pressure metamorphism is clear

CHAPTER 4 – REACTION TEXTURES IN SAPPHIRINE GRANULITES

and is described in the subsequent chapter. It seems reasonable to assume that there would have been some localized melting of the host rock during emplacement of the eclogite protolith and that the resulting rock might be slightly enriched in Mg and Fe due to its interaction with the eclogite protolith. This would explain the localized growth of sapphirine assemblages that disappear within 1-2 m of the contact. In addition, the veins might also be remnants of this melting event, resulting in highly aluminous melts from the host felsic gneiss, and the development of the kyanite veins.

A rich variety of reaction textures are preserved in both the sapphirine granulites and eclogites from the East Athabasca mylonite triangle, northern Saskatchewan. All of these reaction textures imply a decompression P - T path. However, the reaction textures preserved in the eclogites appear to have equilibrated at significantly higher pressures (1.1-1.0 GPa) than the reaction textures involving sapphirine and spinel in the aluminum silicate veins (~0.6 GPa). In addition the reactions textures involving the breakdown of garnet in the eclogite margin rocks appear to record similar conditions to the eclogite decompression textures (~1.1 GPa). This implies that the development of the various reaction textures was not isochronous and that these rocks record the crossing of multiple univariant reactions with decreasing pressure. Based on our modeling results, the final equilibration recorded in the sapphirine-bearing vein rocks is on the order of 0.6 GPa and 600-700°C. These P - T conditions are significantly lower than what is generally inferred for decompression textures in sapphirine formed in exhumed eclogites (Möller, 1999; Rötzler & Romer, 2001). These results imply that these rocks were exhumed to mid-crustal levels following the high-PT metamorphism at 1.9 Ga.

References

- Baba, S., 1999. Sapphirine-bearing orthopyroxene-kyanite/sillimanite granulites from South Harris, NW Scotland: evidence for Proterozoic UHT metamorphism in the Lewisian. *Contributions to Mineralogy and Petrology*, **136**, 33-47.
- Baer, A. J., 1969. The Precambrian geology of Fond-du-Lac map-area (74-0), Saskatchewan. *Geological Survey of Canada Paper 68-61*, 17p.
- Baldwin, J. A., Bowring, S. A. & Williams, M. L., 2000. A unique view of Archean lower crust. *EOS Transactions, American Geophysical Union*, **81**(48), 1250.
- Baldwin, J. A., Bowring, S. A. & Williams, M. L., 2003. Petrological and geochronological constraints on high pressure, high temperature metamorphism in the Snowbird tectonic zone, Canada. *Journal of Metamorphic Geology*, **21**, 81-98.
- Berman, R. G., 1991. Thermobarometry using multi-equilibrium calculations: a new technique, with petrological applications. *Canadian Mineralogist*, **29**, 833-855.
- Berman, R. G. & Aranovich, L. Y., 1996. Optimized standard state and solution properties of minerals: I. Model calibration for olivine, orthopyroxene, cordierite, garnet, and ilmenite in the system FeO-MgO-CaO-Al₂O₂-TiO₂-SiO₂. *Contributions to Mineralogy and Petrology*, **126**, 1-24.
- Brown, M. & Raith, M., 1996. First evidence of ultrahigh-temperature decompression from the granulite province of southern India. *Journal of the Geological Society of London*, **153**, 819-822.
- Carswell, D. A., Möller, C. & O'Brien, P. J., 1989. Origin of sapphirine-plagioclase symplectites in metabasites from Mitterbachgraben Dunkelsteinerwald granulite complex, Lower Austria. *European Journal of Mineralogy*, **1**, 455-466.
- Connolly, J. A. D. & Petrini, K., 2002. An automated strategy for calculation of phase diagram sections and retrieval of rock properties as a function of physical conditions. *Journal of Metamorphic Geology*, **20**, 697-708.
- Coscombe, B., 1992. Silica-undersaturated sapphirine, spinel and kornerupine granulite facies rocks, NE Strangways Range, Central Australia. *Journal of Metamorphic Geology*, **10**, 181-201.
- Cumming, G. L., Krstic, D. & Wilson, J. A., 1987. Age of the Athabasca Group, northern Alberta. *Geological Association of Canada - Mineralogical Association of Canada Annual Meeting Abstracts*, **12**, 35.
- Droop, G. T. R., 1989. Reaction history of garnet-sapphirine granulites and conditions of Archean high-pressure granulite-facies metamorphism in the Central Limpopo Belt, Zimbabwe. *Journal of Metamorphic Geology*, **7**, 383-403.
- Flowers, R. M., Baldwin, J. A., Bowring, S. A. & Williams, M. L., 2002. Age and significance of the Proterozoic Chipman dike swarm, Snowbird Tectonic Zone, northern Saskatchewan. *Geological Association of Canada - Mineralogical Association of Canada Annual Meeting Abstracts*.
- Godard, G. & Mabit, J.-L., 1998. Peraluminous sapphirine formed during retrogression of a kyanite-bearing eclogite from Pays de Léon, Armorican Massif, France. *Lithos*, **43**, 15-29.

CHAPTER 4 – REACTION TEXTURES IN SAPPHIRINE GRANULITES

- Goodacre, A. K., Grieve, R. A. F., Halpenny, J. F. & Sharpton, V. L., 1987. Horizontal gradient of the Bouguer gravity anomaly map of Canada, Canadian Geophysical Atlas, Map 5, Geological Survey of Canada, Ottawa.
- Green, D. H. & Ringwood, A. E., 1967. An experimental investigation of the gabbro to eclogite transformation and its petrological applications. *Geochimica et Cosmochimica Acta*, **31**, 767-833.
- Hanmer, S., 1994. Geology, East Athabasca mylonite triangle, Saskatchewan. In: *Geological Survey of Canada Map 1859A*.
- Hanmer, S., 1997. Geology of the Striding-Athabasca mylonite zone, northern Saskatchewan and southeastern District of Mackenzie, Northwest Territories. *Geological Survey of Canada Bulletin*, **501**, 1-92.
- Hanmer, S., Parrish, R., Williams, M. & Kopf, C., 1994. Striding-Athabasca mylonite zone: Complex Archean deep-crustal deformation in the East Athabasca mylonite triangle, northern Saskatchewan. *Canadian Journal of Earth Sciences*, **31**, 1287-1300.
- Hanmer, S., Williams, M. & Kopf, C., 1995a. Modest movements, spectacular fabrics in an intracontinental deep-crustal strike-slip fault: Striding-Athabasca mylonite zone, NW Canadian Shield. *Journal of Structural Geology*, **17**(4), 493-507.
- Hanmer, S., Williams, M. & Kopf, C., 1995b. Striding-Athabasca mylonite zone: implications for the Archean and Early Proterozoic tectonics of the western Canadian Shield. *Canadian Journal of Earth Sciences*, **32**, 178-196.
- Harley, S. L., 1989. The origins of granulites: a metamorphic perspective. *Geological Magazine*, **126**(3), 215-247.
- Harley, S. L., 1998. On the occurrence and characterization of ultrahigh-temperature crustal metamorphism. In: *What Drives Metamorphism and Metamorphic Reactions?* (eds Treloar, P. J. & O'Brien, P. J.), pp. 81-107, Geological Society Special Publications, London.
- Harley, S. L., Hensen, B. J. & Sheraton, J. W., 1990. Two-stage decompression in orthopyroxene-sillimanite granulites from Forefinger Point, Enderby Land, Antarctica; implications for the evolution of the Archaean Napier Complex. *Journal of Metamorphic Geology*, **8**(6), 591-613.
- Hensen, B. J. & Green, D. H., 1973. Experimental study of the stability of cordierite and garnet in pelitic compositions at high pressures and temperatures. III. Synthesis of experimental data and geological applications. *Contributions to Mineralogy and Petrology*, **38**, 151-166.
- Hensen, B. J. & Harley, S. L., 1990. Graphical analysis of P-T-X relations in granulite facies metapelites. In: *High Temperature Metamorphism and Crustal Anatexis* (eds Ashworth, J. R. & Brown, M.), pp. 427-457, Unwin Hyman, London.
- Higgins, J. B., Ribbe, P. H. & Herd, R. K., 1979. Sapphirine: Crystal chemical contributions. *Contributions to Mineralogy and Petrology*, **68**, 349-356.
- Holland, T. J. B. & Powell, R., 1998. An internally-consistent thermodynamic data set for phases of petrological interest. *Journal of Metamorphic Geology*, **16**, 309-343.
- Johansson, L. & Möller, C., 1986. Formation of sapphirine during retrogression of a basic high-pressure granulite, Roan, Western Gneiss Region, Norway. *Contributions to Mineralogy and Petrology*, **94**, 29-41.

CHAPTER 4 – REACTION TEXTURES IN SAPPHIRINE GRANULITES

- Kopf, C. F., 1999. Deformation, metamorphism, and magmatism in the East Athabasca mylonite triangle, northern Saskatchewan: implications for the Archean and Early Proterozoic crustal structure of the Canadian Shield, *University of Massachusetts, Unpublished Ph.D. thesis*.
- Kriegsman, L. M. & Schumacher, J. C., 1999. Petrology of sapphirine-bearing and associated granulites from central Sri Lanka. *Journal of Petrology*, **40**(8), 1211-1239.
- Liati, A. & Seidel, E., 1994. Sapphirine and högbomite in overprinted kyanite-eclogites of central Rhodope, N. Greece: first evidence of granulite-facies metamorphism. *European Journal of Mineralogy*, **6**, 733-738.
- Mahan, K. H., Williams, M. L. & Baldwin, J. A., in press. Juxtaposition of deep crustal and middle crustal rocks along the Legs Lake shear zone, western Churchill Province, Canadian Shield. *Canadian Journal of Earth Sciences*.
- McDade, P. & Harley, S. L., 2001. A petrogenetic grid for aluminous granulite facies metapelites in the KFMASH system. *Journal of Metamorphic Geology*, **19**, 45-59.
- Möller, C., 1999. Sapphirine in SW Sweden: a record of Svecnorwegian (-Grenvillian) late-orogenic tectonic exhumation. *Journal of Metamorphic Geology*, **17**, 127-141.
- O'Brien, P. J., 1992. The formation of sapphirine and orthopyroxene during overprinting of Mariánské Lázně Complex eclogites. *Zentralblatt Geol. Paläontol.*(7/8), 827-836.
- Ouzegane, K., Guiraud, M. & Kienast, J. R., 2003. Prograde and retrograde evolution in high-temperature corundum granulites (FMAS and KFMASH systems) from In Ouzal terrane (NW Hoggar, Algeria). *Journal of Petrology*, **44**, 517-545.
- Rötzler, J. & Romer, R. L., 2001. P-T-t evolution of ultrahigh-temperature granulites from the Saxon Granulite Massif, Germany. Part I: Petrology. *Journal of Petrology*, **42**, 1995-2013.
- Sandiford, M., Neall, F. B. & Powell, R., 1987. Metamorphic evolution of aluminous granulites from Labwor Hills, Uganda. *Contributions to Mineralogy and Petrology*, **95**, 217-225.
- Schreyer, W. & Abraham, K., 1975. Peraluminous sapphirine as a metastable reaction product in kyanite-gedrite-talc schists from Sar e Sang, Afghanistan. *Mineralogical Magazine*, **40**, 171-180.
- Slimmon, W. L., 1989. Compilation bedrock geology Fond-du-Lac, NTS area 74-0, Saskatchewan Geological Survey, Map247A, 1:250000.
- Snoeyenbos, D. R., Williams, M. L. & Hanmer, S., 1995. Archean high-pressure metamorphism in the western Canadian Shield. *European Journal of Mineralogy*, **7**, 1251-1272.
- Vogt, T., 1947. Mineral assemblages with sapphirine and kornepirine. *Bull. Commission Geol. de Finlande*, **XXIV**, 140, 15-23.
- Williams, M. L. & Hanmer, S., in press. Structural and metamorphic processes in the lower crust: evidence from the East Athabasca mylonite triangle, Canada, a deep-crustal isobarically cooled terrane. In: *Evolution and Differentiation of the Continental Crust* (eds Brown, M. & Rushmer, T.), Cambridge University Press.

CHAPTER 4 – REACTION TEXTURES IN SAPPHIRINE GRANULITES

- Williams, M. L., Hanmer, S., Kopf, C. & Darrach, M., 1995. Syntectonic generation and segregation of tonalitic melts from amphibolite dikes in the lower crust, Striding-Athabasca mylonite zone, northern Saskatchewan. *Journal of Geophysical Research*, **100**(B8), 15717-15734.
- Williams, M. L., Melis, E. A., Kopf, C. & Hanmer, S., 2000. Microstructural tectonometamorphic processes and the development of gneissic layering: a mechanism for metamorphic segregation. *Journal of Metamorphic Geology*, **18**, 41-57.
- Windley, B. F., Ackermann, D. & Herd, R. K., 1984. Sapphirine/kornerupine-bearing rocks and crustal uplift history of the Limpopo Belt, Southern Africa. *Contributions to Mineralogy and Petrology*, **86**, 342-358.

Figure Captions

Figure 1. Geologic map of the western Canadian Shield showing major tectonic elements (inset shows location of map). Abbreviations are as follows: AB – Athabasca basin, BL – Baker Lake basin, KX – Kramanitaur Complex, STZ – Snowbird tectonic zone, THO – Trans-Hudson Orogen, TO – Talston Orogen, TMZ – Thelon Magmatic Zone, UX – Uvauk Complex, VR – Virgin River Shear Zone. The Striding-Athabasca mylonite zone occurs within the East Athabasca mylonite triangle, the northern tip of the Athabasca lozenge, as well along the eastern margin of the Selwyn lozenge to the northeast (shown in black). Other examples of high-pressure granulites in the STZ include the Kramanitaur Complex and Uvauk Complex. Outline shown for East Athabasca mylonite triangle shown in Figure 2.

Figure 2. (A) Lithotectonic domains of the East Athabasca mylonite triangle, northern Saskatchewan. Outline of study area shown in B, (B) Geologic map of the northern extent of the southern domain showing the location of the eclogite and sapphirine granulites. Locations of samples described in this study are marked with stars.

Figure 3. Outcrop photos of sapphirine granulites. (A) Sapphirine granulite from margin of eclogite unit, (B) Aluminum silicate veins in the eclogite crosscutting foliation, (C) Interlayered aluminum silicate veins and Opx + Grt zones within eclogite

CHAPTER 4 – REACTION TEXTURES IN SAPPHIRINE GRANULITES

Figure 4. Photomicrographs from margin granulites. (A)-(C) Coronitic texture in marginal sapphirine rocks. Corona of plagioclase surrounds garnet, which is surrounded by a thin layer of orthopyroxene. Quartz is present on outside of corona microstructure, (D) Garnet with rim of sapphirine+anorthite. Rutile is a common accessory phase, (E) Kyanite with reaction rim of sapphirine+spinel+anorthite. Matrix is predominantly quartz, (F) Cluster of kyanite porphyroblasts with reaction rims of sapphirine+spinel+anorthite.

Figure 5. BSE images of margin granulites. (A) Garnet with coronitic texture of plagioclase surrounded by orthopyroxene, (B) Elongate garnet with similar microstructure to (A), (C) Garnet with relatively thick corona of plagioclase and thin rim of orthopyroxene. Garnet contains inclusions of kyanite, quartz, and plagioclase., (D) Kyanite porphyroblast with reaction rim of Spr+Spl+An, (E) Opx is present throughout matrix as rim around quartz grains, (F) Spl+Pl symplectite occur as clusters surrounded by rim of orthopyroxene.

Figure 6. X-ray map of corona texture in 01SZ40A. (A) Ca map showing corona of plagioclase around garnet. Ca is depleted at rim of garnet since it is being consumed to produce plagioclase. Some small garnets show high Ca cores. (B) Mg map showing corona of orthopyroxene. (C) Fe map. Ilmenite occurs in upper left corner.

Figure 7. Sketch of a full thin section of the sapphirine-bearing veins within the eclogite. Approximate dimensions are 25 x 50 mm. Large Opx porphyroblasts are surrounded by symplectites of Opx-Cpx-Hbl-Pl and kyanite veins are surrounded by symplectites of Spr-Spl-Crn-An. Resorbed Grt is distributed throughout the rock.

CHAPTER 4 – REACTION TEXTURES IN SAPPHIRINE GRANULITES

Figure 8. Photomicrographs from veins within eclogite. (A) Als vein with reaction rim of Spr+An, Spl+An, and Crn+An. Bottom of field of view is Opx+Pl symplectite with plagioclase in between. (B) Crn+An symplectite at edge of vein. (C) Sapphirine crystals along edge of vein. (D) Large Opx porphyroblast reacting to Opx+Pl symplectite at margins. (E) Opx+Pl symplectite around garnet. Note asymmetry to reaction rim. Adjacent to Opx domains garnet reacts to Opx+Pl, but adjacent to sapphirine+Als vein garnet reacts to nearly pure An and shows corresponding depletion in Grs near bottom rim. (F) Large garnet with Opx+Pl symplectite. Spl+Pl symplectite occurs at bottom of field of view.

Figure 9. BSE images from vein. (A) Spr crystals along Als vein margin. (B) Spl + Pl symplectite surrounding Sil. Bright spots are monazite and allanite inclusions. (C) Garnet rimmed by sapphirine. Bright spots are rutile.

Figure 10. X-ray compositional maps from veins. (A) Mg map of garnet surrounded by Opx+Pl symplectite along top edge. Spr+Spl+Pl symplectite occurs below garnet. Yellow phase is Spr, Orange phase is Spl. This probably represents the site of a former kyanite porphyroblast, first reacting to Spl+Pl, then rimmed by Spr+Pl. (B) Ca map showing pure anorthite in symplectite (white) and more sodic plagioclase around garnet. (C) Mg map of vein showing Opx (white) at bottom with elongate garnet above. Spr+Spl+Pl symplectite (orange and yellow) occurs between garnet and Als vein (dark). (D) Ca map of vein showing extremely high Ca content of plagioclase associated with vein. Slightly more sodic plagioclase is adjacent to garnet. (E) Mg map of vein with adjacent Spr+Spl symplectite. Spr is yellow and Spl is red-orange. White phase is Opx. (F) Corundum crystals are present as inclusions inside vein surrounded by plagioclase (white). Plagioclase is more sodic adjacent to the Opx.

Figure 11. Asymmetric garnet zoning profile in sapphirine granulite. Profile is shown for garnet in Fig. 7d. Left side of profile is adjacent to the Opx symplectite at the

CHAPTER 4 – REACTION TEXTURES IN SAPPHIRINE GRANULITES

bottom of garnet. Right side is adjacent to plagioclase that is adjacent to the Spr-Pl symplectites at edge of vein (off the field of view in Fig. 7d). Profile shows depletion in Grs on side of garnet towards the vein since Ca is being consumed to produce the plagioclase. The AlmPrp component in garnet is more depleted adjacent to Opx since Fe and Mg are consumed to produce the Opx and coexisting plagioclase in this symplectite is less anorthitic.

Figure 12. Si versus $Al+Fe^{3+}+Cr$ in sapphirine. The line indicates the ideal CaTs substitution $2Al = Mg+Si$. Sapphirine is more aluminous than the 7:9:3 endmember indicating that it is peraluminous as defined by Schreyer and Abraham (1975) and is considered to be metastable.

Figure 13. Petrogenetic grid for the CMAS system.

Figure 14. Petrogenetic grid for the CFMAS system showing near-Mg endmember reactions in brown. Blue lines show pseudo-univariant reactions for the compositions in 01SZ100e.

CHAPTER 4 - REACTION TEXTURES IN SAPPHIRINE GRANULITES

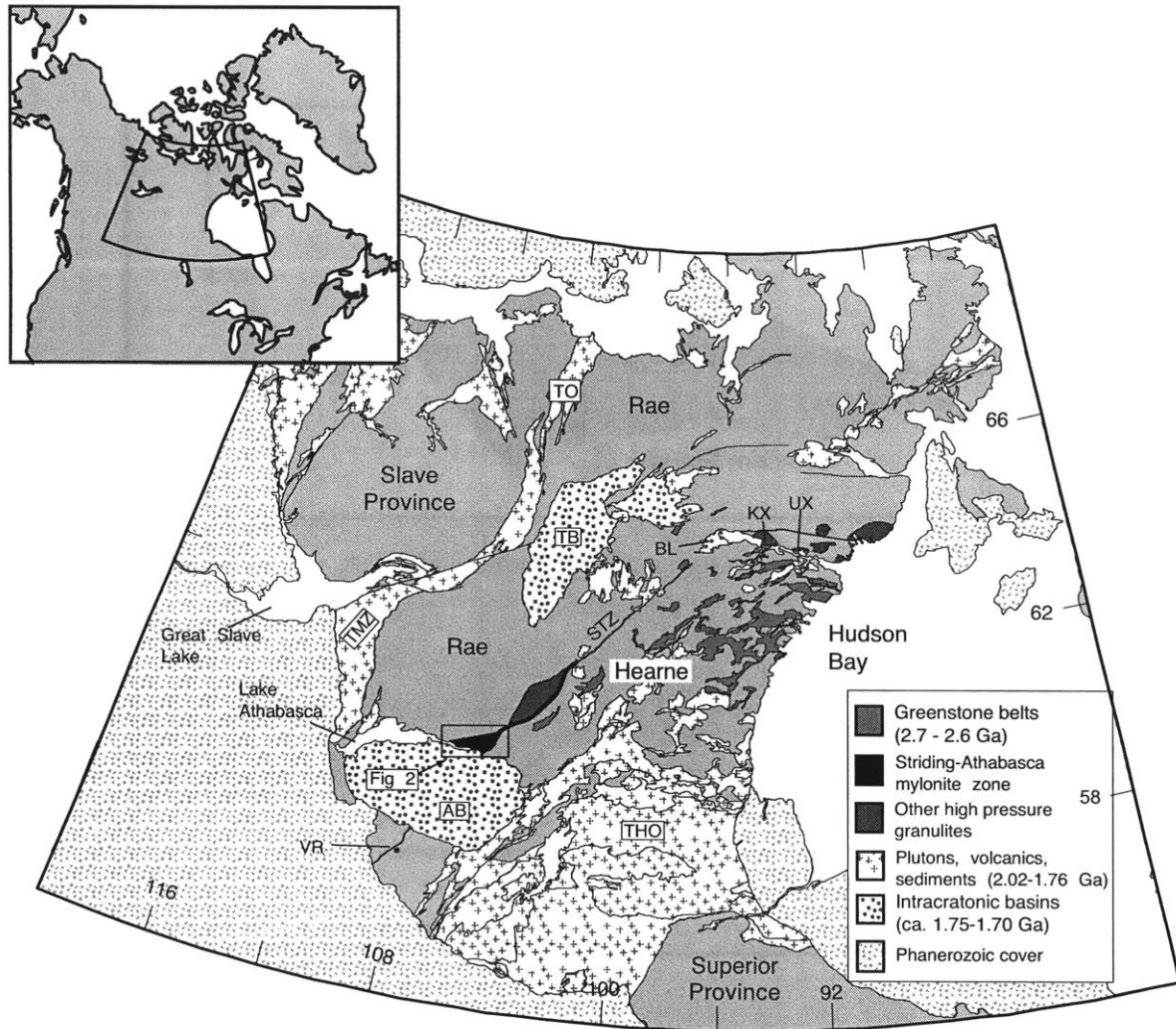


Figure 1

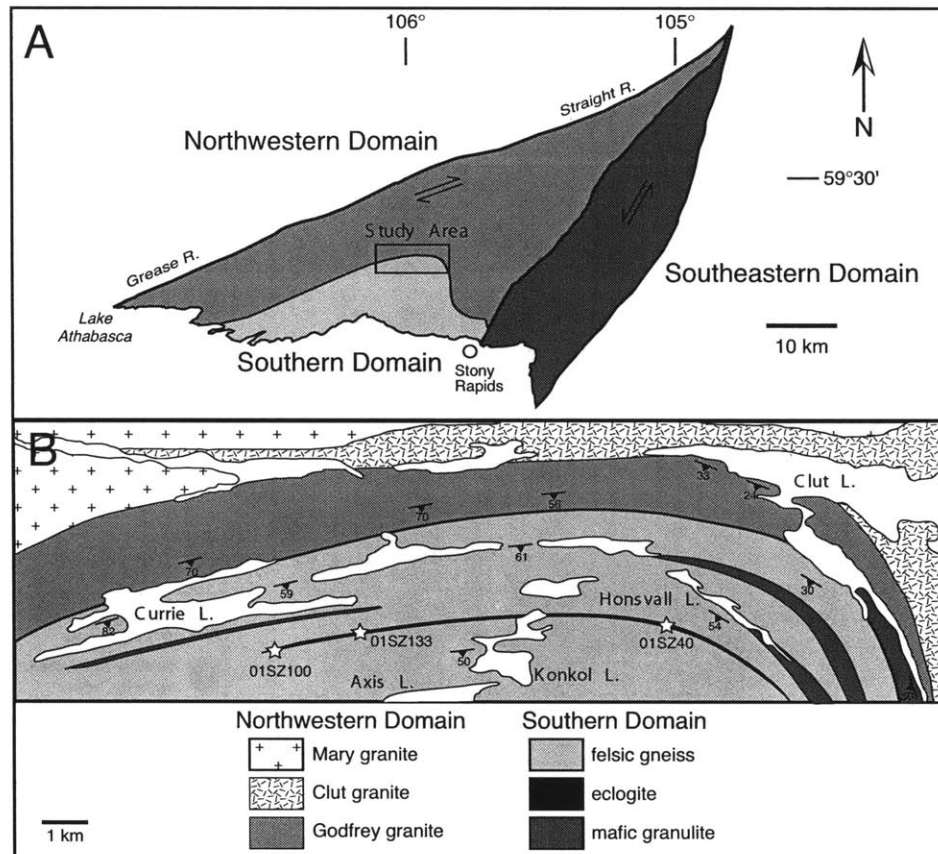


Figure 2

CHAPTER 4 - REACTION TEXTURES IN SAPPHIRINE GRANULITES

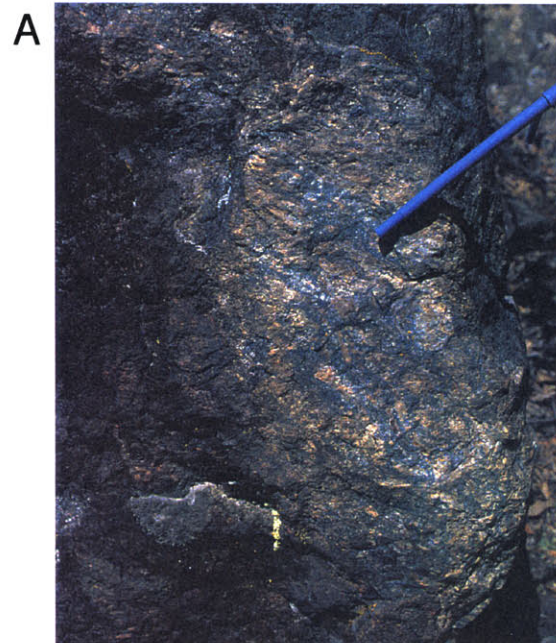


Figure 3

CHAPTER 4 - REACTION TEXTURES IN SAPPHIRINE GRANULITES

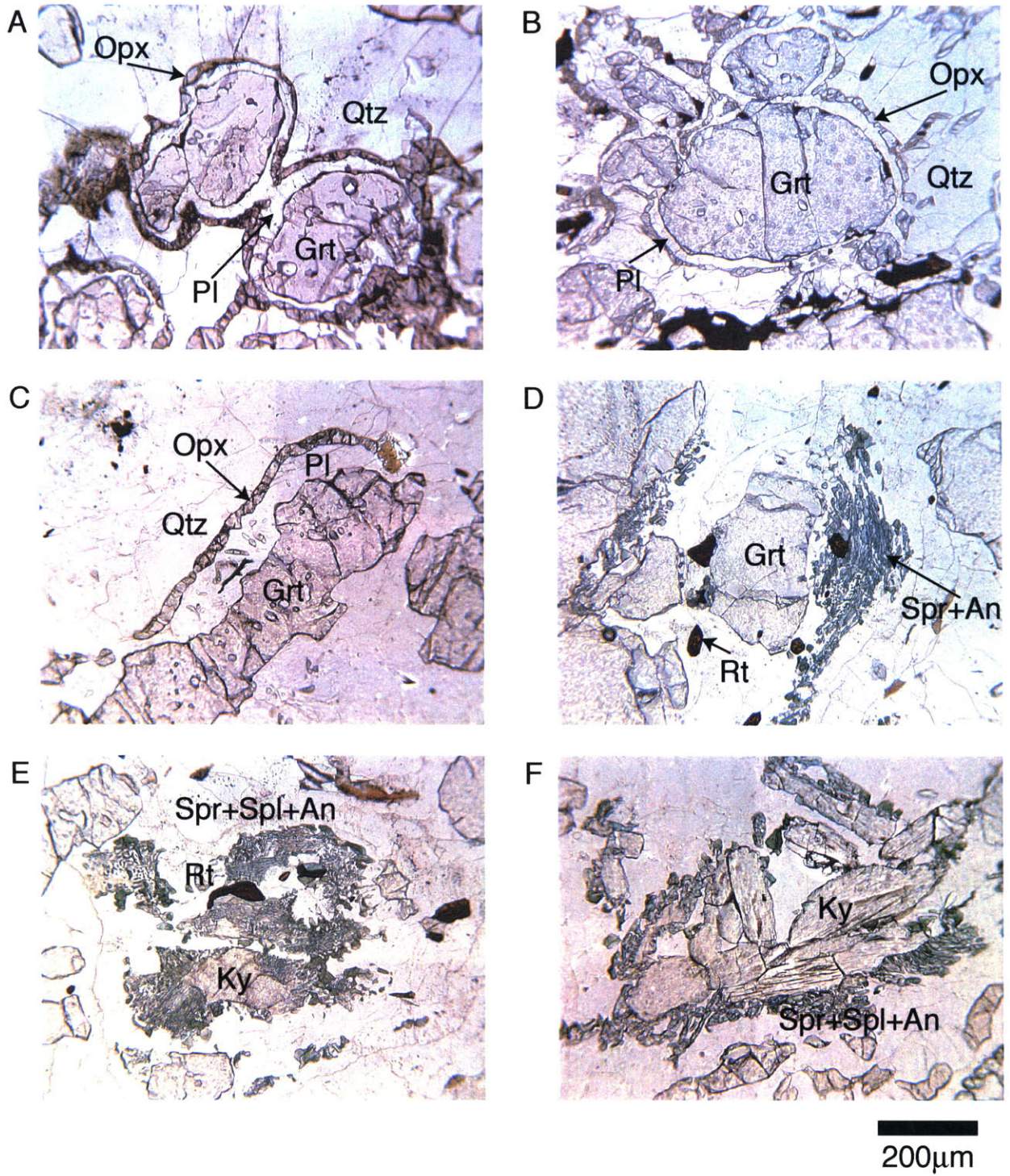


Figure 4

CHAPTER 4 - REACTION TEXTURES IN SAPPHIRINE GRANULITES

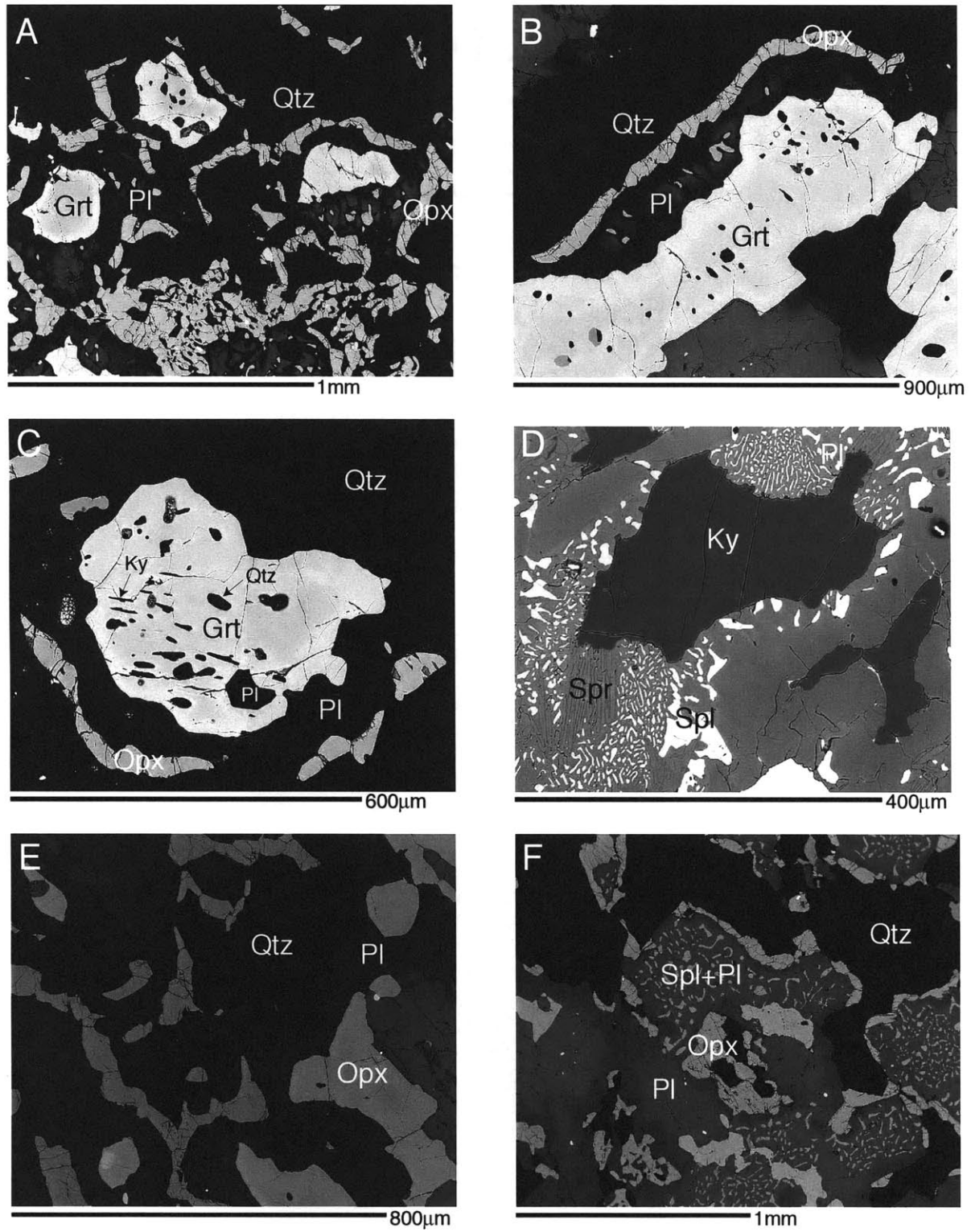


Figure 5

CHAPTER 4 - REACTION TEXTURES IN SAPPHIRINE GRANULITES

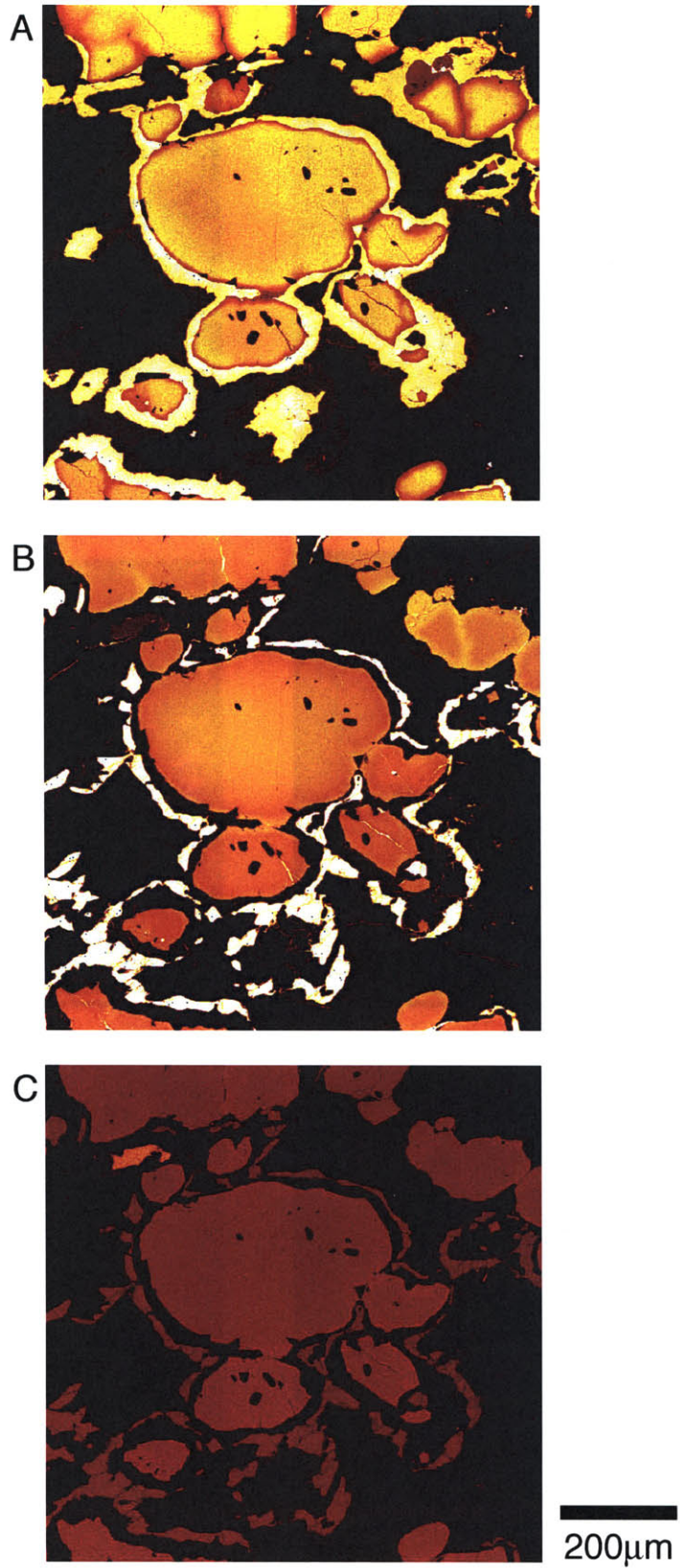


Figure 6

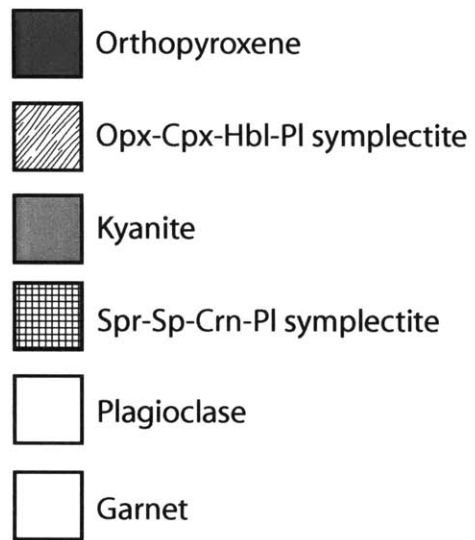
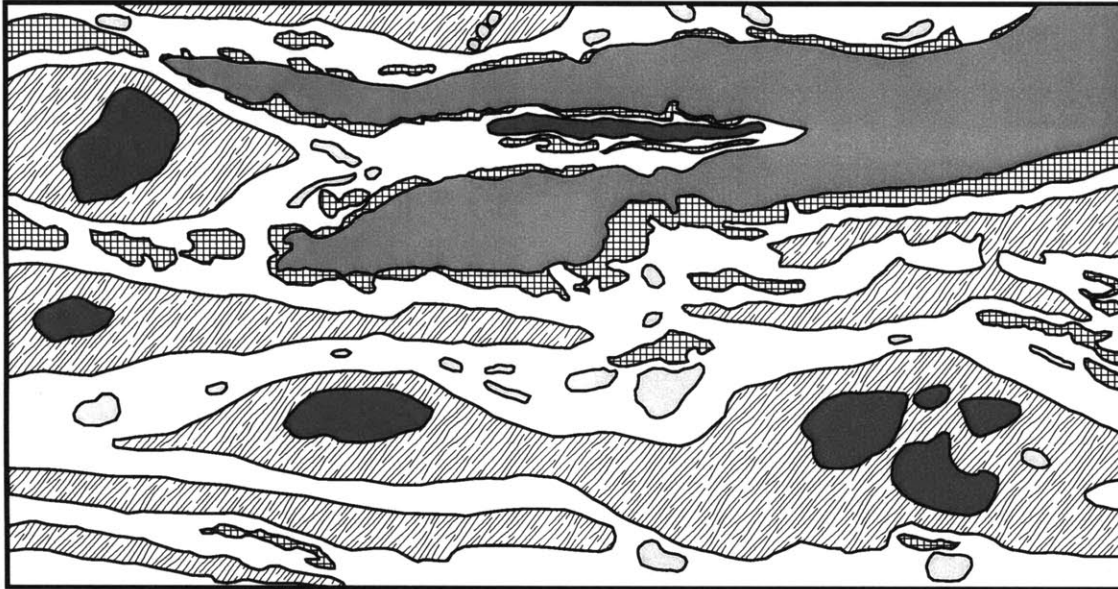


Figure 7

CHAPTER 4 - REACTION TEXTURES IN SAPPHIRINE GRANULITES

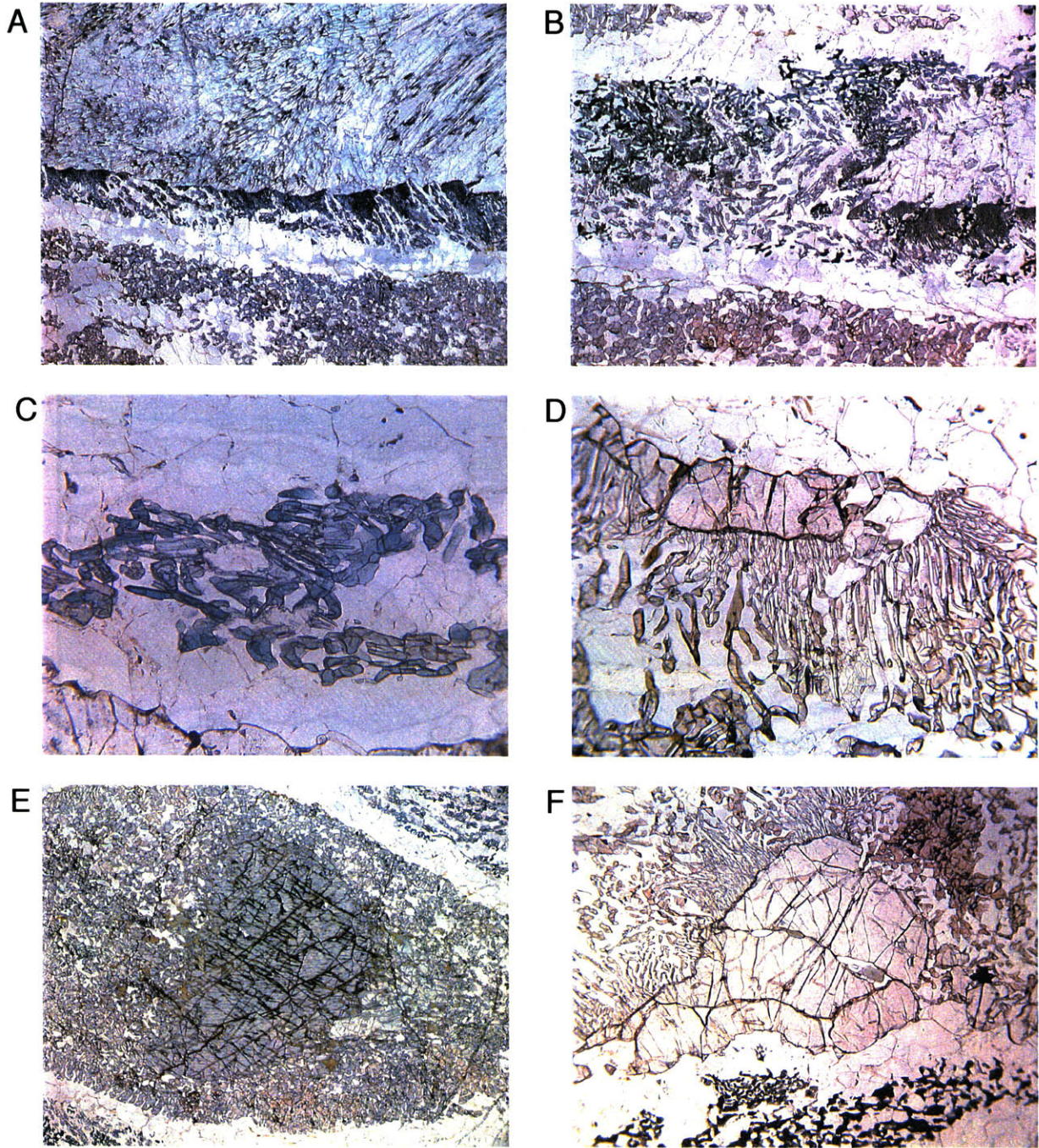


Figure 8

CHAPTER 4 - REACTION TEXTURES IN SAPPHIRINE GRANULITES

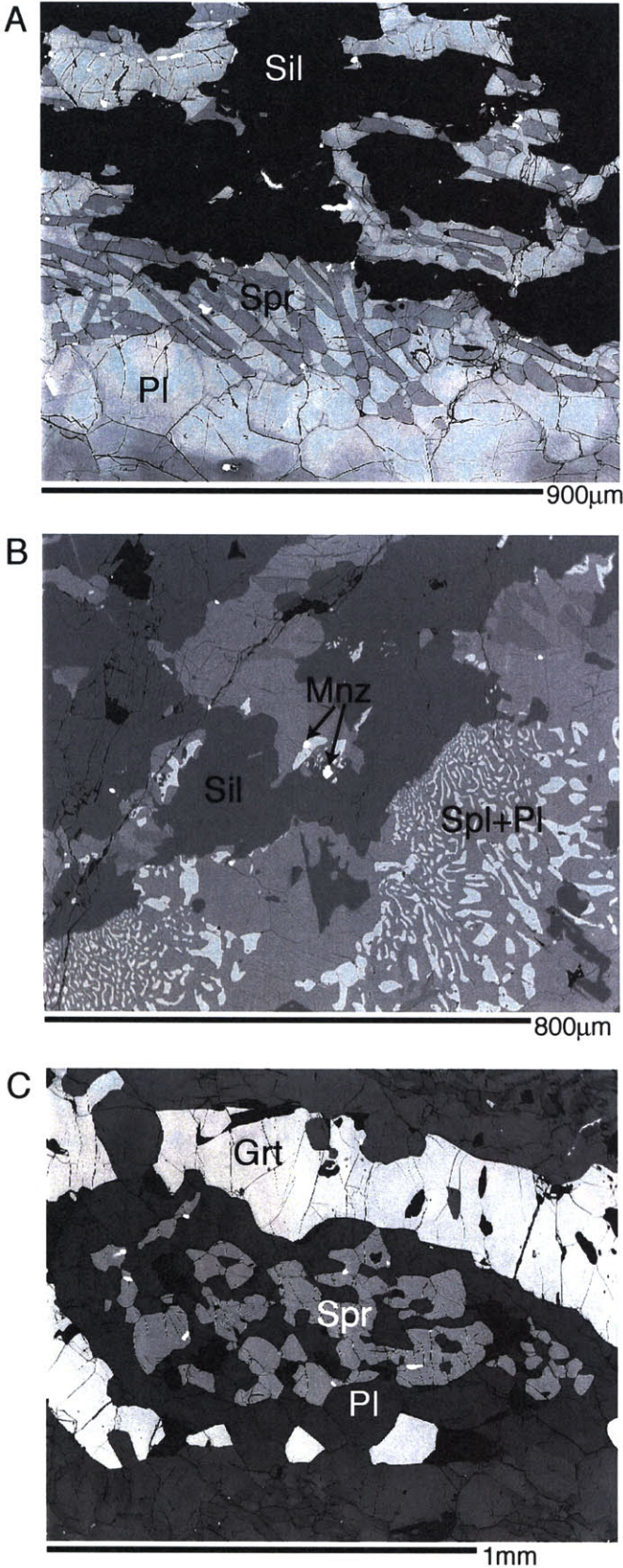


Figure 9

CHAPTER 4 - REACTION TEXTURES IN SAPPHIRINE GRANULITES

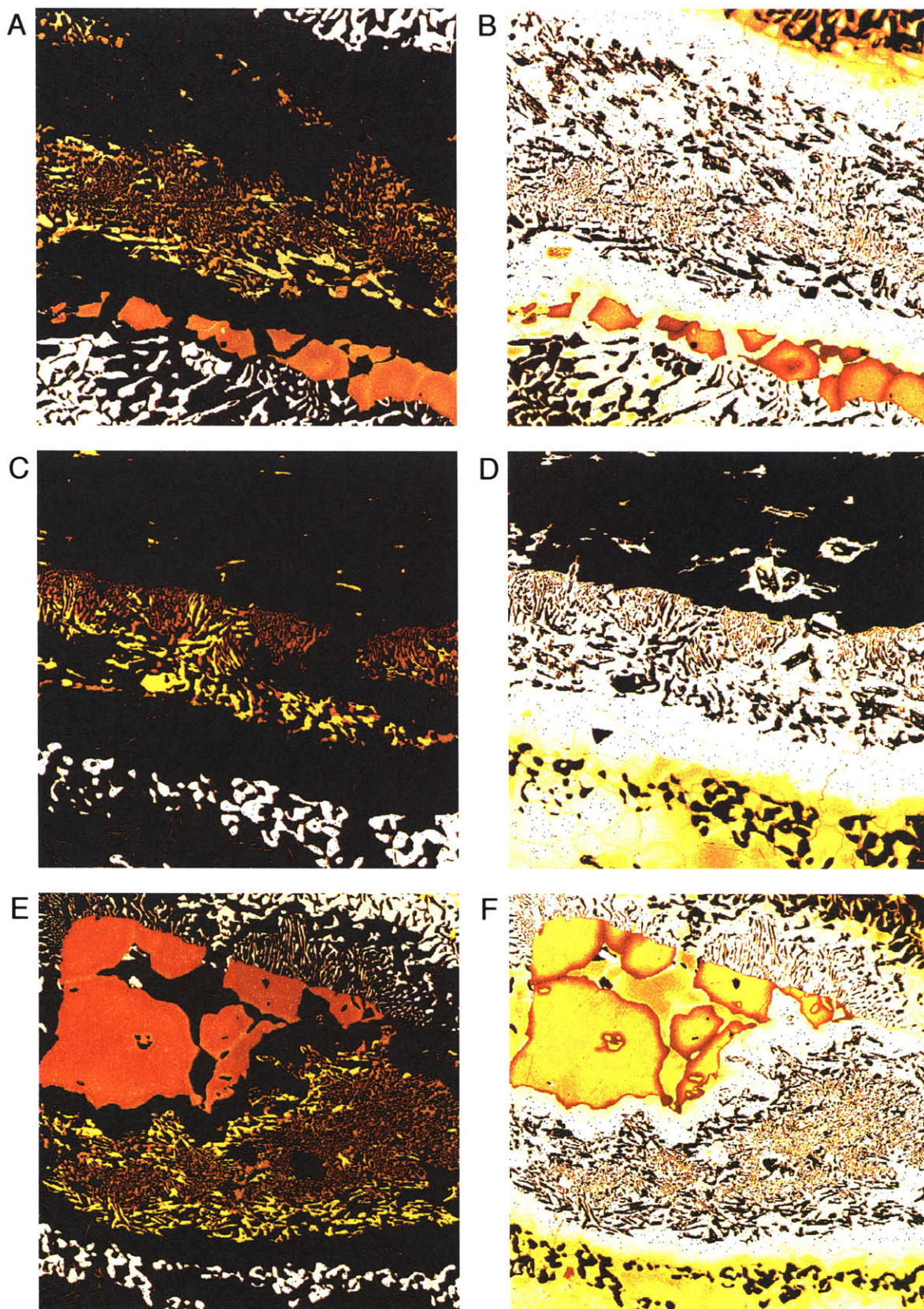


Figure 10

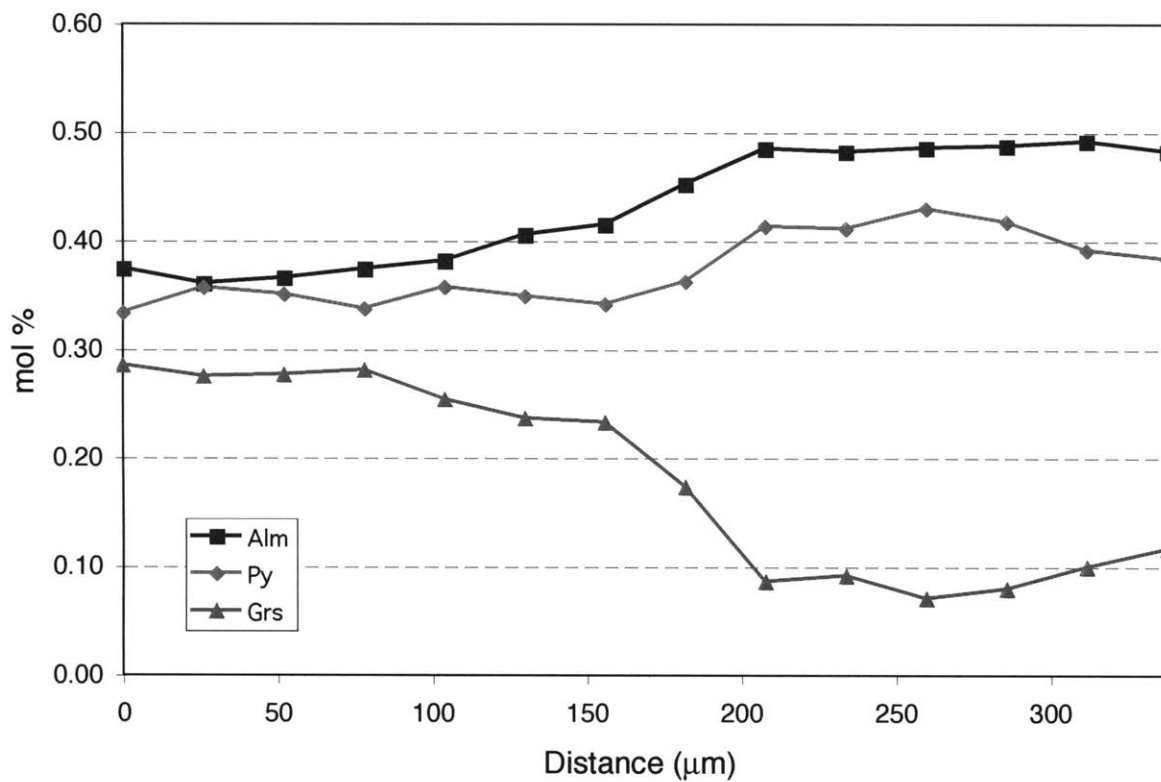


Figure 11

CHAPTER 4 - REACTION TEXTURES IN SAPPHIRINE GRANULITES

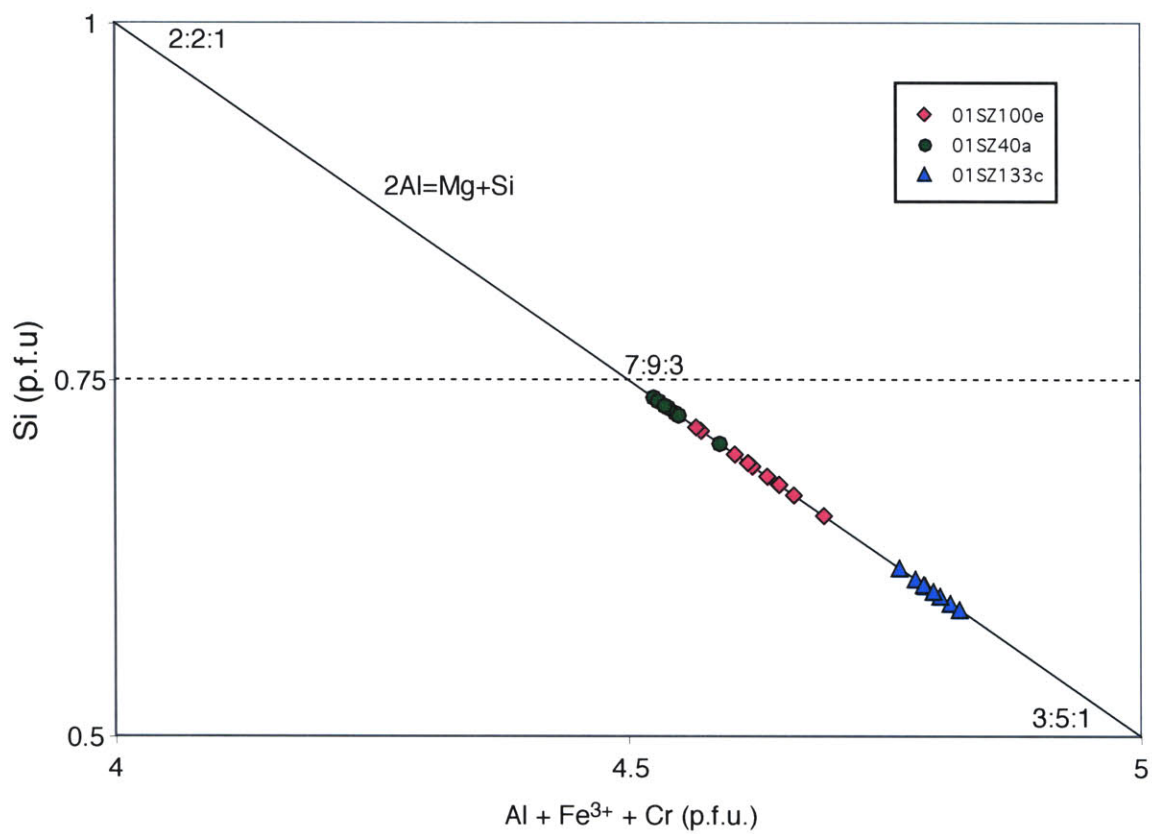


Figure 12

CHAPTER 4 - REACTION TEXTURES IN SAPPHIRINE GRANULITES

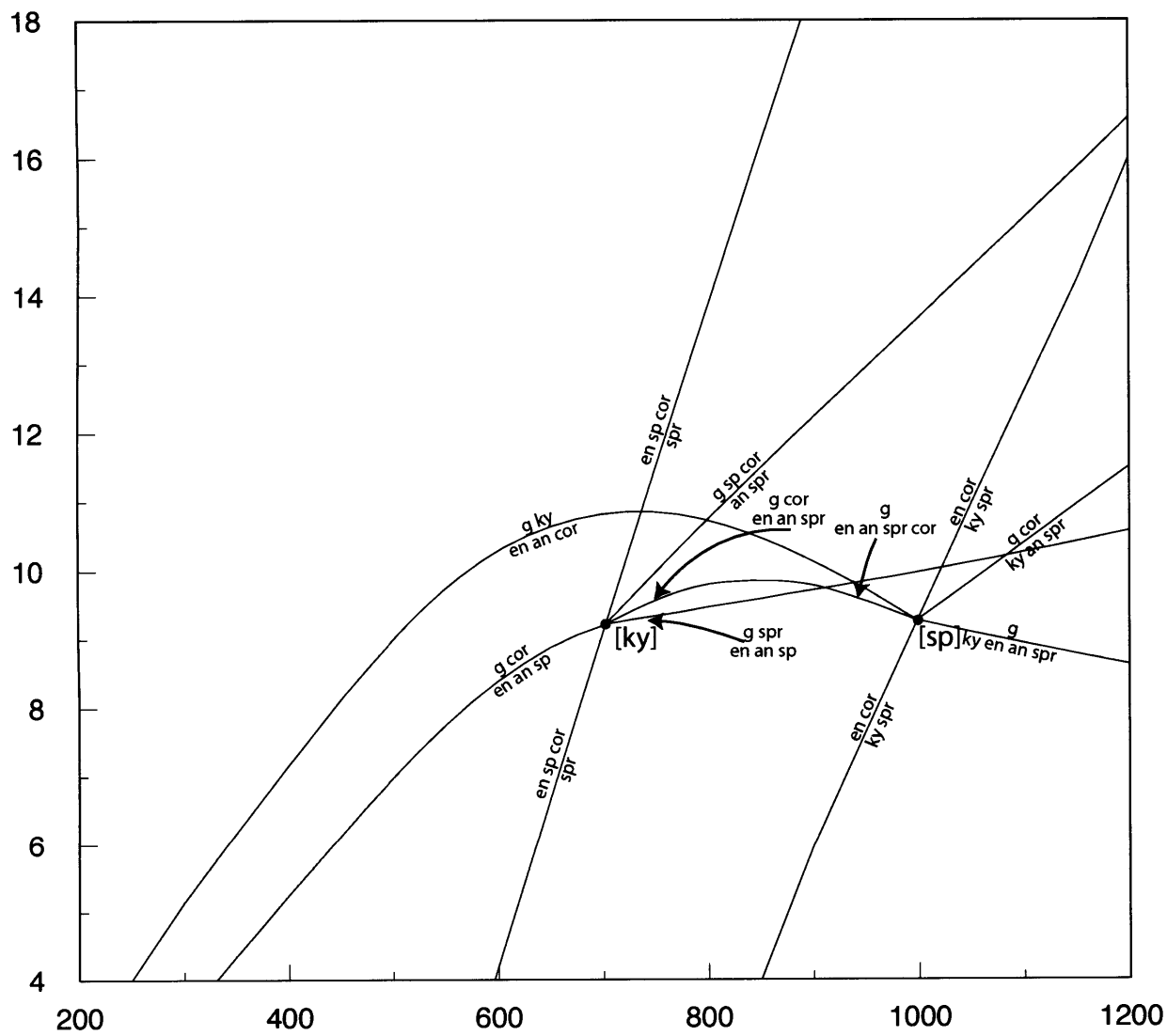


Figure 13

CHAPTER 4 - REACTION TEXTURES IN SAPPHIRINE GRANULITES

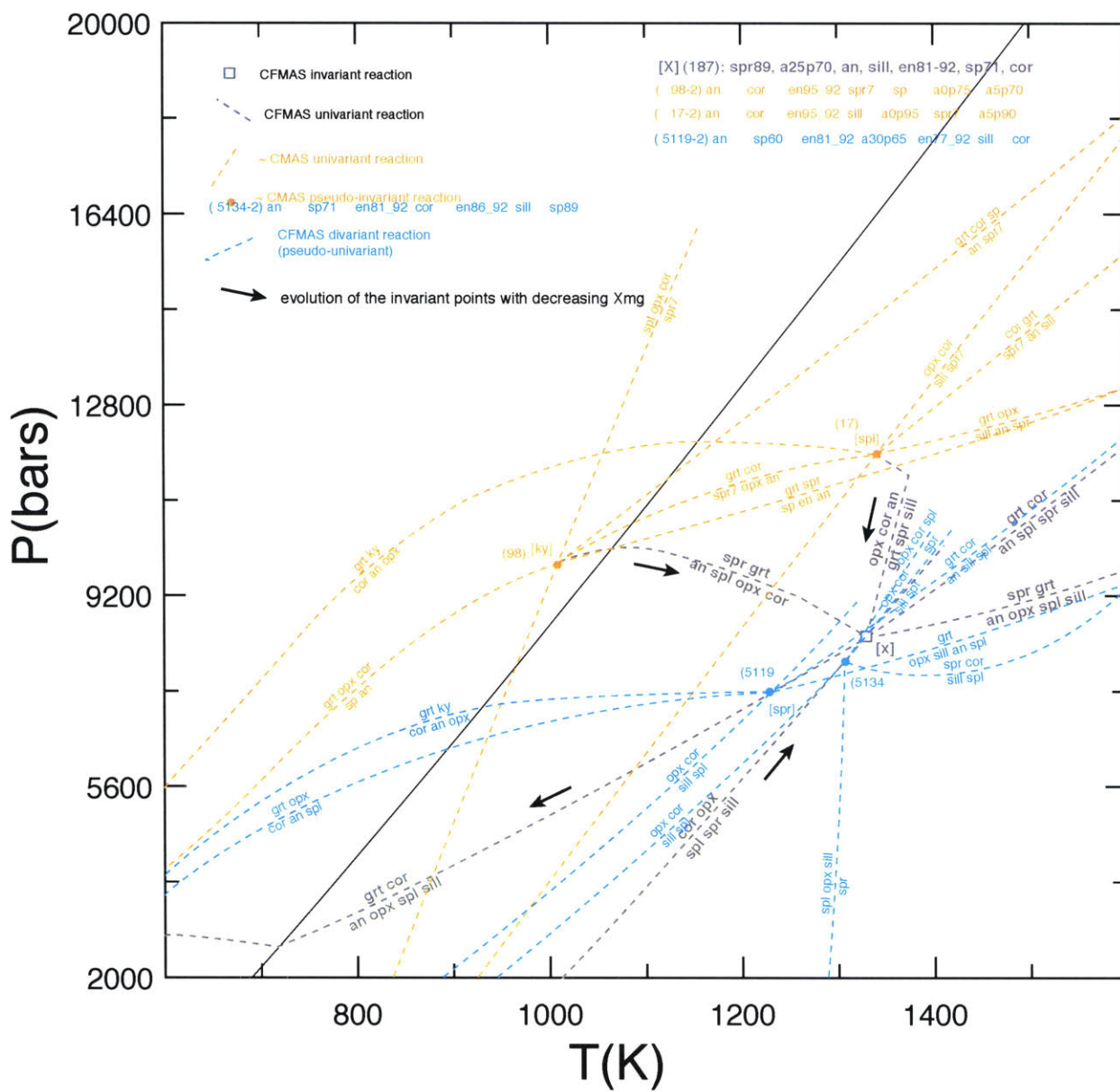


Figure 14

CHAPTER 4 - REACTION TEXTURES IN SAPPHIRINE GRANULITES

Table 1. Representative garnet microprobe analyses from sapphirine granulites.

Sample	01SZ40A	01SZ40A	01SZ133C	01SZ133C	01SZ133C	01SZ133C	01SZ133C	01SZ100E	01SZ100E
Type	core	rim	core	near pl incl	rim nr pl	rim nr opx	rim nr plag	adj pl	adj opx
SiO ₂	39.78	38.89	39.76	39.39	39.07	39.58	39.51	39.37	39.68
TiO ₂	0.05	0.04	0.09	0.02	0.06	0.03	0.07	0.02	0.05
Al ₂ O ₃	22.91	22.61	23.03	23.11	22.44	22.83	22.37	23.10	22.78
Cr ₂ O ₃	0.064	0.077	0.02	bd	bd	bd	0.02	bd	bd
FeO	20.11	23.26	17.10	22.71	23.62	23.16	22.43	22.74	17.04
MnO	0.18	0.22	0.33	0.51	0.61	0.58	0.51	0.74	0.32
MgO	10.65	8.19	7.91	9.24	9.57	10.85	9.93	10.92	9.46
CaO	6.38	6.62	12.38	5.51	4.77	3.37	5.89	2.90	10.15
Na ₂ O	0.06	0.01	bd	bd	bd	bd	0.01	bd	bd
Total	100.17	99.92	100.63	100.48	100.15	100.41	100.73	99.78	99.47
Si	2.985	2.975	2.982	2.977	2.976	2.983	2.982	2.978	2.991
Ti	0.003	0.003	0.005	0.001	0.004	0.002	0.004	0.001	0.003
Al	2.026	2.039	2.035	2.059	2.015	2.028	1.990	2.059	2.024
Cr	0.004	0.005	0.001	0.000	0.000	0.000	0.001	0.000	0.000
Fe ²⁺	1.262	1.488	1.072	1.435	1.505	1.460	1.416	1.439	1.074
Mn	0.011	0.014	0.021	0.033	0.039	0.037	0.032	0.047	0.020
Mg	1.191	0.934	0.884	1.041	1.086	1.219	1.117	1.231	1.062
Ca	0.513	0.543	0.994	0.446	0.389	0.272	0.477	0.235	0.819
Na	0.009	0.002	0.000	0.000	0.000	0.000	0.002	0.000	0.000
X _{Grs}	0.17	0.18	0.33	0.15	0.13	0.09	0.16	0.08	0.28
X _{Sps}	0.00	0.00	0.01	0.01	0.01	0.01	0.01	0.02	0.01
X _{Alm}	0.42	0.50	0.36	0.49	0.50	0.49	0.47	0.49	0.36
X _{Prp}	0.40	0.31	0.30	0.35	0.36	0.41	0.37	0.42	0.36

Normalized to 12 oxygens. bd, below detection limit.

CHAPTER 4 - REACTION TEXTURES IN SAPPHIRINE GRANULITES

Table 2. Representative orthopyroxene microprobe analyses from sapphirine granulites

Sample	01SZ40A	01SZ133C	01SZ133C	01SZ100E
Type	corona	corona	nr pl	core
SiO ₂	52.37	52.96	52.30	54.73
TiO ₂	0.05	0.07	0.09	0.04
Al ₂ O ₃	3.16	2.26	4.62	1.50
Cr ₂ O ₃	0.17	bd	0.17	0.02
FeO	21.10	20.49	18.00	16.83
MnO	0.04	0.14	0.14	0.20
MgO	23.21	23.87	25.22	26.73
CaO	0.12	0.16	0.17	0.41
Na ₂ O	0.01	bd	bd	bd
Total	100.24	99.95	100.71	100.46
Si	1.928	1.949	1.890	1.970
Ti	0.001	0.002	0.003	0.001
Al	0.137	0.098	0.197	0.063
Cr	0.005	0.000	0.005	0.001
Fe ²⁺	0.649	0.631	0.544	0.507
Mn	0.001	0.004	0.004	0.006
Mg	1.273	1.310	1.359	1.434
Ca	0.005	0.006	0.007	0.016
Na	0.001	0.000	0.000	0.000
X_{Mg}	0.66	0.67	0.71	0.74

Normalized to 6 oxygens. bd, below detection limit. $X_{Mg} = Mg/(Mg+Fe^{2+})$

Table 3. Representative plagioclase microprobe analyses from sapphirine granulites.

Sample	01SZ40A	01SZ40A	01SZ40A	01SZ40A	01SZ40A	01SZ133C	01SZ133C	01SZ133C	01SZ133C	01SZ133C	01SZ133C	01SZ100E	01SZ100E	01SZ100E
Type	corona	matrix	adj spl	adj spl	adj spr	incl in grt	corona	nr qtz	nr spr	adj ky	crn sym	adj spr	adj spl	nr grt
SiO ₂	55.57	56.90	48.79	53.87	48.65	57.86	57.55	59.88	44.63	44.99	44.17	46.31	46.71	49.50
Al ₂ O ₃	28.42	27.95	33.75	30.16	33.58	26.50	27.26	25.61	35.64	35.49	36.39	35.12	35.16	32.74
FeO	0.24	0.15	0.22	0.27	0.32	0.19	0.25	bd	0.15	0.09	0.02	0.09	0.16	0.27
MgO	0.02	0.02	0.12	0.05	0.20	bd	bd	bd	bd	0.01	bd	0.01	bd	bd
CaO	9.84	9.58	15.52	11.79	15.82	8.32	9.10	6.94	18.82	18.51	18.52	17.58	18.00	15.35
Na ₂ O	5.81	6.15	2.56	4.84	2.32	6.75	6.52	7.50	0.78	0.93	0.73	1.40	1.40	2.84
K ₂ O	0.10	0.19	0.06	0.13	0.06	0.09	0.09	0.17	0.02	0.02	0.02	bd	0.01	0.02
Total	99.99	100.95	101.02	101.11	100.96	99.71	100.77	100.10	100.03	100.04	99.85	100.51	101.44	100.72
Si	2.500	2.533	2.208	2.411	2.205	2.597	2.563	2.664	2.060	2.074	2.040	2.117	2.119	2.246
Al	1.506	1.466	1.800	1.591	1.794	1.402	1.431	1.343	1.939	1.928	1.981	1.892	1.880	1.751
Fe ²⁺	0.009	0.005	0.009	0.010	0.012	0.007	0.009	0.000	0.006	0.004	0.001	0.004	0.006	0.010
Mg	0.001	0.001	0.008	0.003	0.014	0.000	0.000	0.000	0.000	0.001	0.000	0.000	0.000	0.000
Ca	0.474	0.457	0.753	0.565	0.768	0.400	0.434	0.331	0.931	0.914	0.916	0.861	0.875	0.746
Na	0.507	0.531	0.224	0.420	0.204	0.588	0.563	0.647	0.070	0.083	0.065	0.124	0.123	0.250
K	0.006	0.011	0.003	0.008	0.004	0.005	0.005	0.010	0.001	0.001	0.001	0.000	0.001	0.001
X _{An}	0.48	0.46	0.77	0.57	0.79	0.40	0.43	0.34	0.93	0.92	0.93	0.87	0.88	0.75

Normalized to 8 oxygens. bd, below detection limit.

CHAPTER 4 - REACTION TEXTURES IN SAPPHIRINE GRANULITES

Table 4. Representative sapphirine and spinel microprobe analyses from sapphirine granulite.

Sample	01SZ40A	01SZ40A	01SZ133C	01SZ133C	01SZ100E	01SZ100E
Mineral	spr	spl	spr	spl	spr	spl
SiO ₂	12.06	0.05	11.54	0.02	11.59	0.01
TiO ₂	0.02	0.01	0.01	0.01	bd	bd
Al ₂ O ₃	62.68	62.55	64.25	61.71	64.40	61.90
Cr ₂ O ₃	0.18	0.69	bd	0.01	bd	bd
FeO	8.69	24.09	8.86	26.73	9.05	26.28
MnO	bd	0.02	0.07	0.10	0.08	0.09
MgO	15.49	11.68	14.91	10.84	14.91	11.44
CaO	0.02	0.05	0.01	0.07	bd	0.05
NiO	bd	0.45	bd	0.13	bd	0.06
Total	99.13	99.59	99.65	99.62	100.03	99.84
Si	0.725	0.001	0.691	0.000	0.691	0.000
Ti	0.001	0.000	0.001	0.000	0.000	0.000
Al	4.440	1.969	4.531	1.956	4.527	1.951
Cr	0.009	0.015	0.000	0.000	0.000	0.000
Fe ³⁺	0.100	0.013	0.086	0.042	0.090	0.048
Fe ²⁺	0.337	0.525	0.357	0.559	0.362	0.539
Mn	0.000	0.000	0.003	0.002	0.004	0.002
Mg	1.388	0.465	1.330	0.435	1.326	0.456
Ca	0.001	0.001	0.001	0.002	0.000	0.002
Ni	0.000	0.010	0.000	0.003	0.000	0.001
X _{Mg}	0.80	0.47	0.79	0.44	0.79	0.46

Sapphirine normalized to 10 and spinel to 4 oxygens. Ferric iron calculated by charge balance.

Abbreviations: bd, below detection; X_{Mg} = Mg/(Mg+Fe²⁺)

Chapter 5

High-pressure metamorphism of lower crustal felsic granulites, Snowbird tectonic zone, northern Saskatchewan, Canada: Implications for the U-Pb systematics of monazite

To be submitted to *Contributions to Mineralogy and Petrology*

Baldwin, J.A., Bowring, S.A., and Williams, M.L.

Abstract

An investigation of the U-Pb and Sm-Nd systematics of monazite from felsic high-pressure granulites from the East Athabasca mylonite triangle, northern Saskatchewan, has been carried out in an attempt to deconvolve the timing of metamorphism. This terrane is a 400 km² package of "white gneisses" interpreted to represent pelitic rocks that were metamorphosed at conditions of 1.5-2.0 GPa and 1000°C. These high-pressure mineral assemblages are interpreted to have formed primarily as the result of high-pressure partial melting, which is consistent with the observed garnet-kyanite-ternary feldspar assemblage. Detailed investigations using combined EPMA and ID-TIMS techniques, reveal that monazite records a complicated growth history from 2.6 to 1.9 Ga. Well-armored monazite inclusions in garnet yield the oldest observed U-Pb dates at 2.62 Ga. In contrast, matrix grains and inclusions in garnet rims that are not well-armored show much more complicated U-Pb systematics and contain multiple age domains. One matrix monazite grain examined yields a U-Pb date of 1.90 Ga. Sm-Nd isotope systematics of single monazite indicate that inclusions in garnet are similar to the whole rock signature with a limited range of slightly negative $\epsilon_{Nd(i)}$. In contrast, grains that show geochronological evidence for a Paleoproterozoic component show more positive $\epsilon_{Nd(i)}$, most simply interpreted as reflecting derivation from a source containing garnet. Further evidence for the discrete sources for the two populations is given by Y concentrations in monazite. Inclusions in garnet show high-Y implying crystallization in the absence of garnet whereas matrix grains show significant depletion in Y. These results have important implications for the U-Pb systematics of monazite under extreme high-T conditions, and show empirically that even at temperatures of 1000°C there has not been any significant diffusional Pb loss, providing empirical evidence that the closure temperature for monazite is likely >1000°C in agreement with experimental data.

Key words: geochronology, high-pressure granulite, monazite, partial melting, Snowbird tectonic zone

1. Introduction

The lower continental crust contains a complex record of lithospheric evolution including both mass and thermal fluxes from the underlying mantle as well as deformation caused by interaction of lithospheric plates. Lower crustal samples come from either xenolith suites brought to the surface in volcanic rocks or from rare exposures of lower crustal rocks exhumed by tectonic processes (e.g., Percival et al., 1992; Rudnick, 1992). High-precision U-Pb geochronology combined with quantitative geothermobarometry permits a comprehensive analysis of the metamorphic and exhumational history of such rocks. However, unlike xenolith suites, exposed deep crustal sections also permit such rocks to be studied within a structural framework. Exposures of the lower crust typically preserve evidence for multiple metamorphic and deformational events spanning in some instances hundreds of millions of years, yet petrologically only the final decompression segment of a P - T path is typically preserved, making the interpretation of multiple generations of accessory phase growth difficult. Additionally, the exhumation mechanism for exposing such lower crustal sections may be completely unrelated to the processes that produced the observed high-pressure assemblages.

Deciphering complex metamorphic histories of polydeformed lower crustal rocks relies on dating minerals with high-closure temperatures. Determining when accessory phases grew relative to peak metamorphic assemblages and fabrics is a key part of temporally calibrating an observed P - T path. Monazite is a mineral of choice for dating metamorphic rocks because it is relatively common, has high concentrations of U and Pb, low concentrations of common Pb, and like zircon, is highly resistant to diffusive Pb loss. Monazite can be an important geochronometer for dating high-grade metamorphic events, although the behavior of monazite during granulite facies metamorphism is far from well-understood. Monazite can have a greater propensity for growth during metamorphism compared to zircon due to its participation in a number of metamorphic reactions and reactivity with fluids. However, an incomplete understanding of the reactions that produce and consume monazite hinders accurate interpretation of the geochronological data (Foster et al., 2002).

CHAPTER 5 – MONAZITE SYSTEMATICS IN HIGH-PRESSURE GRANULITES

It has been known for over a decade that monazite has at least a moderately high closure temperature ($>725^{\circ}\text{C}$, Copeland et al., 1988; Smith & Barreiro, 1990; Smith & Giletti, 1997). However, recent experimental work suggests that the closure temperature for Pb diffusion in monazite may meet or exceed that of zircon ($>1000^{\circ}\text{C}$, Cherniak & Watson, 2001; Cherniak et al., 2002; Harrison et al., 2002). Although monazite commonly yields concordant U-Pb dates (e.g., Parrish, 1990), recent studies have shown that there are a variety of processes that can result in discordant U-Pb dates (e.g., Hawkins & Bowring, 1997). Additionally, even in cases where concordant dates are obtained, they commonly span a range of as much as 20-30 Ma along concordia (e.g., Bingen & van Breemen, 1998; Hawkins & Bowring, 1999; Spear & Parrish, 1996). Given the evidence for a high closure temperature for Pb diffusion in monazite, this implies that in most geological situations, either the dissolution and reprecipitation of monazite due to reactions with hydrous phases and fluids or episodic or protracted growth rather than Pb diffusion results in discordant U-Pb dates. Therefore in some rocks, discordant ages are a complicated mixture of fluid interactions that may have no geologically meaningful significance. Thus development of dating techniques where knowledge of the petrographic setting of monazite crystals is preserved combined with the capability to analyze subgrain domains is crucial to understanding the significance of the dates obtained (e.g., Foster et al., 2002; Zhu & O'Nions, 1999b).

The electron microprobe dating of monazite combined with high resolution X-ray compositional mapping is an important reconnaissance tool for evaluating the complexities of monazite growth in metamorphic rocks (Crowley & Ghent, 1999; Montel et al., 2000; Williams & Jercinovic, 2002; Williams et al., 1999). The main advantages of the EPMA technique are high spatial resolution, non-destructive nature, and the ability to obtain in situ analyses. This technique when combined with high-resolution mapping of elements such as Th, Y, U, Pb, and Ca can provide information that aids in the interpretation of the dates obtained. However, the EPMA technique does not afford the high precision of U-Pb isotope dilution thermal ionization mass spectrometry (ID-TIMS) analysis as well as the ability to evaluate closed system behavior. Thus, obtaining ID-TIMS dates on grains that have been imaged and dated by the EPMA method is essential

CHAPTER 5 – MONAZITE SYSTEMATICS IN HIGH-PRESSURE GRANULITES

in order to evaluate the geological significance of EMPA dates and to test the assumption that the system has remained closed to diffusional Pb loss. This study presents data from a representative felsic granulite sample from the Snowbird tectonic zone, Canada. Monazite from this sample has been analyzed using both the EPMA and ID-TIMS techniques and thus provides a broad comparison of the two methods. In addition, this study also shows how the EPMA method can be used to target and characterize different populations of monazite based on its petrographic setting, and perhaps fingerprint the populations based on compositional differences. These well-characterized grains can subsequently be dated by high-precision ID-TIMS in order to better understand the metamorphic histories of polydeformed rocks.

Granulites of the Snowbird tectonic zone (STZ), northern Saskatchewan, Canada provide a superb natural laboratory for understanding lower crustal processes and, in particular, high-pressure metamorphism and partial melting of granulites in the lower crust. The high-pressure felsic granulites contain the diagnostic assemblage of kyanite + K-feldspar and have experienced peak metamorphic conditions of >1.5 GPa and 1000°C (Snoeyenbos et al., 1995). The timing of high-pressure metamorphism in these rocks was previously reported to be 2.62-2.60 Ga, although detailed geochronological data were not available (Snoeyenbos et al 1995). This study shows that, in addition to a Late Archean metamorphism, a previously unrecognized episode of Paleoproterozoic metamorphic growth of monazite occurred. However, the correlation of monazite growth to specific *P-T* conditions and tectonometamorphic events remains problematic.

Textural relationships of high-P minerals in the felsic granulite, Ca-zoning in garnet, and regional geochronology indicate that these rocks underwent high pressure metamorphism at 1.90 Ga, resulting in monazite growth from 2.6 to 1.9 Ga. For example, well-armored inclusions of monazite in garnet always preserve Late Archean monazite dates whereas monazite along grain boundaries or in contact with fractures records younger dates. This study provides important empirical evidence for a high closure temperature of Pb diffusion in monazite and provides an example of how the textural setting of monazite affects its ability to participate in metamorphic reactions. In addition, we examine the Sm-Nd isotopic systematics of both whole rock samples and

single monazite grains in order to evaluate potential isotopic source regions during the crystallization of monazite from 2.6 to 1.9 Ga.

2. Regional Geologic Setting

The Snowbird tectonic zone is a 3000-km-long linear element in the horizontal gravity gradient map of the Canadian Shield that extends from the Canadian Cordillera northeast to Hudson Bay (Goodacre et al., 1987). It occurs at the boundary between the Rae and Hearne Archean domains of the western Churchill Province (Hoffman, 1988). In northern Saskatchewan, a well-exposed 125 x 80 x 75 km wedge-shaped segment of the Snowbird tectonic zone has been described as the East Athabasca mylonite triangle (EAmt), and consists of anastomosing lower crustal high-grade granulite facies mylonites (Hanmer, 1997; Hanmer et al., 1994; Hanmer et al., 1995a; Hanmer et al., 1995b). The EAmt is the southwestern segment of the Striding-Athabasca mylonite zone that has been interpreted as an Archean intra-continental strike-slip shear zone (Hanmer, 1994; Hanmer et al., 1994; Hanmer et al., 1995a; Hanmer et al., 1995b) (Fig. 1).

The EAmt is bounded to the northwest and southeast by wallrocks of the Rae and Hearne provinces, respectively, and is overlain to the south by the *ca.* 1.77 Ga Athabasca sandstone (Cumming et al., 1987). The wallrocks of the Rae and Hearne domains adjacent to the EAmt are lithologically similar, consisting dominantly of pelitic schist, paragneiss, amphibolite, and largely undated granitoid rocks, however they were metamorphosed at different crustal levels. Recent work in the Rae wallrocks west of the EAmt suggests that much of the Rae Province in this area experienced intermediate-P granulite facies conditions (~0.8 GPa, 900 C) at *ca.* 1.9 Ga (Williams & Hanmer, in press). In contrast, the Hearne Province wallrocks are separated from the EAmt by a major amphibolite-facies shear zone and record lower pressure amphibolite facies metamorphic conditions (0.5 GPa, 600-700°C, at <1.9 Ga) (Mahan et al., in press).

The EAmt is divided into three structural domains (Fig. 2a). The northwestern and southeastern domains are dominated by felsic to mafic plutonic rocks metamorphosed at uniform pressures and temperatures of 1.0 GPa, 800°C (Williams et al., 1995; Williams et al., 2000). The southern domain consists of both felsic and mafic

granulite as well as minor lenses of eclogite metamorphosed at minimum conditions of 1.5 GPa, 900-1000°C (Baldwin et al., 2003; Snoeyenbos et al., 1995).

3. The Southern Domain

Within the southern domain there are two apparent subdivisions, composed of three dominant lithological units in varying proportions: felsic gneiss, eclogite, and mafic granulite (Fig. 2b). Structurally higher levels in the southern extent are dominated by mafic granulite, whereas lower structural levels to the north are dominated by felsic gneiss. The most abundant lithology in the northern extent of the southern domain is a massive felsic garnet-kyanite quartzofeldspathic gneiss. This felsic gneiss is an anhydrous mylonitic rock (garnet+feldspar+quartz+kyanite/sillimanite+rutile) with a shallow SW-plunging lineation. Garnet is ubiquitous throughout the felsic gneiss, and typically comprises 5-40% of the rock. Kyanite-bearing assemblages are locally preserved, and are particularly well-preserved in the ~5 km thick zone between Axis Lake and Currie Lake (Fig. 2b).

Mafic granulite occurs as layers that are typically several-m-thick, but are locally more than 10 m thick. They contain a foliation that dips steeply to the south and is parallel to the foliation in the host felsic gneiss. At map scale, the strike of this foliation is sub-parallel to the boundary between the southern domain and the northwestern and southeastern domains of the lower deck. Most mafic granulite layers and the host gneisses have a strong mineral lineation that plunges shallowly to the southwest. These mafic granulite layers have been interpreted as a series of intrusive sills with northeast-striking intrusive contacts (Baer, 1969; Slimmon, 1989). Pressures and temperatures have been calculated for mafic granulite layers within the felsic gneiss at 890-960°C, 1.3-1.9 GPa (Baldwin et al., 2003). The timing of high-pressure metamorphism is constrained by U-Pb geochronology of zircon at 1904 ± 0.9 Ma (Baldwin et al., 2003).

A distinctive and important lithological unit for constraining the pressure-temperature history of the southern domain, is a thin 10-15 m-thick band of eclogite that has been mapped along strike for ~15 km (Fig. 2b) (Chapter 3). It consists of garnet + omphacite, with kelyphitic reaction rims of pargasite + plagioclase around garnet and

orthopyroxene + plagioclase symplectite rims around clinopyroxene. Garnet contains abundant inclusions of kyanite \pm zoisite. Pressures and temperatures are constrained at 920-1000°C, 1.8–2.0 GPa (Chapter 3). A near-isothermal decompression path to granulite facies conditions is inferred from the retrograde reaction textures. U-Pb geochronology of eclogitic zircons yields a weighted mean $^{207}\text{Pb}/^{206}\text{Pb}$ date of 1904.2 \pm 0.2 Ma, which is interpreted as the age of eclogite facies metamorphism (Chapter 3).

4. The Snowbird Felsic High-Pressure Granulites

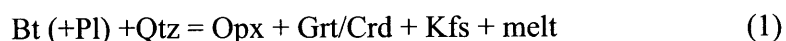
4.1 Petrology of the “White” Gneiss

The dominant rock type in the southern domain is a richly garnetiferous quartzofeldspathic gneiss. The felsic gneiss is petrologically similar to the “Weiss-stein” granulites of the type locality for granulites, the Saxonian granulite massif (O'Brien & Rötzler, 2003; Weiss, 1803), hence the term “white” gneiss has been used to describe them. The petrology of the felsic gneisses has been described by Snoeyenbos et al. (1995). The felsic gneisses are predominantly ribbon mylonites that contain abundant garnet, set in a matrix of quartz ribbons and ternary feldspar. Kyanite is preserved in much of the felsic gneiss and occurs as either inclusions in garnet or as a matrix phase, and is commonly rimmed by sillimanite. The characteristic high-pressure granulite facies assemblage in these rocks is garnet-ternary feldspar-quartz-kyanite-rutile, with the accessory phases monazite, zircon, apatite, and graphite. Biotite is present as a retrograde phase rimming sillimanite or garnet.

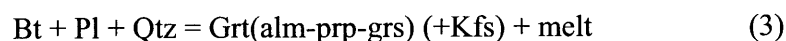
Feldspars of ternary composition occur as ribbons along with quartz in the matrix of the felsic gneiss. These feldspars are typically mesoperthites, and are exsolved into narrow rods of almost pure K-feldspar in a plagioclase host ($\sim\text{Ab}_{70}$). Ternary feldspar rehomogenization thermometry of these mesoperthites yields temperatures of 1000°C (Snoeyenbos et al., 1995). The coexistence of kyanite with these feldspars constrains minimum pressures of \sim 1.5 GPa. In addition, the occurrence of eclogite within the felsic gneiss that has experienced pressures as high as 1.8–2.0 GPa implies that the felsic gneiss has seen similar peak pressures (Chapter 3).

CHAPTER 5 – MONAZITE SYSTEMATICS IN HIGH-PRESSURE GRANULITES

Garnet in the felsic gneiss invariably contains a marginal ridge of high grossular content. Snoeyenbos et al. (1995) proposed that this rim might be related to a partial melting reaction at high pressure. In their experimental study on the partial melting of metagraywackes, Vielzeuf & Montel (1994) observe that grossular content in garnet is strongly pressure dependent. Two important melting reactions in metapelites are commonly observed:



The important observation is that both of these reactions produce Opx during melting, which is a required phase in medium-pressure granulite facies rocks. However, at high pressures, the Bt-out curve changes from a positive to negative slope and intersects with the Opx-in curve between 1.5 and 2.0 GPa (Fig. 3). At pressures above ~1.5 GPa the reaction:



produces Grt and Kfs but no Opx. Thus biotite may completely react with plagioclase and quartz to produce garnet and melt without producing orthopyroxene. Typically, high-pressure felsic granulites are Opx-absent and a reaction such as this at high pressure might provide an explanation for this observation (O'Brien & Rötzler, 2003).

Other observations made by Vielzeuf & Montel (1994) were that with increasing pressure garnet has a characteristic spongy appearance with abundant inclusions and that the modal proportion of garnet increases with increasing pressure, two commonly observed characteristics of the Snowbird felsic granulites. In these experiments, it was observed that grossular content of garnet increased from about 4 mol% at 0.5 GPa to ~15 mol% at 2.0 GPa, which closely parallels the observed grossular increase in the Snowbird felsic granulites. These results show that some melt reactions, particularly those involving a calcic phase are pressure dependent as well as temperature dependent. Other

studies have observed this characteristic as well. In their study of fluid-absent melting of semi-pelites, Nair & Chacko (2002), show that at 1.5 GPa, an increase in Grs from 7 mol% at 950°C to 12 mol% at 1050°C occurs. In addition, Opx was absent from experiments at 1.5 GPa and 1050°C.

4.2 Petrographic description of 01SZ90

A variety of samples were selected for geochemical analysis, but one sample in particular was chosen for a detailed monazite U-Pb and Sm-Nd geochronological study. This sample, 01SZ90, was selected because of its superb preservation of the high-pressure granulite facies assemblage. The sample consists of garnet-kyanite-K-feldspar and displays a protomylonitic fabric with a well-developed lineation. The sample is segregated into discrete layers of alternating K-feldspar and quartz ribbons and layers rich in garnet and kyanite. Garnet is typically 1-10 mm in diameter and kyanite is typically <1 mm. Secondary sillimanite and biotite rim kyanite and garnet. The predominant feldspar is orthoclase with lesser amounts of plagioclase, which typically forms as a secondary phase. Accessory minerals include rutile, monazite, zircon, apatite, pyrite, and graphite.

Garnet is anhedral, ~1 mm to several cm in size, and rich in inclusion phases. Garnet compositional maps show a marked increase in Grs content in the outer few hundred microns (Fig. 4). There is no variation in Fe or Mg suggesting that garnet fully re-equilibrated with respect to Fe-Mg diffusion. Large (100s of μm to >1mm) inclusions of quartz are common (Fig. 5a). These quartz inclusions are typically rimmed by a thin layer of Ksp and/or plagioclase. In addition, polyphase inclusions of Qtz \pm Ky in garnet are rimmed by plagioclase (Fig. 5b). Other inclusions in garnet include sillimanite, rutile, biotite, monazite, and zircon. Minute fluid inclusions are also present in some garnet cores. Sillimanite inclusions occur as fine needles and are present only in the outer region of the garnet. Fractures are common in garnet and are typically filled with late biotite.

Kyanite grains are commonly rimmed by a thin mantle of nearly pure Ksp with scarce exsolution lamellae (<5%) of plagioclase (Fig. 5c). These rims of Ksp are adjacent to matrix quartz grains. Kyanite occurs both in direct contact with garnet as well

CHAPTER 5 – MONAZITE SYSTEMATICS IN HIGH-PRESSURE GRANULITES

as throughout the quartz-feldspar matrix. Matrix feldspar is a fine-grained mixture of discrete orthoclase and plagioclase grains with 80% Ksp and 20% plagioclase.

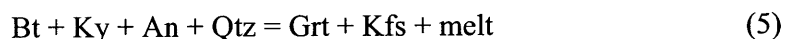
Monazite is an abundant accessory phase that occurs throughout the rock as a matrix phase and as inclusions in garnet. It ranges in size from <10 μ m to >100 μ m. The petrographic setting of each of the individual monazite grains analyzed will be described in a section below. Zircon is a less abundant accessory phase, is more rarely observed as an inclusion in garnet, and most commonly occurs in the quartzofeldspathic matrix. Zircon is typically spheroidal and concentric growth zones are evident.

4.3 Evidence for Partial Melting of a Pelitic Protolith?

Sample 01SZ90 contains abundant evidence for dehydration melting reactions implying a significant modal proportion of mica in the protolith. Muscovite dehydration melting would occur by a reaction such as:



This reaction can explain the predominance of matrix orthoclase feldspar and the abundance of kyanite. In order for this reaction to produce kyanite as the stable aluminosilicate phase, the minimum *P-T* conditions of melting would be >8 kbar, >700°C (Spear, 1993). Because there is no Opx present in the sample, a reaction such as (3) could also explain the production of garnet. Alternatively, kyanite may also be a reactant and garnet could be produced through the reaction:



Either of these reactions would cease once all the biotite is consumed and partial melt is extracted, resulting in an anhydrous restite. The thin rims of orthoclase around kyanite would be produced by a reactions such as (5). An increase in pressure conditions could explain the high Grs rims observed on garnet. Experimental data suggests that minimum *P-T* conditions for biotite dehydration melting without the production of Opx are ~1.5-2.0 GPa, 850-950°C (Vielzeuf & Montel, 1994). Late stage hydration at lower pressure

conditions is evident through the secondary growth of sillimanite replacing kyanite and biotite rimming garnet and sillimanite.

The textures in this sample are consistent with formation of the observed assemblage due to biotite and muscovite fluid-absent melting reactions. Figure 6 shows a schematic petrogenetic grid for fluid-absent melt reactions in the KCMASH system, highlighting those assemblages that involve the anorthite component in plagioclase (Vielzeuf & Montel, 1994). The relevant reactions to the Snowbird felsic gneisses are reactions (3) and (4). Reaction (3) corresponds to the biotite-out reaction at high pressure. The Opx-in reaction is given by:



This is analogous to the high-pressure to medium-pressure granulite facies transition of Green and Ringwood (1967) for mafic granulites. The area shaded in Figure 6 schematically indicates the region of stability for the assemblage observed in the felsic gneisses. This region occurs above the minimum temperatures for muscovite and biotite dehydration melting (reactions 3 and 4) and at sufficiently high pressure that Opx does not form (reaction 6). The *P-T* conditions for this region have been constrained experimentally at >1.6 GPa at temperatures > 950°C (Fig. 3) (Vielzeuf & Montel, 1994).

5. Geochemistry of the Felsic Gneiss

Major and trace element concentrations of representative samples of the felsic gneiss were determined by XRF and ICPMS, respectively (Table 1). The geochemistry is broadly consistent with a granitic or pelitic protolith. Bulk compositions range from 55.7-74.7 wt.% SiO₂, and are aluminous with 13.0-23.5% Al₂O₃. Most of these variations can be traced to the modal proportion of garnet, presence or absence of aluminosilicate, and relative abundances of feldspar versus quartz. Potassium content ranges from 0.34-4.96 wt.% and Ti is generally low (0.12-1.24 wt.%). It is important to note that this variety of lower crust is geochemically distinct from average lower crustal compositions in the literature that generally infer a more mafic composition (Rudnick & Fountain,

1995). Because of the high modal proportion of garnet, these granulites have high densities, however they are considerably depleted in Mg and Ca, compared to average lower crustal compositions.

The whole rock samples investigated for trace elements show substantial LREE enrichment ($\text{La/Yb} = 5.7\text{-}216.3$) and generally display positive Eu anomalies ($\text{Eu/Eu}^* = 1.69\text{-}10.1$) (Fig. 7). These patterns show gently sloping HREE patterns and a wide variation in total HREE between individual samples. The Snowbird felsic granulites are considerably more LREE-enriched than average lower crust, but similar in the HREE. Th/U ratios range from 1.64-19.87 compared to the average lower crustal value of 5.9 (Rudnick & Fountain, 1995).

6. Electron Microprobe Characterization and Dating of Monazite

6.1 Mapping and Characterization of Monazite in Thin Section

We used the methods described by Williams & Jercinovic (2002) and Jercinovic & Williams (in prep.) to identify and characterize the textural setting of individual monazite grains. All of the mapping and analyses were done on the Cameca SX-50 electron microprobe at the University of Massachusetts at Amherst. The distribution of monazite in a thin section was determined by collecting full thin section maps of Ce and a reference element such as Ca, used to characterize the overall texture, structure, and mineralogy. This allows for a first step in evaluating the textural setting of monazite on the thin section scale. High resolution X-ray compositional maps of Th, Y, U, Pb and/or Ca were then obtained for specific monazite grains of interest. These compositional maps identify the potential complexities in the individual grains that may correlate with different age domains. Major element analyses were acquired for representative compositional domains in monazite as depicted on X-ray maps (Table 2). Analyses of the trace elements, Th, U, Pb, and Y were made using an accelerating voltage of 15 kV, 200 nA beam current, and 600 sec count time, except where Pb is lower than 1000 ppm, when a 900 sec count time is used. A chemical date was calculated for each point based on the equation from Montel et al. (1996).

CHAPTER 5 – MONAZITE SYSTEMATICS IN HIGH-PRESSURE GRANULITES

Monazite occurs in a variety of textural settings in 01SZ90. The most common are as inclusions within garnet or matrix grains that are interstitial to feldspar and/or kyanite. Within garnet, the monazite ranges from isolated well-armored grains to grains that are in contact with fractures. Invariably fractures in garnet that lead to monazite inclusions contain biotite. Figure 8 shows Th X-ray compositional maps for eight monazite grains from a single thin section of 01SZ90, all processed with the same brightness scale. These grains show dramatic variation in Th composition that is correlated to the petrographic setting of the monazite grains. High Th grains (Fig. 8 – m2, m5, and m6) are inclusions in garnet, whereas intermediate to low Th grains occur throughout the matrix. The effect of armoring by garnet on Th variation in monazite is shown by comparing m2 with m6. Monazite m2 is a well-armored grain with no evidence for surrounding fractures. In contrast, m6 is connected to the matrix through fractures filled with biotite, and the resulting Th map shows patchy zoning, yet is still high in Th compared to the matrix grains. Matrix grains have a range in Th content. Grain m3 is a medium content Th grain that shows very homogeneous distribution of Th in the core, and a very thin slightly lower Th rim. Grains m1, m4, m7, and m8 are all low Th matrix grains that show evidence for slightly high Th cores regions and low Th homogeneous rims. Thus, Th content can be correlated to the petrographic setting of the monazite and may be an important monitor of the timing of melting, fluid infiltration, or growth of additional phases that may scavenge REE.

Seven monazite grains were selected for a detailed EPMA and TIMS study from three different thin sections that were interpreted to represent the range of petrographic settings of monazite observed in 01SZ90. One section was a 30- μm -thick standard thin section. The other two were cut 80- μm -thick in order to allow for easier extraction of the grains from the thick sections for later analysis by ID-TIMS. These sections are referred to throughout this chapter as thin (th), thick1 (tk1), and thick2 (tk2). Trace element analyses were acquired using information primarily from Th maps as a guide to evaluating age domains within the individual monazite grains. The grains were then extracted and dated by high-precision ID-TIMS, allowing for a direct comparison

between the EPMA and TIMS methods. Trace element compositional data are presented in Table 3.

6.2 *Electron Microprobe Results*

Monazite m1tk1 occurs as a matrix grain in textural equilibrium with kyanite (Fig. 9a). It is anhedral, ~90 in length, and is adjacent to a small rutile grain that is in contact with biotite (Fig. 9a). X-ray compositional maps reveal two distinct domains that correlate with both Th and Ca, and to a lesser extent U (Fig. 10a). The grain contains a high Th core with a low Th overgrowth. However, a thin rim that is not apparent in the BSE image is evident in both the Ca and Th maps. This rim is higher in Ca and intermediate in Th with respect to the other domains. Y concentrations are low (<1000 ppm). The EPMA results yield a range in chemical dates of 2500-2100 Ma for the core region and 2330-2130 for the rim.

Monazite m2tk1 is an elongate matrix grain (~55 μm long) that occurs adjacent to kyanite and K-feldspar (Fig. 9b,c). The Th and Y maps are homogeneous and Y concentration is ~100 ppm (Fig. 10b). No significant composition or age variation is observed in this grain, and the EPMA date based on the weighted mean of eight analyses is 1896 ± 23 Ma.

Monazite m5tk1 is a spherical inclusion in garnet (56 μm diameter) (Fig. 9d,e). There are some small cracks leading away from the monazite, but they do not connect with any fractures leading out to the matrix (Fig. 9e). The Th map and BSE image are predominantly homogeneous; however, a slight thin rim of higher Th monazite is apparent at the lower right edge of the Th map (Fig. 10c). The Y concentration for this grain is relatively high (~8000 ppm), but the compositional maps show a significant variation in Y content within the grain (Fig. 10c). The EPMA date obtained for this grain based on the weighted mean of four analyses is 2592 ± 13 Ma.

Monazite m6tk1 is a matrix grain that occurs between ternary feldspar and kyanite. It is elongate (~74 μm long) with a slightly irregular rim (Fig. 9f). The BSE image does not show any significant variations, however, both the Th and Ca map reveal a high Th, low Ca core with a substantial low Th overgrowth (Fig. 10d). Y is

CHAPTER 5 – MONAZITE SYSTEMATICS IN HIGH-PRESSURE GRANULITES

homogeneous and low. The two domains were analyzed separately, and EPMA chemical dates for the high Th core based on 5 analyses was 2050 ± 18 Ma. For the overgrowth, the weighted mean of four analyses yielded a date of 1940 ± 29 Ma.

Monazite m1tk2 is a large ($175 \times 110 \mu\text{m}$) ovoid inclusion in garnet (Fig. 9g,h). It is well-armored with no evidence for fractures leading to the matrix. It occurs in the inner low Grs region of garnet. The BSE image and Th map indicate that the grain is homogeneous and unzoned (Fig. 10e). Y concentrations are relatively high (~ 8000 ppm), but show significant variability in the compositional map (Fig. 10e). This grain was probed on two different days with different background measurements, and gives an indication of the reproducibility in the measured compositions. The weighted mean averages from each session were 2627 ± 10 Ma ($n=18$) and 2583 ± 10 Ma ($n=9$). The rim yielded an average date of 2396 ± 27 Ma ($n=7$).

Monazite m5tk2 is also a large ovoid inclusion in garnet ($110 \times 66 \mu\text{m}$) (Fig. 9i,j). It occurs in the outer high Grs region of garnet (Fig. 9i) and is surrounded by extensive fractures leading out to the matrix. Although the BSE image does not show any significant complexity, the Th, Y, and Ca maps all show a chaotic internal structure (Fig. 10f). Overall, the outer region of the grain is higher in Th than the core, but there is a highly irregular boundary delineating these two domains. Y zoning is patchy and highly variable (Fig. 10f). The weighted mean of five analyses yields an EPMA date of 2460 ± 17 Ma.

Monazite m3th is an elongate matrix grain ($\sim 155 \mu\text{m}$ long) that occurs adjacent to kyanite and ternary feldspar. It is intermediate in Th content (same grain shown in Fig. 8, m3, above). It is relatively homogeneous with respect to Th and Y, and Y concentration is relatively low (~ 600 ppm) (Fig. 10g). A thin outer rim of slightly lower Th content was analyzed separately from the intermediate Th core. EPMA results for the core region based on 29 analyses yielded a date of 1899 ± 12 Ma. The outer low Th rim yielded an EPMA date of 1844 ± 6 Ma based on three analyses.

The seven grains studied can be classified into two categories based on their Th and Y distribution. Inclusions in garnet are homogeneous and relatively high with respect to Th, and yield Archean EPMA chemical dates. These grains also show

significant variability in Y concentration within the grains. The overall Y concentrations are significantly higher than matrix grains, implying that they grew in the absence of garnet, a phase that would readily scavenge available HREE and Y (Foster et al., 2002; Pyle & Spear, 1999). The one grain that occurs as an inclusion in the garnet rim that is not well-armored (m5tk2, Fig. 9i), shows significantly more variability in the compositional maps (Fig. 10f), and domains with lower Y than the well-armored inclusions. This grain yields Archean chemical dates that are somewhat younger than dates from well-armored grains. The second population are matrix grains that most commonly contain high Th cores with low Th rims. Y is significantly lower than in monazite inclusions in garnet, and these grains typically show evidence for multiple chemical and age domains. Low Y concentrations likely indicate that garnet was crystallizing during this later monazite growth.

7. U-Pb ID-TIMS Geochronology

7.1 ID-TIMS monazite data from thin sections

Analytical procedures for U-Pb ID-TIMS analysis are described in Appendix A. The seven monazite grains characterized and dated by EPMA were extracted from thin sections and dated by ID-TIMS. Results are shown in Figure 11a and Table 4. The advantage of this technique is that it allows for high precision analysis combined with the knowledge of the petrographic setting of individual monazite grains. Three of the larger grains (m1tk1, m2tk1, and m1tk2) were broken into two fragments each and analyzed separately. Table 5 shows a comparison of the EPMA and TIMS results.

Monazite m1tk1, a matrix grain within kyanite yielded $^{207}\text{Pb}/^{206}\text{Pb}$ dates of 2394.8 ± 2.0 Ma (m1tk1A, 1.67% discordant) and 2295.2 ± 2.6 Ma (m1tk1B, 1.36% discordant). Fragment m1tk1A consisted mostly of high Th core material whereas fragment m1tk1B contained more of the lower Th rim material from the bottom half of the grain (Fig. 9a).

Monazite m2tk1, a matrix grain, was broken approximately in half and the two fragments yielded $^{207}\text{Pb}/^{206}\text{Pb}$ dates of 1960.3 ± 1.1 Ma (m2tk1A, 1.08% discordant) and 1998.4 ± 1.3 Ma (m2tk1B, 1.65% discordant). These dates are significantly older than the

CHAPTER 5 – MONAZITE SYSTEMATICS IN HIGH-PRESSURE GRANULITES

EPMA date of 1896 Ma. However, the imaged section of this grain only reached into the outer rim of the grain. When extracted from the thin section, the grain actually was much larger and extended well into the section. Therefore the the TIMS dates most likely reflect mixing with possible core material underneath that was not analyzed by the electron microprobe.

Monazite m5tk1, a well-armored inclusion in garnet, yielded a concordant analysis with a $^{207}\text{Pb}/^{206}\text{Pb}$ date of 2613.2 ± 1.8 Ma. This date is 21 million years older than the EPMA date.

Monazite m6tk1, a matrix grain within feldspar and kyanite, yielded a negatively discordant analysis with a $^{207}\text{Pb}/^{206}\text{Pb}$ date of 1947.7 ± 6.3 Ma. This analysis contained a particularly high amount of common Pb (52 pg), resulting in significant errors on this analysis. However, the date obtained is in agreement with the core domain of 1940 Ma identified by the electron microprobe. It is impossible to assess the amount of material sampled for ID-TIMS compared to the two-dimensional slice sampled by the electron microprobe.

Monazite m1tk2, a large, well-armored inclusion in garnet, yielded concordant analyses with $^{207}\text{Pb}/^{206}\text{Pb}$ dates of 2615.6 ± 0.7 Ma and 2612.0 ± 0.7 Ma. This grain was probed during two sessions on different days with different background measurements. The results for each of these sessions was 2627 ± 10 and 2583 ± 10 Ma. This shows the reproducibility in the EPMA technique and both measurements agree with the TIMS date within ~15 million years. These data show that though within error the results for the microprobe and ID-TIMS analysis do not overlap, they are within a million years of each other (using the older EMPA data). This comparison highlights the need for more accurate background measurements, since this clearly is one of the largest sources of error in the EMPA technique, resulting in variability of as much as 50 Ma in the measured chemical dates.

Monazite m5tk2, a relatively unarmored inclusion in the outer rim of garnet, yielded a $^{207}\text{Pb}/^{206}\text{Pb}$ date of 2525.3 ± 0.7 Ma (2.11% discordant). This date is considerably older than the EPMA date of 2460 ± 17 Ma, highlighting the difficulty in comparing TIMS and EPMA dates for discordant grains. These results imply that for

discordant grains, the TIMS and EPMA dates are not in agreement. The most likely explanation for this is that the system has not remained closed to subsequent modification of the Th and Pb distribution in the grain. This is apparent in the compositional maps for this grain (Fig. 10f), which show heterogeneous distribution of Th and Y. These results show that monazite grains with complex distribution of trace elements are not concordant and therefore the EPMA date obtained is not a precise measure of any geologically meaningful event. This grain has likely been subsequently modified through alteration during dehydration melting or fluid-mediated Pb dissolution and reprecipitation.

Monazite m3th, an elongate matrix grain, yielded a negatively discordant $^{207}\text{Pb}/^{206}\text{Pb}$ date of 1898.1 ± 3.8 . As in the case with m6tk1, this analysis was relatively high in common Pb (163 pg). This date is however in good agreement with the EPMA date of 1899 ± 12 Ma. The EPMA data indicate the presence of a younger, ~ 1850 Ma rim, however this was not apparent from the ID-TIMS date.

7.2 Summary of comparison between EPMA and ID-TIMS data

The seven monazite grains analyzed can broadly be divided into two categories petrographically and geochemically. The first population occurs as inclusions in garnet that are high in Y and Th. Y compositional maps show patchy zonation, but typical concentrations are ~ 1 wt.% Y_2O_3 . The U-Pb systematics of these grains are fairly simple, with ID-TIMS dates for the well-armored inclusions of 2.61 Ga. EMPA chemical dates are in relatively good agreement for these grains within ~ 10 Ma. The inclusion in the garnet rim does not yield consistent results between the EMPA and ID-TIMS techniques, probably due to alteration of the chemical composition of this grain during dehydration melting or later metamorphism following the initial crystallization.

The four matrix grains studied display more complicated U-Pb systematics, are typically lower in Th and Y, morphologically tend to be elongate rather than rounded in shape. These grains show uniformly low Y (< 1000 ppm), and in two of the grains contain a higher Th core than the surrounding rim. The results of the ID-TIMS and EPMA comparison are variable. This can largely be explained by mixtures of age domains that are sampled by each of the techniques. For the EPMA technique, $1 \mu\text{m}$

spots across a two-dimensional cross-section of the grain are analyzed, whereas in the ID-TIMS method, a portion of the whole grain is dissolved and analyzed. The ID-TIMS data is consistent with multiple component mixtures of variable age domains, largely producing discordant analyses. However, the EPMA technique is broadly consistent with the identification of these domains. In the case of grain m1tk1 the EPMA domains of 2500-2100 were identified, and the ID-TIMS data indicated a range of ~2.3 to 2.4 Ga, which is consistent with a complex mixture of chemical age domains.

7.3 Imaged monazite grains in epoxy mounts

In order to investigate a larger number of grains with high precision analysis, ~100 grains were mounted in epoxy grain mounts, polished to half their original thicknesses, and imaged by BSE. Then twelve grains (labeled 90.1.# in Fig. 12 and Table 4) of representative morphologies and zoning patterns were extracted from the grain mounts and dated by ID-TIMS (Fig. 11b). This larger population of ID-TIMS analyses can be compared to the microprobe dates in order to judge whether there were any systematic biases generated by hand picking from a mineral separate versus studying grains in situ. The electron microprobe has the advantage of being to analyze grains as small as ~5 μm , whereas grains analyzed by TIMS are typically hand-picked in the 50-100 μm range.

Of the twelve grains analyzed, four displayed extremely homogeneous BSE images (1.1, 1.18, 1.21, and 1.37). These grains are yellow, glassy, and inclusion-free and are of variably morphology; two are elongate and two are more equant. These four grains preserved the oldest U-Pb analyses with concordant $^{207}\text{Pb}/^{206}\text{Pb}$ dates ranging from 2607-2617 Ma. These were the most concordant analyses out of the twelve grains analyzed. This spread in dates is interpreted to reflect protracted crystallization during an early prograde metamorphism.

Another common feature in BSE images, is a mottled texture, possibly indicating redistribution of REE through recrystallization and reprecipitation. Four of the grains show this texture (1.26, 1.44, 1.52, and 1.69) (Fig. 12). The pattern of the mottled appearance takes on a striated appearance for a few of the grains. These grains are of variable morphologies, ranging from round to ovoid in shape. Two grains (1.26 and

CHAPTER 5 – MONAZITE SYSTEMATICS IN HIGH-PRESSURE GRANULITES

1.52) have inclusions of biotite and grain 1.44 has a composite inclusion of Ky + Ksp. These four grains are more discordant and have domains that are younger than the previous population, with $^{207}\text{Pb}/^{206}\text{Pb}$ dates ranging from 2467-2601 Ma (0.36-3.99% discordant). The oldest of these grains (2601±0.7 Ma) is the monazite with inclusions of the high P assemblage, Ky-Ksp (1.44).

Two of the grains analyzed (1.54 and 1.57) display a patchy zonation, and contain fractures and minute inclusions. Grain 1.57 contains a large biotite inclusion. These grains are also discordant with $^{207}\text{Pb}/^{206}\text{Pb}$ dates of 2534 Ma and 2541 Ma (0.92 % and 1.81% discordant, respectively). Of the two remaining grains, one showed evidence for a thin bright overgrowth surrounded by a thicker dark overgrowth (1.63) (Fig. 12). The core of this grain is homogeneous similar to the first population described. This grain yielded a $^{207}\text{Pb}/^{206}\text{Pb}$ date of 2474±0.7 Ma and was discordant (2.84%). The final grain (1.45) showed an extremely complicated BSE pattern, with a brighter core with oscillatory zoning, and outer dark homogeneous region, and a thick bright overgrowth. This grain yielded a $^{207}\text{Pb}/^{206}\text{Pb}$ date of 2541±0.7 Ma (2.47% discordant).

Interestingly, none of the grains analyzed from grain mounts yielded 1.9 Ga dates, however a number of the grains are discordant and are likely mixtures of several age components. A statistically significant discordia cannot be fit through the data, indicating that these analyses do not represent simple two-component mixtures. These results suggest that a significant fraction of the monazite grains have undergone some degree of recrystallization at some time after their initial growth. However, there is not one significant time at which the system appears to have been perturbed.

7.4 Zircon data from 01SZ90

Five zircon grains were analyzed from 01SZ90A (table 4). Zircon in the felsic gneiss is spherical, without any crystal faces evident from optical inspection. Zircon analyzed from 01SZ90 ranged in diameter from 75-185 μm , are light brown, clear, and inclusion-free. $^{207}\text{Pb}/^{206}\text{Pb}$ dates obtained for these grains ranged from 2478-2582 Ma (Fig. 11c, Table 4). The most concordant analysis (z6) was 2551±0.7 Ma (0.47% discordant). Importantly, all of the zircon grains analyzed are younger than the oldest monazite (2617 Ma from 90.1.18) by at least 35 million years. This age difference has

also been observed in other white gneiss samples from the Snowbird zone (see concluding chapter). An explanation for this could be that either the conditions for zircon crystallization were not favorable during the earliest metamorphism at 2.6 Ga or that it was consumed during metamorphism. If the protolith to the felsic gneiss were igneous, it is unusual not to preserve the timing of igneous crystallization. Additionally, if the protolith were sedimentary, it is interesting that there is no evidence for detrital zircon substantially older than 2.6 Ga present in these rocks.

8. Sm-Nd isotopic systematics

Whole rock Sm-Nd isotopic systematics of fourteen felsic granulites from the southern domain of the EAmt have a range in present day ϵ_{Nd} of -49.1 to -18.4 (Table 6). ϵ_{Nd} values at the age of the earliest metamorphism at 2.6 Ga have a restricted range from -2.3 to 0.9 . Depleted mantle Nd model ages (T_{DM}) range from 2.77 to 2.93 Ga. All samples reflect time-integrated LREE enrichment and are consistent with the protolith of the white gneiss being Archean in age. The lack of any zircon in the white gneiss that is older than 2.7 Ga is broadly consistent with the narrow range of T_{DM} 's, and indicates that older crust such as the 3.2-3.0 Ga Chipman batholith did not contribute to the protolith. Plotting these fourteen samples on an isotope correlation diagram yields an "isochron" of 2730 ± 150 Ma (MSWD = 10.6) with an initial $^{143}\text{Nd}/^{144}\text{Nd}$ of 0.50915 ($\epsilon_{\text{Nd}(i)}=1.09$) (Fig. 13).

In order to evaluate the potential source regions for the discrete populations of monazite in 01SZ90, we analyzed eight single monazite grains from 01SZ90 for Nd isotopic composition (Table 6). In Figure 14, we plot ϵ_{Nd} versus time for the whole rock and single monazites. The $\epsilon_{\text{Nd}(i)}$ is calculated for the $^{207}\text{Pb}/^{206}\text{Pb}$ dates for each of the monazite grains analyzed by ID-TIMS. This diagram shows the remarkable similarity between the older monazite grains and the whole rock in terms of the $\epsilon_{\text{Nd}(i)}$ and the slope of the trajectories towards present-day values. However, the younger monazite grains that have $^{207}\text{Pb}/^{206}\text{Pb}$ dates that are between 2.6 Ga and 1.9 Ga show distinct Nd isotope systematics, with higher initial ϵ_{Nd} and steeper trajectories. Even taking into account large errors in the $^{143}\text{Nd}/^{144}\text{Nd}$ measurement on some of the grains, it is apparent that the

grains with the younger dates record a contribution from a distinctly different reservoir than the whole-rock and older monazites. We also plot a whole-rock sample of eclogite that was metamorphosed at 1905 Ma for comparison. Although the eclogite sample has a similar $\epsilon_{Nd(i)}$ to the 1.9 monazite m3th, it falls on a trajectory with a slope consistent with a similar source to the 01SZ90 whole rock sample. The U-Pb systematics of grains m1tk1, m2tk1, and m6tk1, all indicate complicated mixtures of domains of different chemical dates that correlate with Th distribution and relative concentration. The source for these grains was a reservoir that shows time-integrated Sm enrichment, with positive initial ϵ_{Nd} similar to depleted mantle. One possible interpretation is that Archean monazite grains were derived from an initial source with slightly negative ϵ_{Nd} . During this early metamorphism, much of the REE elements were trapped as monazite inclusions in garnet, effectively isolating their participation in subsequent crystallization of monazite. Grain m1tk1 (2.3-2.4 Ga) shows slightly positive initial ϵ_{Nd} , reflecting growth from a higher Sm/Nd reservoir such as garnet. The U-Pb systematics of this grain are complicated, however, and it is difficult to identify a discrete mixture of Archean and Paleoproterozoic components. EPMA results indicate a range in chemical dates from 2500-2100 Ma. Similar results were obtained on grains m6tk1 and m2tk1, which also show complex U-Pb systematics. However, grain m3th, which is a simple 1.9 Ga monazite shows a significantly more negative initial ϵ_{Nd} , but is slightly more positive than the whole rock and Archean monazite reservoir at 1.9 Ga. These systematics are mostly easily explained by mixing a high-Sm garnet source with the lower Sm whole rock source, resulting in an intermediate initial ϵ_{Nd} .

9. Discussion

9.1 Nature of the felsic gneiss protolith

The felsic gneiss of the EAmt occurs over a 400 km² area and is remarkably homogeneous throughout its extent. The poikilitic texture of garnet with large enclosed alkali feldspar points to a HP-HT migmatitic origin for the rocks. The textural features and mineralogy of the Snowbird felsic gneiss strongly resembles features known from incongruent garnet-producing melt reactions (Waters & Whales, 1984). Similar high-

pressure granulites in the Bohemian Massif have also been proposed to have an origin by melting processes (Kotkova & Harley, 1999). These rocks are interpreted to have formed from HP leucogranitic melts with peritectic Grt + Kfs + Ky as likely protoliths for the granulites, either from granitic or pelitic protoliths. The bulk geochemistry and mineralogy of the felsic gneiss is consistent with an origin by high-pressure melt processes in the lower crust. The absence of orthopyroxene, and significant garnet and K-feldspar production is consistent with pressures >1.5 GPa for these dehydration melting reactions (Vielzeuf & Montel, 1994).

Garnet in the felsic gneiss contains profound Ca-zonation. This zoning profile of a near-marginal rim of high Grs content surrounding a homogeneous low Grs core is interpreted as recording the last phase of prograde growth of garnet under high-pressure conditions, followed by rapid exhumation so as to lock in the observed zoning profiles. Unlike other examples of high-pressure granulites, where a decrease in Grs at the rim is usually attributed to plagioclase growth during decompression (Kotkova & Harley, 1999), garnet from the Snowbird felsic gneiss is interpreted to preserve growth zoning related to the transport of these crustal rocks down to mantle depths (>1.5 GPa). Additionally, the presence of nearly pure meter-scale garnetite layers (possible residues of melt processes) associated with the felsic gneiss, and the presence of quartz-rich rocks and calc-silicates in a large-scale package of predominantly quartzofeldspathic rocks, is consistent with the interpretation that the Southern Domain of the EAmt is largely of metasedimentary origin and has undergone a significant degree of partial melting.

9.2 Significance of U-Pb Geochronological Dates

The geochronology of accessory phases in the felsic gneisses is difficult to interpret, despite the techniques employed in this study to understand the petrographic setting of dated accessory phases. The monazite in 01SZ90 as well as other felsic gneiss samples studied (see Ch. 6), records a complicated growth history from >2.6 Ga to 1.9 Ga. The felsic gneiss chosen for this study is representative of the larger suite of samples that have been studied for both their monazite and zircon systematics (Ch. 6). However, sample 01SZ90 is particularly important because of its excellent preservation of the high-pressure mineral assemblage and occurrence of distinct chemical and age populations of

CHAPTER 5 – MONAZITE SYSTEMATICS IN HIGH-PRESSURE GRANULITES

monazite. The integrated EPMA/TIMS comparison study of seven monazite grains from 01SZ90 reveals the complexity of monazite in high-grade granulite facies rocks. Two general chemical populations can be identified. The first are relatively high ThO₂ (3-4 wt. %) inclusions in garnet that are homogeneous and well-armored. These grains record the oldest phase of monazite growth in the felsic gneiss at 2616-2612 Ma. This is consistent with concordant dates obtained from homogeneous grains imaged prior to analysis that record dates ranging from 2617-2606 Ma. A second chemical population of grains consists of matrix monazites that either consist of high Th cores with low Th overgrowths, or uniformly low Th. These grains are homogeneous and low with respect to Y. These grains record a range of discordant dates ranging from 2395-1948 Ma. These grains are interpreted as mixtures of multiple age domains. These grains typically occur in the matrix and their U-Pb systematics are interpreted to have been disturbed by dissolution and reprecipitation during either fluid infiltration or melting. Only one grain analyzed in this study records a ~1900 Ma date. This grain occurs within the matrix, and consists of ~2.5 wt % ThO₂. Based on both the ID-TIMS and EPMA results, other grains appear to reflect a mixture of 1.9 Ga and some older components.

An important point to make based on this study is that the identification of these distinct age domains, and in particular the evidence for 1.9 Ga monazite growth, is possible using the electron microprobe in situ chemical dating technique. None of the grains dated through conventional mineral separation and BSE imaging contained a significant younger component. One possible explanation for this observation is that the microprobe can be used to characterize grains as small as 5 μm, a grain size not currently possible to analyze with ID-TIMS. Additionally, through compositional mapping of full thin sections, the electron microprobe can identify all monazite grains in a single thin section, which can then be examined relatively quickly in order to identify and target grains with different chemical characteristics.

The grains dated in this study have a significant Paleoproterozoic component and were all substantially smaller than the average grain size analyzed for the conventionally-separated, TIMS grains. One drawback to the microprobe technique is that only a two-dimensional slice through the grain is characterized, resulting in some uncertainty as to

CHAPTER 5 – MONAZITE SYSTEMATICS IN HIGH-PRESSURE GRANULITES

whether than surface is representative of the domains that are present on the scale of an entire grain. For example, grain m2tk1, was characterized by the microprobe as consisting of one homogeneous domain with a chemical date of ~1900 Ma. This was because the area of the grain mapped consisted of a thin slice of rim material. The TIMS data identified an older component within the core of the grain, and the monazite reflects a mixture of a likely 1900 and ~2000 Ma components. This is an important observation that one must take into account when characterizing grains by EPMA. The grains are all randomly oriented, and the planes that are mapped and analyzed may not be representative of the entire grain if it were analyzed as a true cross section area cut halfway through as is done in grain mounts.

A major question that must be addressed using a combination of geochronology and metamorphic petrology is the age of garnet in the white gneiss. Well-armored inclusions of 2.6 Ga monazite occur within garnet and have not experienced any Pb-loss since their encapsulation. Monazite inclusions in garnet with younger dates can be explained by the connectivity of these grains by fractures to the matrix and thus the subsequent recrystallization of these monazites during dehydration melting. This armoring effect of garnet has been observed in other localities (Montel et al., 2000; Zhu & O'Nions, 1999b). Garnet zoning in the felsic gneiss is interpreted to reflect the changing P-T conditions during garnet growth. The low Grs cores are interpreted to have grown at lower pressures than the rims. Therefore it is possible that most of the garnet was produced during an early granulite facies metamorphism at mid- to lower-crustal levels unrelated to the high-pressure event. Then at 1.9 Ga, the rocks were taken to higher pressure forming the high Grs rims, followed by rapid exhumation in order to preserve the zoning profiles and mineral assemblages. The U-Pb systematics of monazite of well-armored in garnet were unaffected by this event due to its encapsulation in garnet and short-lived duration of the high-pressure metamorphism. The preservation of old xenocryst ages and protection of zircon during UHP metamorphism has been recognized for quite some time (Claoué-Long et al., 1991), but this is one of the first studies that provides empirical evidence that monazite may behave similar under high-temperature conditions.

CHAPTER 5 – MONAZITE SYSTEMATICS IN HIGH-PRESSURE GRANULITES

A 1.9 Ga age of high-pressure metamorphism is well-constrained in the eclogite and mafic granulite units (Baldwin et al., 2003) (Ch. 2 & 3). Because the felsic gneiss is the host to these high-pressure rocks it is inferred that it experienced the same high-pressure metamorphism. The peak metamorphic conditions and P - T paths recorded in all three lithologies are remarkably similar indicating that this entire 400 km² package of rocks was “subducted” to mantle depths in the Paleoproterozoic. It is problematic, however, that the felsic gneiss, does not record significant 1.9 monazite growth. In addition to 01SZ90, discrete 1.9 Ga monazite growth has been observed in only one other felsic gneiss sample at 1906-1909 Ma (Ch. 6). One possibility is that the REE budget simply was not favorable for the production of abundant monazite following the earliest metamorphism. It is apparent in the complicated systematics of the monazite growth that matrix grains were severely affected by fluid and melt recrystallization resulting in heterogeneous distribution of REE in the monazite grains.

Interestingly, zircon in the felsic gneiss is almost always younger than the oldest monazite. This observation is apparent in a variety of felsic gneiss samples where monazite typically records dates >2.6 Ga and the oldest zircon is typically 20 to >100 million years younger than the oldest monazite (Ch. 6). Zircon in the felsic gneisses appears to be metamorphic in origin with the characteristic “soccer ball” shape, and concentric growth shells apparent in CL and BSE images. Zircon typically records discordant U-Pb dates and has likely experienced a substantial component of Pb-loss. Petrographically, zircon is most commonly observed in the matrix and occurs less commonly as inclusions in garnet.

9.3 Implications for behavior of monazite under high-grade metamorphic and anatexis conditions

The rate of Pb volume diffusion has been debated considerably in recent literature. Early estimates of the closure temperature of Pb diffusion of around 700°C were based on field studies of amphibolite facies rocks (Copeland et al., 1988; Kingsbury et al., 1993). Diffusion laboratory experiments appeared to be in agreement with these results (e.g., Smith & Giletti, 1997). However, numerous field-based studies over the last decade have shown that detrital and inherited monazite can persist through upper-amphibolite and even granulite-facies conditions of >700-750°C (Möller et al., 2000;

CHAPTER 5 – MONAZITE SYSTEMATICS IN HIGH-PRESSURE GRANULITES

Montel et al., 2000; Schaltegger et al., 1999; Spear & Parrish, 1996). In addition, there is now evidence from lower crustal xenoliths that monazite can be resistant to Pb loss even under UHT conditions (Schmitz & Bowring, 2003). These data provide strong evidence that the closure temperature for Pb volume diffusion in monazite is significantly higher than previously thought. Recent diffusion laboratory experimental results confirm this, with recent estimates as high as 1000°C (Cherniak & Watson, 2001; Cherniak et al., 2002;).

This study has important implications for the behavior of monazite under high-grade metamorphic and anatexis conditions. These rocks afford an exceptional opportunity to examine monazite systematics at or near its closure temperature for Pb volume diffusion. Other studies have noted the armoring effect of garnet on the U-Pb systematics (e.g., Montel et al., 2000). This study supports this conclusion and also shows that monazite may be noticeably unaffected by diffusional modification during extreme crustal metamorphism at temperatures as high as 1000°C. However, as has been noted in numerous other studies (e.g., Hawkins & Bowring, 1997), the U-Pb isotopic system in monazite can be influenced by a variety of processes that partially obscure the early growth history. A variety of primary and secondary processes may result in discordant monazite dates. Volume diffusional Pb loss from the grain notwithstanding, these include: 1) the incorporation of xenocrystic monazite that results in an inherited component; 2) protracted growth; 4) episodic growth resulting in secondary overgrowths; 3) Dissolution and resorption of the grain during interaction with fluids or melt resulting in fluid-mediated Pb loss. The latter three points are particularly valid for the monazite examined in this study.

First, there is evidence for protracted monazite growth during the earliest metamorphism at 2.6 Ga. Monazite within a single sample records concordant U-Pb dates spanning a 16 Ma range from 2617-2601 Ma. Petrographically, these oldest dates correspond to well-armored inclusions in garnet and are interpreted to have crystallized prior to garnet formation. The salient point is that these monazite grains armored in garnet did not suffer any diffusional Pb-loss during subsequent metamorphic events. There is abundant evidence in these monazite grains for episodic secondary growth. The

CHAPTER 5 – MONAZITE SYSTEMATICS IN HIGH-PRESSURE GRANULITES

compositional maps of matrix monazite grains commonly show younger overgrowths on older cores and the resulting U-Pb dates obtained for these grains are complex mixtures. However, more commonly zoning is not preserved as simple rim overgrowths, and the Th and Y distribution within single grains is patchy and chaotic. This implies that a dissolution and reprecipitation process has taken place, resulting in a heterogeneous redistribution of REE within single grains. This would likely be due to interaction of the grain with metamorphic fluids or melts. Unarmored matrix grains are open to these reactions and readily dissolve and recrystallize under high-grade anatectic conditions resulting in complicated U-Pb isotope systematics.

9.4 Implications of geochemical data for melt sources and processes

The Sm-Nd isotope systematics of the white gneiss indicate a homogeneous source for its formation around 2.7 Ga, without evidence for older crust involved in its formation. However, the individual monazite systematics indicate a different source for the Archean and Proterozoic components. The Archean monazite reflects the whole rock signature within error whereas the monazite grains with a Paleoproterozoic component reflect an enriched Sm source with positive initial ϵ_{Nd} values, and these inferred ϵ_{Nd} values at 1.9 Ga are consistent with mantle-derived fluids. The grains that clearly show some mixture of components slightly older than 1.90 Ga have more positive initial ϵ_{Nd} values than the one monazite grain that yields a 1.9 Ga $^{207}\text{Pb}/^{206}\text{Pb}$ date. The simplest explanation for this pattern is that some of the garnet Nd mixed with the initial source to produce more positive ϵ_{Nd} values.

The Y concentration in monazite also serves as a chemical fingerprint to identify different sources. Monazite that is included in garnet is high in Y (1-1.5 wt %) whereas matrix monazite typically contains <0.1 wt % Y. Pyle & Spear (1999) have shown that monazite in equilibrium with garnet is typically lower in Y because Y more readily partitions into garnet. Therefore, the high-Y inclusions in garnet most likely formed before garnet began to crystallize. Other workers have noticed similar patterns (Foster et al., 2002; Zhu & O'Nions, 1999a). In order to explain the Nd isotope systematics, a breakdown or recrystallization of garnet is required to release Nd. This process might also be expected to liberate Y. However, if Y readily partitioned into the garnet core

during the earliest metamorphism, then it might be depleted in the rim of garnet. This hypothesis can be tested by collecting garnet Y compositional maps. If the garnet is zoned with respect to Y, then the breakdown of garnet rims may not be effective in liberating Y, whereas Nd would readily partition into coexisting monazite. Pyle & Spear (1999) have shown that Y in migmatitic garnet typically decreases from core to rim. The authors also observe an increase in $[Y]_{\text{Grt}}$ and $[\text{HREE}]_{\text{Grt}}$ that they attribute to the dissolution of phosphates in the melt such that Y and the HREE readily partition into garnet.

10. Conclusions

The felsic gneiss of the East Athabasca mylonite triangle, northern Saskatchewan, is a 400 km² package of supracrustal pelitic rocks that was metamorphosed at minimum conditions of at least 1.5 GPa and 1000°C (Snoeyenbos et al., 1995). These high-pressure mineral assemblages are interpreted to have formed primarily as the result of high-pressure partial melting, which is consistent with the observed Grt-Ky-ternary feldspar assemblage. Monazite records a complicated growth history from 2.6 Ga to 1.9 Ga, largely reflecting its reaction with fluids in the lower crust during dehydration melting. Well-armored monazite inclusions occur in garnet and yield the oldest observed U-Pb dates at 2.60-2.62 Ga. However, we interpret these dates to represent growth during an earlier metamorphism before significant production of garnet occurred. High-pressure metamorphism at 1.9 Ga is recorded in zircon dates from the enclosed eclogitic and mafic granulite lithologies (Ch. 2 and 3). Minor growth of 1.9 Ga monazite in the felsic gneiss occurred at this time. During a nearly isothermal loading and unloading *P-T* path that is preserved in these rocks, it is possible that the metamorphic assemblage, particularly garnet and monazite, did not experience significant reaction progress, and thus these minerals were not a particularly valuable recorder of the 1.9 Ga episode. The high-pressure metamorphism is preserved in prograde zoning in garnet evident by a significant increase in grossular at garnet rims. Archean monazite mimic the signature of the whole rock, however the Nd in younger monazite was likely derived from a different, more depleted source.

CHAPTER 5 – MONAZITE SYSTEMATICS IN HIGH-PRESSURE GRANULITES

The Southern Domain felsic gneiss poses unusual petrological and tectonic problems and is an unparalleled natural laboratory for unraveling the complex polymetamorphic history of the lower crust. For the most part tangible samples of the lower crust occur only as xenoliths, and the EAmT provides a superb example of the lower crust within a well-constrained structural context. The ability to obtain large volumes of samples over a broad area highlight the complexities in accessory phase growth that is not always apparent from a small xenolith sample. Studying these complexities within a constrained tectonic framework sheds insight into the behavior of these accessory minerals under lower crustal high grade metamorphic and anatexis conditions.

Acknowledgements

This research was supported by National Science Foundation grant EAR-0001131 to SAB and MLW and a research grant from the Mineralogical Society of America to JAB. Helpful discussions with Paddy O'Brien, Joe Pyle, and John Hanchar are appreciated. A constructive and thoughtful review by Jennifer Matzel greatly improved this manuscript.

Appendix A: Analytical Techniques

Monazite and zircon were isolated from the sample by standard crushing, heavy liquid, and magnetic separation techniques. Fractions of accessory minerals consisting of single grains were carefully picked and separated into different populations based on morphology, color, and grain size. Individual grains were measured and recorded by digital photography. Two techniques were used for identification of growth domains in monazite prior to analysis. From the mineral separate, individual grains of similar size were mounted in epoxy, polished halfway through the grains, carbon-coated, and imaged by back-scattered electron (BSE) imaging on the MIT JEOL-733 Superprobe using an accelerating voltage of 15 keV and 30 nA beam current. Other grains were sampled directly from either 30- or 80-micron-thick petrographic thin sections following careful elemental mapping and characterization using the EPMA. Grains were extracted from

CHAPTER 5 – MONAZITE SYSTEMATICS IN HIGH-PRESSURE GRANULITES

the sections using a sharpened sewing needle, carefully excavating around the perimeter of the grain.

For U-Pb analysis, zircon crystals were air-abraded with pyrite after the method of (Krogh, 1982), and acid rinsed in 3M HNO₃ for 5-6 hours, followed by ultrasonication. Accessory mineral fractions were loaded into Teflon FEP microcapsules and washed again in 3M HNO₃ (zircon) or high-purity water (monazite) at *c.* 50°C for 3-4 hours, followed by rinsing with several capsule volumes of 3M HNO₃ (zircon) or water (monazite). Samples were spiked with a mixed ²⁰⁵Pb-²³³U-²³⁵U tracer and dissolved in 29M HF at 220°C for 48-96 hours (zircon) or 12M HCl at 180°C for 48 hours (monazite), followed by conversion to 6M HCl at 180°C for 24 hours. Pb and U were separated from all mineral solutions using anion exchange chromatography procedures modified after (Krogh, 1973). U-Pb ID-TIMS analyses were done at the Massachusetts Institute of Technology on the VG Sector 54 thermal ionization multicollector mass spectrometer. Pb and U were loaded on single Re filaments with a dilute silica gel-0.1 H₃PO₄ emitter solution with U run as an oxide. U-Pb data as well as the details of fractionation and blank corrections are given in Table 4.

For Sm-Nd isotopic analyses, whole rock powders (100-200 mg) or single monazite crystals were spiked with a mixed ¹⁴⁹Sm-¹⁵⁰Nd tracer and completely dissolved with HF-HNO₃ or 12M HCl (monazite) in teflon pressure vessels at 220°C for five days, followed by conversion to 6M HCl at 180°C for 24 hours. Final dissolution of whole rock powders was achieved through repeated fluxing in 6M HCl at 120°C. The separation and purification of Sm and Nd were accomplished with a standard two-stage cation exchange-HDEHP reverse chromatography procedure. Sm was loaded onto single Ta filaments with 1μl of 1M H₃PO₄ and analyzed as metal ions in multicollector static mode with a ¹⁵²Sm ion beam of 2.5x10⁻¹¹A. Nd was loaded on triple Re filaments with 1 μl of 0.1M H₃PO₄ and analyzed as metal ions in dynamic multicollector mode with a ¹⁴⁴Nd ion beam of 1.5x10⁻¹⁰A. Sm and Nd data were fractionation corrected with an exponential law, normalizing to ¹⁵²Sm/¹⁴⁷Sm = 1.783 and ¹⁴⁶Nd/¹⁴⁴Nd = 0.7219 respectively.

References

- Baer, A. J., 1969. The Precambrian geology of Fond-du-Lac map-area (74-0), Saskatchewan. *Geological Survey of Canada Paper 68-61*, 17p.
- Baldwin, J. A., Bowring, S. A. & Williams, M. L., 2003. Petrological and geochronological constraints on high pressure, high temperature metamorphism in the Snowbird tectonic zone, Canada. *Journal of Metamorphic Geology*, **21**, 81-98.
- Bingen, B. & van Breemen, O., 1998. U-Pb monazite ages in amphibolite- to granulite-facies orthogneiss reflect hydrous mineral breakdown reactions: Sveconorwegian Province of SW Norway. *Contributions to Mineralogy and Petrology*, **132**, 336-353.
- Cherniak, D. J. & Watson, E. B., 2001. The influence of diffusion on U-Pb systematics. *11th Annual V.M. Goldschmidt Conference*, **Abstract 3260**.
- Cherniak, D. J., Watson, E. B., Grove, M. & Harrison, T. M., 2002. Pb diffusion in monazite. *Geological Society of America Abstracts with Programs*.
- Claoué-Long, J. C., Sobolev, N. V., Shatsky, V. S. & Sobolev, A. V., 1991. Zircon response to diamond-pressure metamorphism in the Kokchetav massif, USSR. *Geology*, **19**, 710-713.
- Copeland, P., Parrish, R. R. & Harrison, T. M., 1988. Identification of inherited radiogenic Pb in monazite and its implications for U-Pb systematics. *Nature*, **333**, 760-763.
- Crowley, J. L. & Ghent, E. D., 1999. An electron microprobe study of the U-Th-Pb systematics of metamorphosed monazite: the role of Pb diffusion versus overgrowth and recrystallization. *Chemical Geology*, **157**, 285-302.
- Cumming, G. L., Krstic, D. & Wilson, J. A., 1987. Age of the Athabasca Group, northern Alberta. *Geological Association of Canada - Mineralogical Association of Canada Annual Meeting Abstracts*, **12**, 35.
- Foster, G., Gibson, H. D., Parrish, R., Horstwood, M., Fraser, J. & Tindle, A., 2002. Textural, chemical, and isotopic insights into the nature and behaviour of metamorphic monazite. *Chemical Geology*, **191**, 183-207.
- Goodacre, A. K., Grieve, R. A. F., Halpenny, J. F. & Sharpton, V. L., 1987. Horizontal gradient of the Bouguer gravity anomaly map of Canada, Canadian Geophysical Atlas, Map 5, Geological Survey of Canada, Ottawa.
- Hanmer, S., 1994. Geology, East Athabasca mylonite triangle, Saskatchewan. In: *Geological Survey of Canada Map 1859A*.
- Hanmer, S., 1997. Geology of the Striding-Athabasca mylonite zone, northern Saskatchewan and southeastern District of Mackenzie, Northwest Territories. *Geological Survey of Canada Bulletin*, **501**, 1-92.
- Hanmer, S., Parrish, R., Williams, M. & Kopf, C., 1994. Striding-Athabasca mylonite zone: Complex Archean deep-crustal deformation in the East Athabasca mylonite triangle, northern Saskatchewan. *Canadian Journal of Earth Sciences*, **31**, 1287-1300.
- Hanmer, S., Williams, M. & Kopf, C., 1995a. Modest movements, spectacular fabrics in an intracontinental deep-crustal strike-slip fault: Striding-Athabasca mylonite zone, NW Canadian Shield. *Journal of Structural Geology*, **17**(4), 493-507.

CHAPTER 5 – MONAZITE SYSTEMATICS IN HIGH-PRESSURE GRANULITES

- Hanmer, S., Williams, M. & Kopf, C., 1995b. Striding-Athabasca mylonite zone: implications for the Archean and Early Proterozoic tectonics of the western Canadian Shield. *Canadian Journal of Earth Sciences*, **32**, 178-196.
- Harrison, T. M., Catlos, E. J. & Montel, J. M., 2002. U-Th-Pb dating of phosphate minerals. In: *Phosphates: Geochemical, Geobiological, and Materials Importance* (eds Kohn, M. J., Rakovan, J. & Hughes, J. M.) *Reviews in Mineralogy and Geochemistry*, pp. 523-558, Mineralogical Society of America, Washington, D.C.
- Hawkins, D. P. & Bowring, S. A., 1997. U-Pb systematics of monazite and xenotime: case studies from the Paleoproterozoic of the Grand Canyon, Arizona. *Contributions to Mineralogy and Petrology*, **127**, 87-103.
- Hawkins, D. P. & Bowring, S. A., 1999. U-Pb monazite, xenotime and titanite geochronological constraints on the prograde to post-peak metamorphic thermal history of Paleoproterozoic migmatites from the Grand Canyon, Arizona. *Contributions to Mineralogy and Petrology*, **134**, 150-169.
- Hoffman, P. F., 1988. United Plates of America, the birth of a craton: Early Proterozoic assembly and the growth of Laurentia. *Annual Reviews of Earth and Planetary Science Letters*, **16**, 543-603.
- Kingsbury, J. A., Miller, C. F., Wooden, J. L. & Harrison, T. M., 1993. Monazite paragenesis and U-Pb systematics in rocks of the eastern Mojave Desert, California, U.S.A.: implications for thermochronometry. *Chemical Geology*, **110**, 147-167.
- Kotkova, J. & Harley, S. L., 1999. Formation and evolution of high-pressure leucogranulites: experimental constraints and unresolved issues. *Phys. Chem. Earth (A)*, **24**, 299-304.
- Krogh, T. E., 1973. A low-contamination method for hydrothermal decomposition of zircon and extraction of U and Pb for isotopic age determination. *Geochimica Cosmochimica Acta*, **46**, 485-494.
- Krogh, T. E., 1982. Improved accuracy of U-Pb zircon ages by the creation of more concordant systems using an abrasion technique. *Geochimica et Cosmochimica Acta*, **46**, 637-649.
- Mahan, K. H., Williams, M. L. & Baldwin, J. A., in press. Juxtaposition of deep crustal and middle crustal rocks along the Legs Lake shear zone, western Churchill Province, Canadian Shield. *Canadian Journal of Earth Sciences*.
- Möller, A., Mezger, K. & Schenk, V., 2000. U-Pb dating of metamorphic minerals: Pan-African metamorphism and prolonged slow cooling of high pressure granulites in Tanzania, East Africa. *Precambrian Research*, **104**, 123-146.
- Montel, J. M., Foret, S., Veschambre, M., Nicollet, C. & Provost, A., 1996. Electron microprobe dating of monazite. *Chemical Geology*, **131**, 37-53.
- Montel, J. M., Kornprobst, J. & Vielzeuf, D., 2000. Preservation of old U-Th-Pb ages in shielded monazite: example from the Beni Bousera Hercynian kinzigites (Morocco). *Journal of Metamorphic Geology*, **18**, 335-342.
- Nair, R. & Chacko, T., 2002. Fluid-absent melting of high-grade semipelites: P-T constraints on orthopyroxene formation and implications for granulite genesis. *Journal of Petrology*, **43**, 2121-2142.

CHAPTER 5 – MONAZITE SYSTEMATICS IN HIGH-PRESSURE GRANULITES

- O'Brien, P. J. & Rötzler, J., 2003. High-pressure granulites: formation, recovery of peak conditions and implications for tectonics. *Journal of Metamorphic Geology*, **21**, 3-20.
- Parrish, R. R., 1990. U-Pb dating of monazite and its application to geological problems. *Canadian Journal of Earth Sciences*, **27**, 1431-1450.
- Percival, J. A., Fountain, D. M. & Salisbury, M. H., 1992. Exposed crustal cross sections as windows on the lower crust. In: *Continental Lower Crust* (eds Fountain, D. M., Arculus, R. & Kay, R. W.) *Developments in Geotectonics*, pp. 317-362, Elsevier, Amsterdam.
- Pyle, J. M. & Spear, F. S., 1999. Yttrium zoning in garnet: Coupling of major and accessory phases during metamorphic reactions. *Geological Materials Research*, **1**(6), 1-49.
- Rudnick, R. L., 1992. Xenoliths - samples of the lower continental crust. In: *Continental Lower Crust* (eds Fountain, D. M., Arculus, R. & Kay, R. W.), pp. 269-316, Elsevier, Amsterdam.
- Rudnick, R. L. & Fountain, D. M., 1995. Nature and composition of the continental crust: a lower crustal perspective. *Reviews of Geophysics*, **33**, 267-309.
- Schaltegger, U., Fanning, C. M., Gunther, D., Maurin, J. C., Schulmann, K. & Gebauer, D., 1999. Growth, annealing and recrystallization of zircon and preservation of monazite in high-grade metamorphism: conventional and in-situ U-Pb isotope, cathodoluminescence and microchemical evidence. *Contributions to Mineralogy and Petrology*, **134**, 186-201.
- Schmitz, M. D. & Bowring, S. A., 2003. Ultrahigh-temperature metamorphism in the lower crust during Neoproterozoic Ventersdorp rifting and magmatism, Kaapvaal Craton, southern Africa. *Geological Society of America Bulletin*, **115**, 533-548.
- Slimmon, W. L., 1989. Compilation bedrock geology Fond-du-Lac, NTS area 74-0, Saskatchewan Geological Survey, Map247A, 1:250000.
- Smith, H. A. & Barreiro, B., 1990. Monazite U-Pb dating of staurolite grade metamorphism in pelitic schists. *Contributions to Mineralogy and Petrology*, **105**, 602-615.
- Smith, H. A. & Gilletti, B. J., 1997. Lead diffusion in monazite. *Geochimica Et Cosmochimica Acta*, **61**, 1047-1055.
- Snoeyenbos, D. R., Williams, M. L. & Hanmer, S., 1995. Archean high-pressure metamorphism in the western Canadian Shield. *European Journal of Mineralogy*, **7**, 1251-1272.
- Spear, F. S., 1993. *Metamorphic Phase Equilibria and Pressure-Temperature-Time Paths*. Mineralogical Society of America, Washington, D.C.
- Spear, F. S. & Parrish, R. R., 1996. Petrology and cooling rates of the Valhalla Complex, British Columbia, Canada. *Journal of Petrology*, **37**(4), 733-765.
- Sun, S. S. & McDonough, W. F., 1989. Chemical and isotopic systematics of oceanic basalts: implications for mantle composition and processes. In: *Magmatism in the Ocean Basins*, *Geological Society Special Publications* (eds Saunders, A. D. & Norry, M. J.), pp. 313-345.

CHAPTER 5 – MONAZITE SYSTEMATICS IN HIGH-PRESSURE GRANULITES

- Vielzeuf, D. & Montel, J. M., 1994. Partial melting of metagreywackes. Part I. Fluid-absent experiments and phase relationships. *Contributions to Mineralogy and Petrology*, **117**, 375-393.
- Waters, D. J. & Whales, C. J., 1984. Dehydration melting and the granulite transition in metapelites from southern Namaqualand, S. Africa. *Contributions to Mineralogy and Petrology*, **88**, 269-275.
- Weiss, C. S., 1803. Über die Gebirgsart des sächsischen Erzgebirges, welche unter dem Namen Weiss-Stein neuerlich bekannt gemacht worden ist. *Neue Schriften Gesellschaft Naturforschender Freunde*, **4**, 342-366.
- Williams, M. L. & Hanmer, S., in press. Structural and metamorphic processes in the lower crust: evidence from the East Athabasca mylonite triangle, Canada, a deep-crustal isobarically cooled terrane. In: *Evolution and Differentiation of the Continental Crust* (eds Brown, M. & Rushmer, T.), Cambridge University Press.
- Williams, M. L., Hanmer, S., Kopf, C. & Darrach, M., 1995. Syntectonic generation and segregation of tonalitic melts from amphibolite dikes in the lower crust, Striding-Athabasca mylonite zone, northern Saskatchewan. *Journal of Geophysical Research*, **100**(B8), 15717-15734.
- Williams, M. L. & Jercinovic, M. J., 2002. Microprobe monazite geochronology: putting absolute time into microstructural analysis. *Journal of Structural Geology*, **24**, 1013-1028.
- Williams, M. L., Jercinovic, M. J. & Terry, M. P., 1999. Age mapping and dating of monazite on the electron microprobe: Deconvoluting multistage tectonic histories. *Geology*, **27**, 1023-1026.
- Williams, M. L., Melis, E. A., Kopf, C. & Hanmer, S., 2000. Microstructural tectonometamorphic processes and the development of gneissic layering: a mechanism for metamorphic segregation. *Journal of Metamorphic Geology*, **18**, 41-57.
- Zhu, X. K. & O'Nions, R. K., 1999a. Monazite chemical composition: some implications for monazite geochronology. *Contributions to Mineralogy and Petrology*, **137**, 351-363.
- Zhu, X. K. & O'Nions, R. K., 1999b. Zonation of monazite in metamorphic rocks and its implications for high temperature thermochronology: a case study from the Lewisian terrain. *Earth and Planetary Science Letters*, **171**, 209-220.

Figure Captions

Figure 1. Geologic map of the western Canadian Shield showing major tectonic elements (inset shows location of map). Abbreviations are as follows: AB – Athabasca basin, BL – Baker Lake basin, KX – Kramanitaur Complex, STZ – Snowbird tectonic zone, THO – Trans-Hudson Orogen, TO – Talston Orogen, TMZ – Thelon Magmatic Zone, UX – Uvauk Complex, VR – Virgin River Shear Zone. The Striding-Athabasca mylonite zone occurs within the East Athabasca mylonite triangle, the northern tip of the Athabasca lozenge, as well along the eastern margin of the Selwyn lozenge to the northeast (shown in black). Other examples of high-pressure granulites in the STZ include the Kramanitaur Complex and Uvauk Complex. Outline shown for East Athabasca mylonite triangle shown in Figure 3.

Figure 2. (a) Lithotectonic domains of the East Athabasca mylonite triangle, northern Saskatchewan. Outline of study area shown in (b), (b) Geologic map of the northern extent of the southern domain showing the location of 01SZ90.

Figure 3. P-T diagram showing experimental melting reactions of Vielzeuf and Montel (1994). Where the Opx-in curve and Bt-out curve intersect at high-pressure, the melting reaction favors the production of Grt + Kfs without production of Opx.

Figure 4. X-ray compositional maps of garnet from 01SZ90. (a) Ca map from inclusion-rich garnet. Plagioclase coronas forming around quartz inclusions in garnet. Note the high Grs rim surrounding garnet, and matrix plagioclase. (b) Al map from same garnet shown in (a). Kyanite shown in yellow surrounding garnet. Note how some kyanite grains are rimmed by an aluminous phase (red), which is K-feldspar. Inclusions of sillimanite needles occur within garnet. Note abundant ribbons of K-feldspar and quartz in the matrix. (c) Ca map from inclusion-free garnet showing same high Grs rim. (d) Al map from garnet shown in (c).

Abundant kyanite surrounds garnet. Note in upper left corner the two large kyanite grains that are surrounded by K-feldspar. These are the same grains shown in Fig. 3c. K-feldspar also occurs throughout the matrix.

Figure 5. (a) Inclusion of quartz within garnet. Rim of K-feldspar mantles quartz grain. Thin rim of plagioclase between quartz and k-feldspar. (b) Polyphase inclusion of qtz + ky rimmed by plagioclase and K-feldspar. (c) Kyanite grains mantled by K-feldspar adjacent to quartz grains.

Figure 6. Schematic petrogenetic grid showing important fluid-absent melt reactions in the KCMASH system (after Vielzeuf and Montel, 1994). Shaded region shows stable region of assemblage investigated in this study. Scales on P and T are schematic, but the intersection of the Opx-in and Bt-out reactions should correspond to the experimentally calibrated reactions shown in Figure 2.

Figure 7. REE diagram for felsic gneiss samples. Chondrite values from Sun & McDonough (1989).

Figure 8. X-ray Th compositional maps from 01SZ90 monazite. Maps have been simultaneously processed to show relative differences in Th between individual grains. m2, m5, and m6 are high-Th inclusions in garnet. m1, m4, m7, and m8 are low Th matrix grains. m1, m7, and m8 show higher Th cores. m3 is a matrix grain that shows an intermediate Th composition with a lower Th rim. This grain was extracted and dated by ID-TIMS.

Figure 9. BSE image showing petrographic setting of monazite. (a) m1tk1, matrix grain adjacent to kyanite and rutile (b) m2tk1, matrix monazite petrographic setting (c) m2tk1, grain is adjacent to kyanite and K-feldspar (d) m5tk1, inclusion in garnet core (e) m5tk1, showing well-armored nature of inclusion (f) m6tk1, matrix grain adjacent to kyanite and K-feldspar (g) m1tk2, inclusion in garnet (h) m1tk2,

CHAPTER 5 – MONAZITE SYSTEMATICS IN HIGH-PRESSURE GRANULITES

showing well-armored nature of inclusion (i) m5tk2, inclusion in garnet rim (j) m5tk2, showing multiple fractures and cracks around grain (Scale??)

Figure 10. X-ray compositional maps of monazite. Th, Ca, Y and U are shown for all grains with the exception of m3th (g), which shows Pb instead of Ca. Circles correspond to trace element analysis locations, squares correspond to the location of background measurements, and stars show the location of a complete suite of major element analysis. (a) m1tk1, high Th core surrounded by lower Th overgrowth. Homogeneous Y distribution. (b) m2tk1, Elongate matrix grain with homogeneous Th and Y. (c) m5tk1, Inclusion in garnet with high Y core surrounded by low Y overgrowth. Homogeneous Th distribution. (d) m6tk1, elongate matrix grain with high Th core and lower Th overgrowth. Homogeneous Y distribution. (e) m1tk2, Large inclusion in garnet. Patch Y zoning, but homogeneous Th distribution. Note Ca in garnet is lower than in monazite. (f) m5tk2, inclusion in garnet rim. Patchy Y distribution, slightly higher Th rim than core. Note Ca in garnet is higher than monazite since grain occurs in outer high-Gr_s garnet rim. (g) m3th, elongate matrix grain. Slightly lower Th and Y rim, but core shows homogeneous distribution of Th and Y.

Figure 11. Concordia diagrams for 01SZ90 zircon and monazite. (a) EPMA/TIMS comparison data. A and B refer to fragments of the same grains. (b) Grains from monazite mineral separate. m1.# refers to grains that were imaged in epoxy grain mounts prior to analysis. Grains m1, m2, and m4 were not imaged prior to analysis. Inset shows area outlined in box. (c) Zircon data from 01SZ90. Monazite data shown in gray for comparison. Oldest zircon is ~35my younger than the oldest monazite.

CHAPTER 5 – MONAZITE SYSTEMATICS IN HIGH-PRESSURE GRANULITES

Figure 12. BSE images of monazites from 01SZ90 that were imaged prior to analysis. Grains are labeled with an analysis I.D., 90.1.#, followed by the $^{207}\text{Pb}/^{206}\text{Pb}$ date, amount of discordance, and inclusions are noted where present. See text for discussion.

Figure 13. Isotope correlation diagram for felsic gneiss samples.

Figure 14. Nd isotope evolution diagram for 01SZ90 whole rock and single monazite grains. Dashed lines are the whole rock and *ca.* 2.6 Ga grains as determined by ID-TIMS analysis. Solid lines are grains that show a mixture of Archean and Paleoproterozoic components.

CHAPTER 5 - MONAZITE SYSTEMATICS IN HIGH-PRESSURE GRANULITES

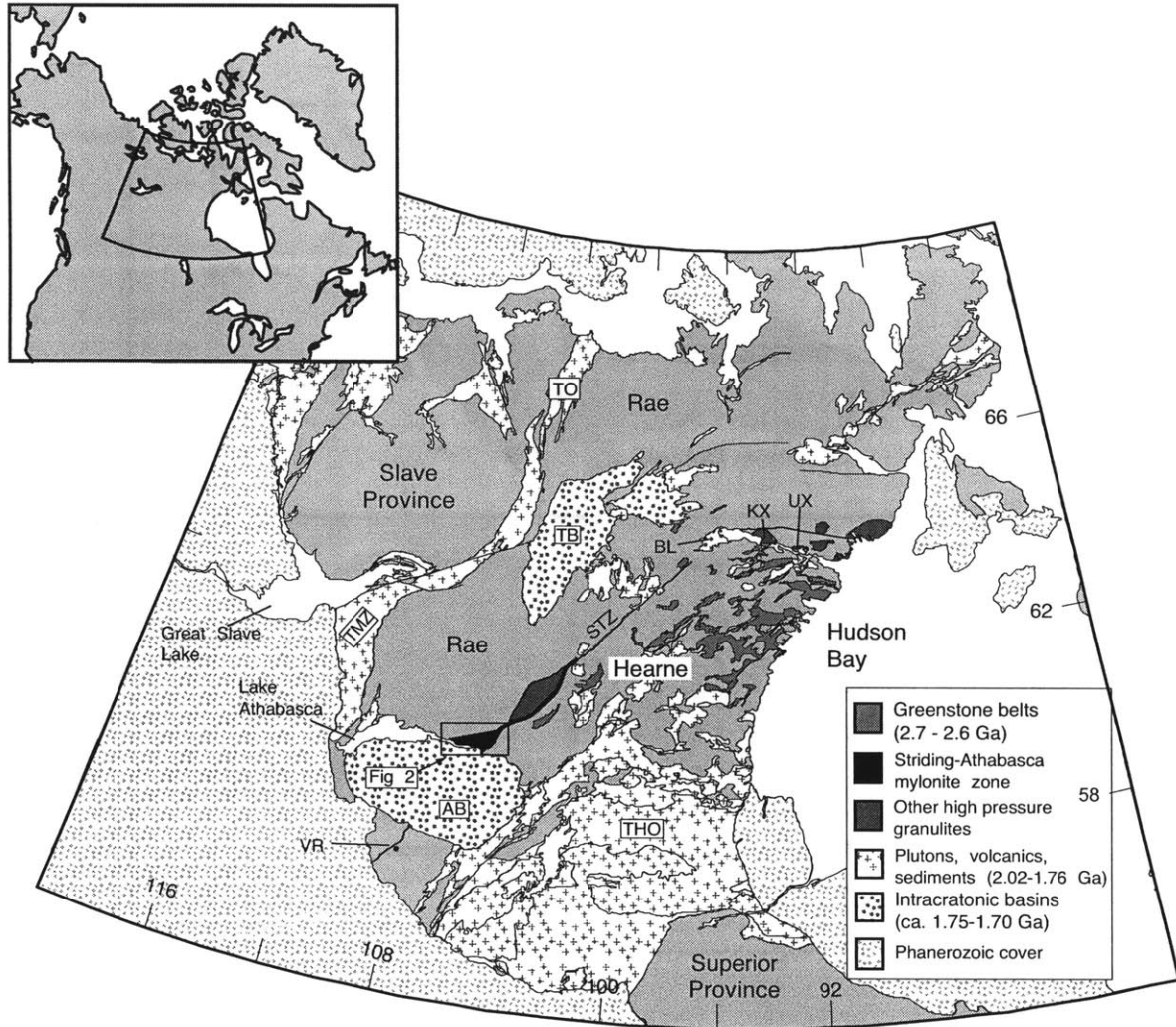


Figure 1

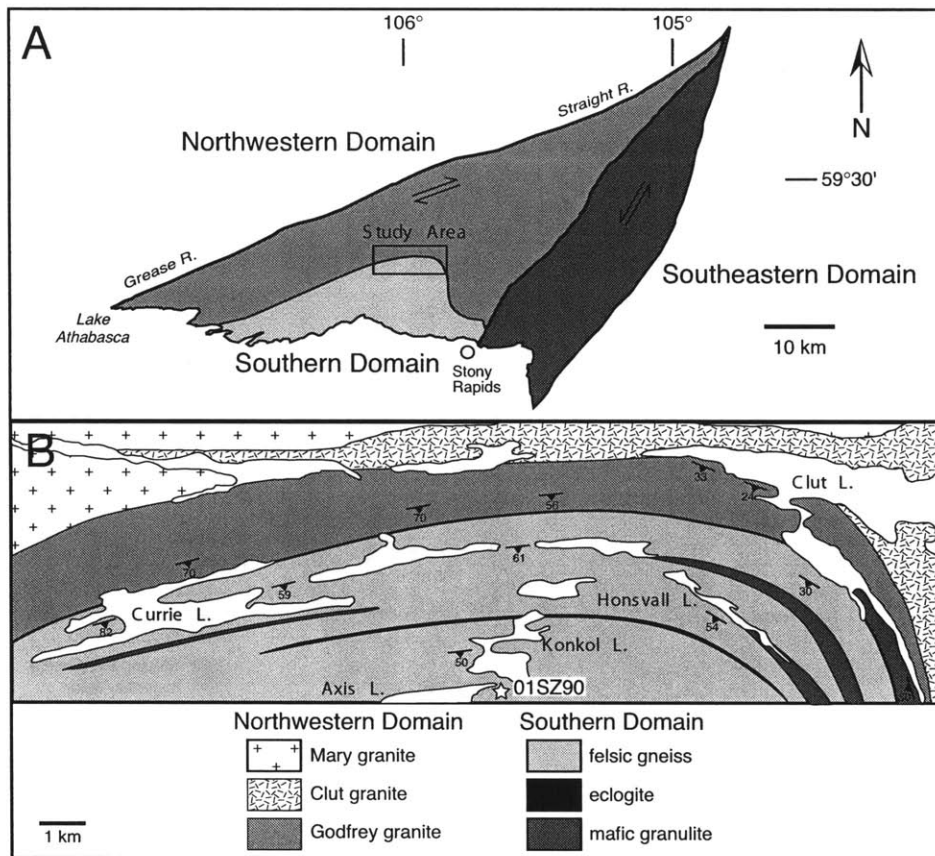


Figure 2

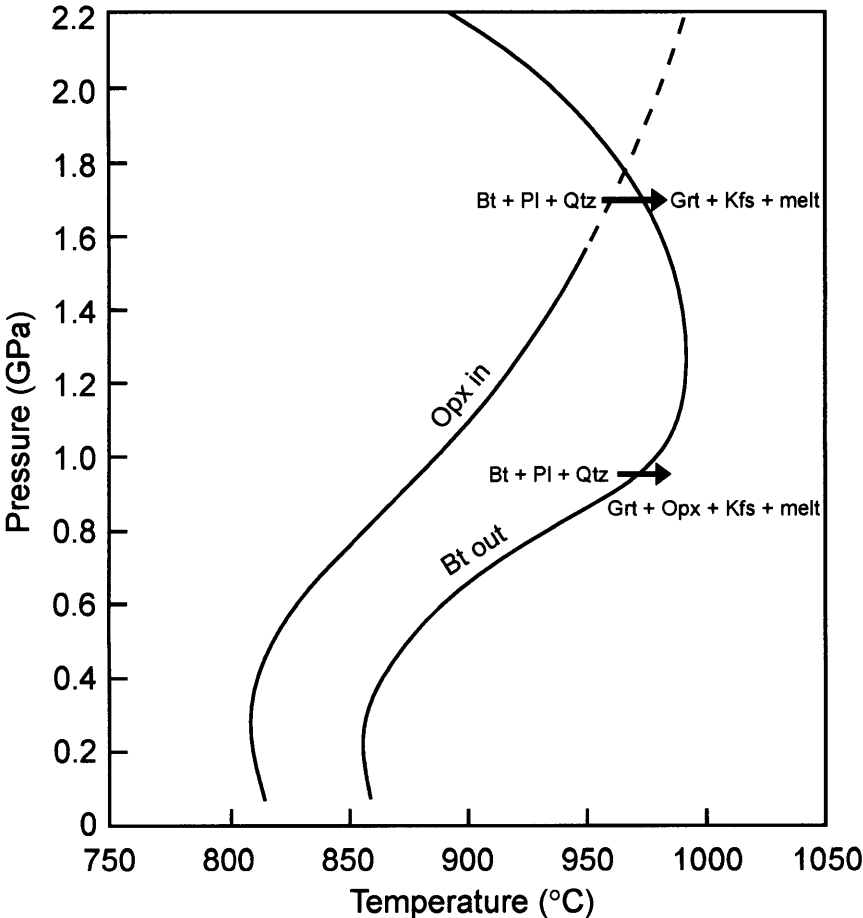


Figure 3

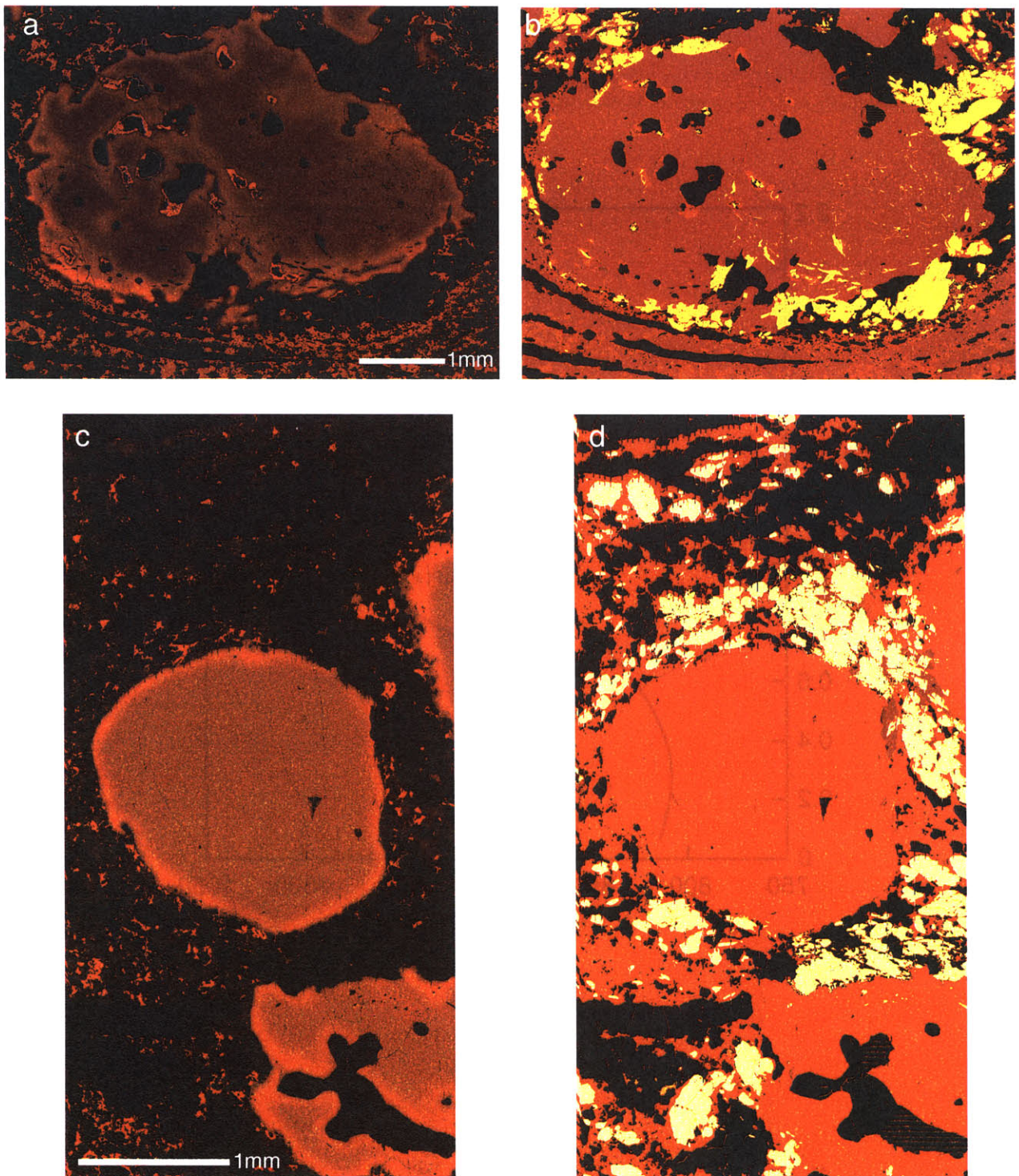


Figure 4

CHAPTER 5 - MONAZITE SYSTEMATICS IN HIGH-PRESSURE GRANULITES

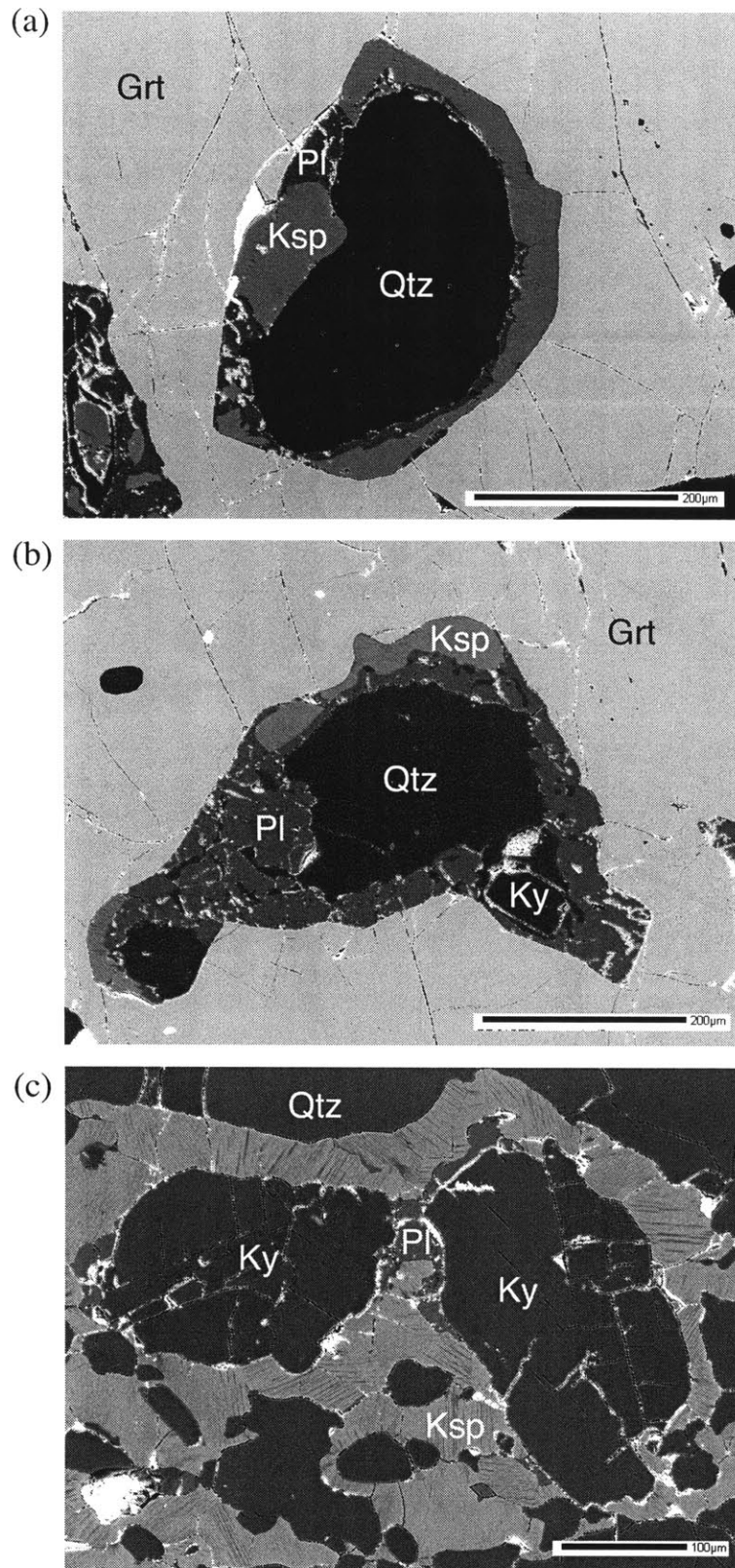


Figure 5

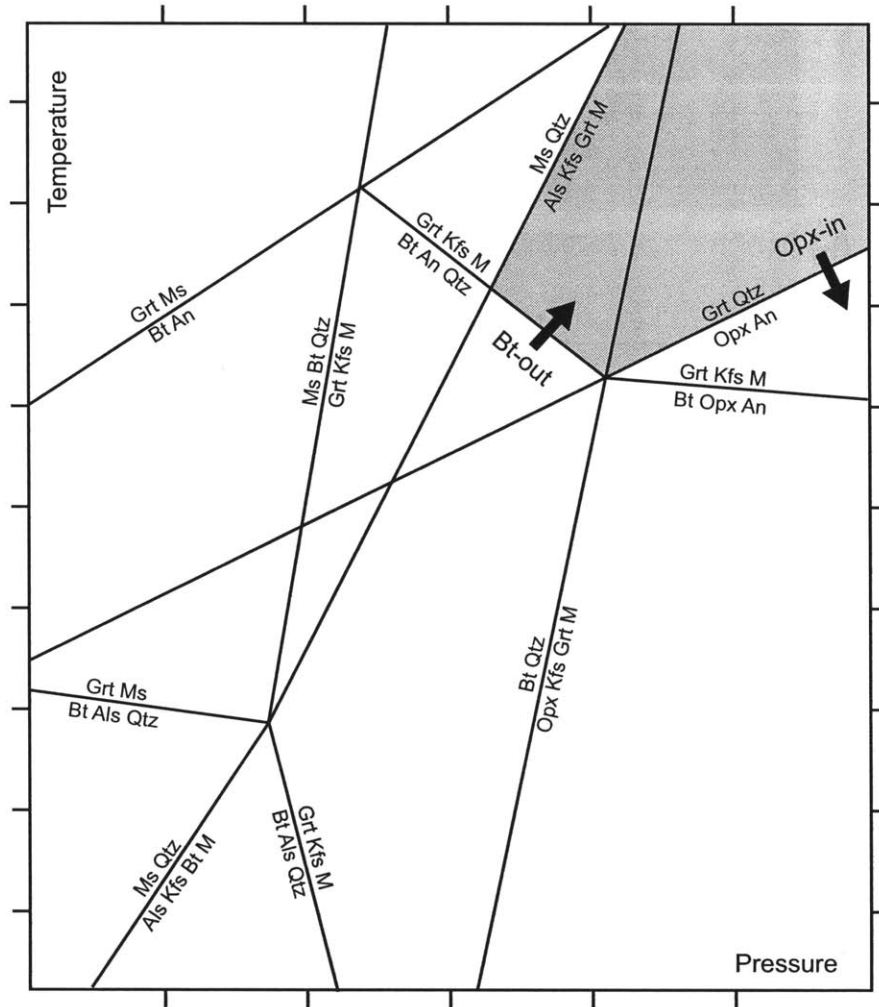
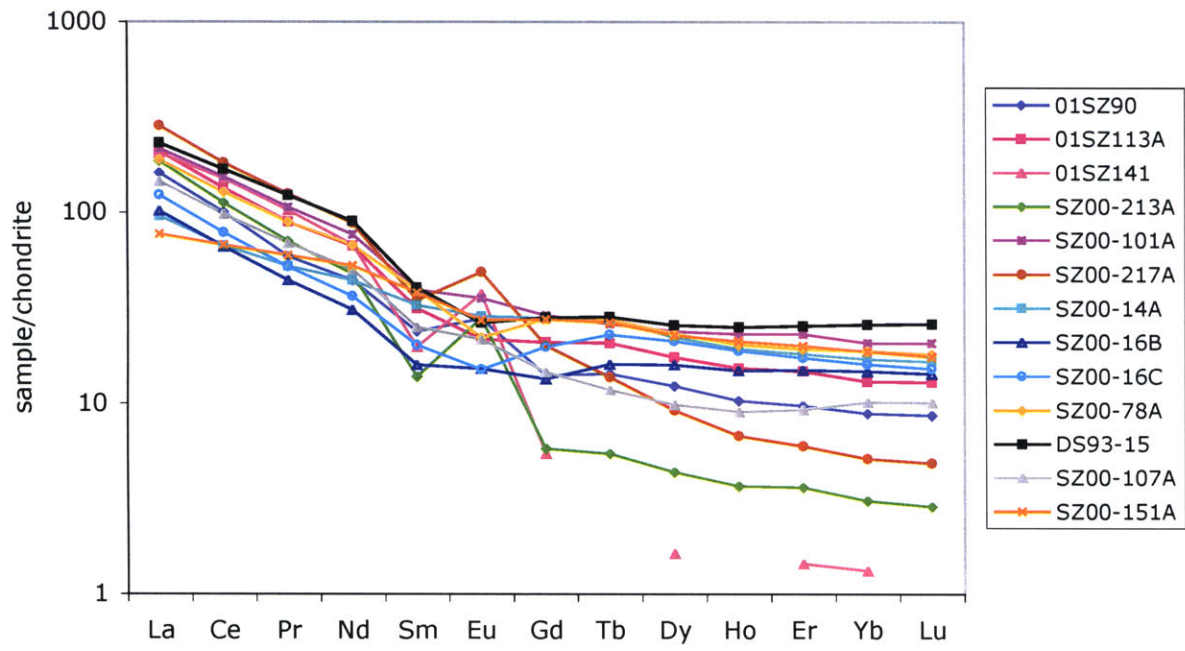


Figure 6

CHAPTER 5 - MONAZITE SYSTEMATICS IN HIGH-PRESSURE GRANULITES



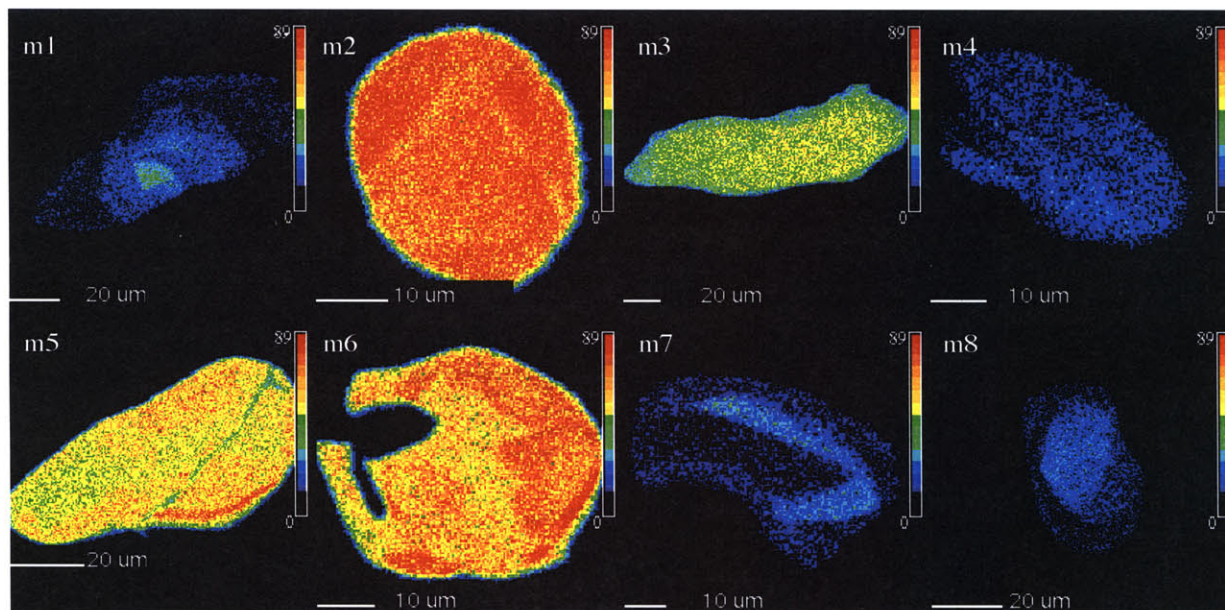


Figure 8

CHAPTER 5 - MONAZITE SYSTEMATICS IN HIGH-PRESSURE GRANULITES

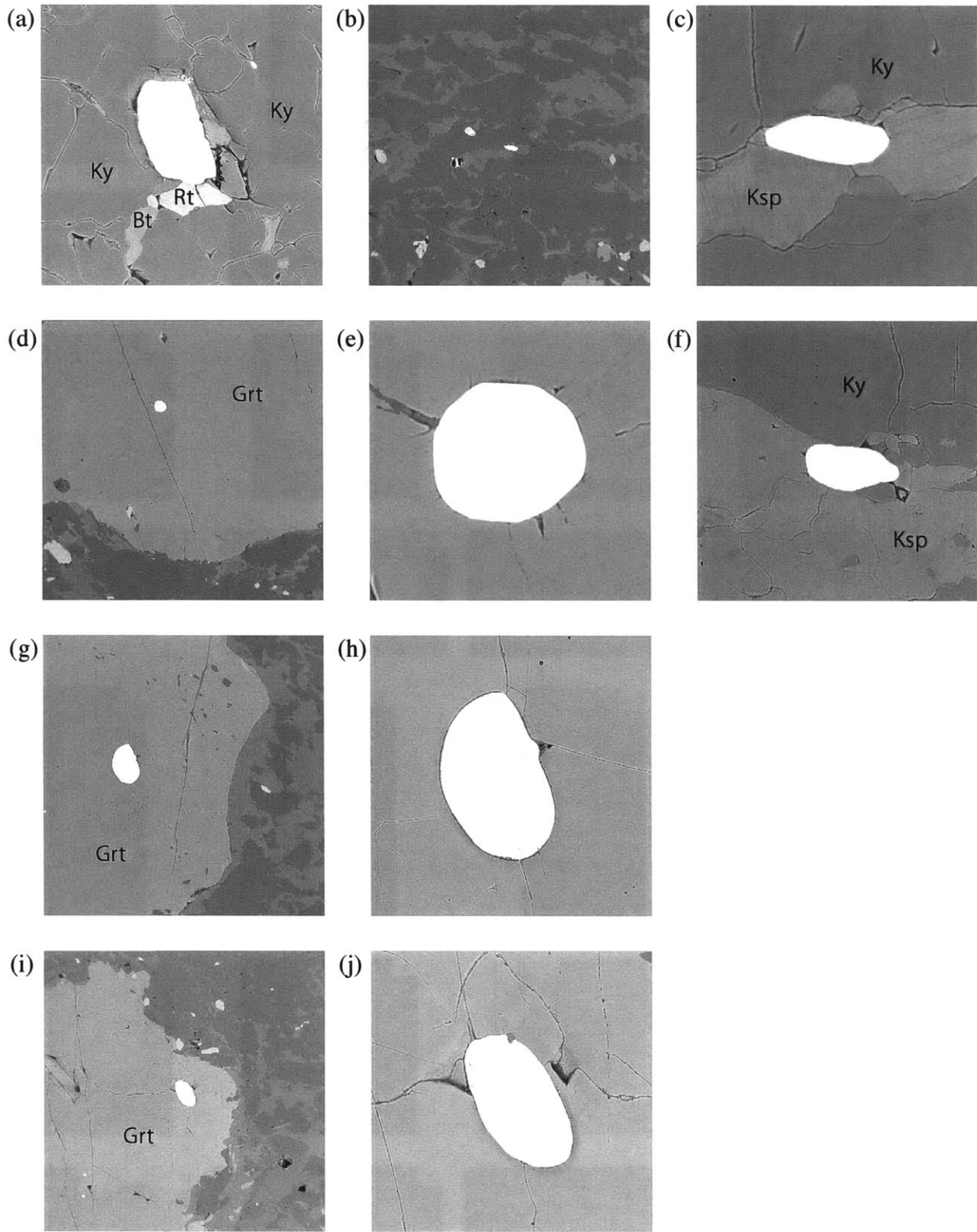


Figure 9

CHAPTER 5 - MONAZITE SYSTEMATICS IN HIGH-PRESSURE GRANULITES

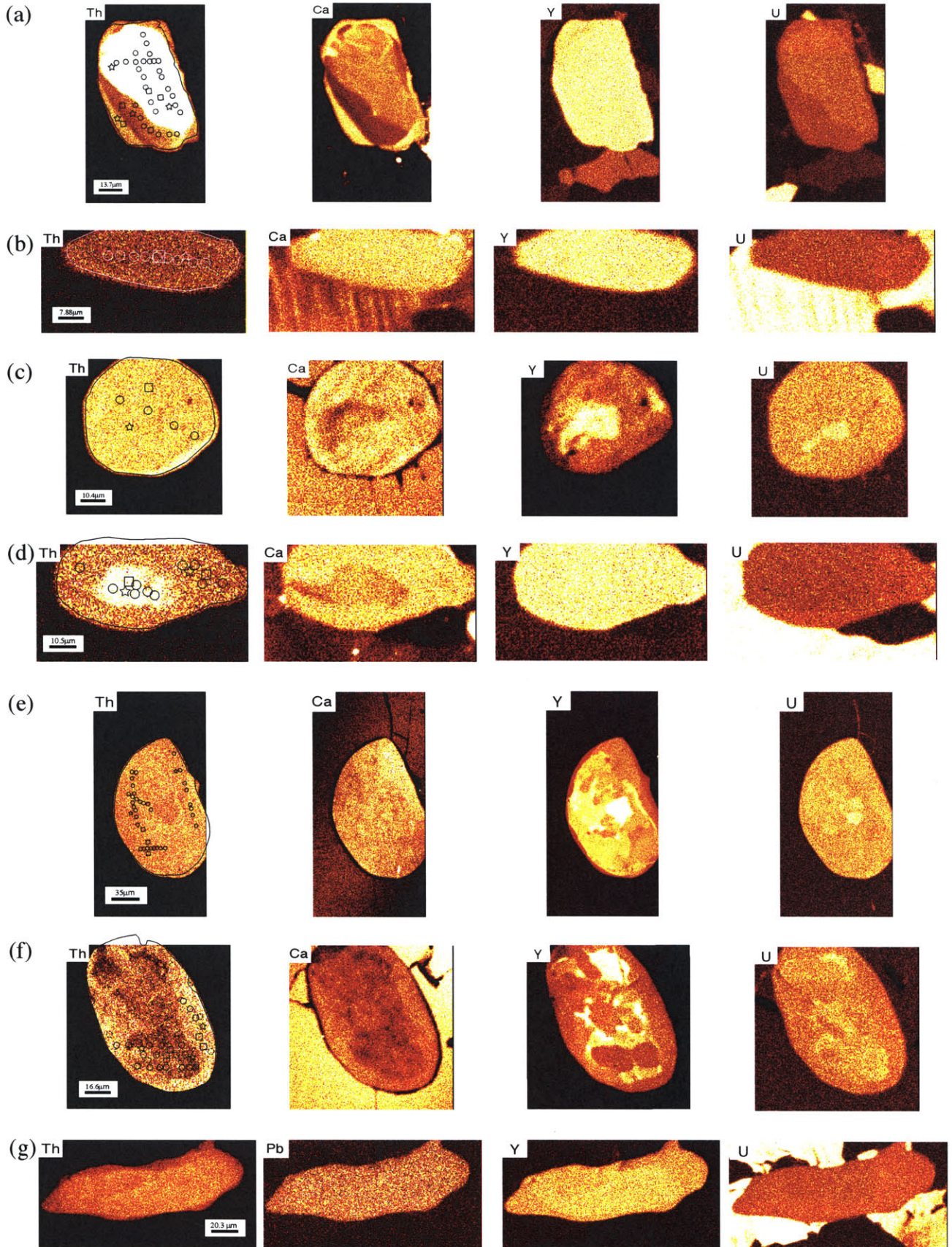


Figure 10

CHAPTER 5 - MONAZITE SYSTEMATICS IN HIGH-PRESSURE GRANULITES

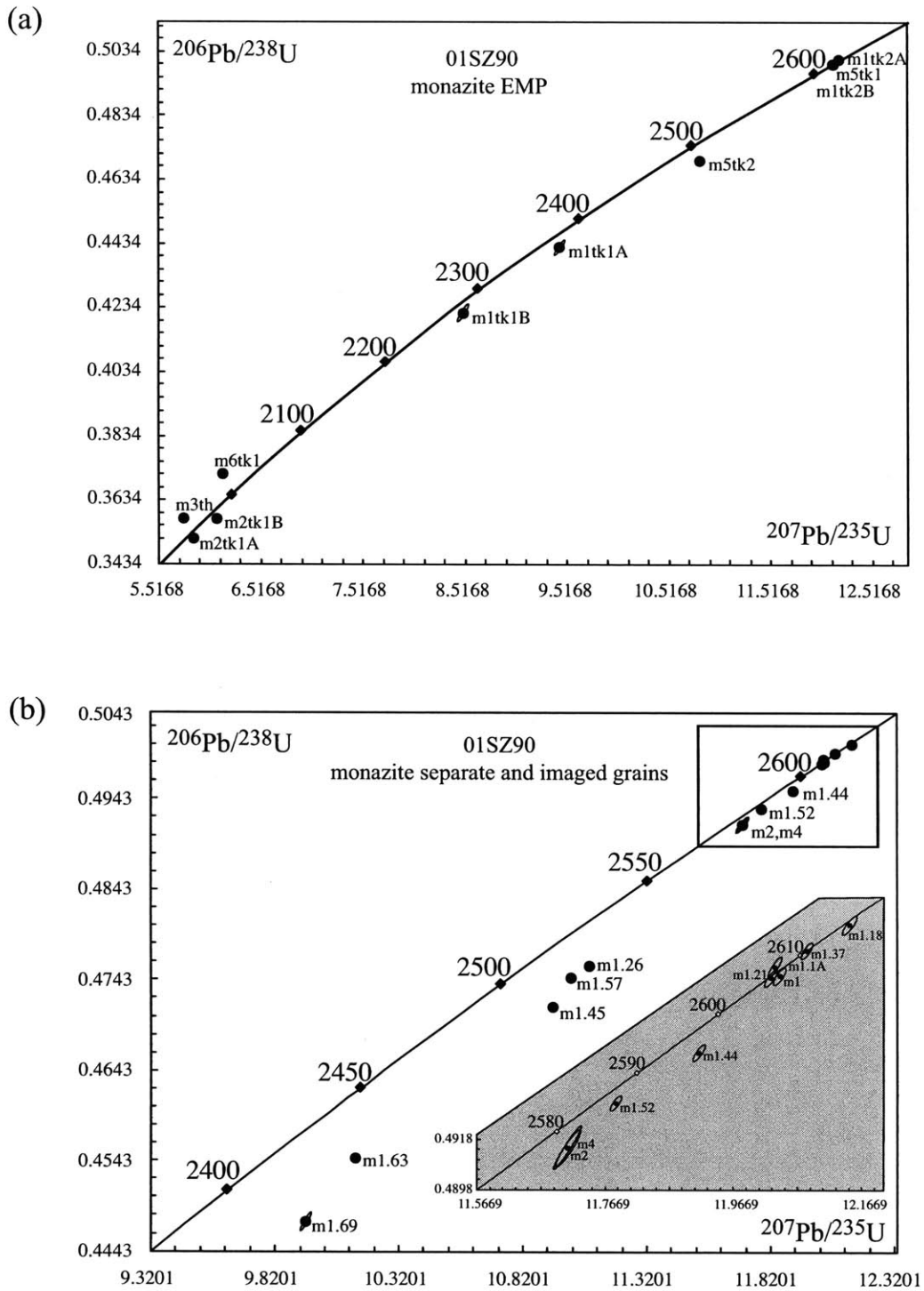


Figure 11

CHAPTER 5 - MONAZITE SYSTEMATICS IN HIGH-PRESSURE GRANULITES

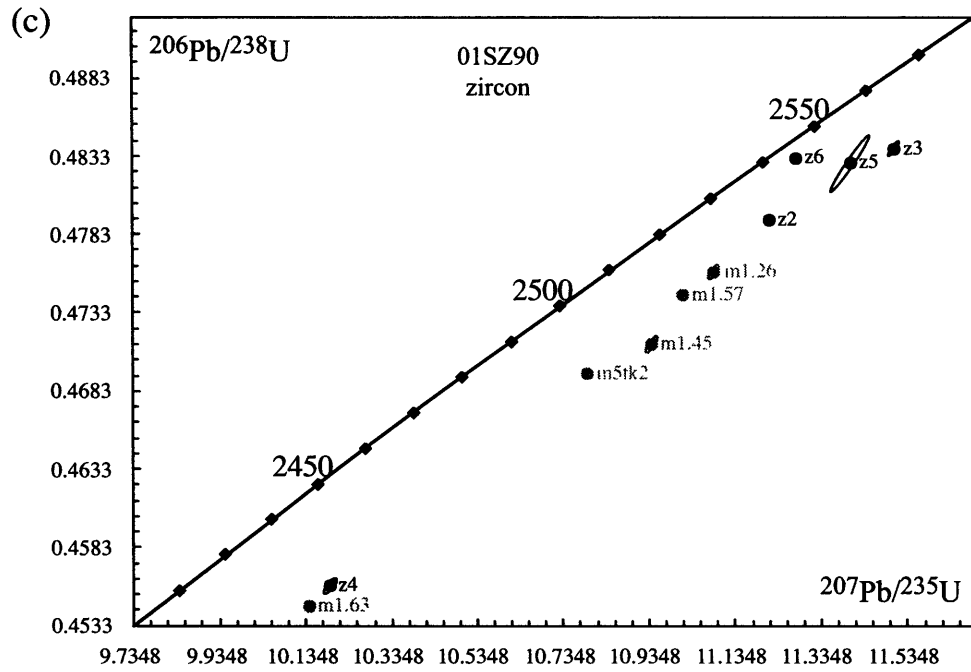


Figure 11, cont'd.

CHAPTER 5 - MONAZITE SYSTEMATICS IN HIGH-PRESSURE GRANULITES

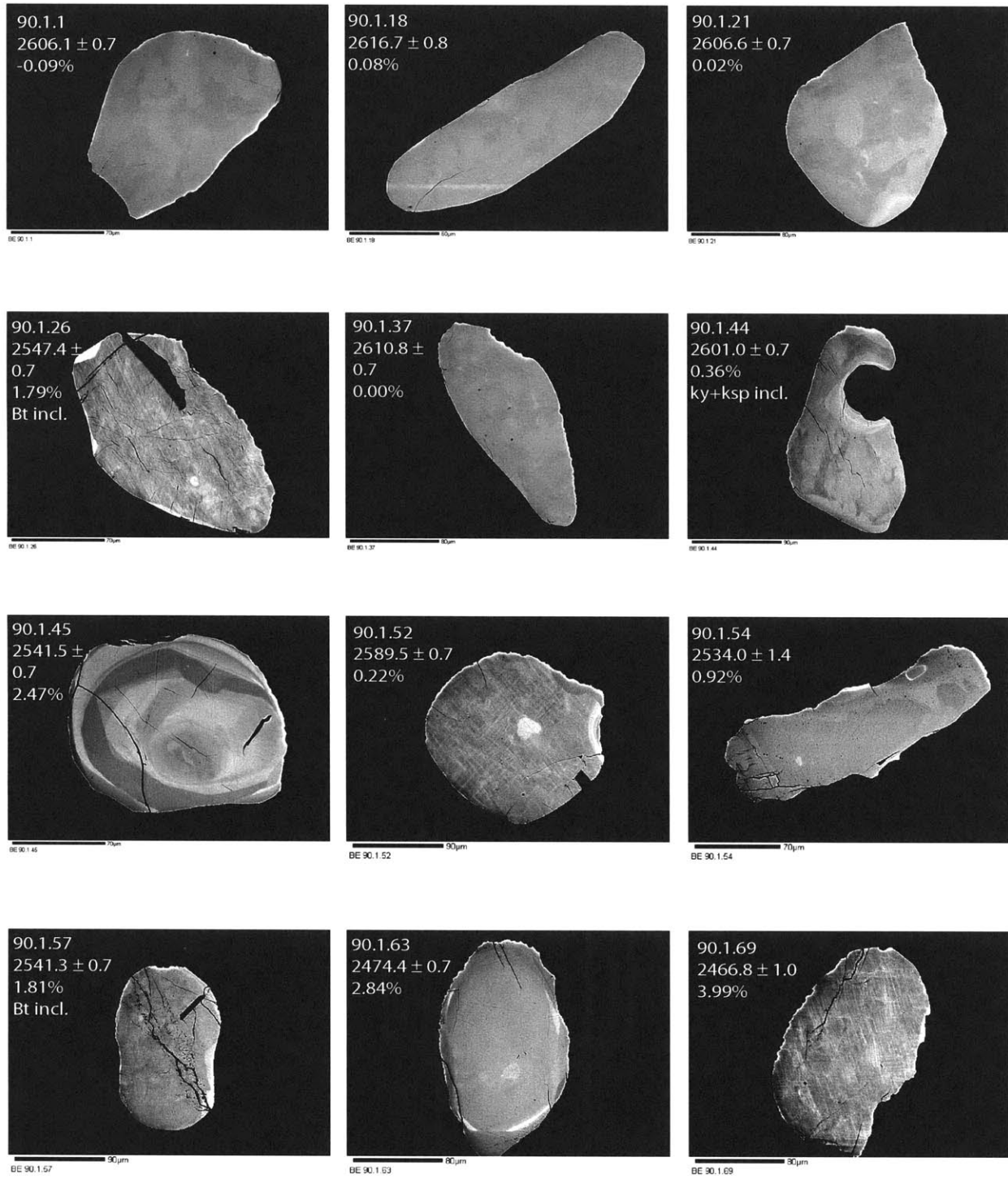
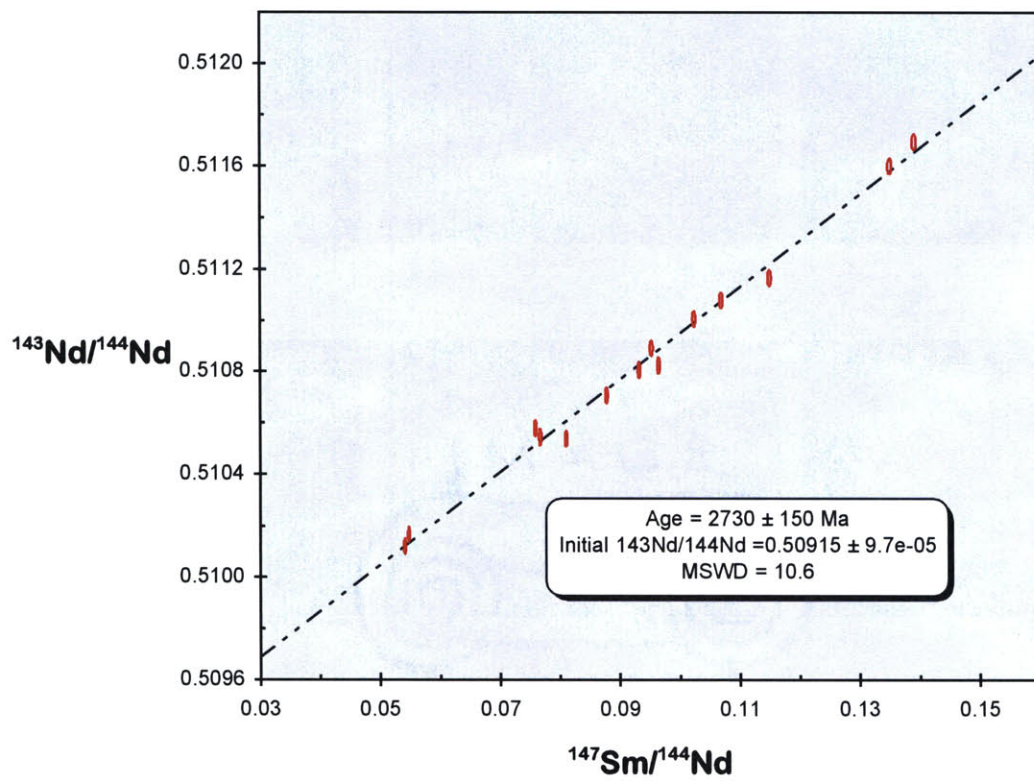


Figure 12



CHAPTER 5 - MONAZITE SYSTEMATICS IN HIGH-PRESSURE GRANULITES

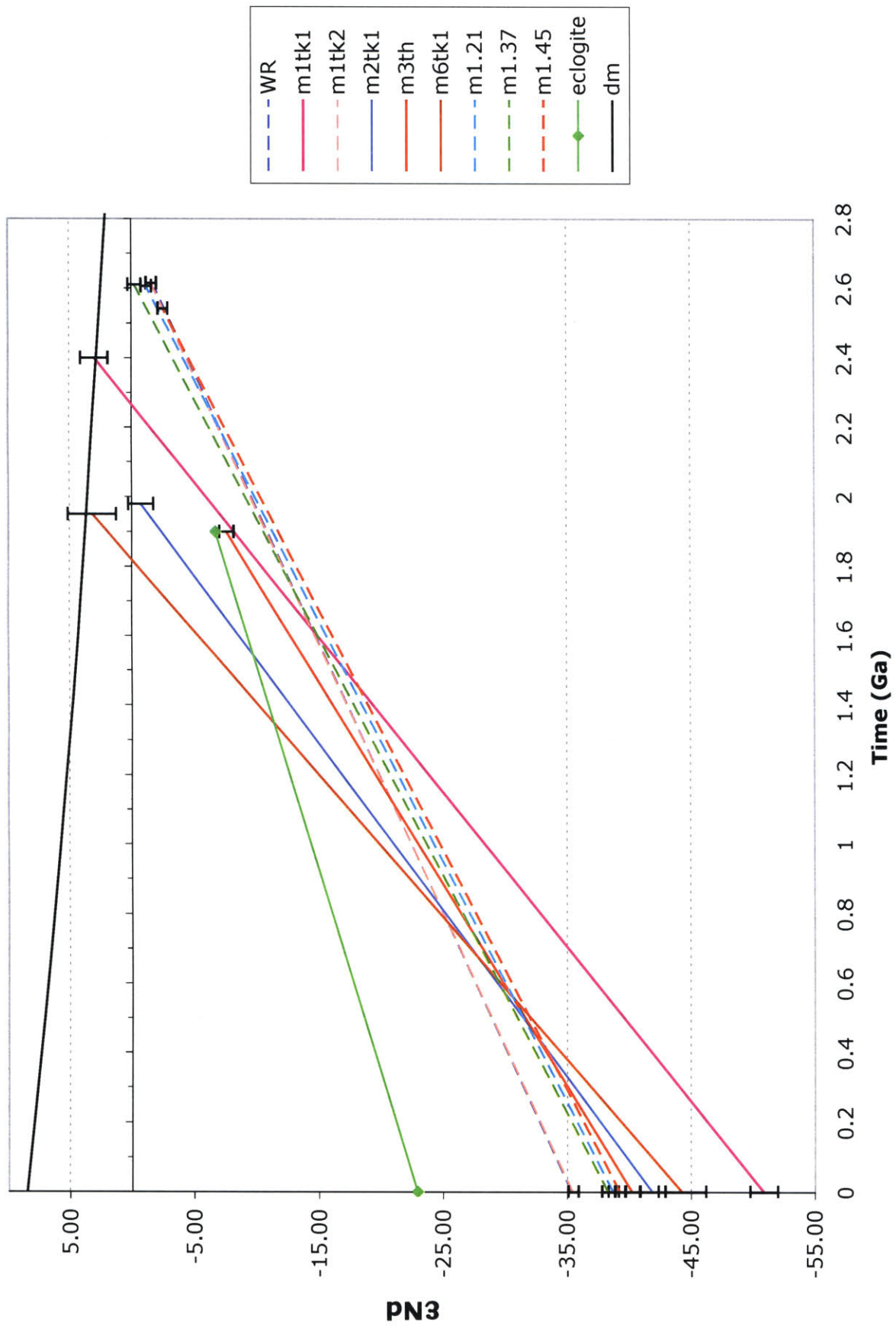


Table 1. Major and trace element geochemistry of the white gneiss

Sample	01SZ90	01SZ113A	01SZ141	SZ00-213A	SZ00-101A	SZ00-217A	SZ00-14A	SZ00-16B	SZ00-16C	SZ00-78A	DS93-15	SZ00-107A	SZ00-151A
SiO ₂	66.31	71.93	73.55	74.70	59.16	55.67	56.83	67.65	73.89	62.09	58.87	66.10	56.52
Al ₂ O ₃	18.93	13.93	15.39	14.16	23.53	21.88	18.98	16.26	12.96	16.89	18.56	16.13	18.10
Fe ₂ O ₃	4.00	4.23	1.39	1.35	6.16	8.77	11.60	5.03	4.70	10.67	11.89	4.02	11.45
MnO	0.04	0.04	0.01	0.02	0.09	0.061	0.213	0.095	0.089	0.133	0.133	0.076	0.129
MgO	1.89	1.43	0.50	0.42	2.65	2.33	1.36	1.86	1.51	3.09	4.24	1.70	3.29
CaO	0.71	0.90	3.02	1.71	1.59	3.97	5.90	3.41	2.07	2.87	2.80	2.80	6.18
Na ₂ O	1.73	2.91	4.32	3.75	1.79	4.41	3.81	3.42	2.94	2.90	2.19	3.04	2.79
K ₂ O	4.48	3.99	1.28	3.23	4.31	1.69	0.60	1.45	1.15	0.99	0.87	4.96	0.34
TiO ₂	0.44	0.44	0.18	0.12	0.73	1.24	1.22	0.51	0.44	0.39	0.63	0.55	1.21
P ₂ O ₅	0.04	0.05	0.03	0.06	0.07	0.04	0.24	0.03	0.05	0.05	0.05	0.14	0.21
L.O.I.	0.17	-0.05	0.27	0.29	-0.03	-0.15	-0.53	0.39	0.30	-0.14	-0.03	0.51	-0.16
Total	98.75	99.78	99.94	99.81	100.06	99.91	100.22	100.11	100.09	99.93	100.21	100.03	100.05
Sc	13	11	2	3	18	8	22	14	11	25	25	12	21
Be	0	0	0	2	1	0	1	1	0	0	0	1	2
V	86	54	19	12	139	93	139	92	64	81	158	89	165
Cr	124	92	26	0	121	86	0	70	58	109	225	83	25
Co	10	11	3	2	7	14	21	13	10	19	26	16	23
Cu	0	0	0	0	13	16	0	32	22	33	44	19	117
Zn	0	45	0	0	78	92	69	59	0	64	76	70	109
Ga	20	15	19	16	35	24	20	19	13	16	21	18	23
Ge	0	2	0	0	2	2	2	1	0	2	2	1	2
Rb	102	76	13	36	98	22	5	38	14	16	11	91	3
Sr	226	222	449	331	397	759	314	331	234	305	333	517	457
Y	16	22	2	6	38	11	31	25	30	32	38	15	31
Zr	81	240	99	64	149	455	126	77	264	188	165	127	75
Nb	7	9	5	2	8	6	10	5	5	4	16	7	7
Ba	1,800	1,240	564	1,310	1,840	584	381	449	299	316	312	935	168
La	38.2	49.7	48.7	44.5	51.5	67.6	22.6	24.0	29.3	44.9	55.0	34.6	18.2
Ce	61.2	82.2	92.1	69.0	94.1	112.0	40.8	40.3	47.9	78.4	103.7	59.6	41.4
Pr	5.59	8.45	9.71	6.73	10.1	11.9	4.96	4.17	4.94	8.48	11.7	6.57	5.66
Nd	20.6	31.0	31.5	22.2	35.6	40.9	20.6	14.5	17.0	31.5	42.0	23.5	24.7
Sm	3.6	4.8	3.0	2.1	6.0	5.3	5.0	2.4	3.1	6.0	6.2	3.8	5.8
Eu	1.61	1.26	2.18	1.62	2.05	2.82	1.66	0.88	0.87	1.29	1.54	1.25	1.59
Gd	2.9	4.3	1.1	1.2	5.9	4.1	5.7	2.8	4.0	5.7	5.8	3.0	5.6
Tb	0.5	0.8	0.0	0.2	1.0	0.5	1.0	0.6	0.9	1.0	1.1	0.4	1.0
Dy	3.1	4.4	0.4	1.1	6.0	2.3	5.6	4.0	5.4	5.9	6.5	2.5	5.7
Ho	0.6	0.9	0.0	0.2	1.3	0.4	1.1	0.8	1.1	1.2	1.4	0.5	1.2
Er	1.6	2.4	0.2	0.6	3.8	1.0	3.0	2.5	2.9	3.2	4.2	1.5	3.3
Tm	0.23	0.37	0.00	0.08	0.57	0.13	0.46	0.39	0.45	0.52	0.69	0.25	0.52
Yb	1.5	2.2	0.2	0.5	3.5	0.9	2.9	2.5	2.7	3.2	4.4	1.7	3.2
Lu	0.22	0.33	0.0	0.07	0.53	0.12	0.42	0.36	0.39	0.46	0.66	0.26	0.45
Hf	2.6	6.8	2.8	2.0	4.2	13.0	3.4	2.2	7.5	5.1	4.8	3.4	2.3
Ta	0.4	0.5	0.2	0.0	0.5	0.2	0.6	0.1	0.2	0.0	1.3	0.3	0.4
Tl	0.3	0.5	0.0	0.2	1.1	0.1	0.0	0.3	0.0	0.0	0.0	0.6	0.0
Pb	9	22	12	22	32	23	0	6	0	6	8	18	0
Th	3.4	7.3	0.4	0.2	6.5	3.0	1.2	0.5	0.7	8.7	13.0	5.6	2.1
U	0.5	0.7	0.3	0.1	0.6	0.8	0.4	0.2	0.3	1.4	0.7	0.8	0.7
Eu/Eu*	3.03	1.69	7.27	6.24	2.10	3.10	4.10	5.10	6.10	7.10	8.10	9.10	10.10
Th/U	7.31	10.84	1.64	1.87	10.53	3.59	2.92	2.80	2.25	6.04	19.87	7.05	2.88

Table 2. Major element electron microprobe data for 01SZ90.

Pt		FeO	CaO	SiO ₂	P ₂ O ₅	As ₂ O ₃	ThO ₂	U ₂ O ₃	Y ₂ O ₃	La ₂ O ₃	Ce ₂ O ₃	Nd ₂ O ₃	Pr ₂ O ₃	Sm ₂ O ₃	Gd ₂ O ₃	Dy ₂ O ₃	Er ₂ O ₃	Eu ₂ O ₃	Tm ₂ O ₃	Yb ₂ O ₃	F	SO ₂	Total	
3	m1th2 core1	bd	1.13	0.40	27.57	0.13	4.26	0.88	1.26	14.63	29.25	11.61	2.99	1.36	0.89	0.58	0.08	0.69	bd	bd	0.66	0.02	98.40	
4	m1th2 rim1	0.04	1.18	0.31	27.52	0.06	4.38	0.80	0.59	14.68	28.65	11.64	3.32	1.47	1.29	0.35	bd	0.57	bd	0.15	0.64	0.01	97.65	
5	m2th2 hiTh1	bd	0.16	0.49	26.66	0.01	1.78	0.16	bd	14.35	35.10	14.80	4.16	0.55	0.58	0.01	bd	0.56	bd	bd	0.87	0.03	100.25	
6	m2th2 rim1	bd	0.18	0.20	26.98	bd	0.73	0.10	0.09	23.31	32.10	9.08	2.59	1.06	bd	bd	bd	0.54	bd	0.02	0.64	0.01	97.62	
7	m4th2 pt1	bd	0.18	0.22	26.86	0.05	0.42	0.12	bd	24.13	31.18	9.54	2.58	1.16	bd	bd	bd	0.49	0.03	0.01	0.61	0.02	97.58	
8	incl. in grt rim	m5tk2 1	bd	0.75	0.45	27.34	0.11	3.54	0.74	0.11	15.58	30.28	12.34	3.29	1.49	bd	bd	bd	0.72	0.24	bd	0.64	bd	97.62
9	incl. in grt rim	m5tk2 rim	0.19	0.89	0.46	27.23	0.04	4.38	0.35	0.26	15.60	30.68	11.99	3.13	1.48	bd	0.12	0.09	0.32	0.05	bd	0.49	bd	97.76
10	incl. in grt rim	m5tk2 hiY	bd	0.66	0.49	27.45	bd	3.47	0.48	0.46	15.75	30.16	11.88	3.23	1.58	0.04	0.29	0.06	0.56	0.10	bd	0.78	0.02	97.47
11	m6tk2 core1	bd	0.12	0.43	27.52	0.04	0.34	bd	0.09	16.14	34.03	14.08	3.38	0.86	0.39	0.14	bd	0.66	bd	0.14	0.67	0.02	99.05	
12	m6tk2 rim1	bd	0.16	0.20	28.50	0.04	1.00	0.14	0.07	25.60	32.31	9.34	2.43	1.14	0.17	0.09	bd	0.53	bd	0.16	0.65	0.04	102.57	
13	m6tk2 rim2	bd	0.24	0.19	27.89	bd	0.61	0.18	0.13	23.54	31.68	9.12	2.24	0.98	0.46	0.10	0.04	0.60	0.15	bd	0.79	bd	98.94	
14	m8tk2 pt1	bd	0.06	0.22	27.85	0.07	0.35	0.10	bd	16.32	35.47	14.17	3.75	0.94	bd	bd	bd	0.74	0.04	0.04	0.80	bd	100.93	
15	matrix	m1tk1 core1	bd	0.48	2.76	24.86	0.03	11.62	0.19	0.04	11.40	28.82	12.85	3.45	0.56	0.33	bd	0.24	0.77	0.19	0.10	0.62	0.06	99.36
16	matrix	m1tk1 core2	bd	0.44	3.74	22.99	0.08	15.79	0.27	bd	10.20	26.57	12.45	2.85	0.52	bd	bd	0.08	0.67	0.15	0.04	0.57	0.04	97.43
17	matrix	m1tk1 inner rim	bd	0.23	0.81	27.06	bd	3.18	bd	bd	15.96	34.39	12.78	2.74	0.50	bd	bd	bd	0.76	0.07	bd	0.68	0.02	99.18
18	matrix	m1tk1 outer rim	bd	0.66	0.51	27.91	bd	3.86	0.04	bd	19.74	31.26	10.17	2.63	0.83	bd	bd	bd	0.71	0.17	bd	0.63	0.03	99.15
19	incl. in grt core	m5tk1 hi Y	0.07	0.85	0.63	27.18	0.09	4.51	0.69	1.45	14.25	29.63	11.65	2.91	1.30	1.04	0.47	0.04	0.54	0.09	bd	0.48	bd	97.85
21	m7tk1 core1	bd	0.14	0.43	27.94	0.11	1.40	bd	bd	15.83	35.61	13.12	3.31	0.35	bd	0.05	bd	0.81	0.16	bd	0.65	0.05	99.94	
22	m7tk1 rim1	bd	0.20	0.21	28.93	0.07	0.53	0.09	0.08	24.52	31.58	9.57	2.57	1.06	bd	bd	bd	0.65	0.20	bd	0.69	0.04	101.00	
23	matrix	m6tk1 core1	bd	0.14	0.43	27.84	0.12	1.41	0.12	0.06	15.87	34.97	14.01	3.57	0.34	bd	bd	bd	0.91	0.09	bd	0.80	0.05	100.71
24	matrix	m6tk1 rim1	bd	0.18	0.21	28.31	0.01	0.59	0.07	bd	24.71	32.69	8.78	2.71	0.48	bd	0.12	bd	0.80	0.09	0.05	0.60	0.03	100.44
25	m2tk1 pt1	bd	0.15	0.14	27.98	0.02	0.25	0.06	bd	24.59	32.76	8.64	2.26	0.56	bd	bd	bd	0.69	0.14	bd	0.61	0.03	98.88	

bd Below detection limit

CHAPTER 5 - MONAZITE SYSTEMATICS IN HIGH-PRESSURE GRANULITES

Table 3. Electron microprobe trace element compositions and age data.

Label	Y	Th	Pb	U	Chemical Date
mltk1-core					
1	0	149512	18284	1031	2518
2	0	157241	18768	993	2466
3	0	148172	16801	894	2353
4	0	157986	18050	1018	2366
5	0	134692	15048	789	2322
6	0	124040	13793	738	2311
33	309	145752	18021	2257	2467
34	339	134527	16422	2127	2435
35	411	161100	19299	2441	2398
36	418	146801	17348	2222	2368
37	438	147830	16552	2231	2253
38	505	146476	16137	2122	2224
39	355	138694	16689	2140	2406
40	415	137377	16080	2078	2348
41	424	138491	16161	2195	2335
42	473	138033	15929	2112	2315
43	495	140012	15727	2097	2260
44	523	144254	15761	2166	2202
45	511	143707	14835	2033	2095
46	512	128775	13559	1756	2138
47	477	133767	14079	1847	2136
48	483	137242	14407	1901	2130
Range					2095-2518
mltk1-rim					
7	0	30416	3593	521	2351
8	0	29746	3549	568	2357
9	0	29840	3487	556	2316
10	0	29727	3449	530	2307
11	0	29638	3488	495	2346
49	313	31644	3608	1042	2161
50	283	29738	3288	965	2103
51	296	28219	3193	1012	2126
52	290	31683	3649	992	2192
53	352	36934	4084	1064	2128
54	314	39155	4238	1108	2090
Range					2090-2357
m2tk1					
6	173	2130	563	1192	1853
7	164	2149	564	1164	1876
8	167	2079	596	1192	1956
9	158	2166	605	1257	1901
10	141	2093	612	1279	1917
12	113	2096	581	1235	1872
13	107	2133	605	1251	1914
14	76	2426	606	1212	1882
Ave	137	2159	592	1223	1896
2*StdErr					23
m5tk1					
1	8714	42598	8029	5576	2595
2	5251	41339	7587	5077	2585
3	11758	42490	7562	4791	2578
4	7099	42101	8071	5675	2610

CHAPTER 5 - MONAZITE SYSTEMATICS IN HIGH-PRESSURE GRANULITES

Table 3. Electron microprobe trace element compositions and age data.

Label	Y	Th	Pb	U	Chemical Date
Ave	8206	42132	7812	5280	2592
2*StdErr					13
m6tk1-core					
1	46	14296	1658	804	2047
2	55	13716	1615	773	2074
3	36	13472	1556	755	2040
4	46	11588	1371	776	2022
5	38	12189	1476	815	2066
Ave	44	13052	1535	785	2050
2*StdErr					18
m6tk1-rim					
1	122	5089	835	1093	1953
2	125	4895	784	1057	1908
3	118	4699	827	1144	1974
4	136	3449	744	1303	1924
Ave	125	4533	798	1149	1940
2*StdErr					29
m1tk2-core					
1	7274	42558	8040	5430	2620
2	6977	42369	7930	5299	2614
3	7541	42058	7915	5268	2625
4	7355	41882	7857	5239	2619
5	7780	41704	7873	5205	2634
6	7983	42112	8064	5414	2643
7	8256	41573	7982	5484	2630
8	7962	41215	7974	5555	2630
9	7544	41170	7906	5227	2659
10	7467	41519	8046	5525	2643
11	6812	41160	8086	5925	2611
12	6911	40629	7913	5718	2610
13	10355	43538	8707	6452	2626
14	9246	42687	8522	6559	2593
15	4665	41927	7815	4993	2641
16	6665	41662	8520	6772	2597
17	7435	42168	8341	6165	2613
18	9597	41666	8521	6157	2677
Ave	7657	41866	8112	5688	2627
2*StdErr					10
m1tk2-rim					
1	9578	40861	8639	7269	2589
1	7062	43758	8520	6541	2562
2	9075	39383	8713	7843	2582
3	6277	41619	8204	6117	2602
4	5895	41167	7913	5606	2608
5	10888	44017	8694	6675	2581
6	8224	42198	8176	6224	2562
7	9607	41998	8352	6410	2590
8	9811	42644	8398	6495	2571
Ave	8491	41961	8401	6576	2583
2*StdErr					10
m1tk2-rim					
19	0	15110	1912	330	2465
20	0	15458	1928	443	2378

CHAPTER 5 - MONAZITE SYSTEMATICS IN HIGH-PRESSURE GRANULITES

Table 3. Electron microprobe trace element compositions and age data.

Label	Y	Th	Pb	U	Chemical Date
21	0	15595	1937	442	2372
22	0	15353	1914	452	2371
23	0	15525	2009	511	2426
24	0	15569	1987	555	2375
25	0	15434	1991	580	2384
Ave	0	15435	1954	473	2396
2*StdErr					27
m5tk2					
1	310	40870	5737	2293	2433
2	593	33778	6189	4750	2481
3	633	33435	6307	5186	2466
4	726	32504	6729	6292	2471
5	767	33509	6448	5577	2450
Ave	606	34819	6282	4820	2460
2*StdErr					17
m3th-core					
11	336	25192	2454	960	1838
12	461	29733	2899	1003	1864
13	456	31204	3048	1132	1853
14	705	31683	3288	1305	1932
15	821	31651	3308	1458	1916
16	833	32187	3316	1438	1899
17	720	31655	3199	1294	1886
18	582	29994	3073	1190	1917
19	588	30880	3111	1191	1894
20	725	32264	3360	1396	1926
21	958	34127	3603	1656	1920
22	878	33761	3441	1572	1869
23	763	33084	3452	1551	1909
24	769	32736	3381	1512	1895
25	739	31761	3338	1418	1934
26	899	33593	3614	1665	1948
27	1005	33820	3575	1747	1905
28	821	32868	3502	1535	1947
29	825	32539	3413	1548	1914
30	752	31894	3316	1471	1907
31	504	32790	3172	1088	1854
32	498	32150	3162	988	1897
33	458	30563	2991	1008	1875
34	250	22653	2314	957	1898
1	302	24402	2405	983	1846
2	293	24984	2461	995	1848
1	367	31636	3277	1221	1943
2	409	31612	3261	1269	1927
3	581	32602	3402	1452	1922
Ave	631	31035	3177	1310	1899
2*StdErr					12
m3th-rim					
11	336	25192	2454	960	1838
1	302	24402	2405	983	1846
2	293	24984	2461	995	1848
Ave	310	24859	2440	979	1844
2*StdErr					6

Table 4. U-Pb isotopic data for 01SZ90.

01SZ90	Weight ^b Fractions ^a (μg)	Compositions						Isotopic Ratios						Age (Ma)			Dis- cordance %		
		U (ppm)	Pb (ppm)	Th (ppm)	Th U	Pb _c (pg)	Pb*/Pb _c ^d	206 Pb* ^c 204 Pb	208 Pb 206 Pb	206 Pb ^f 238 U	% err	207 Pb ^f 235 U	% err	207 Pb ^f 206 Pb	% err	206 Pb 238 U		207 Pb 235 U	207 Pb ^e 206 Pb
m1	5.0	1600	2866	16688	10.7	4.2	3359.2	58377	2.980	0.49828	(.07)	12.03983	(.08)	0.17525	(.04)	2606.4	2607.5	2608.4 \pm 0.7	0.09
m2	3.3	2150	4439	27453	13.1	58.3	250.2	3311	3.663	0.49146	(.15)	11.70881	(.17)	0.17279	(.06)	2577.0	2581.4	2584.9 \pm 1.1	0.37
m4	2.3	2120	3582	20619	10.0	26.9	299.0	4878	2.788	0.49152	(.18)	11.70831	(.19)	0.17276	(.05)	2577.3	2581.4	2584.6 \pm 0.8	0.34
m1.1A	2.2	5823	7083	33597	5.9	15.9	982.5	22798	1.645	0.49865	(.08)	12.03200	(.09)	0.17500	(.04)	2608.0	2606.9	2606.1 \pm 0.7	-0.09
m1.18	0.2	2624	4489	25517	10.0	3.4	227.6	4302	2.776	0.50028	(.07)	12.14868	(.09)	0.17612	(.05)	2615.0	2616.0	2616.7 \pm 0.8	0.08
m1.21	5.2	2446	3304	16769	7.0	25.4	670.0	13822	1.957	0.49822	(.07)	12.02569	(.08)	0.17506	(.04)	2606.1	2606.4	2606.6 \pm 0.7	0.02
m1.26	1.2	2685	11327	83319	31.8	17.7	768.7	4939	9.049	0.47593	(.07)	11.08740	(.08)	0.16896	(.04)	2509.5	2530.5	2547.4 \pm 0.7	1.79
m1.37	1.8	5251	7051	35594	7.0	7.8	1653.8	36073	1.934	0.49929	(.06)	12.08201	(.07)	0.17550	(.04)	2610.7	2610.8	2610.8 \pm 0.7	0.01
m1.44	2.1	6957	10561	57427	8.5	30.5	714.9	13000	2.365	0.49524	(.07)	11.91364	(.08)	0.17447	(.04)	2593.3	2597.6	2601.0 \pm 0.7	0.36
m1.45	3.1	1245	8882	68864	56.7	73.5	378.4	1405	16.242	0.47133	(.10)	10.94157	(.11)	0.16837	(.04)	2489.4	2518.2	2541.5 \pm 0.7	2.47
m1.52	2.0	1901	3218	18515	10.0	10.3	622.2	10470	2.788	0.49325	(.06)	11.78388	(.07)	0.17327	(.04)	2584.7	2587.4	2589.5 \pm 0.7	0.22
m1.54	0.6	903	3399	23634	26.8	88.4	22.9	181	7.568	0.47713	(.11)	11.02725	(.14)	0.16762	(.08)	2514.7	2525.4	2534.0 \pm 1.4	0.92
m1.57	0.7	3578	4871	26277	7.5	10.3	305.7	6200	2.142	0.47450	(.06)	11.01424	(.07)	0.16835	(.04)	2503.3	2524.3	2541.3 \pm 0.7	1.81
m1.63	2.2	964	2626	18718	19.9	11.3	509.6	4926	5.748	0.45461	(.07)	10.14094	(.08)	0.16178	(.04)	2415.7	2447.7	2474.4 \pm 0.7	2.84
m1.69	2.9	135	316	2197	16.7	3.7	246.7	3035	4.872	0.44758	(.17)	9.93899	(.18)	0.16105	(.06)	2384.5	2429.1	2466.8 \pm 1.0	3.99
m1tk1A	0.4	348	5332	45918	135.3	4.4	421.9	777	38.754	0.44238	(.51)	9.41512	(.52)	0.15436	(.12)	2361.3	2379.3	2394.8 \pm 2.0	1.67
m1tk1B	0.2	399	4675	41588	106.9	9.7	110.4	251	30.705	0.42185	(.69)	8.47015	(.71)	0.14562	(.15)	2268.9	2282.7	2295.2 \pm 2.6	1.36
m2tk1A	0.6	331	214	1120	3.5	1.9	62.8	2212	1.015	0.35156	(.14)	5.83019	(.16)	0.12028	(.06)	1942.1	1950.9	1960.3 \pm 1.1	1.08
m2tk1B	0.5	394	283	1572	4.1	3.8	38.9	1256	1.199	0.35742	(.38)	6.05531	(.39)	0.12287	(.07)	1969.9	1983.8	1998.4 \pm 1.3	1.65
m5tk1	0.9	3343	5081	27248	8.4	24.5	190.0	3516	2.327	0.49951	(.13)	12.10494	(.17)	0.17576	(.11)	2611.7	2612.6	2613.2 \pm 1.8	0.07
m6tk1	0.3	403	515	2511	6.4	52.2	2.4	72	1.754	0.37156	(.43)	6.11846	(.58)	0.11943	(.35)	2036.7	1992.9	1947.7 \pm 6.3	-5.33
m1tk2A	5.6	3415	4759	24443	7.3	15.7	1684.1	34280	2.039	0.50110	(.07)	12.16043	(.08)	0.17600	(.04)	2618.5	2616.9	2615.6 \pm 0.7	-0.14
m1tk2B	2.1	4400	5984	30411	7.1	8.1	1523.2	32751	1.972	0.49963	(.08)	12.09855	(.09)	0.17562	(.04)	2612.2	2612.1	2612.0 \pm 0.7	-0.01
m5tk2	1.5	2040	3510	21362	10.7	4.9	1098.3	18431	3.067	0.46943	(.06)	10.79328	(.07)	0.16676	(.04)	2481.1	2505.5	2525.3 \pm 0.7	2.11
m3th	0.3	1970	5593	50400	26.2	163.0	10.7	100	7.277	0.35769	(.16)	5.72925	(.28)	0.11617	(.21)	1971.2	1935.8	1898.1 \pm 3.8	-4.47
z2	2.5	245	126	61	0.3	1.8	177.7	10723	0.072	0.47925	(.06)	11.21662	(.07)	0.16975	(.04)	2524.0	2541.3	2555.1 \pm 0.7	1.47
z3	2.0	259	161	285	1.1	2.3	137.1	6882	0.320	0.48379	(.08)	11.50784	(.09)	0.17252	(.05)	2543.8	2565.2	2582.2 \pm 0.8	1.80
z4	1.0	275	133	63	0.2	1.4	93.9	5731	0.068	0.45587	(.10)	10.19082	(.12)	0.16213	(.07)	2421.3	2452.2	2478.0 \pm 1.1	2.74
z5	0.9	184	103	97	0.5	4.7	18.7	1032	0.153	0.48286	(.37)	11.40635	(.38)	0.17133	(.09)	2539.7	2556.9	2570.6 \pm 1.6	1.46
z6	9.9	208	122	173	0.9	1.4	842.4	44705	0.239	0.48315	(.04)	11.27878	(.06)	0.16931	(.04)	2541.0	2546.5	2550.8 \pm 0.7	0.47

^a Abbreviation m for monazite and z for zircon. All fractions are single grains or fractions of single grains. m1, m2, and m4 were not imaged prior to analysis. m1 # refers to grains that were imaged in epoxy grain mounts prior to analysis.

tk1, tk2, and th refer to thick sections 1 and 2 and thin section, respectively. These grains were mapped and dated on the EMP prior to TIMS analysis. A and B refer to fragments of individual grains.

^b Sample weights were estimated to within 40% using measured grain dimensions and nominal density 5.0g/cm³ for monazite, 4.5g/cm³ for zircon, and 4.2g/cm³ for rutile.

^c common Pb

^d Radiogenic to common Pb ratio

^e Measured ratio corrected for fractionation and spike contribution, Pb fractionation correction is 0.12 \pm 0.04% per a.m.u. (2s) for multicollector analyses and 0.15 \pm 0.04% per a.m.u. (2s) for single collector analyses based on repeated daily analysis of NBS 981.

^f Pb/U isotopic ratios corrected for fractionation, spike, blank, and initial common Pb. U blank = 0.1 pg \pm 50%; data was reduced using a Pb blank of 3.5 pg \pm 50%; initial common Pb composition was estimated using the model for terrestrial

Pb evolution of Stacey & Kramers (1975), numbers in parentheses are the % error reported at the 2-sigma confidence interval.

^g Uncertainty in the Pb-Pb date in My at the 2-sigma confidence interval.

Table 5. EMP and TIMS comparison data.

Fraction	Comment	Petrographic Setting	TIMS Age	% Discordant	EMP
m1tk1A	fragment consists primarily of higher Th core	matrix, in Als, rutile adj	2394.8 ± 2.0	1.67	2500-2100 (hi Th core)
m1tk1B	fragment consists primarily of lower Th rim	matrix, in Als, rutile adj	2295.2 ± 2.6	1.36	2330-2130 (low Th rim)
m2tk1A	broke in half, large grain, EMP just caught rim	matrix, elongate, adj Ksp and Als	1960.3 ± 1.1	1.08	1896±23
m2tk1B	broke in half, large grain, EMP just caught rim	matrix, elongate, adj Ksp and Als	1998.4 ± 1.3	1.65	
m5tk1		inclusion in garnet, well-armored	2613.2 ± 1.8	0.07	2592±13
m6tk1	high common Pb	matrix, adj to Ksp and Als	1947.7 ± 6.3	-5.33	2050±18 (core), 1940±29 (rim)
m1tk2A	larger core fragment	inclusion in garnet, well-armored	2615.6 ± 0.7	-0.14	2627±10, 2583±10*
m1tk2B	smaller rim fragment	inclusion in garnet, well-armored	2612.0 ± 0.7	-0.01	2583±10
m5tk2		inclusion in garnet (near rim), fractures around grain	2525.3 ± 0.7	2.11	2460±17
m3th	high common Pb	matrix, elongate	1898.1 ± 3.8	-4.47	1899±12 (core), 1844±6 (rim)

* Difference in dates for this grain reflect two different microprobe sessions on different days with different background measurements

CHAPTER 5 - MONAZITE SYSTEMATICS IN HIGH-PRESSURE GRANULITES

Table 6. Sm-Nd isotopic data for the felsic gneisses.

Sample	Lithology	[Sm] ¹	[Nd] ¹	¹⁴⁷ Sm/ ¹⁴⁴ Nd ²	¹⁴³ Nd/ ¹⁴⁴ Nd ³	ε _{Nd}	ε _{Nd(t)} ⁴	t _{CHUR} ⁵	t _{DM} ⁶
SZ00-217A	w.gneiss	4.80	35.82	0.0810	0.510538 ± 5	-40.96	-2.27	2.78	2.90
SZ00-14A	w.gneiss	4.70	20.44	0.1391	0.511694 ± 3	-18.42	0.86	2.51	2.79
SZ00-16B	w.gneiss	2.17	13.77	0.0953	0.510891 ± 3	-34.08	-0.15	2.63	2.79
SZ00-16C	w.gneiss	2.96	17.50	0.1024	0.511006 ± 3	-31.84	-0.29	2.65	2.81
SZ00-78A	w.gneiss	5.41	28.46	0.1150	0.511165 ± 3	-28.73	-1.40	2.78	2.93
DS93-15	w.gneiss	7.74	61.06	0.0767	0.510544 ± 3	-40.85	-0.70	2.67	2.80
SZ00-101A	w.gneiss	6.04	34.15	0.1069	0.511079 ± 4	-30.41	-0.38	2.65	2.83
SZ00-107A	w.gneiss	4.25	27.58	0.0932	0.510806 ± 3	-35.74	-1.12	2.71	2.85
SZ00-151A	w.gneiss	6.12	27.41	0.1351	0.511601 ± 3	-20.23	0.40	2.57	2.83
SZ00-85D	w.gneiss	2.37	18.87	0.0758	0.510580 ± 3	-40.14	0.29	2.60	2.74
SZ00-213A	w.gneiss	2.02	22.32	0.0547	0.510166 ± 3	-48.22	-0.73	2.66	2.77
01SZ113A	w.gneiss	4.47	30.82	0.0878	0.510706 ± 3	-37.68	-1.25	2.71	2.85
01SZ141	w.gneiss	3.37	37.72	0.0541	0.510121 ± 4	-49.09	-1.39	2.70	2.81
01SZ90	w.gneiss	3.23	20.24	0.0965	0.510824 ± 4	-35.39	-1.88	2.77	2.91
01SZ90 (2400)	m1tk1	1951	53370	0.0221	0.510030 ± 25	-50.88	3.02	2.28	2.40
01SZ90 (2615)	m1tk2	9834	61953	0.0960	0.510819 ± 4	-35.48	-1.59	2.76	2.90
01SZ90 (1980)	m2tk1	1411	24566	0.0347	0.510490 ± 23	-41.90	-0.72	2.03	2.18
01SZ90 (1900)	m3th	16925	163372	0.0626	0.510574 ± 11	-40.27	-7.61	2.35	2.50
01SZ90 (1950)	m6tk1	491	42792	0.0069	0.510368 ± 46	-44.28	3.24	1.83	1.97
01SZ90 (2606)	m1.21	7071	50458	0.0847	0.510653 ± 4	-38.73	-1.19	2.71	2.85
01SZ90 (2611)	m1.37	11356	82371	0.0834	0.510674 ± 7	-38.31	-0.23	2.65	2.79
01SZ90 (2541)	m1.45	21020	150863	0.0842	0.510625 ± 4	-39.27	-2.53	2.74	2.87

¹ Concentrations in ppm, as determined by isotope dilution.

² Internal errors in measured ¹⁴⁷Sm/¹⁴⁴Nd are <0.1% (2σ s.d.)

³ Measured ¹⁴³Nd/¹⁴⁴Nd with internal error (2σ s.e.)

⁴ initial ε_{Nd} calculated at 2.6 Ga for whole rock samples and at corresponding ²⁰⁷Pb/²⁰⁶Pb date for single monazite grains (given in () in first column.)

⁵ t_{CHUR} (Ga) calculated with (¹⁴⁷Sm/¹⁴⁴Nd)_{CHUR} = 0.1967 and (¹⁴³Nd/¹⁴⁴Nd) = 0.512638

⁶ t_{DM} (Ga) = (1/λ₁₄₇) * ln[((¹⁴³Nd/¹⁴⁴Nd)_{sample} - (¹⁴³Nd/¹⁴⁴Nd)_{DM}) / ((¹⁴⁷Sm/¹⁴⁴Nd)_{sample} - (¹⁴⁷Sm/¹⁴⁴Nd)_{DM}) + 1]; present-day (¹⁴³Nd/¹⁴⁴Nd)_{DM} = 0.513151, (¹⁴⁷Sm/¹⁴⁴Nd)_{DM} = 0.2137

Chapter 6

Synthesis of Thesis Findings and New Directions:

Regional U-Pb geochronological constraints on the metamorphism and juxtaposition of crustal blocks across the East Athabasca mylonite triangle, northern Saskatchewan, Canada

Introduction

The research presented in this thesis was originally motivated by the occurrence of unusual high-pressure rocks that seemingly lie in the center of a large Archean craton along a major shear zone in the western Canadian Shield called the Snowbird tectonic zone. A major goal of this research was to elucidate the metamorphic history of these rocks and place geochronological constraints on the inferred P - T paths in order to understand the large-scale significance of the Snowbird tectonic zone (STZ) and its importance in the history and assembly of Laurentia. The Striding-Athabasca (S-A) mylonite zone segment of the STZ is one of the world's exceptional exposures of lower crustal rocks, and thus provides a rare window to the base of the crust of an Archean craton. The high-pressure granulites and eclogites investigated in this study have afforded an opportunity to explore issues of critical importance to the thermal evolution of the lower crust as it records the processes of growth and stabilization of the Canadian Shield. This integrated petrological and geochronological approach has resulted in a re-evaluation of the tectonic history of this region and has elucidated the important Paleoproterozoic history of this segment of the STZ. In this final chapter, I revisit the controversy surrounding the tectonic significance of the STZ and summarize the important conclusions drawn from this thesis research. I also present additional U-Pb geochronological data that bears on the regional juxtaposition of large-scale crustal blocks within the S-A mylonite zone. Finally, I discuss how these new data change the previous interpretation of the STZ for the assembly of Laurentia, and explore new directions that will further expand our understanding of the Snowbird zone and its tectonic significance.

The debate surrounding the STZ

One of the most striking features of the western Canadian Shield is the Snowbird tectonic zone (STZ). This NE-trending structural discontinuity is the 2800 km-long boundary between the Rae and Hearne crustal provinces and is marked by dramatic gravity and magnetic anomalies and gradients (Fig. 1). The Striding-Athabasca (S-A) mylonite zone is a well-exposed 400 km-long segment in northern Saskatchewan and the

CHAPTER 6 - SYNTHESIS OF THESIS FINDINGS

Northwest Territories (Fig. 2). Two end-member models have been proposed to explain the STZ. In the first, the structure is fundamentally an Archean intracratonic shear zone with only local Paleoproterozoic reactivation (Hanmer et al., 1994; Hanmer et al., 1995a; Hanmer et al., 1995b). In the second, it is a Paleoproterozoic suture that accommodated tectonic escape of the Hearne Province during assembly of Laurentia (Hoffman, 1988), and is an 1850-1800 Ma accretionary suture along its southernmost extent (Ross et al., 1991). One of the major contributions of this thesis research is the identification of a much larger component of Paleoproterozoic metamorphism and deformation than originally hypothesized by Hanmer. Specifically, the results presented in this study from the East Athabasca mylonite triangle (EAmt) of the S-A mylonite zone indicate high-pressure metamorphism (2.0 GPa), intrusion of an immense mafic dike swarm, and exhumation from *ca.* 1.9-1.8 Ga. Distinguishing between Paleoproterozoic and Archean tectonothermal events has proven to be extremely difficult and although this research has made important strides in our understanding of the STZ, there are still challenging problems for the interpretation of the geology of the western Churchill Province and the Canadian Shield as a whole.

Although the western Churchill Province has a complex Archean history, it is surrounded by Paleoproterozoic collisional orogens and probably accommodated far-field stresses from 2.0-1.8 Ga. The western Churchill Province is bounded on the north by the Great Slave Lake shear zone–Thelon orogen (2.20-1.89 Ga); to the west by the Talston arc (1.99-1.91 Ga) and to the southeast by the Trans-Hudson orogen 1.9-1.8 Ga. Hoffman (1988; 1989) following Gibb (1983) and Gibb et al. (1983), suggested a model in which a large system of transcurrent faults, including the Striding-Athabasca segment of the STZ, accommodated extrusion of crustal blocks related to *ca.* 2.0-1.8 Ga indentation of the Superior and Slave Provinces. This hypothesis was based on regional geophysical data suggesting that the STZ truncates the Proterozoic Taltson magmatic zone of the Thelon orogen. This truncation relationship has been supported by further analysis of the subsurface geology along the southwestern extension of the STZ in Alberta (Ross et al., 1991). In addition, mapping and geochronology along the Virgin River shear zone (Bickford et al., 1994; Orell et al., 1999) also indicates Proterozoic tectonism along the southern segment of the STZ.

CHAPTER 6 - SYNTHESIS OF THESIS FINDINGS

In contrast, earlier field and geochronological results by the Geological Survey of Canada supported a model for the STZ as an Archean suture that was reactivated in the Paleoproterozoic (Hanmer, 1994; Hanmer et al., 1994; Hanmer et al., 1995a; Hanmer et al., 1995b). This interpretation was based on regional similarities between the Rae and Hearne provinces since 2.6 Ga (Hanmer et al., 1995a; Hanmer et al., 1995b) and more directly on the age of igneous rocks interpreted to be synchronous with deformation and metamorphism in the EAmt (Hanmer, 1997a; Hanmer et al., 1994). These workers suggest that the main part of the STZ is a 2620-2600 Ma mylonite zone localized along the Neoproterozoic collisional suture between the Rae and Hearne provinces. In this model, this lithospheric-scale heterogeneity or anisotropy was then repeatedly the site of reactivation but with very limited tectonic displacements. In order to explain the apparent contradiction between Archean mylonitization and a major Proterozoic truncation to the southwest, Hanmer et al. (1995b) proposed a model in which the Virgin River shear zone acted as a transform fault during Proterozoic convergence 2.08-1.75 Ga within an embayment bounded by the Virgin River shear zone and the Great Slave Lake shear zone.

Summary of Thesis Findings

Nature of the Southern Domain – Northwestern Domain boundary

Chapter 2 (Baldwin et al., 2003) examined the boundary between the high-*PT* rocks of the Southern Domain and the adjacent 2.6 Ga Godfrey granitic gneiss of the Northwestern Domain. This petrological and geochronological study showed that the high-*PT* rocks of the Southern Domain experienced a high-pressure event not recorded in the adjacent Godfrey granite. In contrast to the clear evidence for minimum *P-T* conditions of >1.5 GPa and 900-1000°C in the Southern Domain, well-preserved corona textures in the Godfrey granite constrain igneous crystallization and early metamorphism in the intermediate-pressure granulite field (Opx+Pl) at 1.0 GPa, 775°C. The reaction textures indicate that this was followed by metamorphism in the high-pressure granulite field (Grt+Cpx+Pl) at 1.2 GPa, 860°C. There is no geochronological evidence for 1.9 Ga high-*P* metamorphism preserved in the Godfrey granite, which has a minimum crystallization age of 2.61 Ga. In contrast, data from mafic granulites in the Southern

CHAPTER 6 - SYNTHESIS OF THESIS FINDINGS

Domain indicate that an early granulite facies event occurred at *ca.* 2.55-2.52 Ga, but at 1.9 Ga the Southern Domain underwent high-*P-T* metamorphism, then, based on titanite cooling ages and decompressional reaction textures, decompressed to 0.9-1.0 GPa relatively rapidly. Juxtaposition of the southern domain and Godfrey granite must have occurred during or following the decompression. In this model, the high-*P-T* rocks were exhumed quickly following the high-pressure metamorphism. Notably, this style of metamorphism is typically associated with collisional orogenesis, which has important implications for the Snowbird tectonic zone as a fundamental boundary in the Canadian Shield.

First record of eclogite facies metamorphism in the STZ

Chapter 3 (Baldwin et al., in review) continued to explore the idea that some component of collisional overthickening and collapse occurred in the STZ through a detailed study of eclogites that occur in the Southern Domain. This study examined the petrology, geochemistry, and geochronology of high-temperature eclogites from the Southern Domain. Temperatures were constrained by garnet-clinopyroxene exchange thermometry at 920-1000°C. At these temperatures, minimum pressure conditions in the eclogite are recorded by the $Jd + Qtz = Ab$ geobarometer at 1.8-2.0 GPa. A near-isothermal decompression path to granulite facies conditions is inferred from retrograde reaction textures. Geochemical data and inclusion patterns in garnet are consistent with a protolith characterized by low-pressure plagioclase accumulation.

The timing of high-pressure metamorphism was constrained by dating zircons contained in the eclogite. Inclusion suites of high-pressure phases, sector zoning patterns, and the petrographic setting of zircon are a direct link between zircon growth and eclogite facies metamorphism. Zircon from one eclogite samples yield a timing for the high-pressure metamorphism at 1904 Ma. However, zircon grains from one eclogite sample have older cores that are 2.54 Ga, which is a minimum age for the emplacement or earliest metamorphism of the gabbroic protolith. This age is also similar to dates obtained from zircons in the mafic granulite (Chapter 2). U-Pb rutile data indicate slow cooling at $\sim 1^\circ\text{C}/\text{Ma}$ below $\sim 500^\circ\text{C}$ from 1883 to 1851 Ma.

Of the two models that have emerged to explain the STZ, the eclogite data are consistent with a model of transport of continental crust to mantle depths during the

CHAPTER 6 - SYNTHESIS OF THESIS FINDINGS

Paleoproterozoic, followed by rapid buoyancy-driven exhumation to normal lower crustal depths. This study, combined with the data from Chapter 2, presents a tectonic scenario that is fundamentally different than the intracontinental Archean transpressional shear zone model of Hanmer et al. (1994; 1995a; 1995b).

Decompression P-T path of the eclogite and sapphirine granulites

Chapter 4 established the decompressional *P-T* path for the eclogite unit from associated sapphirine-bearing granulites. Peak pressures and temperatures from garnet-kyanite-quartz granulites yield pressures consistent with the mafic granulite and eclogite of ~2.0 GPa. The reaction textures in these rocks preserve a much later and lower pressure segment of the *P-T* path. The results of this study suggest that these rocks re-equilibrated at mid-crustal depths (0.6 GPa) following the high-*PT* metamorphism. Spectacular reaction textures are preserved in these rocks that allow for detailed petrological modeling and construction of petrogenetic grids that are applicable to a variety of sapphirine assemblages in decompressed kyanite eclogites in the literature.

Metamorphic evolution of the high-pressure felsic granulite

Chapters 2 & 3 established clear evidence for high-pressure metamorphism in the Southern Domain eclogite and mafic granulite at 1.9 Ga. In contrast, Chapter 5 presented important evidence for an Archean metamorphic history in the host rock to the mafic lithologies, the white gneiss. This rock is intriguing from all perspectives: petrologically, geochemically, and geochronologically. Detailed geochronological investigations of monazite from the white gneiss using combined electron microprobe and ID-TIMS methods, revealed that monazite records a complex history from 2.6 to 1.9 Ga. This study documented how the petrographic setting of monazite controls its participation in later metamorphic reactions and also showed how the geochemistry of the individual grains changes depending on the petrographic setting as inclusions in garnet or as matrix grains.

The felsic gneiss is largely a product of dehydration melting in the lower crust, but the precise timing, nature, and relative importance of the 2.6 and 1.9 events in this rock remain elusive. Nevertheless, an important conclusion of this study was the empirical verification of the high closure temperature for Pb diffusion in monazite. This

CHAPTER 6 - SYNTHESIS OF THESIS FINDINGS

study provided evidence that despite temperatures as great as 1000°C, monazite that is well-armored in garnet does not show any evidence for diffusional Pb loss.

Regional U-Pb geochronological constraints from the EAmt

Additional U-Pb geochronological data collected over the course of this four-year study are presented in Table 1. These data are from representative lithologies from each of the three lithotectonic domains of the EAmt (Fig. 3). Below, I present these data and discuss the implications of these data for the regional metamorphism and juxtaposition of these large-scale crustal domains.

Northwestern Domain (Bohica mafic complex)

The Bohica mafic complex in the northwestern domain consists of metanorite, gabbro and diorite (Fig. 3). The main body of the Bohica mafic complex is divided into well-foliated garnet-pyroxene mafic rocks with relict igneous textures, and is flanked to the northwest by hornblende-bearing granulite ribbon mylonite. Much of the mylonite is retrogressed, consisting of hornblende-bearing assemblages, although anhydrous Grt-Cpx and Opx-Cpx-bearing assemblages are also well-preserved. The mafic rocks are interfingered with granitic compositions, which are likely related to the Mary granite intrusion.

U-Pb geochronological data from a variety of lithologies in the Bohica mafic complex record Archean through Paleoproterozoic accessory phase growth (Table 1). U-Pb zircon and monazite dates from two mafic rocks, 96C-39 and 96C-37, record Paleoproterozoic lower intercepts of 1856 ± 10.2 and 1838 ± 19.2 Ma, with Archean upper intercepts (Fig. 4). Zircon and monazite from deformed granites within the Bohica complex are variably discordant with $^{207}\text{Pb}/^{206}\text{Pb}$ dates ranging from 2414 to 2599 Ma, which are interpreted as magmatic crystallization ages.

Southeastern Domain (Chipman dikes and tonalite)

Zircon and titanite from several Chipman dike samples record Paleoproterozoic dates (Fig. 5). Zircon from two migmatitic dikes in which garnet is associated with cm-scale leucosomes yields $^{207}\text{Pb}/^{206}\text{Pb}$ dates ranging from 1907-1863 Ma (96W47e, W29b, & SZ00-202G, Table 1). In one of these samples, W29b, zircon from a ~2-cm garnet and its associated melt tail yields $^{207}\text{Pb}/^{206}\text{Pb}$ dates of 1894 and 1885 Ma. This is interpreted

CHAPTER 6 - SYNTHESIS OF THESIS FINDINGS

reflect the time of melting and garnet growth. Titanite from both migmatitic and nonmigmatitic dikes yields $^{207}\text{Pb}/^{206}\text{Pb}$ dates of *ca.* 1900 Ma (96w47e and M112b). Zircon from two large (tens of cm) tonalitic melt segregations (96W42 and W2-27D) yield $^{207}\text{Pb}/^{206}\text{Pb}$ dates of 1896-1893 Ma. From these data, it is inferred that dike emplacement and melting were synchronous with or closely followed migmatization at granulite facies. Dates from both titanite and zircon are similar, indicating that this domain may have experienced rapid decompression and cooling following or cocomitant with deformation.

In addition to the dike samples, zircon from a deformed granite (96w-50a) that intrudes the Chipman tonalite and cross-cuts nonmigmatitic Chipman dikes were analyzed and yield $^{207}\text{Pb}/^{206}\text{Pb}$ dates of *ca.* 3.1 Ga. This zircon likely reflects inheritance from the host Chipman batholith. Of all of the intrusive bodies in the EAmt, the Chipman tonalite is the only unit that records zircon growth >3.0 Ga. Protolith ages for all of the other intrusive units are ~ 2.6 Ga.

Southern Domain (High-pressure granulites)

Additional U-Pb geochronological data from the Southern Domain high-pressure granulites are presented in Table 1. These data supplement the geochronological data from Chapters 2 and 5. Monazite and zircon data from several other felsic gneiss samples complement the data presented in Chapter 5. These samples consistently show the same complex polymetamorphic history from 2.6 to 1.9 Ga. The oldest monazite from these samples is typically 2625-2600 Ma (Fig. 6). Numerous discordant analyses with $^{207}\text{Pb}/^{206}\text{Pb}$ dates between 2.6 and 1.9 Ga are common. In addition, one sample (DS93-15) records monazite growth at 1906-1909 Ma. Zircon dates are commonly, but not always (e.g., DS93-15, Table 1), younger than the oldest monazite (Fig. 6). However, the oldest zircon analyzed from the felsic gneisses is 2615 Ma, which is within the range of Archean monazite dates. Rutile data from the felsic gneiss range from 1883-1824 Ma, which is a similar range seen in the eclogite, although the range extends to younger dates. These are interpreted to reflect cooling ages during protracted exhumation following an initial rapid exhumation that is indicated by titanite dates from adjacent mafic granulites.

Zircon from an underformed pegmatite sample that cross-cuts the felsic gneiss was analyzed (01SZ94). Zircon is clear, pink, and inclusion-free, and ranges in size from 90-200 μm . The morphology of the grains ranges from ovoid to short, stubby, equant

CHAPTER 6 - SYNTHESIS OF THESIS FINDINGS

grains. Ten zircons were analyzed, and one of the ten was clearly an inherited grain with a $^{207}\text{Pb}/^{206}\text{Pb}$ date of 2562 Ma. However, the remaining nine grains yield $^{207}\text{Pb}/^{206}\text{Pb}$ dates ranging from 1906-1938 Ma (Fig. 7). It is likely that the older zircon grains contain some inherited component, and I interpret the youngest $^{207}\text{Pb}/^{206}\text{Pb}$ date to reflect the maximum age for the crystallization of the pegmatite. The timing of this pegmatite emplacement places a minimum constraint on the deformation of the felsic gneiss that is approximately coincident with the timing of high-pressure metamorphism (1906.4±1.9 Ma, pegmatite emplacement and 1904.2±0.2 Ma, high-P metamorphism).

Additional zircon data for one sapphirine granulite (01SZ40a) and one mafic granulite (01SZ41b) are also presented in Table 1. These samples are adjacent to the eclogite outcrop that is described in Chapter 3 (Baldwin et al., in review). Zircon from the sapphirine granulite is similar in morphology to the felsic gneiss zircon, with the characteristic “soccer-ball” morphology with concentric shells of bright and dark BSE image domains. Nine zircon grains were analyzed from this sample and yield $^{207}\text{Pb}/^{206}\text{Pb}$ dates ranging from 2723-2070 Ma. The oldest date is interestingly the oldest zircon analyzed so far from the Southern Domain high-P rocks, and likely reflects an inherited component. The range of dates for the remaining zircon grains, excluding the youngest analysis, is 2640-2533 Ma. The younger dates are similar to the cores preserved in the eclogite, whereas the older dates are broadly consistent with the timing of Archean metamorphism in the host felsic gneiss. Five zircon grains analyzed from the mafic granulite sample yield $^{207}\text{Pb}/^{206}\text{Pb}$ dates ranging from 2623-2523 Ma, which is broadly similar to the range recorded in the sapphirine granulite, with dates that are similar to the cores of eclogitic zircons as well as some grains that are similar to the timing of the oldest metamorphism in the felsic gneiss.

Summary of regional geochronological data

These additional data provide insight into the relative importance and regional significance of the Paleoproterozoic and Archean histories of this segment of the STZ. The Northwestern Domain records evidence for Paleoproterozoic metamorphism manifested as ca. 1.86 Ga lower intercepts of zircon data from the Bohica mafic complex. The Northwestern Domain consists of primarily of orthogneisses, charnockites, and variety of mafic rocks that all crystallized at 2.6 Ga. The lower intercepts imply there

CHAPTER 6 - SYNTHESIS OF THESIS FINDINGS

was a Paleoproterozoic event that resulted in diffusional Pb loss from zircon grains. However, there is no evidence for discrete zircon or monazite growth at 1.9 Ga in the 2.6 Ga intrusive suite of the Northwestern Domain. This is consistent with the findings in Chapter 2, where no evidence for 1.9 Ga zircon growth was evident in the rocks directly adjacent to the Southern Domain.

In contrast to the Northwestern Domain, the Southeastern Domain preserves excellent evidence for a Paleoproterozoic magmatic and metamorphic event manifested by the Chipman dike swarm. Zircon in the dikes consistently yields ~1890-1895 Ma dates. Additionally, titanite from these rocks is within error the same age as zircon implying rapid cooling at ~1.0 GPa from 800-600°C. Interestingly, data from the Chipman dike swarm are consistently younger than the ~1905 Ma dates recorded in the Southern Domain. The possible connection between these two apparent events will be discussed below.

The geochronological data from the Southern Domain paint a complicated history of accessory phase growth from >2.6 Ga to the high-P metamorphism and decompression of the EAmt from 1.9-1.8 Ga. The data presented in Chapters 2 and 3 give the evidence for high-pressure metamorphism in the mafic lithologies at 1.9 Ga, but indicate that the timing of emplacement or earliest metamorphism in these rocks is at 2.52-2.55 Ga. The additional data presented in this chapter indicate zircon growth during the ~2.50 to 2.55 Ga interval as well as older 2.60-2.64 Ga zircon growth. The older dates are consistent with the timing of earliest metamorphism in the felsic gneiss presented in Chapter 5. The felsic gneiss does record some evidence for monazite growth at 1.9 Ga, but it is typically preserved as young rims on older cores, and these observations are summarized in Chapter 5, as well as the evidence for 1.9 Ga high-pressure metamorphism in all three lithologies of the Southern Domain. The complicated geochronology and U-Pb systematics of accessory phases in the felsic gneiss thus highlights the difficulties in deciphering complex metamorphic histories of lower crustal granulites. The important observation from a regional perspective is that the high-pressure event recorded in the Southern Domain occurred at *ca.* 1904 Ma, approximately 10 Ma earlier than the magmatism and metamorphism of the Chipman dike swarm. The decompression of these two domains was coeval, however, with titanite data from both domains recording similar

CHAPTER 6 - SYNTHESIS OF THESIS FINDINGS

dates, indicating decompression and cooling by ~1890 Ma. More protracted exhumation following this initial cooling is apparent from the broad range in rutile data from ~1.88-1.82 Ga.

Tectonic model for the Snowbird tectonic zone

The initial motivation of this thesis was to set out to solve the “problem” of whether or not the Snowbird tectonic zone represents an intracontinental Archean transpressional shear zone (Hanmer, 1997a; Hanmer, 1997b; Hanmer et al., 1994; Hanmer et al., 1995a; Hanmer et al., 1995b), or a Paleoproterozoic orogen (Hoffman, 1988; Hoffman, 1989). The main result of this thesis is that there is no simple answer as to what precisely the STZ really does represent. My work has uncovered an important Paleoproterozoic history to the Striding-Athabasca segment that had been predicted before this work began. However, these rocks also have an important Archean history and categorizing the STZ as dominantly Paleoproterozoic or Archean is impossible.

The occurrence of rocks that have experienced peak pressures of 20 kbar in the EAmT segment of the STZ *ca.* 1.9 Ga documents that this boundary records significant movement. The tectonic model put forth by Hanmer et al. (1995b) for the EAmT does not accommodate the formation and exhumation of eclogites. This thesis has shown that the high-P metamorphism that produced the eclogite occurred at 1904 Ma and involved transport of middle-lower crustal rocks to mantle depths. This implies that there was some type of crustal shortening event that occurred at this time, though its nature is not well-constrained. It is possible that an incipient basin developed at this time and that closure of these tectonic blocks, possibly due to far field stresses related to the development of the surrounding Taltson-Thelon and Trans-Hudson orogens occurred. It is intriguing however that the Paleoproterozoic dates recorded in the EAmT generally fall between the ages of the bounding orogens (e.g., Taltson-Thelon (1.99-1.91 Ga) and the Trans-Hudson (1.9-1.8 Ga)). This implies that a discrete event that occurred following the accretion of the Taltson-Thelon arc and prior to the Trans-Hudson collision resulted in this high-P metamorphism followed shortly by the mafic magmatism.

This study has placed firm timing constraints on the *P-T* evolution of the Southern Domain of the EAmT. Figure 8 shows a summary *P-T* diagram for the rocks investigated in this study. Table 2 lists the major timing constraints from this study. The results of

CHAPTER 6 - SYNTHESIS OF THESIS FINDINGS

this integrated petrological and geochronological study show that all three of the major lithological units of the EAmt experienced high-P metamorphism at 1.9 Ga. Peak metamorphism was followed by rapid exhumation (< 10 Ma) back to normal lower crustal levels recorded in all of the lithologies. It remains unclear what the precise significance of the Archean metamorphic history within the EAmt is. However, it is clear that each of the lithotectonic domains of the EAmt experienced different *P-T* histories prior to their juxtaposition and that this juxtaposition took place in the Paleoproterozoic. The scenario for the formation and exhumation of these high-P rocks must have involved significant crustal shortening followed by rapid, buoyancy driven exhumation, consistent with a model involving collision followed by delamination, which would drive the exhumation.

Future Work

The body of work presented in this thesis represents an attempt to resolve the complex metamorphic history of the high-pressure granulites and eclogites in the STZ. As such, there are still many unresolved issues, some that are directly related to the work presented in this thesis, and others that represent new avenues for future exploration. As far as the issues that relate to the research presented in this thesis, the most outstanding problem is understanding the Archean history of these rocks, particularly the felsic gneiss of the Southern Domain. It is still unclear what *P-T* conditions these rocks resided at at 2.6 Ga during the earliest metamorphism, and what the metamorphic evolution of these rocks was between 2.6 and 1.9 Ga. There still exists a vast area of the Southern Domain that is as of yet unexplored and unsampled. Finding rocks that preserve some evidence for the 2.6 to 1.9 Ga history, rather than just the strong metamorphic overprint at 1.9 Ga is key to understanding the early history of these rocks.

In addition, there is still more work to be done on understanding the significance of the sapphirine granulites from a petrological view. The reaction textures preserved in these rocks afford an excellent opportunity to understand these assemblages. It will be interesting to continue with the theoretical petrological modeling studies in order to construct more robust petrogenetic grids and pseudosections for silica-undersaturated sapphirine granulites.

CHAPTER 6 - SYNTHESIS OF THESIS FINDINGS

Another important question that is touched on, but not completely resolved is the connection between the Chipman mafic dike swarm at ~1895 Ma and its connection to the high-P metamorphism in the Southern Domain approximately 10 Ma earlier. This will require a better understanding of the precise timing constraints age of the mafic magmatism in the Southeastern Domain. The speculation that delamination of the lithosphere occurred in the Southern Domain, which provides an exhumation mechanism for the high-P rocks as well as a causal explanation for the localized magmatism manifested by the Chipman dikes needs to be tested more rigorously.

The overall goals of this research project have been to understand the timing, tempo, and controls on the metamorphism and exhumation of this regional granulite terrane. Through a series of focused studies within the EAmt by myself and others, we are slowly building up a robust dataset that allows us to understand the role of this region within the context of the assembly and stabilization of the western Canadian Shield. Extending these detailed studies to areas outside the EAmt will provide additional constraints on the regional exhumation and significance of this terrane.

Concluding Statement

The work presented in this thesis is really just the beginning of what I hope is a more comprehensive and detailed understanding of one of the most enigmatic and least understood boundaries in all of Laurentia. In many ways, this study has uncovered more complexities than were previously known, resulting in more unanswered questions than resolute answers. However, the many new questions provide exciting new problems to tackle that will ultimately afford a more comprehensive understanding of the nature of deep crustal metamorphic processes, the regional exhumation of high-pressure granulite terranes, and a better understanding of the geological significance of the Snowbird tectonic zone in the evolution of the western Canadian Shield.

References

- Baldwin, J. A., Bowring, S. A. & Williams, M. L., 2003. Petrological and geochronological constraints on high pressure, high temperature metamorphism in the Snowbird tectonic zone, Canada. *Journal of Metamorphic Geology*, **21**, 81-98.
- Baldwin, J. A., Bowring, S. A., Williams, M. L. & Williams, I. S., in review. Eclogites of the Snowbird tectonic zone: evidence for Paleoproterozoic high-pressure metamorphism in the western Canadian Shield. *Contributions to Mineralogy and Petrology*.
- Bickford, M. E., Collerson, K. D. & Lewry, J. F., 1994. Crustal history of the Rae and Hearne provinces, southwestern Canadian Shield, Saskatchewan: constraints from geochronologic and isotopic data. *Precambrian Research*, **68**, 1-21.
- Gibb, R. A., 1983. Model for suturing of Superior and Churchill plates; an example of double indentation tectonics. *Geology*, **11**, 413-417.
- Gibb, R. A., Thomas, M. D., Lapointe, P. L. & Mukhopadhyay, M., 1983. Geophysics of proposed Proterozoic sutures in Canada. *Precambrian Research*, **19**, 349-384.
- Hanmer, S., 1994. Geology, East Athabasca mylonite triangle, Saskatchewan. In: *Geological Survey of Canada Map 1859A*.
- Hanmer, S., 1997a. Geology of the Striding-Athabasca mylonite zone, northern Saskatchewan and southeastern District of Mackenzie, Northwest Territories. *Geological Survey of Canada Bulletin*, **501**, 1-92.
- Hanmer, S., 1997b. Shear zone reactivation at granulite facies: the importance of plutons in the localization of viscous flow. *Journal of the Geological Society of London*, **154**, 111-116.
- Hanmer, S., Parrish, R., Williams, M. & Kopf, C., 1994. Striding-Athabasca mylonite zone: Complex Archean deep-crustal deformation in the East Athabasca mylonite triangle, northern Saskatchewan. *Canadian Journal of Earth Sciences*, **31**, 1287-1300.
- Hanmer, S., Williams, M. & Kopf, C., 1995a. Modest movements, spectacular fabrics in an intracontinental deep-crustal strike-slip fault: Striding-Athabasca mylonite zone, NW Canadian Shield. *Journal of Structural Geology*, **17**(4), 493-507.
- Hanmer, S., Williams, M. & Kopf, C., 1995b. Striding-Athabasca mylonite zone: implications for the Archean and Early Proterozoic tectonics of the western Canadian Shield. *Canadian Journal of Earth Sciences*, **32**, 178-196.
- Hoffman, P. F., 1988. United Plates of America, the birth of a craton: Early Proterozoic assembly and the growth of Laurentia. *Annual Reviews of Earth and Planetary Science Letters*, **16**, 543-603.
- Hoffman, P. F., 1989. Precambrian geology and tectonic history of North America. In: *The Geology of North America - An overview* (eds Bally, A. W. & Palmer, A. R.), pp. 447-512, Geological Society of America, Boulder, Colorado.
- Orell, S. E., Bickford, M. E. & Lewry, J. F., 1999. Crustal evolution and age of thermotectonic reworking in the western hinterland of the Trans-Hudson Orogen, northern Saskatchewan. *Precambrian Research*, **95**, 187-223.

CHAPTER 6 - SYNTHESIS OF THESIS FINDINGS

- Ross, G. M., Parrish, R. R., Villeneuve, M. E. & Bowring, S. A., 1991. Geophysics and geochronology of the crystalline basement of the Alberta Basin, western Canada. *Can. J. Earth Sci.*, **28**, 512-522.
- Sharpton, V. L., Grieve, R. A. F., Thomas, M. D. & Halpenny, J. F., 1987. Horizontal gravity gradient: an aid to the definition of crustal structure in North America. *Geophysical Research Letters*, **14**, 808-811.

Figure Captions

Figure 1. Horizontal Bouguer gravity gradient map of North America from Sharpton et al. (1987). Based on least squares fitting of plane over area of 25 x 25 km to Bouguer anomaly values interpolated to 5-km grid. Number 13 marks the Snowbird tectonic zone, which corresponds to a 1 mGal km⁻¹ over much of its length.

Figure 2. Geologic map of the western Canadian Shield showing major tectonic elements (inset shows location of map). Abbreviations are as follows: AB – Athabasca basin, BL – Baker Lake basin, KX – Kramanitaur Complex, STZ – Snowbird tectonic zone, THO – Trans-Hudson Orogen, TO – Talston Orogen, TMZ – Thelon Magmatic Zone, UX – Uvauk Complex, VR – Virgin River Shear Zone. The Striding-Athabasca mylonite zone occurs within the East Athabasca mylonite triangle, the northern tip of the Athabasca lozenge, as well along the eastern margin of the Selwyn lozenge to the northeast (shown in black). Other examples of high-pressure granulites in the STZ include the Kramanitaur Complex and Uvauk Complex. Outline shown for East Athabasca mylonite triangle shown in Figure 3.

Figure 3. Geological map of the East Athabasca mylonite triangle. Inset shows location of the three lithotectonic domains. The EAMt is bound by the Rae craton to the northwest and the Hearne craton to the southeast.

Figure 4. (a) Concordia diagram for mafic mylonite, 96C-39, from the Bohica mafic complex, NW domain. (b) Concordia diagram for mafic mylonite, 96C-37, from the Bohica mafic complex, NW domain. Upper intercepts are interpreted to

CHAPTER 6 - SYNTHESIS OF THESIS FINDINGS

represent the crystallization age. Lower intercepts reflect Pb loss or new growth at ~1.85 Ga.

Figure 5. Concordia diagram for the Chipman mafic dike samples. Analyses are labeled with fraction and sample number from Table 1. Error ellipses are 2σ .

Figure 6. (a) Concordia diagram for the felsic granulites of the Southern Domain. Results are shown for the samples listed in Table 1. Error ellipses are smaller than size of symbol. (b) CL images of zircon from sample DS93-15, showing “soccer-ball” morphology and concentric growth shells of alternating dark and light zones.

Figure 7. Concordia diagram for pegmatite sample 01SZ94. Error ellipses are 2σ . Analyses are labeled with fraction names from Table 1.

Figure 8. Summary *P-T* diagram and timing constraints on the metamorphic evolution of the lithological units investigated in this study.

CHAPTER 6 - SYNTHESIS OF THESIS FINDINGS

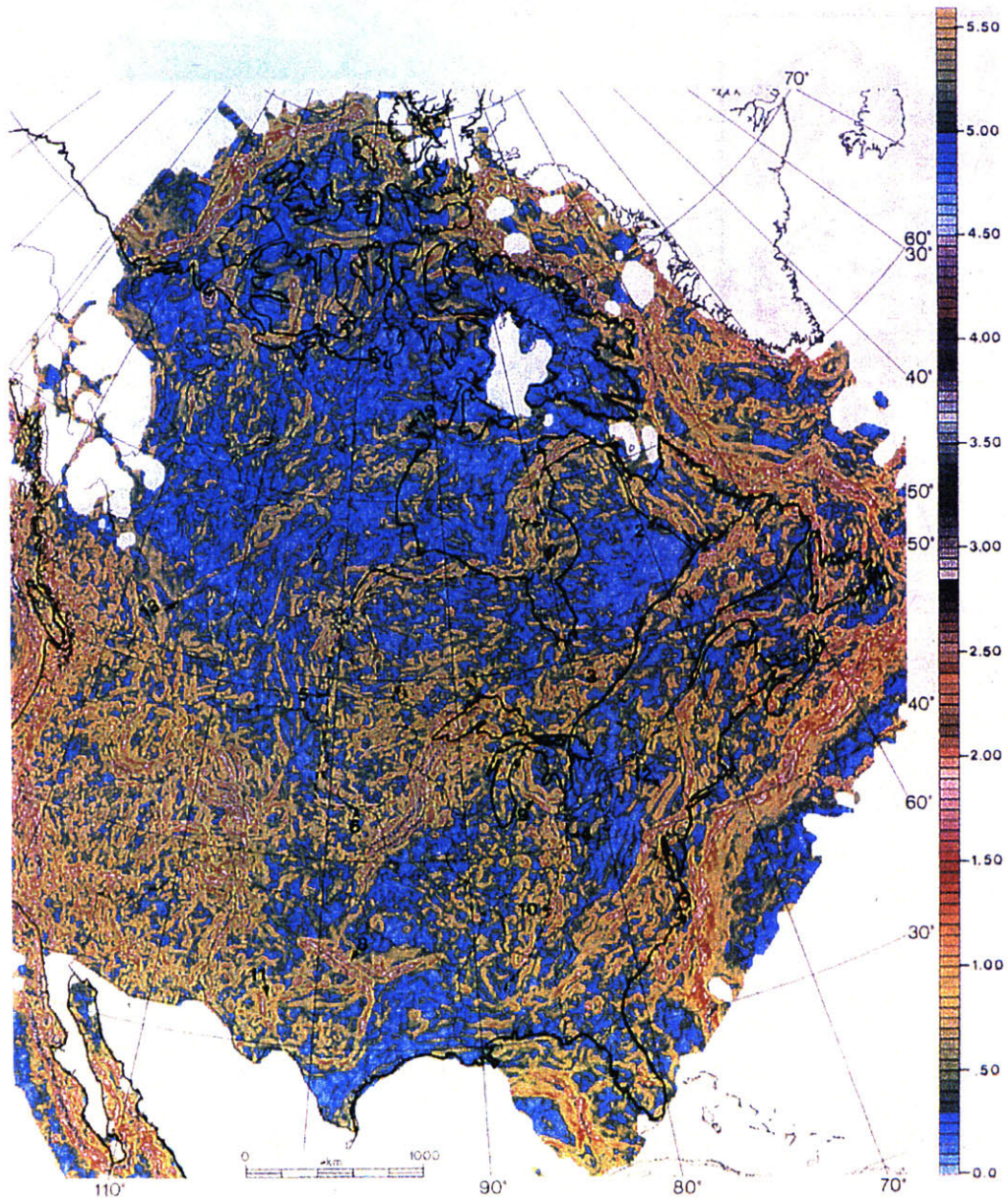


Figure 1

CHAPTER 6 - SYNTHESIS OF THESIS FINDINGS

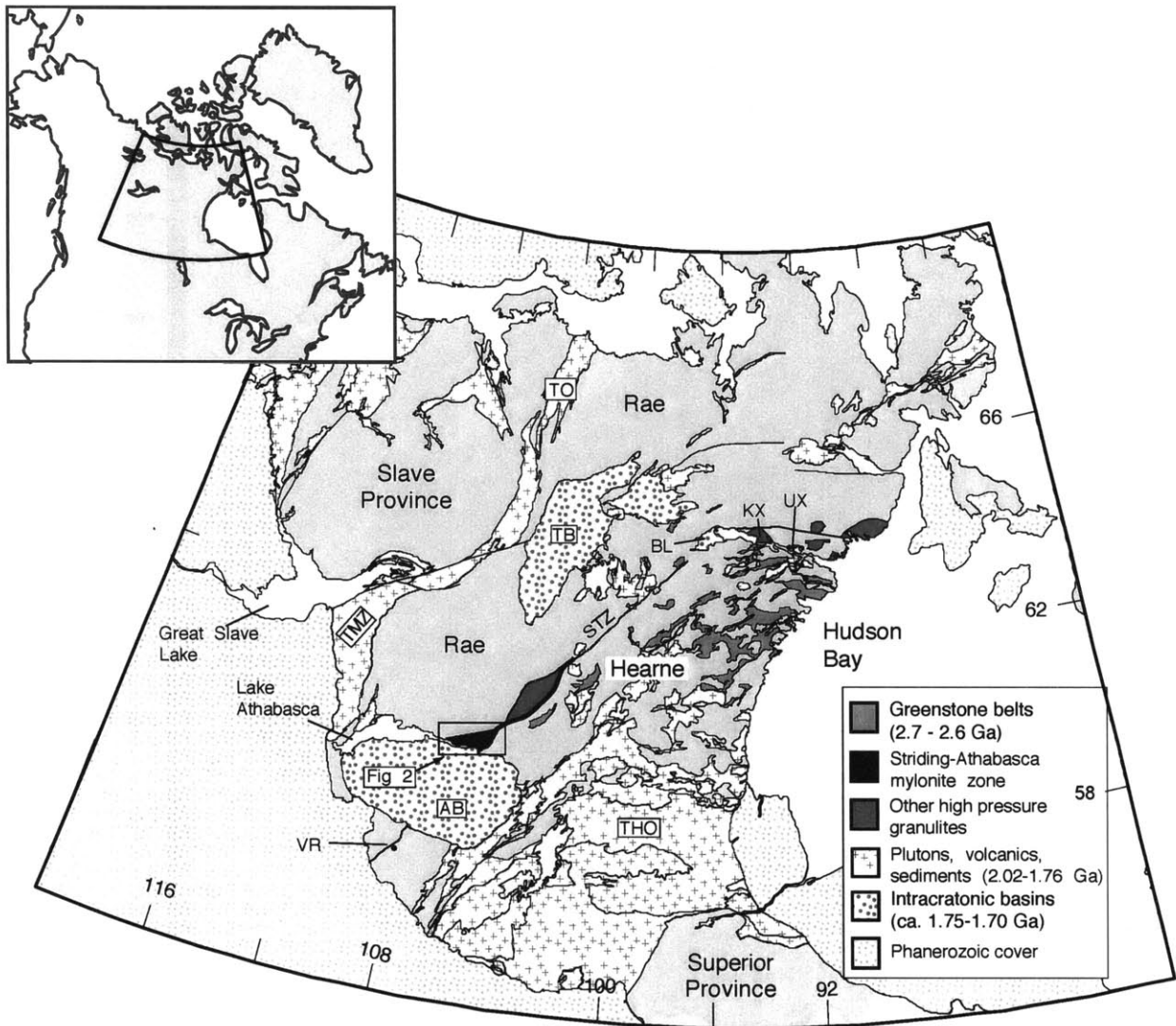


Figure 2

CHAPTER 6 - SYNTHESIS OF THESIS FINDINGS

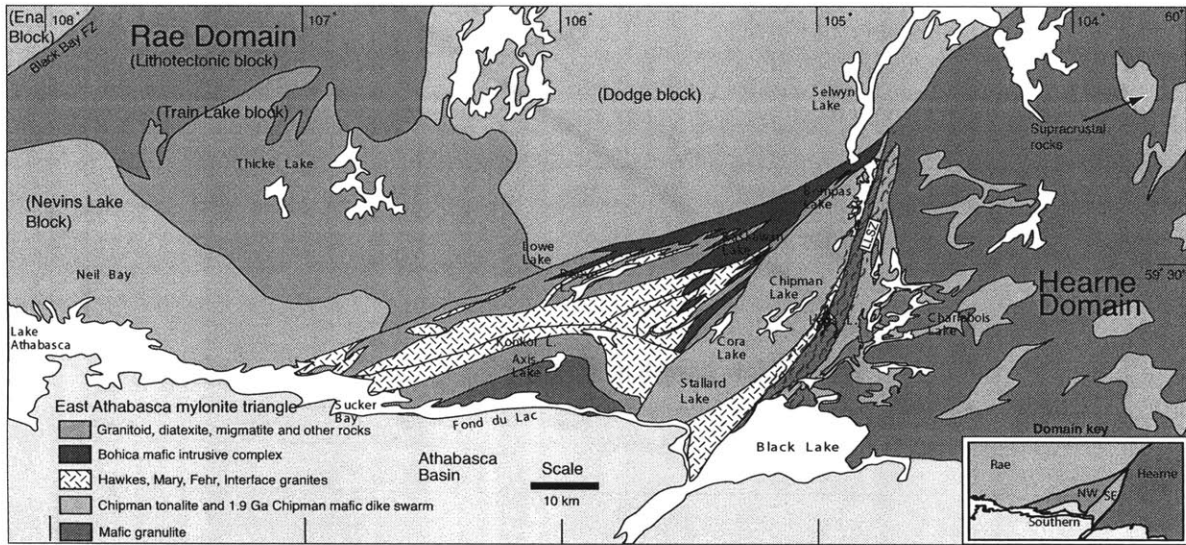


Figure 3

CHAPTER 6 - SYNTHESIS OF THESIS FINDINGS

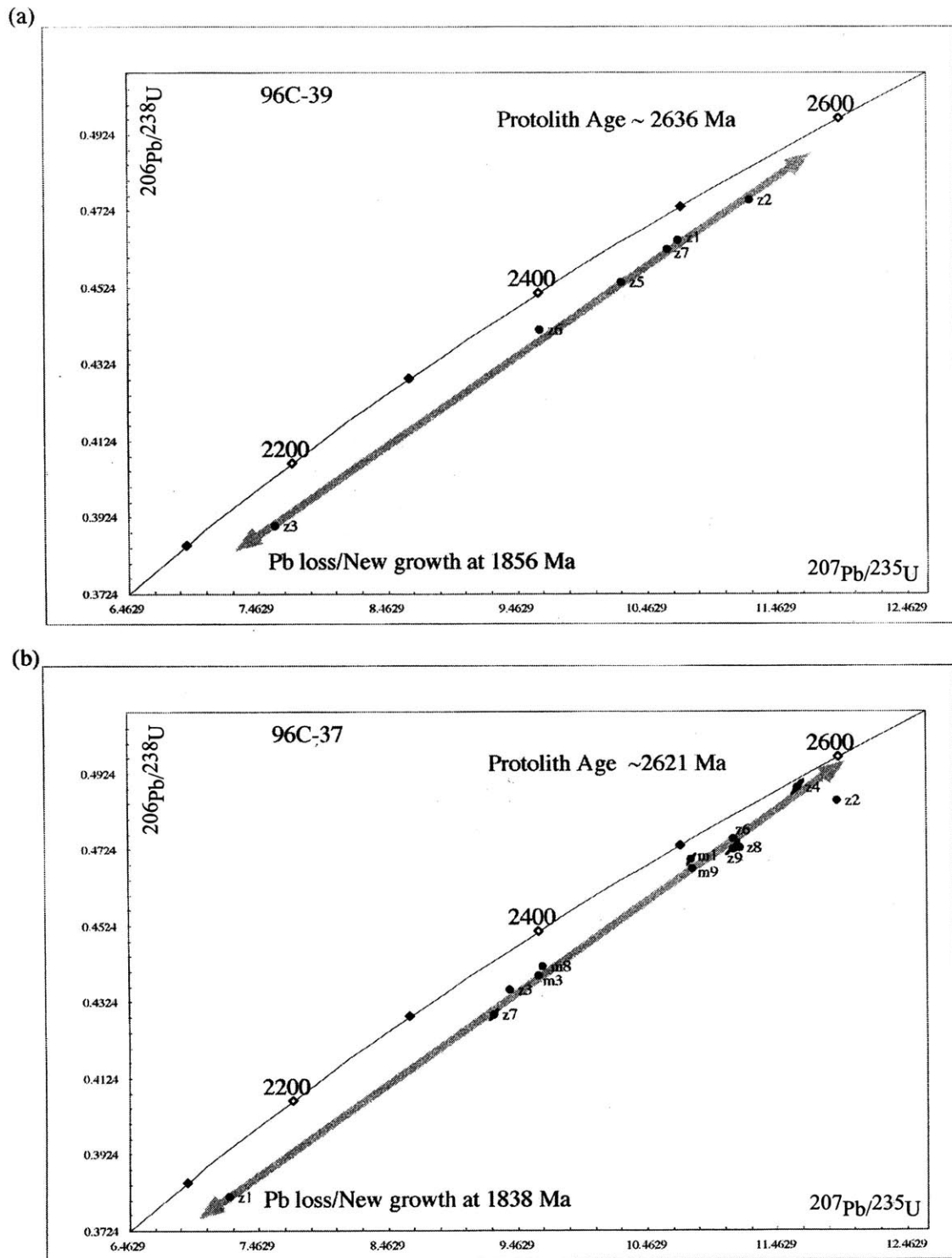


Figure 4

CHAPTER 6 - SYNTHESIS OF THESIS FINDINGS

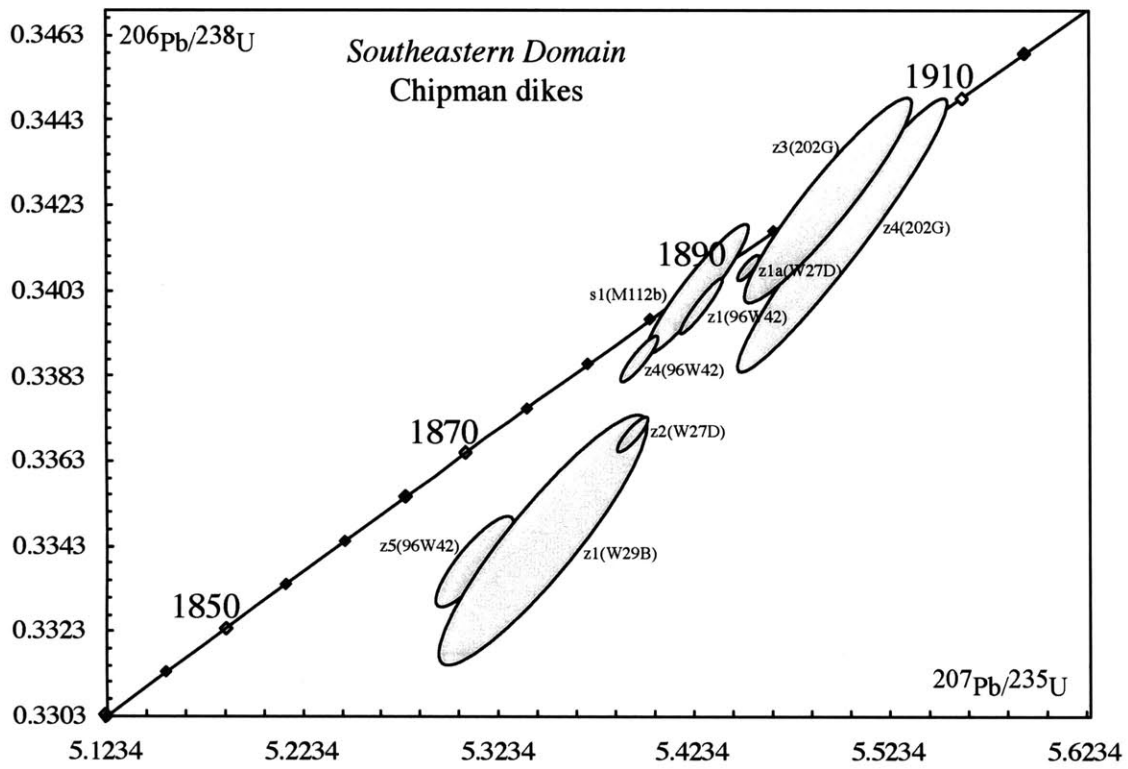
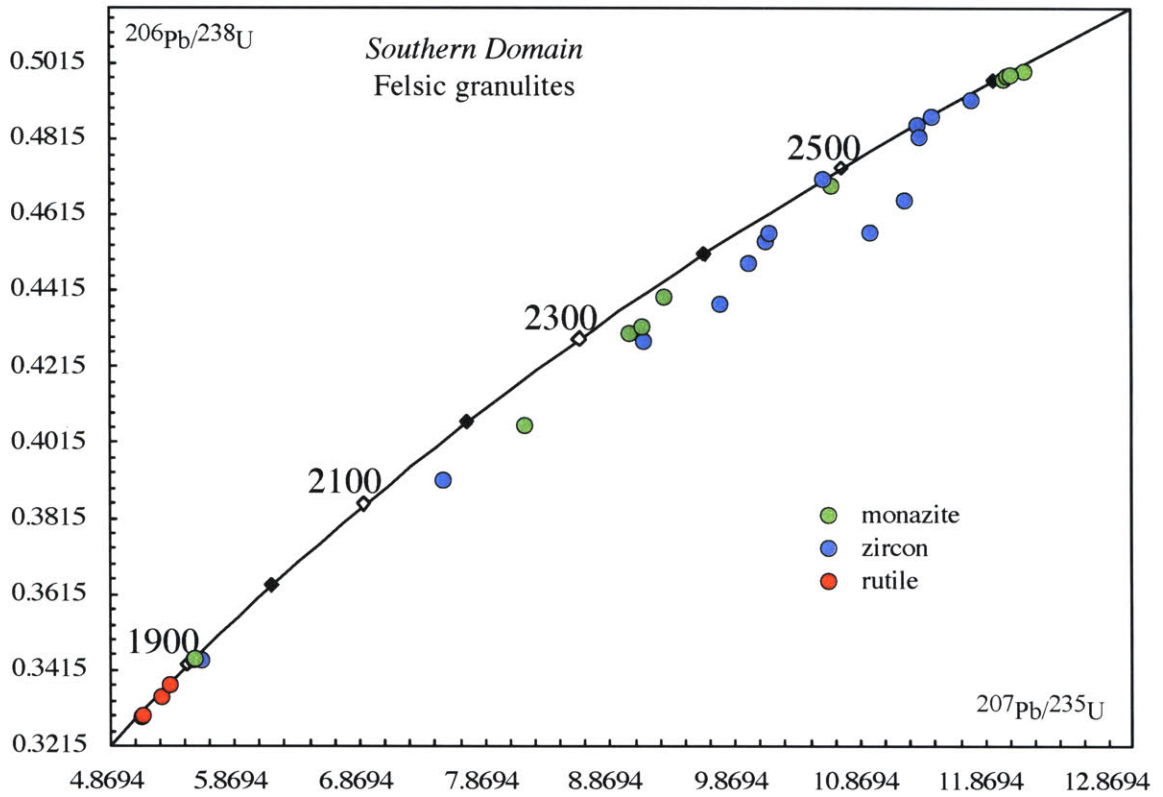


Figure 5

CHAPTER 6 - SYNTHESIS OF THESIS FINDINGS

(a)



(b)

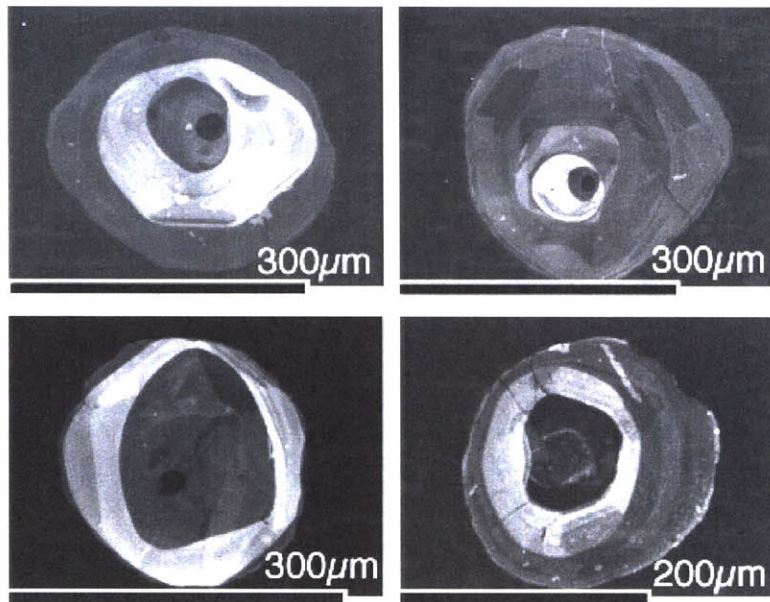


Figure 6

CHAPTER 6 - SYNTHESIS OF THESIS FINDINGS

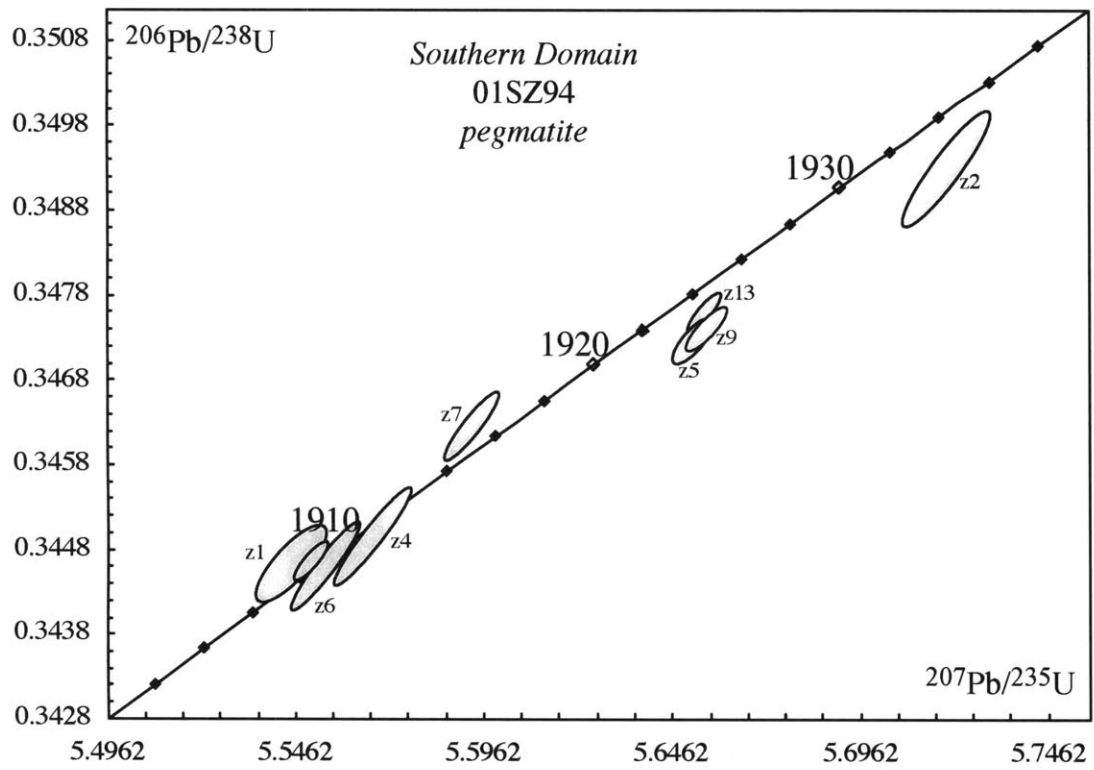


Figure 7

CHAPTER 6 - SYNTHESIS OF THESIS FINDINGS

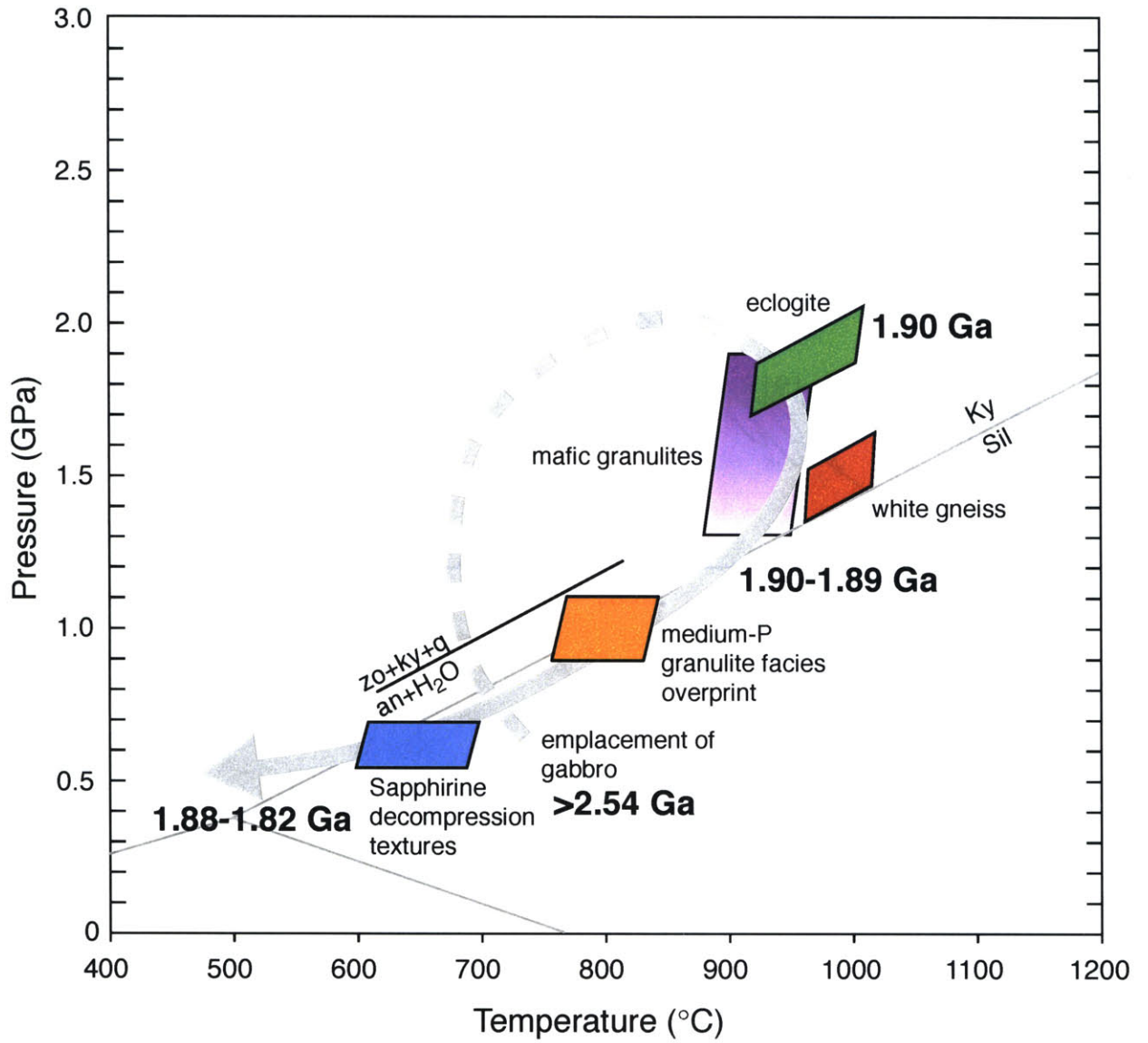


Figure 8

Table 1. U-Pb results for zircon, monazite, titanite, and rutile.

Sample	Weight Fraction (1)	Composition			Isotopic Ratios						Dates (Ma)			Discordance (%)			
		U	Pb	Pbc	Pb*	206Pb*	208 Pb	206 Pb	% err	207 Pb	% err	206 Pb	207 Pb		207 Pb		
		(ppm)	(ppm)	(pg)	(4)	204 Pb	206 Pb	238 U	% err	235 U	% err	238 U	235 U		206 Pb		
NORTHWESTERN DOMAIN																	
Bohica Mafic Complex																	
96C-37	Grt-bt mafic mylonite																
m1	7.7	5015	3425	59.7	439.5	16849	0.5156	0.46974	(.31)	10.81231	(.31)	0.16694	(.04)	2482.4	2507.1	2527.2 ± 0.7	2.13
m3	9.1	1927	2051	14.2	1320.2	31361	1.6421	0.43936	(.18)	9.62291	(.19)	0.15885	(.04)	2347.8	2399.4	2443.5 ± 0.7	4.67
m8	4.3	1027	4512	7.5	2573.4	15382	10.3041	0.44197	(.07)	9.65396	(.08)	0.15842	(.04)	2359.4	2402.3	2438.9 ± 0.7	3.89
m9	9.1	1689	4981	39.8	1134.4	10057	6.1089	0.46754	(.10)	10.81356	(.11)	0.16775	(.04)	2472.8	2507.2	2535.3 ± 0.7	2.97
z1	15.4	251	101	29.8	51.5	2856	0.0673	0.38133	(.07)	7.23813	(.09)	0.13766	(.04)	2082.5	2141.2	2198.0 ± 0.7	6.15
z2	8.0	350	192	49.7	30.0	1531	0.0926	0.48523	(.10)	11.93972	(.14)	0.17846	(.09)	2550.0	2599.7	2638.6 ± 1.5	4.06
z3	3.4	167	81	11.7	22.5	1211	0.0940	0.43560	(.14)	9.40750	(.15)	0.15664	(.06)	2330.9	2378.6	2419.7 ± 0.9	4.37
z4	0.6	239	152	17.9	4.3	235	0.0970	0.48878	(.42)	11.63646	(.44)	0.17267	(.11)	2565.4	2575.6	2583.6 ± 1.8	0.86
z6	5.5	190	101	17.9	30.2	1576	0.0943	0.47531	(.09)	11.12958	(.11)	0.16983	(.06)	2506.8	2534.0	2555.9 ± 0.0	2.32
z7	0.6	388	203	18.4	5.3	299	0.0726	0.42906	(.36)	9.27734	(.38)	0.15682	(.10)	2301.5	2365.8	2421.7 ± 1.7	5.90
z8	1.7	258	131	11.0	20.0	1120	0.0393	0.47281	(.20)	11.18558	(.21)	0.17158	(.05)	2495.9	2538.7	2573.1 ± 0.9	3.62
z9	1.7	104	68	15.5	6.6	317	0.2540	0.47275	(.47)	11.13287	(.48)	0.17079	(.09)	2495.6	2534.3	2565.4 ± 1.5	3.28
96C-39	Grt-hbl-bt mafic mylonite																
z1	25.2	273	139	52.7	65.7	3391	0.0906	0.46469	(.14)	10.70381	(.17)	0.16706	(.09)	2460.3	2497.8	2528.4 ± 1.6	3.24
z2	10.3	578	310	22.4	141.2	7056	0.1327	0.47542	(.10)	11.25397	(.12)	0.17168	(.07)	2507.3	2544.4	2574.1 ± 1.1	3.13
z3	44.1	173	71	14.6	214.5	11863	0.0815	0.39021	(.16)	7.59101	(.17)	0.14109	(.04)	2123.8	2183.8	2240.6 ± 0.7	6.12
z5	9.9	162	79	22.3	34.3	1844	0.0639	0.45394	(.15)	10.27082	(.17)	0.16410	(.07)	2412.7	2459.5	2498.3 ± 1.2	4.11
z6	7.4	132	67	31.6	14.8	787	0.0944	0.44139	(.14)	9.63605	(.16)	0.15834	(.08)	2356.8	2400.6	2438.0 ± 1.3	3.97
z7	8.7	88	46	22.8	16.7	893	0.0802	0.46243	(.10)	10.62099	(.12)	0.16658	(.05)	2450.3	2490.5	2523.6 ± 0.9	3.49
96C-40	Grt-hbl mafic mylonite																
m1	6.5	154	2549	21.8	757.1	1118	43.7900	0.42311	(.11)	9.10680	(.12)	0.15610	(.05)	2274.6	2348.8	2413.9 ± 0.9	6.84
m3	17.6	11	5	26.3	2.4	140	0.2394	0.28747	(.54)	4.15797	(.73)	0.10490	(.45)	1628.9	1665.8	1712.6 ± 8.2	5.53
96C-53	Granitic gneiss																
z1	1.6	681	370	16.5	34.2	1778	0.1024	0.48442	(.12)	11.50208	(.13)	0.17221	(.06)	2546.5	2564.8	2579.2 ± 1.0	1.54
z2	1.0	252	144	16.6	7.8	413	0.1042	0.47129	(.45)	11.32466	(.45)	0.17427	(.08)	2489.2	2550.2	2599.1 ± 1.3	5.09
z3	0.8	310	185	22.0	5.6	305	0.0871	0.47841	(.32)	11.47711	(.36)	0.17399	(.14)	2520.3	2562.7	2596.4 ± 2.4	3.54
z4	0.4	292	186	17.0	3.9	217	0.0978	0.48471	(.47)	11.62320	(.49)	0.17392	(.14)	2547.8	2574.5	2595.7 ± 2.3	2.24
z5	0.4	126	74	9.0	2.9	171	0.1122	0.44428	(1.10)	10.43030	(1.11)	0.17027	(.14)	2369.8	2473.7	2560.3 ± 2.3	8.89
96C-55	Granitic gneiss																
z1a	0.3	982	441	31.5	2.9	168	0.0629	0.32654	(.45)	7.16236	(.61)	0.15908	(.36)	1821.6	2131.8	2445.9 ± 6.1	29.23
z1b	0.5	657	426	71.3	1.9	108	0.1022	0.39170	(.38)	9.05502	(.52)	0.16766	(.32)	2130.7	2343.6	2534.4 ± 5.3	18.67
z1c	0.4	557	426	60.4	2.0	116	0.0903	0.47977	(.24)	11.46355	(.29)	0.17329	(.15)	2526.3	2561.6	2589.7 ± 2.5	2.96
z4	0.9	301	183	33.0	3.9	211	0.1006	0.45173	(.63)	10.79981	(.66)	0.17340	(.18)	2402.9	2506.1	2590.7 ± 2.9	8.67

Table 1. U-Pb results for zircon, monazite, titanite, and rutile.

Sample	Weight Fraction (1)	Composition				Isotopic Ratios					Dates (Ma)				Discordance (%)			
		U	Pb	Pbc	Pb*	206Pb*	208 Pb	206 Pb	207 Pb	207 Pb	206 Pb	207 Pb	206 Pb	207 Pb				
		(ppm)	(ppm)	(pg)	Pbc	204 Pb	206 Pb	238 U	% err	235 U	% err	206 Pb	% err	238 U		235 U	206 Pb	
SOUTHEASTERN DOMAIN																		
Chipman dikes and tonalite																		
96W-47e	Migmatitic Dike																	
s1(1)	54.1	14	7	51.6	6.0	328	0.1697	0.36947	(.12)	5.90471	(.15)	0.11591	(.07)	2026.9	1961.9	1894.1	± 1.3	-8.18
s2(2)	93.9	27	12	171.4	5.8	333	0.0997	0.37234	(.07)	5.96820	(.11)	0.11625	(.07)	2040.4	1971.2	1899.4	± 1.3	-8.67
s3(10)	250.0	9	5	155.5	6.6	334	0.2696	0.39268	(.11)	6.29593	(.13)	0.11628	(.07)	2135.3	2017.9	1899.8	± 1.3	-14.57
z2	4.7	2	1	4.5	0.8	74	0.0017	0.36875	(7.50)	5.79213	(7.77)	0.11392	(1.66)	2023.5	1945.2	1862.9	± 30.0	-10.05
z3	4.6	2	1	6.4	0.5	47	0.0523	0.27769	(7.55)	4.42033	(7.75)	0.11545	(1.25)	1579.7	1716.2	1886.9	± 22.4	18.34
SZ00-202G	Migmatitic Dike																	
z3	0.4	77	28	2.4	4.7	305	0.1050	0.34248	(.71)	5.49198	(.77)	0.116304	(.27)	1898.6	1899.3	1900.2	± 4.8	0.10
z4	0.4	397	180	17.5	3.2	194	0.1164	0.34165	(.95)	5.49972	(.99)	0.116752	(.27)	1894.6	1900.6	1907.1	± 4.8	0.76
W29B	Tonalitic leucosome from migmatitic dike																	
z1	3.7	23	12	18.0	1.6	111	0.0309	0.33717	(.89)	5.38941	(1.00)	0.11593	(.41)	1873.1	1883.2	1894.4	± 7.4	1.30
z2	1.0	19	9	6.2	1.0	78	0.0282	0.31773	(4.14)	5.05273	(4.28)	0.11534	(.89)	1778.6	1828.2	1885.2	± 16.0	6.47
96W-50a	Deformed granite																	
z1a	1.2	690	509	33.9	16.8	795	0.0951	0.61177	(.10)	19.96451	(.11)	0.23668	(.05)	3077.1	3089.6	3097.8	± 0.8	0.84
z1b	2.5	766	548	16.0	85.5	4049	0.1027	0.61477	(.12)	20.24683	(.13)	0.23886	(.04)	3089.1	3103.2	3112.4	± 0.7	0.94
z1c	1.5	471	305	17.0	25.2	1222	0.0852	0.55417	(.10)	17.63592	(.11)	0.23081	(.05)	2842.5	2970.1	3057.7	± 0.7	8.69
z2	0.4	495	222	19.8	4.0	206	0.1147	0.32593	(.42)	9.37627	(.43)	0.20864	(.11)	1818.6	2375.5	2895.0	± 1.7	42.50
z3	1.0	646	403	12.3	31.6	1649	0.0176	0.57116	(.11)	17.61427	(.12)	0.22367	(.05)	2912.6	2968.9	3007.3	± 0.9	3.91
96W-42	Melt pod from migmatitic dike																	
z1	0.5	939	320	8.4	18.2	1146	0.0133	0.34047	(.18)	5.43534	(.19)	0.11578	(.06)	1889.0	1890.4	1892.1	± 1.1	0.19
z4	0.4	1411	468	5.9	32.9	2107	0.0095	0.33874	(.16)	5.39579	(.18)	0.11553	(.08)	1880.6	1884.2	1888.2	± 1.5	3.5
z5	0.4	922	322	13.1	9.6	599	0.0140	0.33397	(.32)	5.31140	(.38)	0.11535	(.19)	1857.6	1870.7	1885.3	± 3.5	3.5
W2-27D	Tonalite melt segregation																	
z1a	17.6	231	78	7.0	195.5	12047	0.0329	0.34093	(.08)	5.45241	(.09)	0.11599	(.04)	1891.2	1893.1	1895.3	± 0.8	0.25
z2	5.0	210	70	6.9	50.1	3106	0.0307	0.33720	(.13)	5.39585	(.14)	0.11606	(.07)	1873.2	1884.2	1896.4	± 1.2	1.41
M112b	Nonmigmatitic, cauliflower dike																	
s1(3)	42.8	6	5	32.3	5.9	177	1.3573	0.34184	(.34)	5.44386	(.39)	0.11550	(.16)	1895.5	1891.8	1887.7	± 2.9	-0.48
s2(5)	44.2	6	6	51.3	3.9	128	1.0893	0.42237	(.25)	6.84411	(.32)	0.11752	(.18)	2271.2	2091.4	1918.9	± 3.3	-21.82
s3(11)	28.2	8	6	23.7	5.9	199	1.0876	0.31619	(.37)	5.04246	(.45)	0.11566	(.25)	1771.1	1826.5	1890.2	± 4.5	7.21
96W-50a	Deformed granite																	
z1a	1.2	690	509	33.9	16.8	795	0.0951	0.61177	(.10)	19.96451	(.11)	0.23668	(.05)	3077.1	3089.6	3097.8	± 0.8	0.84
z1b	2.5	766	548	16.0	85.5	4049	0.1027	0.61477	(.12)	20.24683	(.13)	0.23886	(.04)	3089.1	3103.2	3112.4	± 0.7	0.94
z1c	1.5	471	305	17.0	25.2	1222	0.0852	0.55417	(.10)	17.63592	(.11)	0.23081	(.05)	2842.5	2970.1	3057.7	± 0.7	8.69
z2	0.4	495	222	19.8	4.0	206	0.1147	0.32593	(.42)	9.37627	(.43)	0.20864	(.11)	1818.6	2375.5	2895.0	± 1.7	42.50
z3	1.0	646	403	12.3	31.6	1649	0.0176	0.57116	(.11)	17.61427	(.12)	0.22367	(.05)	2912.6	2968.9	3007.3	± 0.9	3.91

Table 1. U-Pb results for zircon, monazite, titanite, and rutile.

Sample	Weight Fraction	Composition			Isotopic Ratios					Dates (Ma)			Discordance (%)					
		U	Pb	Pbc	Pb*	²⁰⁶ Pb*	²⁰⁸ Pb	²⁰⁶ Pb	% err	²⁰⁷ Pb	²⁰⁷ Pb	²⁰⁶ Pb		²⁰⁷ Pb				
		(ppm)	(ppm)	(pg)	Pbc	204 Pb	206 Pb	238 U	% err	235 U	% err	206 Pb		206 Pb	207 Pb			
(1)	(2)	(3)	(3)	(4)	(5)	(6)	(7)	(7)	(7)	(7)	(7)	(8)	(8)					
SOUTHERN DOMAIN																		
D33S3	felsic gneiss																	
z1	29.4	38	18	10.4	51.2	2850	0.0555	0.45472	(.11)	10.11269	(.12)	0.16130	(.05)	2416.2	2445.1	2469.3	± 0.8	2.58
z2	26.4	49	24	21.2	29.2	1576	0.0654	0.45677	(.08)	10.14140	(.09)	0.16103	(.05)	2425.3	2447.8	2466.5	± 0.9	2.00
z3	10.9	39	18	5.5	34.6	2050	0.0510	0.42821	(.23)	9.14484	(.30)	0.15489	(.16)	2297.7	2352.6	2400.6	± 2.8	5.10
z7	2.1	75	33	7.7	8.3	495	0.0704	0.39177	(.52)	7.53846	(.53)	0.13956	(.12)	2131.0	2177.6	2221.7	± 2.1	4.79
m1	0.9	771	5938	7.4	752.8	2886	16.6290	0.49852	(.12)	12.08191	(.13)	0.17577	(.06)	2607.4	2610.8	2613.4	± 1.0	0.28
m2	1.4	1063	8219	8.9	1329.0	4991	16.7231	0.49821	(.07)	12.05362	(.08)	0.17547	(.05)	2606.1	2608.6	2610.5	± 0.8	0.21
m4	0.5	8206	13433	17.2	390.3	6710	2.6243	0.49700	(.07)	12.01655	(.08)	0.17536	(.04)	2600.9	2605.7	2609.4	± 0.8	0.40
m3	0.9	1281	5012	7.3	615.4	4592	7.9676	0.49366	(.09)	11.84465	(.10)	0.17402	(.05)	2586.5	2592.2	2596.7	± 0.7	0.48
m5	0.6	529	683	6.4	65.1	1440	1.9998	0.46885	(.21)	10.62954	(.22)	0.16443	(.06)	2478.5	2491.3	2501.7	± 1.1	1.12
r1	22.0	36	13	41.7	6.1	382	0.0131	0.32892	(.20)	5.11642	(.30)	0.11282	(.22)	1833.1	1838.8	1845.3	± 4.0	0.76
r2	89.6	3	2	57.5	1.6	108	0.0404	0.33634	(.41)	5.16992	(.71)	0.11148	(.54)	1869.0	1847.7	1823.7	± 9.9	-2.86
r3	27.6	10	3	6.6	12.7	846	0.0038	0.32994	(.44)	5.11148	(.46)	0.11236	(.10)	1838.1	1838.0	1837.9	± 1.8	-0.01
DS93-15	felsic gneiss																	
z1	10.6	1079	584	5.2	1193.6	64712	0.1343	0.48212	(.28)	11.34287	(.28)	0.17064	(.07)	2536.5	2551.7	2563.9	± 1.1	1.29
z2	7.9	781	432	1.8	1890.2	107145	0.1485	0.48735	(.07)	11.45483	(.08)	0.17047	(.04)	2559.2	2560.9	2562.2	± 0.7	0.14
z4	10.9	104	54	20.0	28.5	1372	0.1929	0.42807	(.82)	10.27199	(.82)	0.17403	(.08)	2297.0	2459.6	2596.8	± 1.4	13.70
z5	17.8	74	43	2.5	308.2	16939	0.1879	0.49178	(.13)	11.77143	(.14)	0.17360	(.06)	2578.4	2586.4	2592.7	± 1.0	0.67
z6	4.4	48	26	5.2	21.9	1163	0.1865	0.46967	(.30)	10.75421	(.31)	0.16607	(.06)	2482.1	2502.1	2518.4	± 1.1	1.73
z7	2.5	24	15	4.8	7.4	381	0.2788	0.48561	(1.10)	11.62740	(1.11)	0.17366	(.14)	2551.6	2574.9	2593.2	± 2.4	1.94
z8	3.3	25	15	4.7	10.3	541	0.2381	0.48500	(.71)	11.32810	(.72)	0.16940	(.10)	2549.0	2550.5	2551.7	± 1.6	0.13
z9	4.4	26	16	3.7	19.1	1010	0.2462	0.50466	(.51)	12.24514	(.51)	0.17598	(.08)	2633.8	2623.4	2615.4	± 1.3	-0.86
z10	5.0	71	45	7.6	28.9	1353	0.3041	0.48672	(.27)	11.45755	(.28)	0.17073	(.08)	2556.5	2561.1	2564.8	± 1.3	0.39
m1	8.2	486	593	18.1	268.0	4476	2.9636	0.34459	(.07)	5.55227	(.09)	0.11686	(.05)	1908.7	1908.7	1908.8	± 0.9	0.00
m2	5.3	1319	473	6.4	391.6	22993	0.0943	0.34415	(.07)	5.53597	(.08)	0.11667	(.04)	1906.6	1906.2	1905.7	± 0.8	-0.05
m3	13.4	206	93	2.5	497.2	31302	0.0358	0.43963	(.06)	9.30810	(.07)	0.15356	(.04)	2349.0	2368.8	2385.9	± 0.8	1.85
m4a1	1.5	1338	5698	17.9	478.8	2790	10.2063	0.43184	(.10)	9.12249	(.11)	0.15321	(.05)	2314.0	2350.4	2382.1	± 0.8	3.40
m4b	0.4	2405	8716	39.4	78.8	520	9.0337	0.40619	(.16)	8.18268	(.21)	0.14610	(.13)	2197.5	2251.4	2300.8	± 2.3	5.30
m4e	0.6	1360	5936	45.5	72.1	419	10.4046	0.43035	(.28)	9.03217	(.33)	0.15222	(.15)	2307.3	2341.3	2371.0	± 2.5	3.19
m5	4.7	1897	3431	118.5	135.3	1385	5.4722	0.31462	(.45)	5.06486	(.45)	0.11676	(.07)	1763.4	1830.2	1907.1	± 1.2	8.61
r1	105.0	20	7	31.2	21.9	1355	0.0009	0.33451	(.16)	5.28712	(.21)	0.11463	(.13)	1860.2	1866.8	1874.1	± 2.4	0.86
r2	120.0	22	8	126.5	7.0	436	0.0094	0.34159	(.15)	5.42424	(.19)	0.11517	(.11)	1894.3	1888.7	1882.5	± 1.9	-0.72
96D3A	felsic gneiss																	
z1	5.3	112	44	7.5	30.7	1677	0.1815	0.34398	(.17)	5.60053	(.19)	0.11808	(.09)	1905.8	1916.2	1927.4	± 1.7	1.30
z2	1.9	165	133	78.0	2.2	120	0.2005	0.48202	(.19)	10.87642	(.37)	0.16365	(.28)	2536.1	2512.6	2493.7	± 4.8	-2.05
r1(34)	190	14	7	525	1.7	115	0.0422	0.33769	(.43)	5.35650	(1.17)	0.11504	(.97)	1875.6	1877.9	1880.5	± 17.6	0.31
r2(115)	552	6	3	367	3.0	191	0.0239	0.32935	(.20)	5.13870	(.37)	0.11316	(.28)	1835.2	1842.5	1850.8	± 5.1	0.97

Table 1. U-Pb results for zircon, monazite, titanite, and rutile.

Sample	Fraction	Composition				Isotopic Ratios						Dates (Ma)			Discordance (%)				
		Weight (μg)	U (ppm)	Pb (ppm)	Pbc (pg)	Pb*	206Pb*	208 Pb	206 Pb	207 Pb	207 Pb	206 Pb	207 Pb	206 Pb		207 Pb			
																	204 Pb	206 Pb	238 U
(1)	(2)	(3)	(3)	(4)	(5)	(6)	(7)	(7)	(7)	(7)	(7)	(7)	(7)	(8)					
96D3B	felsic gneiss																		
	z1	8.1	25	15	18.0	6.0	309	0.1800	0.47081	(.29)	10.57113	(.31)	0.16284	(.10)	2487.1	2486.2	2485.4	\pm 1.7	-0.08
	z2	1.1	262	131	5.9	24.4	1359	0.1107	0.44846	(.24)	9.98731	(.26)	0.16152	(.09)	2388.4	2433.6	2471.6	\pm 1.5	4.03
SZ00-149A	felsic gneiss																		
	z1	1.4	179	90	6.4	18.6	1033	0.0925	0.45148	(.26)	10.81422	(.29)	0.17372	(.12)	2401.8	2507.3	2593.8	\pm 2.0	8.86
	z2	0.9	422	194	3.5	50.3	3108	0.0543	0.43818	(.17)	9.75590	(.18)	0.16148	(.05)	2342.5	2412.0	2471.2	\pm 1.8	6.21
	z3	0.8	167	89	4.5	15.1	843	0.1400	0.46524	(.49)	11.23115	(.51)	0.17508	(.13)	2462.6	2542.5	2606.8	\pm 2.1	6.65
	t1m1	16.1	1457	3537	54.5	1041.3	11874	4.4189	0.50047	(.07)	12.23252	(.08)	0.17727	(.04)	2615.8	2622.4	2627.5	\pm 0.7	0.54
	t2m2	6.2	1110	2733	31.0	548.3	6150	4.5637	0.49484	(.06)	11.92131	(.08)	0.17473	(.04)	2591.6	2598.2	2603.4	\pm 0.7	0.55
	t2m5a	2.6	1163	2669	17.8	383.6	4760	4.0827	0.50302	(.05)	12.28720	(.07)	0.17716	(.04)	2626.8	2626.6	2626.5	\pm 0.7	-0.01
	t2m5b	0.5	2601	5324	11.1	252.8	3565	3.5448	0.49953	(.06)	12.13291	(.07)	0.17616	(.04)	2611.8	2614.7	2617.0	\pm 0.7	0.24
	t4m4	7.6	259	707	13.9	388.0	3630	6.0198	0.43899	(.06)	9.06680	(.07)	0.14979	(.04)	2346.1	2344.8	2343.6	\pm 0.7	-0.13
	t3m2	8.4	573	305	44.0	57.2	2505	0.3791	0.40084	(.17)	7.70918	(.18)	0.13949	(.05)	2172.9	2197.7	2220.9	\pm 0.9	2.54
	t5m5	4.5	1792	2923	37.0	351.0	5960	2.6078	0.49718	(.06)	12.05479	(.07)	0.17585	(.04)	2601.7	2608.7	2614.1	\pm 0.7	0.58
01SZ41E	felsic gneiss																		
	z1	1.5	196	105	2.9	51.9	2953	0.1542	0.47004	(.09)	10.84829	(.11)	0.16739	(.06)	2483.7	2510.2	2531.7	\pm 1.0	2.28
	z2	0.8	224	108	2.6	34.4	2070	0.0908	0.44921	(.15)	10.13466	(.16)	0.16363	(.06)	2391.8	2447.1	2493.5	\pm 1.1	4.88
	z4	2.6	264	125	3.6	90.3	5609	0.0326	0.45953	(.10)	10.73100	(.11)	0.16936	(.04)	2437.5	2500.1	2551.4	\pm 0.7	5.36
	z5	1.1	344	164	3.6	50.9	3024	0.0902	0.43816	(.17)	10.45982	(.17)	0.17314	(.05)	2342.4	2476.4	2588.2	\pm 0.8	11.31
	z6	1.1	247	112	1.4	84.5	5259	0.0388	0.43748	(.07)	10.10918	(.09)	0.16759	(.05)	2339.4	2444.8	2533.7	\pm 0.9	9.14
01SZ94	Undeformed pegmatite cross-cutting felsic gneiss																		
	z1	7.7	92	34	7.3	35.1	2065	0.0919	0.34460	(.13)	5.54503	(.17)	0.11670	(.11)	1908.8	1907.6	1906.4	\pm 1.9	-0.15
	z2	3.3	131	48	4.8	32.4	1968	0.0859	0.34926	(.19)	5.71915	(.21)	0.11876	(.08)	1931.1	1934.3	1937.7	\pm 1.5	0.40
	z4	6.2	77	27	3.5	48.2	3013	0.0856	0.34493	(.17)	5.56673	(.18)	0.11705	(.06)	1910.3	1911.0	1911.7	\pm 1.1	0.08
	z5	3.3	146	52	3.0	56.9	3568	0.0826	0.34724	(.08)	5.65189	(.10)	0.11805	(.06)	1921.4	1924.0	1926.9	\pm 1.1	0.33
	z6	4.1	146	54	11.4	18.8	1089	0.0941	0.34458	(.16)	5.55416	(.17)	0.11690	(.06)	1908.7	1909.0	1909.4	\pm 1.1	0.05
	z7	12.1	147	53	3.0	212.3	13247	0.0833	0.34623	(.12)	5.59292	(.13)	0.11716	(.05)	1916.6	1915.0	1913.3	\pm 0.9	-0.19
	z8	7.4	107	38	1.2	237.1	14736	0.0884	0.34462	(.07)	5.55015	(.08)	0.11681	(.05)	1908.8	1908.4	1907.9	\pm 0.9	-0.06
	z9	5.3	88	32	2.5	68.0	4260	0.0809	0.34738	(.08)	5.65561	(.10)	0.11808	(.05)	1922.1	1924.6	1927.4	\pm 1.0	0.32
	z10	1.7	213	120	0.9	235.4	13116	0.1725	0.48640	(.06)	11.43382	(.07)	0.17049	(.05)	2555.1	2559.2	2562.4	\pm 0.8	0.35
	z13	7.0	262	95	4.6	144.8	8766	0.0875	0.34757	(.06)	5.65502	(.08)	0.11800	(.04)	1923.0	1924.5	1926.2	\pm 0.7	0.19

Table 1. U-Pb results for zircon, monazite, titanite, and rutile.

Sample	Weight Fraction (μg) (1)	Composition				Isotopic Ratios						Dates (Ma)			Discordance (%)		
		U (ppm) (3)	Pb (ppm) (3)	Pbc (pg) (4)	Pb* (pg) (4)	$^{206}\text{Pb}^*$ 204 Pb (5)	^{208}Pb 206 Pb (6)	^{206}Pb 238 U (7)	% err (7)	^{207}Pb 235 U (7)	% err (7)	^{206}Pb 238 U (7)	^{207}Pb 235 U (7)	^{207}Pb 206 Pb (8)			
01SZ40A	sapphirine granulite																
z1	5.4	129	78	2.2	195.8	9921	0.3084	0.47852	(.07)	11.12866	(.08)	0.16867	(.04)	2520.8	2534.0	2544.5 \pm 0.7	1.13
z2	1.2	463	176	0.8	261.2	16117	0.0858	0.36394	(.06)	6.42011	(.08)	0.12794	(.05)	2000.8	2035.0	2069.9 \pm 0.8	3.88
z3	3.3	500	290	0.8	1166.4	66985	0.1138	0.51764	(.05)	13.40601	(.07)	0.18783	(.04)	2689.2	2708.7	2723.3 \pm 0.7	1.53
z4	0.9	221	121	7.4	13.9	745	0.1477	0.46606	(.30)	10.76864	(.31)	0.16758	(.07)	2466.3	2503.4	2533.6 \pm 1.2	3.20
z5	1.0	525	293	14.4	19.6	1044	0.0787	0.49613	(.12)	12.21473	(.13)	0.17856	(.05)	2597.1	2621.0	2639.6 \pm 0.8	1.95
z6	1.5	100	57	1.5	56.1	3109	0.1834	0.49187	(.19)	11.75097	(.21)	0.17327	(.07)	2578.8	2584.8	2589.5 \pm 1.2	0.50
z7	2.1	57	31	2.3	27.8	1612	0.1336	0.48527	(.14)	11.39729	(.15)	0.17034	(.07)	2550.2	2556.2	2561.0 \pm 1.2	0.51
z10	1.5	1558	754	9.8	110.8	6270	0.0293	0.46801	(.07)	10.76131	(.08)	0.16677	(.04)	2474.8	2502.7	2525.4 \pm 0.7	2.41
z12	1.1	1548	809	2.8	320.2	19554	0.0509	0.49558	(.07)	11.98013	(.08)	0.17533	(.04)	2594.8	2602.9	2609.1 \pm 0.7	0.67
01SZ41B	mafic granulite																
z1	64.3	82	43	1.5	1843.0	110391	0.0720	0.48356	(.06)	11.78847	(.07)	0.17681	(.04)	2542.7	2587.7	2623.2 \pm 0.7	3.71
z2	31.8	106	54	1.1	1584.8	95314	0.0757	0.47420	(.05)	10.97631	(.06)	0.16788	(.04)	2502.0	2521.1	2536.6 \pm 0.7	1.65
z3	22.0	103	55	3.2	382.0	22978	0.0698	0.49850	(.05)	12.02715	(.06)	0.17498	(.04)	2607.3	2606.5	2605.9 \pm 0.7	-0.07
z4	5.4	98	52	2.5	113.8	6809	0.0797	0.49443	(.07)	11.84923	(.08)	0.17381	(.04)	2589.8	2592.6	2594.7 \pm 0.7	0.23
z5	4.5	91	46	2.1	96.1	5798	0.0780	0.47678	(.10)	10.94881	(.12)	0.16655	(.05)	2513.2	2518.8	2523.3 \pm 0.9	0.48

(1) Fraction includes the type of mineral, z = zircon, m = monazite, s = sphene, a = apatite followed by the analysis number. Analyses are single crystal unless otherwise noted by the number of grains in parentheses.

Fraction numbers followed by a lower case letter are analyses of fragments from individual crystals.

(2) Weights were estimated using measured grain dimensions, an ellipsoidal geometry, and nominal densities of minerals, 5.0g/cc for monazite, 4.5g/cc for zircon, 3.5g/cc for sphene, and 3.2g/cc for apatite.

(3) Expressed as ppm U and Th and ppm radiogenic Pb. Th concentrations and Th/U ratio calculated from radiogenic ^{235}Pb and the $^{235}\text{Pb}/^{207}\text{Pb}$ ratio, respectively, assuming concordance between Th-Pb and U-Pb systems.

(4) Pbc and Pb* represent common Pb and radiogenic Pb respectively.

(5) Measured ratio corrected for fractionation only. Pb fractionation correction is $0.12\% \pm 0.04\%$ per amu for multicollector analyses and $0.15\% \pm 0.04\%$ per amu for single collector analysis based on repeated analyses of NBS 981.

(6) radiogenic Pb.

(7) Pb/U isotopic ratios corrected for fractionation, spike, blank, and initial common Pb, U blank = $1 \text{ pg} \pm 50\%$, data was reduced using a Pb blank of $3.5 \pm 50\%$; initial common Pb composition was estimated using the model for terrestrial Pb evolution of Stacey and Kramers (1975); numbers in parentheses are the % error reported at the 2-sigma confidence interval.

(8) Uncertainty in the Pb-Pb date in My at the 2-sigma confidence interval.

CHAPTER 6 - SYNTHESIS OF THESIS FINDINGS

Table 2. Chronology of events in the EAmt.

Event	Domain	Time (Ma)	Mineral
Decompression of Southern Domain (< ~400°C)	S	1880-1820	(r)
Decompression of SE domain (< ~600°)	SE	1895-1890	(s)
Decompression of Southern Domain (< ~600°)	SE	1900-1894	(s)
Chipman dike emplacement and metamorphism	SE	1890-1895	(z)
Cross-cutting pegmatite in the felsic gneiss	S	1906	(z)
High-pressure metamorphism			
Eclogite	S	1904	(z)
Mafic granulite	S	1904	(z)
Felsic gneiss (M2)	S	1906	(m)
Emplacement of eclogite protolith	S	2540	(z)
Mafic granulite metamorphism	S	2580-2520	(z)
Fehr granite	SE	2580	(z)
Bohica mafic complex emplacement	NW	2600-2580	(z)
Godfrey granite emplacement	NW	2610	(z)
Felsic gneiss early metamorphism (M1)	S	2625-2600	(m)
Emplacement of Chipman batholith	SE	3200-3000	(z)